THE ROLE OF CD82 IN DESMOSOMAL ADHESION

by

Maryam Arab

A thesis submitted to the

University of Birmingham

for the degree of

DOCTOR OF PHILOSOPHY

Institute of Cancer and Genomic Sciences
College of Medical and Dental Sciences
University of Birmingham
September 2019

Abstract

Desmosomes are intercellular junctions that provide tissues with mechanical strength. They are abundant in epithelial tissues and the myocardium. PKCα plays an important role in the assembly of desmosomes and in the regulation of adhesiveness of desmosomes in tissues. Tetraspanins are four-pass transmembrane proteins that are able to interact amongst themselves and with membrane proteins and cytoplasmic signalling proteins to form tetraspanin-enriched microdomains. The tetraspanin CD82 has been shown to strengthen E-cadherin-β-catenin interactions and recruit PKCα to the membrane. The aim of this thesis was to investigate the role of CD82 in desmosomal adhesion.

Overexpression of CD82 in HB2 mammary epithelial cells increases cell-cell adhesion. The CD82 mediated increase in cell-cell adhesion is brought about by an increase in both desmosomal and adherens junction mediated adhesion. Interaction studies revealed that CD82 interacts with PKCα, and PKCα interacts with the C-terminal domain of desmoplakin and phosphorylates it. CD82 does not interact directly with desmoplakin but it could potentially localise PKCα at the membrane, enabling it to phosphorylate desmoplakin, so promoting desmosome assembly and cell adhesion. Direct stochastic optical reconstruction microscopy revealed that CD82 does not affect the clustering of desmosomal proteins but instead alters the organisation of the desmosomal plaque, reducing the distance between desmoplakin C-terminal domains. Overall these findings show that CD82 mediates an increase in desmosomal adhesion by a mechanism that could involve

PKCα-mediated desmoplakin phosphorylation and reorganisation of desmoplakin within the desmosomal plaque.

“Time is how you spend your love”

— Nick Laird

Acknowledgements

I would first like to thank my supervisors Dr Elena Odintsova and Dr Martyn Chidgey, for their mentoring, knowledge, encouragement, and support over the years. Thank you for guiding me with patience and care, and for always making time for me. I would also like to thank Dr Fedor Berditchevski for providing reagents and advice throughout the PhD.

Thank you to past and present members of the Odintsova and Berditchevski laboratories. I would especially like to thank Dr Vera Novitskaya for being a voice of reason and for providing me with a wealth of knowledge and an unlimited supply of chocolate, Dr Regina Andrijes for all the adventures, and Jing Zhang for tolerating my terrible singing and dancing. I am forever grateful for your support and kindness.

Many thanks to Dr Natalie Poulter and Dr Dee Kavanagh for training and support in using the dSTORM microscope and for sharing my excitement of imaging desmosomes. Thank you to Dr Jeremy Pike for his support with dSTORM data analysis and for his patience with all my questions. I would also like to thank Paul Stroe and Dr Ella Claridge for their help with the cell-cell boundary detection software.

Thank you to the BBSRC Midlands Integrative Biosciences Training Partnership (MIBTP) programme for funding this work. A big thanks to the programme organisers for the support throughout the PhD. I would also like to extend my thanks to everyone who has supported me during my various placements, and my fellow MIBTP buddies. Shout out to Caroline Shak for always being there for me, and Terry Tillota for brightening up my commutes.

To my best friend, Zamiya Shire, thank you for being my biggest cheerleader – I am exceptionally lucky to have you in my life.
Thank you to my wonderful siblings for always making me laugh and for making me endless cups of green tea during the writing of this thesis.
And to my amazing parents: thank you for always believing in me and for encouraging me to keep going. This one is for you, with all my love.

Presentations and awards

Conferences attended

BSCB/BSDB Joint Annual Spring Meeting, Warwick, UK, 2019

Quantitative Bioimaging Society Conference, QBI, Rennes, France, 2019

9th International Tetraspanin Conference, Tuscon, Arizona, US, 2018

Midlands Academy of Medical Sciences Research Festival, Loughborough, UK,

2018

8th International Tetraspanin Conference, Sheffield, UK, 2016

Posters and talks given externally

CD82 promotes desmosomal adhesion and reorganises the desmosomal plaque. Poster, Warwick, 2019

Investigation of the cross-talk between desmosomes and tetraspanins. Talk, Rennes, 2019

Investigation of the cross-talk between desmosomes and tetraspanins. Poster, Tuscon, 2018

Investigation of the cross-talk between desmosomes and tetraspanins. Poster, Loughborough, 2018

Awards and prizes

Biochemical Society General Travel Grant, 2018

3rd place poster presentation, Midlands Academy of Medical Sciences Research Festival, 2018

MIBTP BBSRC PhD studentship, 2015

Table of Contents

List of Figures

List of Tables

Abbreviations

CAR	Cell adhesion recognition site
DBSCAN	Density-based spatial clustering of applications with noise
DP	Desmoplakin
DSC	Desmocollin
DSG	Desmoglein
dSTORM	Direct stochastic optical reconstruction microscopy
DTD	Desmoglein terminal domain
E-cad	E-cadherin
EA	Extracellular anchor
EC	Extracellular domain
EC1	Small extracellular loop
EC2	Large extracellular loop
EGF	Epidermal growth factor
EGFR	Epidermal growth factor receptor
GSR	Glycine-serine-arginine
HaCaT	Human keratinocyte cells
HB2	Mammary epithelial cells
IA	Intracellular anchor
ICS	Intracellular cadherin-like sequence
IDP	Inner dense plaque
IF	Intermediate filaments
IPL	Intracellular proline rich linker
MDCK	Madin Darby canine kidney type II cells

MinPts	Minimum number of points
ODP	Outer dense plaque
PG	Plakoglobin
PKA	Protein kinase A
PKC	Protein kinase C
PKCα	Protein kinase C alpha
PKP	Plakophilin
PM	Plasma membrane
PRD	Plakin repeat domain
RUD	Repeat unit domain
SDS-PAGE	Sodium dodecyl sulphate-polyacrylamide gel electrophoresis
siRNA	Small interfering ribonucleic acid
STED	Stimulation emission depleted microscopy
TERMs	Tetraspanin-enriched microdomains
TM	Transmembrane domain
TPA	12-O-Tetradecanoylphorbol 13-acetate
β-cat	β-catenin

Chapter 1 - Introduction

1.1 Cell-cell junctions

Adhesion of cells to one another is important for the maintenance of tissue integrity and communication between cells in tissues. Adhesion between cells is facilitated by cell-cell junctions. Cell-cell junctions are particularly abundant in epithelial tissues and the myocardium (Green and Gaudry, 2000). Cell-cell junctions allow communication between cells and provide strength to tissues that are subject to mechanical stress. There are three main categories of cell-cell junctions: occluding junctions, anchoring junctions and communicating junctions (Figure 1) (Green and Gaudry, 2000). Tight junctions are occluding junctions that seal adjacent cells and regulate the diffusion of solutes and, restrict the diffusion of apical and basolateral membrane proteins (section 1.1.1). There are two types of anchoring junctions that join adjacent cells: adherens junctions and desmosomes (discussed further in section 1.1.2 and 1.3). Both types of junctions provide mechanical strength to tissues as they link to the cell cytoskeleton (discussed further in section 1.2). Gap junctions are communicating junctions that directly couple cells and allow the exchange of ions and molecules (Meşe et al., 2007) (section 1.1.3). In polarised epithelial cells, tight junctions, adherens junctions and desmosomes together form the junctional complex (Green and Gaudry, 2000). Gap junctions are situated on the basal side of this complex.

The cell-cell junctions that make up the junctional complex show that they have broader functions beyond simply providing adhesion, including responding to

signals to control processes such as cell proliferation, mechanotransduction and differentiation (Niessen, 2007; Johnson et al., 2014; Rübsam et al., 2018). For example, the tight junction protein zonula occludens-1 (ZO-1) is involved in regulating cell proliferation, by sequestering the transcription factor ZONAB (ZO-1-associated nucleic acid binding protein)/DbpA, whose targets include cell cycle related genes, in the cytoplasm (Matter and Balda, 2007). The adherens junction protein E-cadherin plays a role in contact inhibition of proliferation, where it inhibits epidermal growth factor receptor (EGFR) signalling (Perrais et al., 2007). Adherens junctions can also sense and respond to mechanical forces during for example tissue remodelling (Yap et al., 2018). Desmosomes play a role in the differentiation of keratinocytes. The desmosomal protein desmoglein 1 (DSG1) promotes differentiation by suppressing EGFR/extracellular signal regulated kinase (ERK1/2) signalling (Getsios et al., 2009). Overall the functions mentioned above suggest that cell-cell junctions play a key role in tissue homeostasis in addition to providing adhesion.

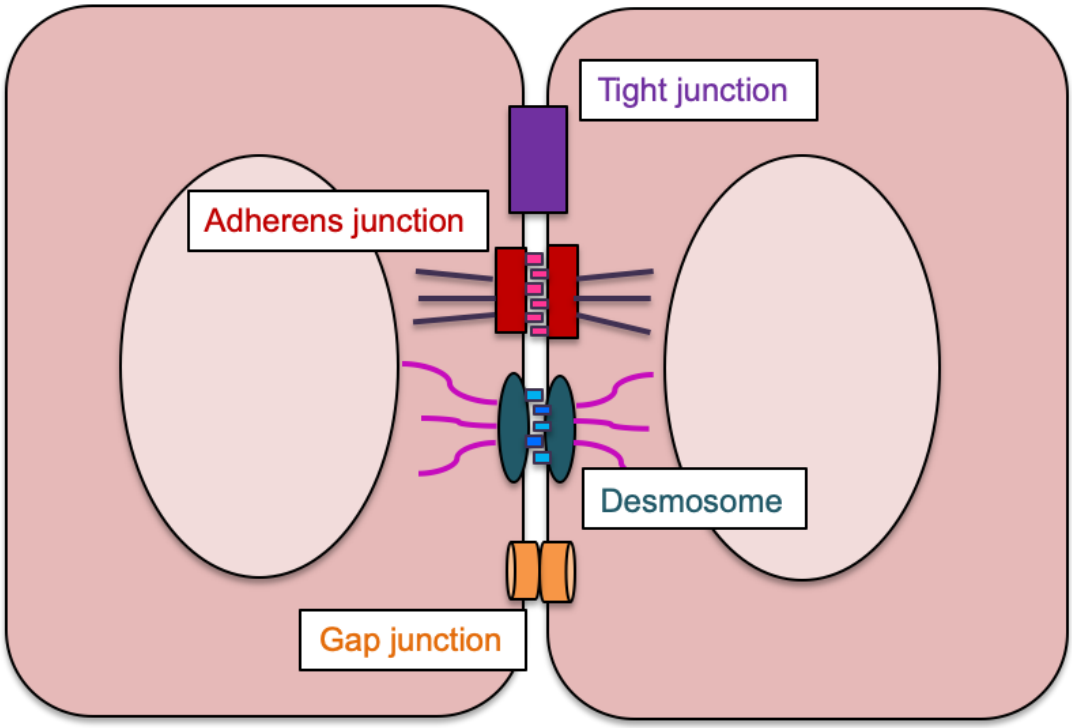

Figure 1 Cell junctions between adjacent epithelial cells

There are four types of cell-cell junctions found in epithelial cells. In an apical to basal direction, these are tight junctions which seal adjacent membranes, adherens junctions and desmosomes which provide mechanical strength to tissues by linking to the cell cytoskeleton, and gap junctions which facilitate communication between cells. Adherens junctions link to actin microfilaments (dark blue) and desmosomes to intermediate filaments (magenta). Adapted from Green and Gaudry (2000).

1.1.1 Tight junctions

Tight junctions are the most apical structure of the junctional complex. Tight junctions mark the border between apical and basolateral membrane domains, preventing proteins in the basolateral domain diffusing into the apical domain and vice versa. They also act as a selective barrier preventing macromolecules and large solutes from diffusing between the cells of epithelial sheets (Niessen, 2007). Tight junctions contain occludins, claudins, and junctional adhesion molecules which are transmembrane proteins that are involved in mediating cell-cell adhesion. These proteins associate with zonula occludens proteins which can provide a link with actin microfilaments (Niessen, 2007).

1.1.2 Adherens junctions

Adherens junctions are situated below tight junctions in the junctional complex. Adherens junctions link transmembrane proteins with the actin cytoskeleton through interactions with linker proteins. In addition to facilitating cell-cell adhesion, adherens junctions play an important role in embryonic development through their link to the actin cytoskeleton (Gumbiner, 2005). Attachment to the actin cytoskeleton helps generate the forces that are required for the development of new tissues. Adherens junctions are composed of two different adhesive complexes: the cadherin-catenin complex and nectin-afadin complex (Gumbiner, 2005; Niessen and Gottardi, 2008). The cadherin-catenin complex contains cadherins, which are single-pass transmembrane proteins that join adjacent cells in a calcium dependent manner. One of the most studied cadherins is E-cadherin. In the presence of calcium, E-cadherin dimerises, the rigidification of the

extracellular domains allows homophilic interaction between E-cadherin molecules on adjacent membranes (Shapiro et al., 1995; Nagar et al., 1996). The cytoplasmic domains of cadherins interact with the armadillo family members, p120 catenin and β-catenin. β-catenin then binds to α-catenin which couples the cadherin-catenin complex to actin microfilaments. α-catenin can also interact with actin microfilaments indirectly through its association with actin associated proteins such as α-actinin, vinculin and formin-1 (Baum and Georgiou, 2011). The nectin-afadin complex is composed of nectin, which is a member of the immunoglobulin superfamily, and the actin binding protein afadin, which connects nectin to the actin cytoskeleton (Gumbiner, 2005; Niessen and Gottardi, 2008). The nectin-afadin complex can associate with the cadherin-catenin complex, to facilitate cell-cell adhesion (Niessen, 2007).

1.1.3 Gap junctions

Gap junctions are found on the basal side of the junctional complex. Gap junctions are assembled from proteins from the connexin family (Meşe et al., 2007). Six connexins oligomerise to form channels called connexons, that facilitate cell-cell communication and the direct exchange of small permeable molecules and ions between adjacent cells (Meşe et al., 2007).

1.2 The cell cytoskeleton

The ability of cells to maintain their structure and coordinate movement in response to intracellular and extracellular signals depends on their cytoskeleton (Fletcher and Mullins, 2010). The three major components of the cytoskeleton are: microtubules, actin microfilaments and intermediate filaments. Microtubules are stiff polymers that are formed by the polymerisation of αβ-tubulin heterodimers (Brouhard and Rice, 2018). Microtubules form the mitotic spindle and direct intracellular trafficking. Actin microfilaments are built from actin monomers that are polymerised into helical filaments (Dogterom and Koenderink, 2019). Actin microfilaments generate the forces that are required for cell migration and changes in cell shape. Intermediate filaments are diverse and built from various types of monomers. They provide resistance to shear stress and are more flexible than microtubules and actin microfilaments (Cheng and Eriksson, 2014). Desmosomes anchor intermediate filaments and are able to provide tensile strength to tissues in this way.

1.2.1 Intermediate filaments

Intermediate filament (IF) proteins are encoded by a large family of related genes (Cheng and Eriksson, 2014). The structure of IF proteins is tripartite in nature and consists of α-helical rod central domain, flanked by a N-terminal head domain and a C-terminal tail domain (Cheng and Eriksson, 2014). IF monomers self-assemble into rope-like structures to give rise to nuclear lamins or cytoplasmic IF networks. The IFs that interact with desmosomes include the keratins, vimentin and desmin (Meng et al., 1997). IFs interact with the desmosomal cytolinker desmoplakin

(discussed further in section 1.3.1.3) through their central rod domain (Fontao et al., 2003; Favre et al., 2018).

1.3 Desmosomes

Desmosomes are cell-cell junctions that provide mechanical strength to tissues by linking to the IF cytoskeleton (Garrod and Chidgey, 2008). They are abundant in epithelial tissues and myocardium which are subject to mechanical stress. Desmosomes were first observed by the pathologist Giulio Bizzozero in 1864 in the spinous layer of the epidermis with a light microscope, where they appeared as dense nodules (Delva et al., 2009; Garrod and Tabernero, 2014). Since then the structure of desmosomes has been studied with electron microscopy and super-resolution microscopy (Odland, 1958; North et al., 1999; Stahley et al., 2016a) (discussed further in section 1.3.2). Desmosomes are approximately 0.2-0.5 μm in diameter, and are characterised by the presence of an electron dense midline between adjacent membranes in the intercellular space (Garrod and Chidgey, 2008; Kowalczyk and Green, 2013). Ultrastructural studies have revealed that the desmosome is resolved into three separate regions: the extracellular core region or desmoglea, outer dense plaque (ODP) and inner dense plaque (IDP) (Figure 2). IDP links the desmosome with the IF cytoskeleton (North et al., 1999). The importance of the link with IFs is highlighted by the severe skin and cardiac defects that arise when this link is compromised (Norgett et al., 2000; Vasioukhin et al., 2001; Jonkman et al., 2005; Yang et al., 2006).

Using immunogold labelling and electron microscopy North et al. (1999) constructed a map of a desmosome by determining the mean distances of each protein domain from the plasma membrane. The width of the desmosomal plaque is approximately 50 nm, with the ODP located 15-20 nm from the plasma membrane. The distance of desmoplakin (DP) C-terminus is about 51 nm from the plasma membrane and is thought to determine the size of the desmosome. This is further supported by the desmosome map constructed by Stahley et al. (2016a) using the super-resolution microscopy technique, direct stochastic optical reconstruction microscopy (dSTORM) (discussed further in section 1.3.2).

1.3.1 Molecular components of the desmosome

Desmosomes contain proteins from the cadherin, armadillo, and plakin family. In the desmosome, the desmosomal cadherins desmoglein (DSG 1-4) and desmocollin (DSC 1-3) couple adjacent cells, and their cytoplasmic tails interact with the armadillo proteins, plakoglobin (PG) and plakophilin (PKP 1-3). PG and PKP in turn bind to the N-terminus of the plakin family member desmoplakin (DP) which links the desmosome with the IF cytoskeleton (Figure 2). The individual components of desmosomes vary depending on the cell type (Dubash and Green, 2011).

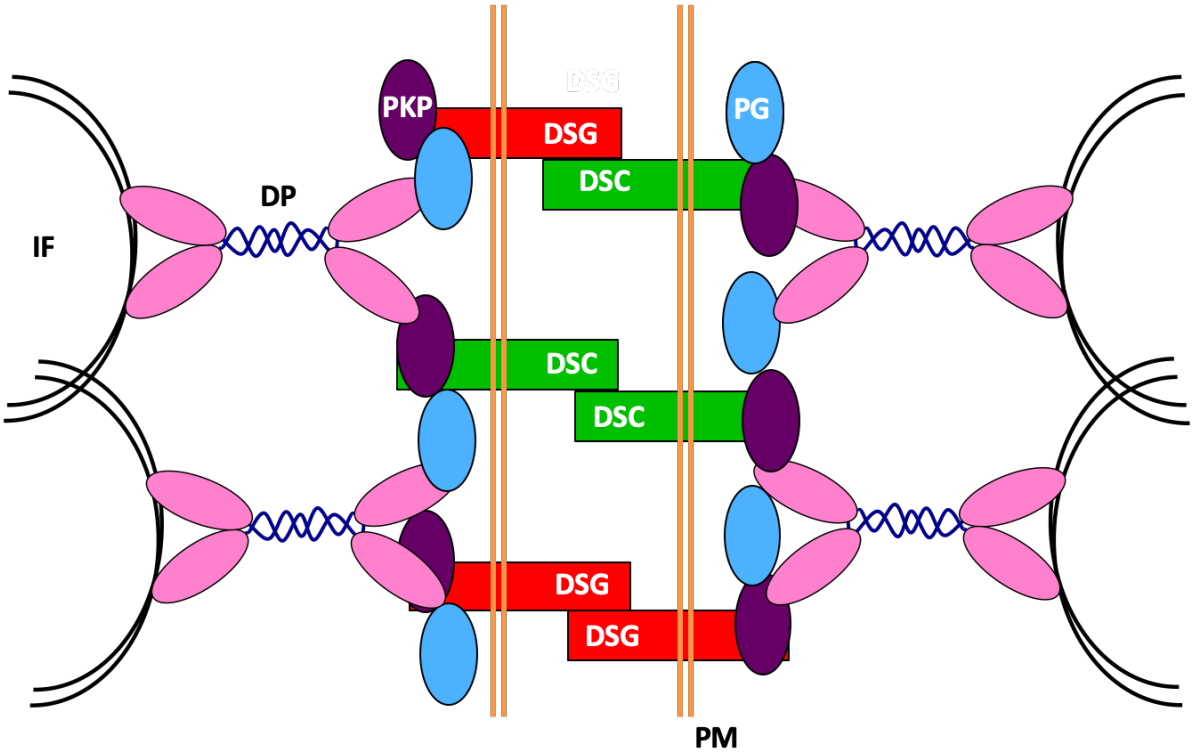

Figure 2 Molecular components of the desmosome

Schematic representation of the arrangement of the molecular components within desmosomes. Desmosomes are comprised of proteins from the desmosomal cadherin, armadillo and plakin families. The desmosomal cadherins, desmogleins (DSG) and desmocollins (DSC) are the adhesive component of the desmosome and interact in the intercellular space. Their cytoplasmic tails bind to the armadillo proteins, plakoglobin (PG) and plakophilin (PKP) which in turn bind to desmoplakin (DP). DP links the desmosome to the intermediate filament (IF) cytoskeleton. PM, plasma membrane. Adapted from Desai et al. (2009).

1.3.1.1 Desmosomal cadherins

The desmosomal cadherins are single pass transmembrane proteins and adhesive components of desmosomes. They belong to the cadherin superfamily of adhesion molecules (Koch and Franke, 1994). Seven desmosomal cadherins have been identified in humans: desmoglein (DSG) isoforms 1-4 and desmocollin (DSC) isoforms 1-3 (Garrod and Chidgey, 2008). The pair of proteins encoded by each DSC gene are alternatively spliced giving rise to an ‘a’ and ‘b’ form, that differ in the length of their cytoplasmic tail (Figure 3). Desmosomal cadherins share similar domain organisation and have four extracellular cadherin (EC) domains, an extracellular anchor (EA) domain, a single pass transmembrane region, and an intracellular domain (Garrod and Chidgey, 2008). The linkers between the EC domains are capable of binding three calcium ions (Garrod et al., 2005). The first EC domain contains a cell adhesion recognition (CAR) site that allows interaction with another desmosomal cadherin (Tselepis et al., 1998; Garrod et al., 2005). While homophilic interactions between desmosomal cadherins are possible (DSG:DSG or DSC:DSC), there is a preference for heterophilic interactions (DSG:DSC) and it is likely that DSG:DSC interactions mediate intercellular adhesion for the most part in desmosomes (Harrison et al., 2016). In addition, both DSG and DSC are required for desmosomal adhesion (Chidgey et al., 1996; Tselepis et al., 1998). The intracellular domain of the desmosomal cadherins contains an intracellular anchor (IA) domain and intracellular cadherin-like sequence (ICS) domain (Garrod and Chidgey, 2008). The ICS domain is only present in the ‘a’ form of DSC. The ICS region is important for interaction with desmosomal plaque components. The DSG cytoplasmic tail contains an

intracellular proline rich linker (IPL) domain, a repeat unit domain (RUD), and glycine rich DSG terminal domain (DTD) (Garrod and Chidgey, 2008). The DSG cytoplasmic tail is intrinsically disordered and provides a binding platform that enables interactions with itself and other desmosomal proteins (Kami et al., 2009; Chen et al., 2012). This region has been implicated in increasing cell-cell adhesion by inhibiting the internalisation of DSG2 which in turn promotes interactions between the DSG2 tails (Chen et al., 2012). Mutations in genes encoding the desmosomal cadherins DSG1 and DSC3, or autoantibodies against DSG1 and DSG3, lead to skin defects, whereas mutations in DSG2 and DSC2 which are expressed in both the skin and heart result in cardiomyopathies (Thomason et al., 2010).

1.3.1.2 Armadillo proteins

The desmosomal armadillo family member proteins are plakoglobin (PG) and plakophilin (PKP) 1-3. There are two isoforms of PKP1 and 2 that are generated by alternative splicing, a short ‘a’ and longer ‘b’ form (Garrod and Chidgey, 2008). Armadillo proteins have a central arm repeat domain, flanked by a N-terminal head and C-terminal tail domain. PG contains 12 central arm repeats (Figure 3). PKPs have a similar structure to PG but instead have 9 central arm repeats and a flexible insert between arm repeat 5 and 6, that makes this domain sickle shaped. The arm repeat domains contain binding sites that are involved in interactions with the desmosomal cadherins and desmoplakin (DP) (Chitaev et al., 1996; Kowalczyk et al., 1997). PG interacts with the cytoplasmic domain of the desmosomal cadherins and the N-terminus of DP. PG also interacts with E-

cadherin in adherens junctions but binds more efficiently to desmosomal cadherins and is therefore predominantly found in desmosomes (Knudsen and Wheelock, 1992; Chitaev et al., 1996).

PG is also present in the nucleus and plays a role in the Wnt/ β-catenin signalling pathway (Green and Simpson, 2007). Similar to PG, PKPs are also found in the nucleus. The 'b' variant of PKP1 is only present in the nucleus. PKP1 and PKP3 associate with RNA binding proteins and may be involved in translation and RNA metabolism (Hofmann et al., 2006). PG and PKP2 knockout mice die at around days 12-16 of embryonic development, due to heart rupture as a result of weakened adhesion between cardiomyocytes (Ruiz et al., 1996; Bierkamp et al., 1996; Grossmann et al., 2004). This highlights the essential role of PG and PKP in desmosomes, and of desmosomes in heart development.

1.3.1.3 Plakins

The plakins are a family of cytolinker proteins that facilitate interactions with the cell cytoskeleton. Four plakin members are able to associate with desmosomes: desmoplakin (DP), periplakin, envoplakin and plectin (Desai et al., 2009). However, of these only DP is a constitutive desmosomal protein that is indispensable for normal desmosomal adhesion. Alternative splicing gives rise to two isoforms of DP, DP I and DP II, that differ in the length of their rod domains (Green et al., 1990) (Figure 3). There is also a minor isoform of DP I, called DP1a (Cabral et al., 2010). DP contains three distinct regions: a N-terminal head domain containing spectrin repeats and a Src homology domain, a central coiled-coil rod

domain that allows dimerisation, and a C-terminal tail containing three plakin repeat domains, a linker domain, and a glycine-serine-arginine (GSR) rich region (Green et al., 1990; Al-Jassar et al., 2013). The N-terminal head domain interacts with the desmosomal armadillo family proteins while the C-terminal tail interacts with the IF cytoskeleton (Stappenbeck et al., 1993; Kowalczyk et al., 1997). Phosphorylation of the C-terminal tail modulates the strength of interaction of DP with the IF cytoskeleton (Stappenbeck et al., 1994). DP knockout mice die early during embryonic development as result of the tissues not being able to withstand mechanical stress during egg cylinder formation (Gallicano et al., 1998). Conditional DP knockout mice keratinocytes show a lack of attachment to IFs which compromises epithelial sheet formation (Vasioukhin et al., 2001).

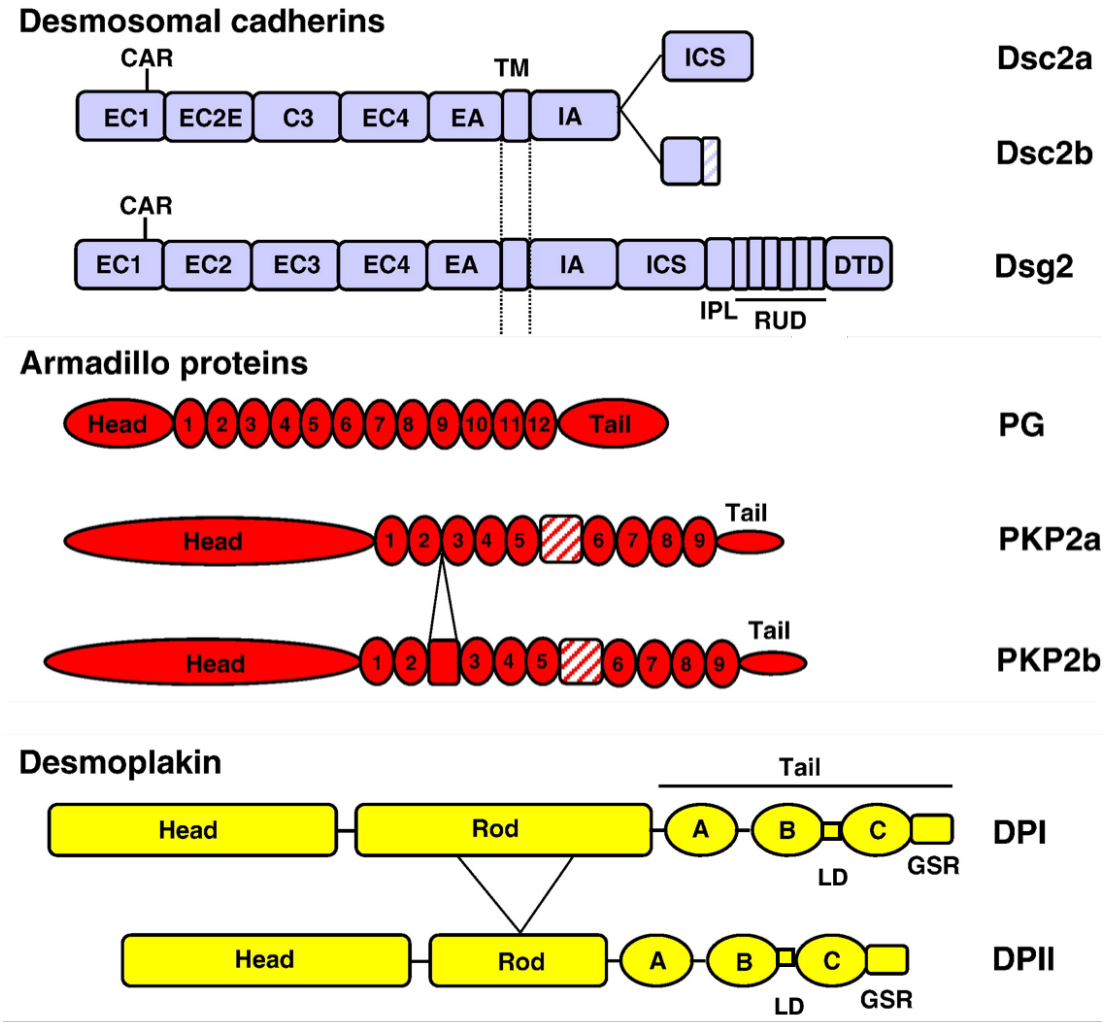

Figure 3 Domain organisation of desmosomal proteins

Schematic representation of the structure of desmosomal proteins. EC, extracellular core domain; CAR, cell adhesion recognition site; EA, extracellular anchor domain; TM, transmembrane domain; IA, intracellular anchor domain; ICS, cadherin-like sequence domain; IPL, intracellular proline rich linker; RUD, repeat unit domain; DTD, DSG terminal domain; GSR, glycine-serine-arginine rich domain. The ICS domain is truncated in DSC2b and the hatched box in PKP2a/b indicates the flexible insert between arm repeat 5 and 6. A, B and C represent plakin repeat domains in the DP C-terminal tail. LD represents the linker domain between PRDs B and C. Adapted from Garrod and Chidgey (2008).

1.3.2 Direct stochastic optical reconstruction microscopy (dSTORM) and desmosomes

The resolution of fluorescence microscopy is limited by the diffraction of light. To overcome the diffraction limit, super-resolution microscopy techniques have been developed. One of these techniques is direct stochastic optical reconstruction microscopy (dSTORM) which can achieve a resolution of 20 nm (Rust et al., 2006). dSTORM relies on the 'blinking' of molecules to determine their localisation. Individual molecules are switched on and off using lasers. This is achieved by labelling samples with photoswitchable fluorophores (Dempsey et al., 2011). The samples are imaged in STORM switching buffer to induce 'blinking' of molecules. STORM imaging buffers often rely on an oxygen scavenging system, to minimise irreversible photobleaching. Buffers that rely on this system contain glucose, glucose oxidase and catalase in combination with reducing agents, such as the thiol cysteamine or tris(2-carboxyethyl)phosphine (TCEP) (Dempsey et al., 2011; Vaughan et al., 2013). During dSTORM acquisition, a subset of fluorophores are switched on and imaged sequentially to determine their positions. Repeated cycles allow the positions of stochastically different subsets of fluorophores to be determined. The fluorescence image from each switch gives a point spread function (PSF). The PSF is then fitted to a Gaussian to find the precise location of the molecule (Rust et al., 2006). A sub-diffraction image can then be reconstructed from the positions of the molecules. For 3D-STORM, a cylindrical lens is inserted in the imaging path to introduce astigmatism (Huang et al., 2008). This results in a stretch in the x or y direction of the fluorophore. The shape of the fluorophore is then used to determine the z coordinate. The data obtained can then be used to

determine the dimensions of structures or used to analyse the clustering behaviour of the proteins being studied. However, clustering analysis requires prior knowledge to reflect the true clustering behaviour of proteins, and this presents a challenge if this data is not available for the structures being studied.

In my study, 3D-STORM was used to investigate whether CD82 affects the clustering of desmosomal proteins and the organisation of a desmosome (see chapter 5). A desmosome is defined by a pair of plaques contributed by adjacent cells. Clustering of desmosomal proteins refers to how tightly packed desmosomal proteins (also referred to as molecules in chapter 5) are in a single desmosome. The organisation of a desmosome was investigated by measuring the distance between protein domains of adjacent plaques of interacting cells. This approach was used by Stahley et al., (2016a) who measured these distances to construct a map of a desmosome and determine desmosome length. Their results showed that overexpression of PKP1 which promotes adhesion results in decreased plaque to plaque distance for DSG3 C-terminal domain, DP rod and C-terminal domains, suggesting that the altered organisation of desmosomes could contribute to increased adhesion. Similarly, using a different super-resolution technique called structured illumination microscopy, Stahley et al. (2016b) have shown in pemphigus vulgaris patient skin samples that desmosomes split and have also demonstrated this in cultured keratinocytes treated with pemphigus vulgaris autoantibodies by subjecting them to mechanical stress. The examples above show that super-resolution microscopy techniques can be used to study the ultrastructure of desmosomes.

1.3.3 Desmosome assembly

Desmosomal proteins are synthesised as soluble proteins that become insoluble at the membrane where they are incorporated into desmosomes (Penn et al., 1987). E-cadherin clustering occurs prior to the initial steps of desmosome assembly in response to cell-cell contact or when the extracellular calcium concentration is raised to approximately 1 mM or greater when culturing cells (Lewis et al., 1994; Green et al., 2010). At >1 mM calcium rigidification of the E-cadherin extracellular domains takes place, and enabling interactions between E-cadherin molecules on adjacent cells (Shapiro et al., 1995; Nagar et al., 1996). It was recently shown that E-cadherin interacts with DSG2 to initiate desmosome assembly (Shafraz et al., 2018). The association between E-cadherin and DSG2 is transient and facilitates the recruitment of desmosomal proteins to the membrane. However, there is also evidence to suggest that DSC2 and DSG2 are sequentially trafficked to the membrane in a microtubule dependent manner to initiate the formation of desmosomes (Nekrasova et al., 2011). DSC2 and DSG2 require different motor proteins, kinesin-2 and kinesin-1 respectively. PKP2 also plays a role in transporting DSC2 to the membrane. This raises the question of whether DSC2 can also interact with E-cadherin to initiate desmosome assembly. Membrane raft microdomains could also play a role in desmosome assembly as desmosomal cadherins can associate with them (Stahley et al., 2014).

Desmosomal assembly also involves the accumulation of DP at cell-cell borders (Godsel et al., 2005). DP containing particles which may or not may not be membrane bound form near the cell cortex which then translocate to nascent

desmosomes (Godsel et al., 2005). PKP2 colocalises with DP containing particles and recruits protein kinase C (PKC) α to DP (Bass-Zubek et al., 2008). PKCα is a member of the protein kinase C family of serine/threonine kinases (section 1.4) and phosphorylation of DP by PKCα modulates its association with IFs and promotes the assembly of desmosomes. Depletion of PKP2 impairs the formation of desmosomes, suggesting that it may be involved in scaffolding and/or trafficking of DP and perhaps desmosomal cadherins to the membrane. The importance of armadillo proteins in the assembly process is further highlighted by the role of the N- and C-terminal domains of PG in regulating the size of desmosomes (Palka and Green, 1997). Overall it is clear that the assembly of desmosomes involves a number of distinct steps, what remains to be fully determined is the order in which these steps occur.

1.3.4 Desmosome downregulation

To facilitate cell migration during development and wound healing desmosomes can downregulate their adhesion (Garrod et al., 2005). In sub-confluent or in newly confluent cultures, chelation of extracellular calcium ions results in the loss of intercellular adhesion which gives rise to half desmosomes. The internalisation of half desmosomes has been demonstrated in Madin Darby canine kidney type II (MDCK) cells, and requires PKC activity and actin microfilaments (McHarg et al., 2014). The half desmosomes are then transported to the centrosome in a microtuble/kinesin dependent manner for degradation. Desmosomal components are degraded by proteasomes and lysosomes (McHarg et al., 2014). DP is

degraded by proteasomes and other desmosomal components (DSG2, DSG3, and PG) by lysosomes.

1.3.5 Hyperadhesion

Desmosomes in tissues and in confluent monolayers grown for an extended time period (i.e. 4 days or more) are strongly adhesive. This state is referred to as ‘hyperadhesion’ (Garrod et al., 2005; Kimura et al., 2007). Hyperadhesive desmosomes are calcium independent, as chelation of extracellular calcium ions does not result in a decrease in adhesion in cultured cells with hyperadhesive desmosomes. This may be as a result of the ordered arrangement of the desmosomal cadherin extracellular (EC) domains, which may trap bound calcium ions in their EC domains (Garrod et al., 2005). Desmosomes found at a wound edge are calcium dependent, lack a midline and are accompanied by a narrower intercellular space (Garrod et al., 2005). The ability to transition between a hyperadhesive, calcium independent state, and a less adhesive calcium dependent state, is unique to desmosomes. PKCα is thought to play a role both in the acquisition of hyperadhesion during desmosome assembly, and the transition from a hyperadhesive to less adhesive desmosomes in wound healing. Thus phosphorylation of residue Ser 2849 in the C-terminal GSR rich region of DP reduces DPs interaction with IFs, promoting assembly (Godsel et al., 2005) and increased adhesiveness. By contrast PKCα becomes associated with desmosomes with wound edge desmosomes and triggers the transition to calcium dependence by phosphorylating desmosomal components, resulting in decreased adhesiveness, perhaps as a result of a loss of organisation of the EC domains

(Wallis et al., 2000; Garrod et al., 2005; Thomason et al., 2012). During the transition from calcium dependence to hyperadhesion, there is no change in the composition of desmosomes, suggesting that modification of pre-existing proteins plays a key role in this transition (Kimura et al., 2007).

Phosphorylation of desmosomal components by PKCα contributes to the assembly (section 1.3.2), and downregulation of desmosomes during wound healing (section 1.3.3), by regulating the strength of interaction of DP with IFs and interactions between desmosomal proteins. All desmosomal proteins can be phosphorylated on serine or tyrosine residues (Parrish et al., 1990; Stappenbeck et al., 1994; Garrod, 2010). Phosphorylation of DP serine residue 2849 by PKCα results in weaker association with IFs, promoting assembly (Stappenbeck et al., 1994; Hobbs and Green, 2012). Epidermal growth factor receptor (EGFR) dependent phosphorylation of desmosomal components can affect interactions between desmosomal proteins. PG and DSG2 can become phosphorylated in response to epidermal growth factor (EGF) treatment (Gaudry et al., 2001). Tyrosine phosphorylated PG does not interact with DP but remains associated with tyrosine phosphorylated DSG2. Prolonged treatment of keratinocytes with EGF results in a decrease in adhesion and a loss of DP (Yin et al., 2005a). Expression of a phospho-deficient mutant in PG null keratinocytes treated with EGF for an extended period of time results in an increase in adhesion and association of PG with DP, suggesting that EGFR dependent phosphorylation of PG is associated with the downregulation of adhesion. This is further supported by evidence suggesting that inhibition of EGFR increases the assembly of

desmosomes which in turn increases cell-cell adhesion (Lorch et al., 2004). However, treatment of MDCK cells with the tyrosine phosphatase inhibitor pervanadate, results in tyrosine phosphorylation of PG and DSG2, which remain capable of interacting, and leads to an increase in the amount of DSG2 found in the soluble fraction that contains desmosomal proteins that are incorporated in desmosomes (Garrod et al., 2008). This implies that tyrosine phosphorylation induced by pervandate treatment increases the strength of interactions of desmosomal proteins in desmosomes. In addition, PG inhibits keratinocyte motility by increasing adhesion and suppressing Src signalling through a mechanism that involves the C-terminal domain of PG (Yin et al., 2005b). These results are line with evidence suggesting that tyrosine phosphorylation of different PG residues can have different effects on its association with desmosomal and adherens junction proteins. Phosphorylation of tyrosine residue 643 of PG by Src increases the association of PG with DP and reduces its association with E-cadherin (Miravet et al., 2003), whereas phosphorylation of tyrosine residue 549 of PG by Fyn or Fer results in a decreased association with DP and, phosphorylation by Fer increases interaction between PG and α-catenin. The studies above suggest that phosphorylation of desmosomal components can have different effects depending on the kinase in question.

While PKP2 plays a key role in recruiting in PKCα to DP (Bass-Zubek et al., 2008) (section 1.3.2), other scaffolding proteins could also be involved in this process. Tetraspanins have been shown to act as scaffolds for PKC isozymes

(Zuidscherwoude et al., 2017; Termini et al., 2016), and the role of tetraspanins will be discussed further in section 1.5.

1.4 PKC

The protein kinase C (PKC) family of serine/threonine kinases play an important role in signalling pathways and are involved in the regulation of processes such as cell cycle control, differentiation, and apoptosis to name a few (Griner and Kazanietz, 2007; Mackay and Twelves, 2007). The PKC isozymes are encoded by nine genes and are grouped into three subclasses: the classical PKCs (cPKCs) (PKCα, PKCβ I, PKCβ II, PKCγ), novel PKCs (PKCδ, PKCε, PKCη and PKCθ), and atypical PKCs (PKCζ and PKCι) (Griner and Kazanietz, 2007). cPKCs contain a pseudosubstrate domain that is autoinhibitory and keeps cPKCs in an inactive state, two C1 domains (A/B) which are involved in binding diacylglycerol, phorbol esters and phoshatidylserine, a C2 domain which binds calcium ions and phosphatidylinositol-4,5-bisphosphate (PIP_2), a serine/threonine kinase domain, and a C-terminal tail that contains conserved phosphorylation sites (Figure 4A) (Griner and Kazanietz, 2007; Newton, 2010).

As described in earlier sections, PKCα plays a key role in the regulation of desmosomal adhesion. PKCα is 672 amino acids in length and is widely expressed (Griner and Kazanietz, 2007). In common with other cPKCs, PKCα is found in its inactive form in the cytoplasm (Newton, 2003). Upon treatment with phorbol esters, such as TPA which mimics diacylglycerol, cPKCs translocate to the membrane (Newton, 2003) (Figure 4B). In physiological conditions, cPKCs are

recruited to the membrane in response to extracellular signals that lead to an increase in diacylglycerol as a result of activation of phospholipase C (PLC) which results in the hydrolysis of phosphatidylinositol-4,5-bisphosphate(PtdIns $(4,5)P_2$) (Newton, 2003; Mochly-Rosen et al., 2012). This reaction also gives rise to inositol-1,4,5-triphosphate ($Ins(1,4,5)P_3$) that stimulates the release of calcium ions from the endoplasmic reticulum leading to an increase in the intracellular calcium concentration. (Newton, 2003; Mochly-Rosen et al., 2012). Calcium ions bind to the C2 domain of cPKCs which allow cPKCs to become tethered to the membrane, this interaction with the membrane is strengthened by binding of diacylglycerol to the C1 domain which results in the release of the pseudosubstrate, allowing cPKCs to adopt an open conformation. In this membrane bound open conformation cPKCs can bind to substrates leading to activation of downstream signalling pathways (Newton, 2003). Receptors for activated C kinase (RACKs), and tetraspanins can interact with and form a scaffold for PKCs (Zhang et al., 2001; Newton, 2010; Zuidscherwoude et al., 2017; Termini et al., 2016), enabling them to mediate downstream signalling pathways such as the MEK-ERK (mitogen activated protein kinase-extracellular signal-regulated kinase) pathway (Mackay and Twelves, 2007).

A

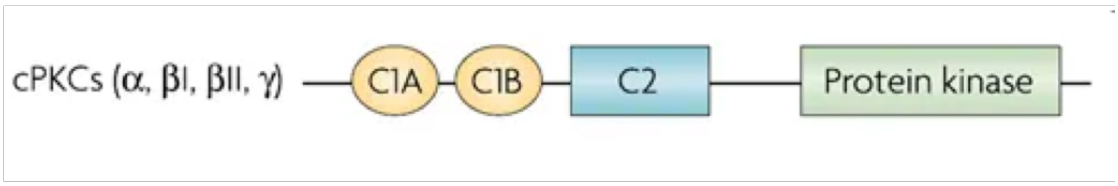

B

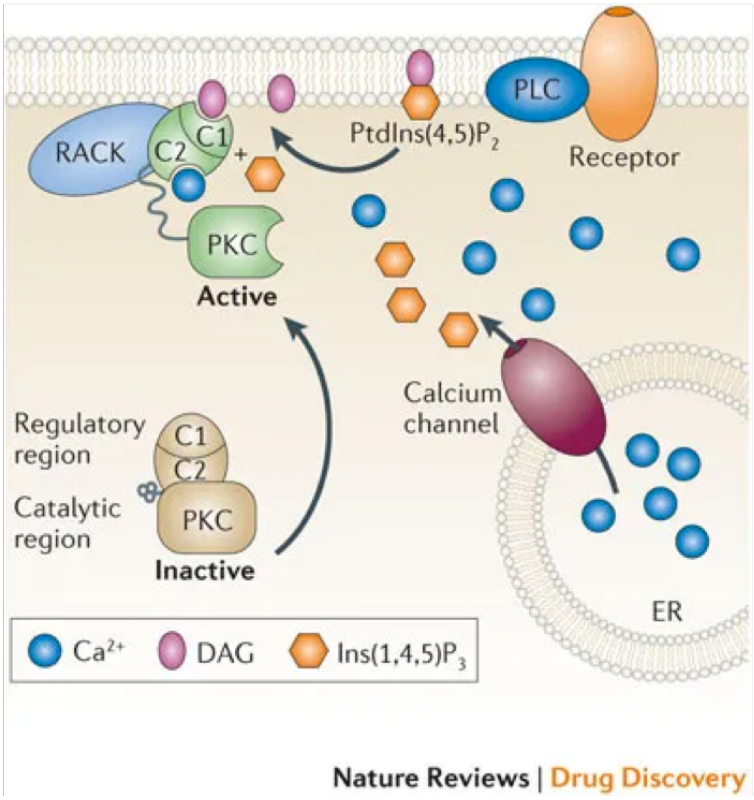

Figure 4 cPKC domain structure and translocation to the membrane

(A) Domain architecture of cPKCs. The C1A domain is preceded by a pseudosubstrate domain (not shown) followed by the C1A/B and C2 regulatory domains and a kinase domain. (B) Depiction of PKC translocation to the membrane. See text. Adapted from (A) Griner and Kazanietz (2007); (B) Mochly-Rosen et al. (2012).

1.5 Tetraspanins

The tetraspanins are a family of four-pass transmembrane proteins that function as membrane organisers. 33 tetraspanins have been identified in humans, and 37 and 20 tetraspanins in *Drosophila Melanogaster* and *Caenorhabditis elegans*, respectively (Charrin et al., 2014). Tetraspanins are small cone-shaped proteins that consist of approximately 200-350 residues and protrude 3-5 nm from the membrane (van Deventer et al., 2017). Some tetraspanins such as CD151 and CD81 are widely expressed in many cell types, whereas the expression of some tetraspanins such as peripherin/ photoreceptor-specific glycoprotein retinal degeneration slow (RDS) is more restricted, with the latter being exclusively expressed in the rod outer segments in the retina (Hemler, 2005). Tetraspanins have been implicated in a number of processes such as cell adhesion, cell migration, cell signalling and cancer progression. The tetraspanins CD9 and CD82 can function as metastasis suppressors whereas other tetraspanins such as CD151 and tetraspanin 8 can promote metastasis (Zöller, 2009).

1.5.1 Structure of tetraspanins

Tetraspanins contain four transmembrane domains, a small (EC1) and large (EC2) extracellular loop, a short intracellular loop between transmembrane domain 2 and 3, and short N- and C-terminal tails (Figure 5) (Hemler, 2005; Yáñez-Mó et al., 2009). The large extracellular loop (EC2) contains a conserved Cys-Cys-Gly motif and two conserved cysteine residues that form disulphide bonds. Four-pass transmembrane proteins must contain these features in order to be considered as part of the tetraspanin family. The EC2 region also contains 5 α helices that are

organised into two subdomains: a constant and a variable region (Kitadokoro et al., 2001; Seigneuret et al., 2001). The variable region is important for tetraspanin protein-protein interactions. Tetraspanins also contain polar residues in transmembrane domains 1, 3 and 4 (Hemler, 2005). The crystal structure of full-length CD81 shows the presence of a cholesterol binding pocket, that could allow the EC2 domain to adopt an open or closed conformation depending on the presence of a cholesterol molecule (Figure 3) (Zimmerman et al., 2016).

Tetraspanins can undergo post-translational modifications. The cytoplasmic cysteine residues of tetraspanins may be palmitoylated which contributes to tetraspanin-tetraspanin interactions (Berditchevski et al., 2002; Charrin et al., 2002; Yang et al., 2002). For example, palmitoylation is important for the interaction of CD151 with CD81, CD63 and CD9, and inhibition of palmitoylation results in weaker association between these tetraspanins (Berditchevski et al., 2002; Yang et al., 2002). Inhibition of palmitoylation of CD151 also decreases its interaction with α3β1 integrin, and the reduced association leads to adhesion dependent activation of the phosphoinositide 3-kinase signalling pathway (Berditchevski et al., 2002).

The EC2 domain of most tetraspanin family members is N-glycosylated (van Deventer et al., 2017), and can regulate their function. Glycosylation of tetraspanin peripherin/RDS is important for the function of cone photoreceptors and its interaction with the related tetraspanin rod outer segment membrane protein 1 (ROM-1). Initially both peripherin/RDS and ROM-1 are found at expected levels in

mice expressing unglycosylated peripherin/RDS (Stuck et al., 2015). However, as these mice age, the levels of peripherin/RDS and ROM-1 decline, which in turn impairs the function of cone photoreceptors (Stuck et al., 2015).

Finally, the cytoplasmic tails of tetraspanins can be ubiquitinated, which regulates their expression level (Lineberry et al., 2008). Ubiquitination of CD82 can have a negative impact on the metastasis suppressing activities of the tetraspanin CD82. CD82 is targeted by the ubiquitin ligase gp78 for degradation (Tsai et al., 2007), and the downregulation of CD82 expression increases the ability of tumour cells to metastasise.

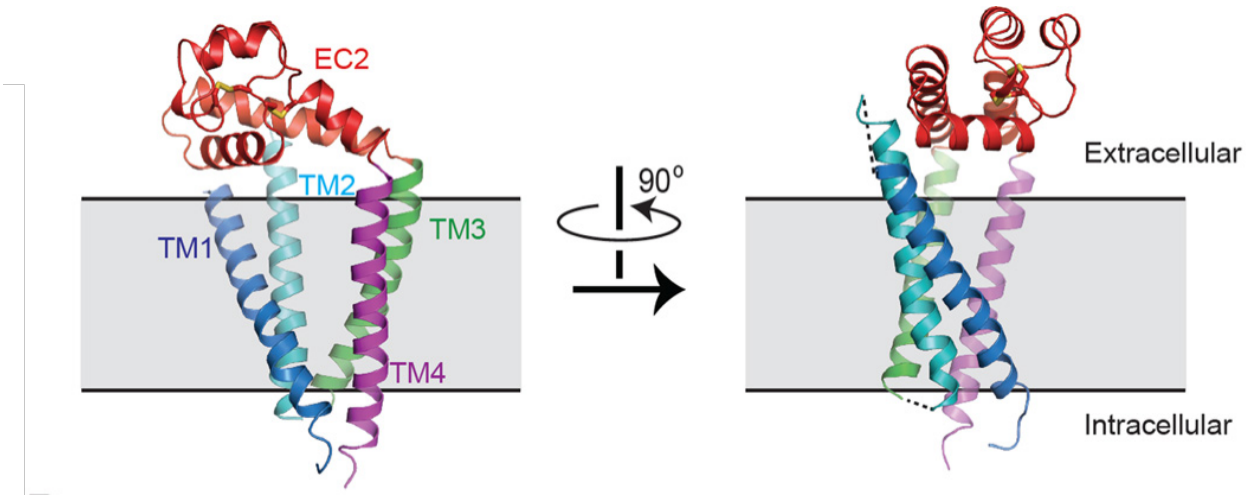

Figure 5 Structure of human CD81

The structure shows a cavity created by the four transmembrane domains (TM) that is covered by the EC2 domain. Molecular dynamics simulations showed that the EC2 domain adopts a closed conformation when a cholesterol molecule is bound, and an open conformation in the absence of cholesterol. TM1, transmembrane domain 1 (blue); TM2, transmembrane domain 2 (cyan); TM3, transmembrane domain 3 (green); TM4, transmembrane domain 4 (magenta); EC2, large extracellular loop (red). Adapted from Zimmerman et al. (2016).

1.5.2 Tetraspanin-enriched microdomains (TERMs)

Tetraspanins can interact amongst themselves and with other membrane proteins and cytoplasmic signalling proteins to form tetraspanin-enriched microdomains (TERMs) (Berditchevski et al., 2002; Termini and Gillette, 2017). They can interact with a wide variety of adhesion receptors, growth factor receptors and enzymes (Figure 6). Within TERMs tetraspanins can regulate the function of associated proteins which can have an effect on a range of cellular processes, such as cell adhesion, migration and trafficking.

The majority of interacting partners of tetraspanins have been identified using biochemical methods, such as immunoprecipitation and chemical cross-linking. Interactions are classified based on the lysis buffer used in the experiment which determines the strength of interaction. Interactions that are maintained in Triton X-100 and NP-40 are considered primary or direct interactions. These include homophilic interactions between tetraspanins and interactions with other membrane proteins such as integrins (Hemler, 2005). Secondary or indirect interactions are maintained in milder buffers such as Brij 96 and Brij 97. These include heterophilic interactions between tetraspanins and other membrane proteins. Palmitoylation of tetraspanins stabilises these interactions (Yang et al., 2002). Finally, tertiary interactions are weak interactions that are preserved in mild buffer conditions such as Brij 98, Brij 99 and CHAPS. In these buffers the specificity of detected interactions decreases as tetraspanin complexes become partially insoluble and the complexes detected contain other tetraspanins and interacting molecules (Hemler, 2005).

The super-resolution microscopy technique, simulation emission depleted (STED) microscopy has been used to study interactions in TERMs in human B cells and dendritic cells (Zuidscherwoude et al., 2015). This revealed that the tetraspanins CD37, CD81 and CD82 tend to form individual clusters, that contain only one type of tetraspanin, that show little overlap with other tetraspanins. These findings challenge the biochemical evidence suggesting that heterophilic tetraspanin interactions are required for the assembly of TERMs (Boucheix and Rubinstein, 2001). Additionally, CD53 and CD81 were in closer proximity to their interacting partners MHC class II and CD19 than to other tetraspanins. Based on this study, the authors proposed to classify tetraspanin interactions based on their functions in TERMs as this may better reflect the organisation of TERMs rather than the biochemical classification of tetraspanin interactions (van Deventer et al., 2017).

Through interactions within TERMs tetraspanins can have far reaching effects on function of their partner/and associated proteins. For example, the interaction between CD151 and α3β1 integrin, which requires the large extracellular loop of CD151 (Berditchevski et al., 2001), has been shown to contribute to neurite outgrowth (Stipp and Hemler, 2000). In a recent study it has been shown that the interaction between CD151 and α3β1 integrin strengthens α3β1 mediated adhesion to laminin (Molder et al., 2019). CD151 can also interact with α6β1, strengthening α6β1 mediated adhesion to laminin (Lammerding et al., 2003). The tetraspanin C8 subgroup of tetraspanins interact with the metalloproteinase ADAM10 and promote the maturation of ADAM10, regulating its trafficking to the membrane and specificity for distinct substrates. This can have far reaching

consequences as ADAM10 is ubiquitously expressed and different cell types express distinct tetraspanin C8s (Haining et al., 2012; Matthews et al., 2017). Tetraspanins can regulate intracellular signalling pathways by interacting with cytoplasmic signalling molecules such as phosphatidylinositol 4-kinase and cPKCs (Berditchevski et al., 1997; Zhang et al., 2001), in particular the interaction of CD82 with PKCα can lead to sustained PKCα signalling, which will be discussed in further in section 1.5.3.2 (Termini et al., 2016).

Tetraspanin interactions also play a role in cell fusion events (Fanaei et al., 2011). The tetraspanin CD9 is essential for sperm-egg fusion, and CD81 can compensate for the loss of CD9 in this process, suggesting cross-talk between these tetraspanins. CD81 has also been implicated in HCV and HIV-1 infections (Fanaei et al., 2011). Finally, tetraspanin 4 containing TERMs are important for the formation of migrasomes, which are organelles that are involved in cell migration and have been shown to be important for development in zebrafish (Huang et al., 2019; Jiang et al., 2019). The examples discussed above highlight the functional relevance of TERMs.

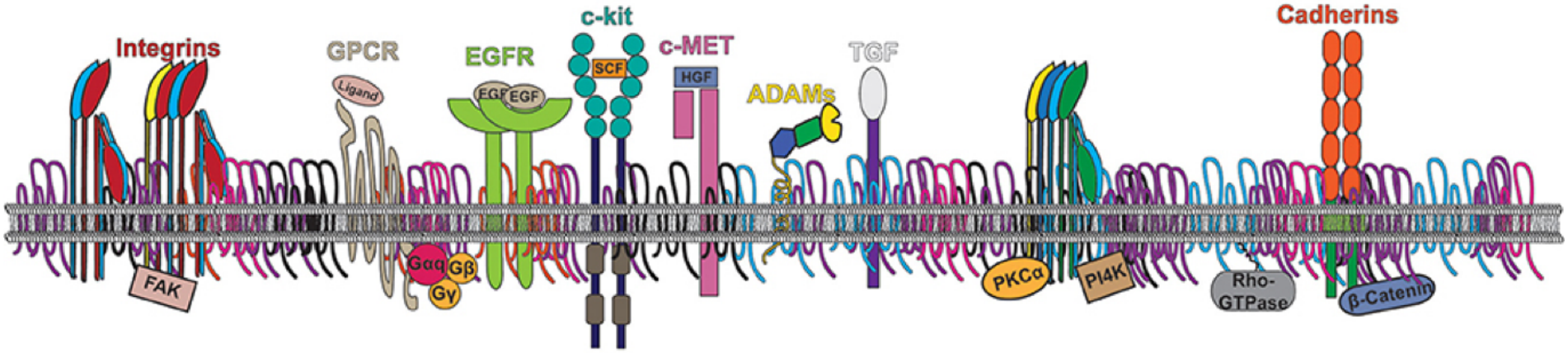

Figure 6 Tetraspanin-enriched microdomains

Schematic representation of tetraspanin-enriched microdomains showing interactions with a range of membrane proteins, including adhesion receptors, growth factor receptors and, cytoplasmic signalling molecules. Adapted from Termini and Gillette (2017).

1.5.3 CD82

The tetraspanin CD82, also known as KAI1 is a metastasis suppressor. CD82 was first identified in a screen for metastasis suppressor genes and shown to suppress metastasis in rat AT6.1 prostate cancer cells (Dong et al., 1995). The downregulation of CD82 is associated with a poor prognosis in number of human cancers (Tonoli and Barrett, 2005). CD82 is 267 residues in length and contains in addition to the typical tetraspanin structural features, 5 membrane proximal cysteine residues that can be palmitoylated, 3 asparagine N-linked glycosylation sites, 4 lysine residues in the cytoplasmic tails that can be ubiquitinated, and a C-terminal tyrosine sorting motif (YSKV) (Termini and Gillette, 2017). As a result of glycosylation CD82 migrates at approximately 25-60 kDa on sodium dodecyl sulphate-polyacrylamide gel electrophoresis (SDS-PAGE) depending on the cell line and appears as a smear (White et al., 1998). So far, no interactions between CD82 and potential interacting proteins that are preserved in Triton X-100 and NP-40 have been identified. Like other tetraspanins, CD82 can regulate the function of associated proteins, affecting cell adhesion, cell migration and trafficking (Abe et al., 2008; Odintsova et al., 2000; Odintsova et al., 2013). More recently CD82 has been identified as a marker for muscle satellite cells and cardiomyocyte fated progenitors and may play a role in muscle stem cell function (Alexander et al., 2016; Takeda et al., 2018).

The majority of studies looking at CD82 focused on its metastasis suppressor properties and are therefore carried out in cell lines that have been derived from metastatic sites, such as DU145 prostate cancer cells and h1299 non-small cell

lung carcinoma cells as described in the next sections. HB2 mammary epithelial cells were used in my study because they are non-cancerous mammary epithelial cells with unchanged phenotype (Caradonna and Luparello, 2014), have been used to study CD82 interactions (Odintsova et al., 2000, Odinitsova et al., 2013), and because they form desmosomes and adherens junctions.

1.5.3.1 CD82 and cell adhesion

Transfection of CD82 into DU145 human prostate cancer cells increases homotypic cell-cell aggregation in a Src dependent manner (Jee et al., 2003). Treating the cells with Src kinase inhibitors or transfection with Src constructs lacking kinase activity reduces cell-cell aggregation. However, it is not clear how CD82 mediates Src signalling to induce cell-cell aggregation. An increase in cell-cell adhesion is also observed in CD82 overexpressing h1299 non-small cell lung carcinoma cells (Abe et al., 2008). The increase in cell-cell adhesion is E-cadherin dependent but there was no change in the amount of E-cadherin at cell-cell borders. However, β-catenin re-localised to the membrane promoting E-cadherin-β-catenin complex formation. Additionally, CD82 overexpression reduced tyrosine phosphorylation of β-catenin, stabilising β-catenin-E-cadherin interactions at the membrane. CD82 may achieve these effects through attenuation of Wnt signalling (Chigita et al., 2012). It does not affect the expression of Wnt proteins but downregulates the expression of Frizzled proteins 2,3,5,7 and 9, and glycogen synthase-3β (GSK-3β) and kinase casein kinase 1 α (CK1α), resulting in reduced β-catenin translocation to the nucleus and its re-localisation to the membrane where it stabilises β-catenin-E-cadherin interactions. In addition, CD82

upregulates E-cadherin expression as a result of reduced binding of the transcription factor Sp1 to the E-cadherin repressor Snail (Lee et al., 2018). Another possibility is that CD82 increases cell-cell adhesion by increasing the clustering of E-cadherin and/or β-catenin molecules which may in turn increase interactions between the two. Inhibition of glycosylation of CD82 increases the size and density of N-cadherin clusters. This results in increased packing of N-cadherin molecules and results in increased adhesion and bone marrow homing of acute myeloid leukaemia cells (Marjon et al., 2016).

Overexpression of CD82 also increases the density of integrin α4 clusters which results in stronger adhesion to the extracellular matrix and could potentially contribute to the adhesion and homing of haematopoietic stem progenitor cells to the bone marrow (Termini et al., 2014). Overall the studies discussed in this section highlight that CD82 can regulate cell-cell and cell-matrix adhesion through mediating signalling pathways or through the clustering of proteins.

1.5.3.2 CD82 and PKCα

CD82 was first shown to interact with PKCα in Jurkat cells when treated with TPA and lysed with 1% Brij 99 (Zhang et al., 2001). In the same study, other tetraspanins were also identified to interact PKCα, these include CD9, CD53 and CD81. In addition, several β1 integrins immunoprecipitated with PKCα leading the authors to suggest that tetraspanins link integrins to PKCα. Recruitment of PKCα by CD82 also plays a role in the suppression of ubiquitylation of EGFR in heparin-binding-epidermal growth factor (HB-EGF) stimulated HB2 mammary epithelial

cells (Odintsova et al., 2013). This results in increased phosphorylation of the EGFR ubiquitylation regulator c-Cbl by PKCα. Using FRET based imaging, Termini et al. (2016) have shown that the organisation of CD82 is important for maintaining the stability of the association between CD82 and PKCα. In addition, in the same study, using the super-resolution microscopy technique direct stochastic optical reconstruction microscopy (dSTORM), the authors showed that CD82 regulates the clustering of PKCα which results in sustained PKCα signalling and activation of ERK1/2, and increased colony formation in acute myeloid leukaemia cells. Hence CD82 may act as a scaffold for PKCα, enabling the phosphorylation of PKCα substrates and activation of signalling pathways.

1.5.3.3 CD82 and cell migration

CD82 can inhibit cell migration through regulating the trafficking of associated proteins. Overexpression of CD82 in HB2 cells suppresses EGF induced cell migration. CD82 interacts with EGFR, and attenuates EGFR signalling by increasing the rate of endocytosis of the activated receptor (Odintsova et al., 2000). In a similar fashion, CD82 downregulates α6 integrin by increasing its rate of internalisation, resulting in reduced adhesion on laminin which in turn results in a decrease in cell migration (He et al., 2005).

CD82 can also inhibit cell migration by regulating c-Met signalling (Takahashi et al., 2007). CD82 associates with the hepatocyte growth factor receptor c-Met, and stimulation of non-small cell lung carcinoma cells overexpressing CD82 with hepatocyte growth factor impairs cell migration (Takahashi et al., 2007). CD82

does not affect the phosphorylation of c-Met but reduces c-Met signalling by inhibiting its association with the adaptor protein, growth factor receptor bound protein 2 (Takahashi et al., 2007).

Finally, CD82 can inhibit cell migration is through its interaction with the immunoglobulin superfamily member, EWI2 (Zhang et al., 2003). Overexpression of EWI2 and CD82 in DU145 cells results in increased EWI2-CD82 complex formation, and further supports the anti-migratory role of CD82, as it results in a greater reduction in migration on laminin and fibronectin compared to DU145 cells overexpressing CD82 alone. However, the mechanism by which this occurs is not clear. Overall it appears that CD82 inhibits cell migration by regulating the trafficking of associated proteins or by interfering with their signalling roles.

1.5.3.4 CD82 and muscle stem cells

CD82 may play a role in muscle stem cell function. CD82 was recently identified as a marker for the isolation of skeletal muscle satellite cells (Alexander et al., 2016). The authors found that the expression of CD82 is not restricted to stem cells and CD82 may have a specific function in skeletal muscle. CD82 interacts with integrin α7β1, which links α-sarcoglycan to the dystrophin-associated glycoprotein complex in human myogenic cells (Alexander et al., 2016). When this complex is compromised it can result in muscular dystrophies. Expression of CD82 is reduced in muscle tissues and myoblasts of patients with Duchenne muscular dystrophy (Alexander et al., 2016). This suggests that CD82 may play a role in the maintenance of this complex.

Human-induced pluripotent stem cell derived cardiomyocyte fated progenitors that express CD82 predominantly differentiate into cardiomyocytes (Takeda et al., 2018). CD82 attenuates Wnt signalling to restrict the fate of these cells to cardiomyocytes, by increasing the secretion of β-catenin containing exosomes and reduces nuclear β-catenin levels (Takeda et al., 2018). Given that CD82 is involved in the differentiation of cardiomyocyte fated progenitors into cardiomyocytes it raises questions of whether CD82 expression is restricted to stem cells and whether CD82 plays a specific role in cardiomyocytes.

1.6 Project aims

Desmosomes are intercellular junctions that provide tissues with mechanical strength (Garrod and Chidgey, 2008). While strong adhesion is important for the maintenance of tissue integrity it is incompatible with processes that require reduced adhesion such as wound healing. The downregulation of adhesion involves phosphorylation of desmosomal components by PKCα (Garrod et al., 2005; Thomason et al., 2012). Phosphorylation of DP by PKCα is also important for the assembly of desmosomes (Bass-Zubek et al., 2008). The tetraspanin CD82 interacts with PKCα, and recruits PKCα to the membrane where it regulates its clustering (Zhang et al., 2001; Termini et al., 2016). This can have an effect on downstream signalling pathways. In addition, CD82 has been shown to strengthen E-cadherin and β-catenin interactions (Abe et al., 2008). However, it is not known whether tetraspanins play a role in desmosomal adhesion. Given that CD82 interacts with PKCα, and regulates PKCα clustering, and contributes to E-cadherin

and β-catenin interactions, I tested the hypothesis that CD82 could play a role in the regulation of desmosomal adhesion. The effect of overexpression of CD82 was investigated in HB2 mammary epithelial cells, whilst HEK293T human embryonic kidney cells were used to investigate the link between PKCα, CD82 and desmosomal proteins. More specifically:

- To determine whether CD82 plays a role in the maintenance of desmosomal adhesion, siRNA oligonucleotides targeting desmosomal components were used and their effects on the adhesiveness of cells assessed by dispase assays. This part of the study was expanded to include the adherens junction proteins E-cadherin and β-catenin.

- To investigate the potential interactions between PKCα, CD82 and desmosomal proteins, and the ability of PKCα to phosphorylate desmosomal proteins, immunoprecipitation and FLAG-agarose pull-down experiments were carried out.

- To investigate the role of CD82 on the intracellular distribution of desmosomal and other cell-cell junction proteins, confocal microscopy and a cell-cell boundary detection software that quantifies fluorescence intensities were used. Further, the super-resolution microscopy technique dSTORM was employed to investigate the clustering and organisation of desmosomal proteins.

Chapter 2 - Materials and Methods

2.1 Cell culture

Control human mammary epithelial (HB2) cells (initially obtained from Berditchevsky et al. (1994) at Cancer Research UK) (HB2PURO), HB2 cells expressing wild-type CD82 (HB2CD82), HB2 cells expressing a CD82 N-terminal deletion mutant with the first 11 amino acids (MGSACIKVTKY) deleted and replaced with a haemagglutinin antigen (HA) tag (YPYDVPDYA) (HB2CD82ΔN), and HB2 cells expressing a palmitoylation deficient mutant of CD82 in which all 5 cysteines have been mutated to alanine (CD82Cys5) were generated by the Odintsova laboratory using a retroviral transduction method (Odintsova et al., 2013). FLY A13 packaging cells were transfected with an empty retroviral expression construct (PURO) with a selectable marker conferring resistance against puromycin, and retroviral constructs encoding CD82, CD82ΔN, and CD82Cys5 with the same selectable marker, together with retroviral packaging and envelope plasmids. The medium on the FLY A13 packaging cells was used to infect HB2 cells. Infected cells were selected for with puromycin.

HB2 cells were cultured in Dulbecco's Modified Eagle Medium (DMEM) (Sigma) containing 10% foetal bovine serum (FBS) (Gibco), 50 U/ml penicillin/streptomycin (Gibco), 10 μg/ml hydrocortisone (Sigma), and 10 μg/ml insulin (Sigma). Human embryonic kidney (HEK293T) cells and immortalised human keratinocytes (HaCaT) cells were cultured in DMEM containing 10% FBS and 50 U/ml penicillin/streptomycin.

All cells were maintained at 37°C in 5% humidified CO_2. Cells were sub-cultured at 80-90% confluence. In brief, cells were dissociated using trypsin-EDTA or TrypLE (Gibco). Cells were then collected in culture medium and centrifuged for 3 min at 1000 rpm. The supernatant was removed, and cells were resuspended in culture medium. Cells were seeded depending on the density required. Cells were cryopreserved using freezing media (10% DMSO (Sigma) in FBS) and initially stored at -80°C and then transferred to liquid nitrogen for long-term storage.

2.2 siRNA knockdown

Cells (2 x10^5) were reverse transfected with siRNA oligonucleotides (Table 1) in 6 well plates using lipofectamine RNAiMax (Invitrogen) according to manufacturer's instructions. For example, for knockdown of PG, 18 pmol siPG was diluted in 500 µl of Opti-MEM medium (Gibco). 5 µl lipofectamine RNAiMax was then added to the mix which was left to incubate for 15-20 min at room temperature. Cells diluted in antibiotic free growth medium were added to the transfection mix which was then made up to a final plating volume of 2 ml. The concentration of non-silencing control used corresponds to the highest concentration used in each experiment. Cells were used for experiments 72 h after transfection. Knockdown efficiency was confirmed by western blotting or immunofluorescence once before being used for dispase assays.

2.3 DNA transfection

Cells were seeded onto a 6 cm dish 24 h before transfection. Constructs (Table 2) were transfected into HEK293T cells using GeneJammer transfection reagent (Agilent technologies) according to manufacturer's instructions. For each transfection, 6 µl GeneJammer transfection reagent was diluted in 194 µl Opti-MEM medium. The GeneJammer-Opti-MEM mix was incubated at room temperature for 5 min. 2 µg DNA (1 µg DNA each for co-transfections) was added to the GeneJammer-Opti-MEM mix, and the mix was incubated at room temperature for 20-25 min. During this incubation, the medium on the cells was replaced. At the end of the incubation, the transfection mix was added dropwise to the cells. Cells were used for experiments 48 h after transfection.

2.4 PKC activator and inhibitor treatment

Cells were treated with 50 nM of TPA (PKC activator), Gö6976 (PKC inhibitor) or DMSO (all from Sigma) for 1 h (Kimura et al., 2007). Dispase assays and immunoprecipitations were carried out as described in 2.5 and 2.9.

2.5 Dispase assay

Cells ($2x10^5$) were seeded in triplicate in 6 well plates. 72 h after seeding, cells were rinsed twice with PBS and incubated with 2 ml of 2.4 U/ml dispase II (Roche) in PBS for 30-45 min at 37°C in 5% humidified CO_2. Released monolayers were subjected to mechanical stress by placing them on a rotating platform at 300 rpm for 1 min. Released and fragmented monolayers were imaged using a

stereomicroscope using a 0.75 x digital camera zoom (Brunel microscopes). The fragments generated were counted manually.

2.6 Gap closure assay

Cells were initially transfected with siRNA in 6 well plates. 48 h after transfection, the cells were detached, and $4.2x10^4$ cells were plated in the chambers of a 35 mm μ-Dish culture insert (Ibidi). 24 h after plating, the silicon insert was removed using forceps, generating gap of 500 μm, and the cells were covered with 2 ml media. Gap closure was observed using a Zeiss Axiovert 25 microscope with a 5x objective. The % gap area was quantified using ImageJ software. Briefly, in each image, the edges of the gap were identified and sharpened. A threshold was applied to clearly delineate the edge of each gap, and the distance of the gap at each timepoint was measured. The % gap area at the 0 h timepoint was considered as 100% for each condition.

Table 1 siRNA oligonucleotides

Oligonucleotides	Supplier/ Catalogue Number	Target sequence	Final concentration
Control siRNA (siCtrl)	1022076 Qiagen	AATTCTCCGAACGTGTCACGT	-
ON-TARGET plus human JUP (3728) siRNA (siPG)	J-011708-10 Dharmacon	AGACAUACACCUACGACUC	9 nM
ON-TARGET DP siRNA	- Dharmacon	AACCCAGACUACAGAAGCAAUUU	9 nM

(custom) (siDP)	(McHarg et al., 2014)		
ON-TARGET plus human DSP (1832) siRNA SMARTpool (siDPpool)	J-019800-00 Dharmacon	CGACAUGAAUCAGUAAGUA GAUAGCCGACCUUGAGUUA GGGAUGAGUUCACCAAACA GUAGAGUGGUCAUAGUUGA	9 nM
ON-TARGET plus human DSG2 (1829) siRNA SMARTpool (siDSG2)	L-011645-00 Dharmacon	CAAUAUACCUGUAGUAGAA GAGAGGAUCUGUCCAAGAA CCUUAGAGCUACGCAUUAA CCAGUGUUCUACCUAAAUA	9 nM
ON-TARGET plus human CDH1 (999) siRNA (siEcad)	J-003877-10 Dharmacon	GGGACAACGUUUAUUACUA	15 nM
ON-TARGET plus human CTNNB1 (1499) siRNA (siβcat)	J-003482-12 Dharmacon	GGUACGAGCUGCUAUGUUC	9 nM
Hs_PRKCA_5 FlexiTube siRNA (siPKCα)	SI00301308 Qiagen	AACCATCCGCTCCACACTAAA	20 nM

Table 2 Constructs

Construct	**Source**
pZeo	Dr Fedor Berditchevski
pcDNA-GFP	Dr Fedor Berditchevski
pGFP-PKCα	Dr Fedor Berditchevski
pZeoCD82	Dr Elena Odintsova

pCD82ΔN(-HA)	Dr Elena Odintsova
pCD82ΔC(-HA)	Dr Elena Odintsova
p931 (DP-FLAG)	Professor Kathleen Green, Northwestern University, USA
pcDNA-DP-ABC-FLAG	Dr Martyn Chidgey
pEGFP-PG	Dr Martyn Chidgey
pmCherry-DSG2	
pcDNA-DP-ABC-GSR-FLAG	

2.7 Cell lysis

Cells were washed twice with ice-cold PBS and lysed on ice with 1x Laemmli sample buffer (0.06 M Tris-HCl pH 6.8, 2% sodium dodecyl sulphate (SDS), 10% glycerol) supplemented with a protease and phosphatase inhibitor cocktail (Cell signalling). Cell lysates were scraped and collected in an Eppendorf tube. Samples were boiled at 100^{o}C for 15 min and centrifuged for 2 min at 13000 rpm. Protein concentration was measured using the Bio-Rad detergent compatible protein assay using bovine serum albumin (BSA) standards according to manufacturer's instructions. The absorbance was measured using an iMark Bio-Rad microplate absorbance reader at 595 nm. Bromophenol blue (0.0025%) was added to samples after determining the protein concentration. Samples were stored at -20^{o}C.

2.8 SDS-PAGE and western blotting

All samples were boiled for 5 min at 100ºC and centrifuged at 13000 rpm for 1 min prior to loading. For reducing conditions, β-mercaptoethanol (1:20) was added to samples before boiling. Samples were loaded at a concentration of 25 µg (or 100 µg) per lane and resolved by 8% SDS-polyacrylamide gel electrophoresis (SDS-PAGE). PageRuler plus prestained protein ladder (Thermo Fisher Scientific) was used as a molecular weight reference. Gels were run at 13 mA for 2 h. Proteins were transferred onto nitrocellulose membranes using wet transfer at 100 V for 1 h at 4ºC (Bio-Rad systems). Membranes were washed with 1 x Tris-buffered saline (20 mM Tris-HCl, pH 7.4, 150 mM NaCl) containing 0.1% Tween-80 (TBST) and blocked in 5% milk or 3% BSA made up in TBST and incubated for 1 h at room temperature. Membranes were washed with TBST and incubated with primary antibodies (Table 3) diluted in 5% milk or 3% BSA in TBST for 1 h at room temperature or overnight at 4ºC. Membranes were washed 3 times for 10 min with TBST and incubated with fluorescently labelled (LI-COR) or HRP conjugated (Dako) secondary antibodies for 1 h at room temperature. Membranes were then washed 3 times for 10 min with TBST, rinsed with dH_2O, and developed using either a LI-COR Odyssey imager or using enhanced chemiluminescence (Perkin-Elmer) and X-ray film (GE-healthcare). Densitometry was carried out using the LI-COR Odyssey software or ImageJ.

2.9 Immunoprecipitation

Cells were washed twice with ice-cold PBS and lysed on ice with 500 µl wash buffer containing 1% Brij 98 (25 mM HEPES, pH 7.4, 150 mM NaCl, 5 mM $MgCl_2$)

or 1% Triton X-100 (10 mM Tris-HCl, pH 7.5, 145 mM NaCl, 5 mM EDTA, 2 mM EGTA) in PBS supplemented with a protease and phosphatase inhibitor cocktail (Cell signalling). Lysates were transferred to an Eppendorf tube and incubated on a rotatory wheel for 45 min at 4 ºC. Lysates were then centrifuged at 13000 rpm for 10 min at 4ºC. The supernatant (400 µl) was transferred to a new Eppendorf tube and incubated with 20 µl protein-G plus agarose beads (Santa-Cruz) (pre-equilibrated in wash buffer) and rotated for 1 h at 4ºC. Remaining lysate was transferred to a new Eppendorf tube and an equal amount of 2x Laemmli sample buffer was added and incubated at 100ºC for 5 min. The supernatant bead mix was centrifuged at 6500 rpm for 1 min and the supernatant was transferred to a new Eppendorf tube. Primary antibody (Table 3) was added to the supernatant and incubated on the rotatory wheel for 90 min at 4ºC. The supernatant was added to 40 µl protein-G plus agarose beads and rotated for 1h at 4ºC. The supernatant was centrifuged at 6500 rpm for 1 min and the majority was removed. 500 µl of wash buffer was added to the beads, vortexed for 10 sec and centrifuged at 6500rpm for 1 min. The majority of the supernatant was removed and this step was repeated four times. After the final wash all of the supernatant was removed, 30µl 2x Laemmli sample buffer was added to the beads and incubated at 100ºC for 5 min. Samples were centrifuged at 13000 rpm for 1 min and the supernatant analysed by SDS-PAGE and western blotting as described in section 2.8.

2.10 Pull-down assay

Cells were washed twice with ice-cold PBS and lysed on ice with 500µl wash buffer containing 1% Brij 98 (25 mM HEPES, pH 7.4, 150 mM NaCl, 5 mM $MgCl_2$)

or 1% Triton-X100 (10 mM Tris-HCl, pH 7.5, 145 mM NaCl, 5 mM EDTA, 2 mM EGTA) in PBS supplemented with a protease and phosphatase inhibitor cocktail (Cell signalling). Lysates were transferred to an Eppendorf tube and rotated for 45 min at 4°C. Lysates were then centrifuged for 10 min at 13000 rpm. 400 µl of the supernatant was added to 20 µl of anti-FLAG M2-agarose beads (Sigma) that were equilibrated in wash buffer. Remaining lysate was transferred to a new Eppendorf tube and an equal volume of 1x Laemmli sample buffer was added to the lysates and incubated for 5 min at 100°C. The supernatant/bead mix was rotated for 2 h at 4°C. The lysates were then centrifuged at 6500 rpm for 1 min. The majority of the supernatant was removed. 500µl of wash buffer was added to the beads and mixed by inversion. The mix was centrifuged at 6500 rpm for 1 min and the majority of the supernatant was removed. This step was repeated four times. After the final wash, all of the supernatant was removed and 30µl of 1x Laemmli sample buffer was added to the beads and incubated at 100°C for 5 min. Samples were centrifuged at 13000 rpm for 1 min and the supernatant analysed by SDS-PAGE and western blotting as described in 2.8.

2.11 Immunofluorescence

Cells were seeded on 12 mm coverslips in 12-well plates. For direct stochastic optical reconstruction microscopy (dSTORM) cells were grown in 3.5 cm MatTek glass bottom culture dishes. Cells were rinsed with PBS and fixed for 10 min with 100% methanol at -20°C. Cells were washed with PBS and blocked for 45 min in 20% heat inactivated goat serum in PBS and incubated overnight at 4ºC with primary antibodies (Table 3), diluted in blocking buffer. Cells were then washed

with PBS three times for 15 min and incubated with Alexa Fluor (AF) conjugated secondary antibodies (AF488,568, 594 or 647) diluted in blocking buffer for 1 h at room temperature in the dark. Cells were then washed with PBS three times for 15 min and rinsed with distilled water. Coverslips were allowed to dry and then mounted on microscope slides using SlowFade Gold Antifade mountant (Thermo Fisher Scientific) and sealed with clear nail varnish. Slides were stored at -20ºC. dSTORM samples were kept in PBS at room temperature and imaged the same day.

2.12 Microscopy

2.12.1 Confocal microscopy

Immunofluorescence images were acquired with a Zeiss LSM 510 confocal laser scanning microscope using a Plan-Apochromat 63x/1.4 oil immersion objective. Z-stack were acquired using a 0.35 µm step size.

2.12.2 Direct stochastic optical reconstruction microscopy (dSTORM)

For STORM imaging, cells were imaged on a Nikon N-STORM system in dSTORM mode using a perfect focus, 100x, 1.49 NA TIRF oil lens objective. Cells were imaged with STORM switching buffer containing 50 µl enzyme stock solution A (20ug/ml catalase, 4mM Tris (2-carboxyethyl) phosphine hydrochloride), 50% glycerol, 25mM KCl, 20 mM Tris-HCl, pH 7.5, 1 mg/ml glucose oxidase), 400 µl glucose stock solution B (100 mg/ml glucose, 10% glycerol), and 100 µl reducing agent stock solution C (1M cysteamine). The STORM switching buffer was made up to 1 ml with PBS. The pH of the STORM switching buffer was adjusted to 7.2-

7.8 with concentrated HCl. AF647 was used for all experiments and excited using the 640 laser line. The 405 laser line was used for reactivation. 20000 frames were captured in 3D-STORM mode using an Andor iXon Ultra EMCCD camera.

2.13 Image analysis

Z-stack confocal image analysis was carried out using a cell boundary detection software (Stroe et al., 2016). The cell boundary detection software runs using a graphical user interface in MATLAB. Pre-processing to reduce noise is initially carried out on the green channel which is then followed by the application of second order steerable Gaussian filters. Further processing involves thresholding, thinning and boundary dilation which then gives rise to the fluorescence intensities of both green and red channels. For STORM, captured frames were reconstructed and processed using ThunderSTORM in Fiji (Ovesný et al., 2014). Molecules that were found in consecutive frames within 50 nm were merged into one molecule. A distance threshold of 50 nm was applied to remove duplicate molecules. Cluster analysis was carried out with KNIME using the Density-based spatial clustering of applications with noise (DBSCAN) algorithm. The KNIME image analysis workflow was developed by Dr Jeremy Pike at the Centre of Membrane Proteins and Receptors (COMPARE). A 2 x 2-μm region of interest containing a single desmosome was used for analysis. To consider a point as part of a cluster a search radius of 30 nm with a minimum of 10 points was applied. Plaque to plaque distances were calculated using the plot profile function in Fiji to determine the intensities of pixels within a selection containing a single desmosome. This was

used to calculate the distance between the two intensity peaks corresponding to each plaque perpendicular to the plasma membrane.

2.14 Statistical analysis

Statistical analysis was carried out using GraphPad Prism (version 8). A two-tailed student's t-test was used to determine statistical significance (with significance set at $P<0.05$).

Table 3 Primary antibodies

Antibodies	Species	Clone/ Product number	Source	WB dilution	IF dilution	IP Volume
DSG1+3	Mouse	32-2B	(Vilela et al., 1987)	1:50	-	-
DSG2	Rabbit	EPR6768	Abcam	1:10000	1:400	-
DSG2	Mouse	33-3D	(Vilela et al., 1995)	-	1:50	-
DSG2	Mouse	3G132	Abcam	1:500	-	2.5 µl
DSC2	Mouse	7G6	Thermo Fisher Scientific	1:1000	-	5 µl
DP I+II	Mouse	11-5F	(Parrish et al., 1987)	1:25	1:100	-
PG	Mouse	610253	BD Biosciences	1:5000	1:1000	-
E-cadherin	Mouse	MB2	Abcam	-	1:300	-
E-cadherin	Mouse	610182	BD Biosciences	1:5000	1:50	-
β-catenin	Mouse	610154	BD Biosciences	1:2000	1:500	-
CD82	Mouse	TS82b	Eric Rubinstein	1:600	-	5 µl
GFP	Rabbit	Ab290	Abcam	-	-	1 µl
Phosphoserine	Rabbit	Ab9332	Abcam	1:1000	-	4 µl

PKCα	Rabbit	2056	Cell signalling	1:1000	-	-
β-Actin	Mouse	AC-15	Sigma	1:20000	-	-
FLAG	Rabbit	F7425	Sigma	1:3000	-	-

2.15 Molecular Biology

2.15.1 Plasmids

A pcDNA-DP-ABC-FLAG construct encoding residues 1960-2822 of DP was used to generate pcDNA-DP-ABC-GSR-FLAG (1960-2871), encoding residues 1960-2871. This new construct was identical to pcDNA-DP-ABC-FLAG but included DNA encoding the carboxyl terminal Gly-Ser-Arg (GSR) rich domain containing GSR repeats.

2.15.2 Polymerase Chain reaction (PCR)

PCR was used to amplify DP residues 2822-2871 (NCBI gene accession number: NM_004415) using a full-length human DP cDNA clone (p931) as a template. Primer 1 (forward) incorporates an *Eco*RV site, and primer 2 (reverse) incorporates a *Xho*I site, stop codon and DNA encoding a FLAG tag (i.e. amino acids DYKDDDDK) (Table 4). The expand high fidelity PCR system was used (Roche). A mastermix containing the following was prepared: 10 µl Buffer 2 (10x) (Roche), 10 µl 2mM dNTPs, 10 µl primers (1 and 2), 64 µl dH_2O, 4 ng p931, 2 µl Expand high fidelity PCR enzyme mix (Roche). A 25 µl reaction volume was used. The PCR was carried out using the following thermal cycling conditions: 95 ºC for

5 min, followed by 20 cycles of 95ºC for 30 sec, 60ºC for 45 sec and 72ºC for 30 sec. The reaction products were pooled and precipitated as described in 2.13.4.

2.15.3 Agarose gel electrophoresis

DNA was resolved on 1% agarose (Invitrogen) gels made up in 1 x TAE buffer (40 mM Tris base, 20 mM glacial acetic acid, 1mM EDTA (pH 8.0)). SYBR safe (1:10000, Thermo Fisher Scientific) was added to molten agarose before casting the gel. Agarose gels were run at 100 V for 30 min. A 1kb HyperLadder (Bioline) was used to estimate the size of DNA bands. Gels were imaged using a UV transilluminator.

2.15.4 Ethanol precipitation of DNA

DNA was precipitated with one half volume of 8 M ammonium acetate and two volumes of 100% ethanol. The solution was vortexed and incubated for a minimum of 40 min at -80ºC. The solution was then centrifuged at 13000 rpm for 10 min. The supernatant was then removed and DNA pellet resuspended in Tris-EDTA (TE) buffer (10 mM Tris-Cl (pH 8.0), 1 mM EDTA (pH 8.0)).

2.15.5 Restriction enzyme digests

Restriction digests were carried out according to manufacturer's instructions. For *Eco*RV/*Xho*I double digests DNA was first digested with *Eco*RV (37ºC for 1 h). The salt concentration was then adjusted with 1M NaCl and the *Eco*RV digested DNA incubated with *Xho*I for an additional hour.

2.15.6 Electroelution

DNA was resolved by agarose gel electrophoresis and the desired DNA band was excised from the gel on a UV transilluminator. The excised band was placed in dialysis tubing with 1 x TAE buffer. The tubing was secured and placed in an electrophoresis tank and the current run at 90 V for 25-30 min. The current was then reversed for 30 sec, and the buffer containing the DNA collected in an Eppendorf tube. The DNA was extracted twice with phenol and once with chloroform. The DNA was then precipitated as described in 2.15.4.

2.15.7 Ligation

Ligation of restriction digests was carried out using a quick ligation kit (New England Biolabs) according to manufacturer's instructions. The ligation mix was incubated at room temperature for 5 min.

2.15.8 Transformation of plasmid DNA into XL-1 blue cells

Competent XL-1 blue cells were thawed on ice for 5 min. 5 µl of ligation mix or 0.5 µl of plasmid DNA was added to the cells and incubated on ice for 30 min. The bacteria were then heat shocked (42ºC for 2 min), the cells immediately placed on ice and 1 ml of Luria Broth (LB) was added. The cells were allowed to recover at 37ºC for 1 h. The cells were then centrifuged at 7000 rpm for 3 min. The supernatant was removed and cells were resuspended in 100 µl of LB. The transformed cells were plated onto LB agar plates containing ampicillin (50 µg/ml) and incubated overnight at 37ºC.

2.15.9 Plasmid DNA isolation

Single colonies were picked and inoculated in 5 ml (for mini preps) or 50 ml (for midi preps) of LB containing ampicillin (50 µg/ml). Cultures were grown overnight at 37ºC with shaking at 200 rpm. The cells were harvested at 4000 rpm for 15 min and plasmid DNA extracted using QIAprep spin mini and midi prep kits (Qiagen) according to manufacturer's instructions. Recovered DNA was dissolved in water for sequencing or TE buffer for long-term storage. DNA concentration was measured using a Nanodrop (Thermo Fisher Scientific) at 260 nm.

2.15.10 Sequencing

Plasmid DNA sequencing was carried out by the Functional Genomics and Proteomics Laboratory (University of Birmingham). Samples provided for sequencing contained 2 µl plasmid DNA, 3 pmol sequencing primer (Table 4) and 5 µl dH_2O. Analysis of sequencing results was carried out using Chromas and NCBI blast alignment tools.

Table 4 Primers used for cloning and sequencing.

Primer	Sequence 5'-3'
Primer 1	GAAGATATCACTGGGCTGCGC
Primer 2	TTCTCGAGCTACTTATCGTCGTCATCCTTGTA ATCGTGCCCAATAGAACTACTGCTA
Sequencing primer	TGGCAACTAGAAGGCACAG

Restriction sites used for cloning are shown in red.

Chapter 3 – CD82 increases intercellular adhesion

3.1 Introduction

Strong adhesion is important for the maintenance of tissue integrity. Desmosomes and adherens junctions are intercellular anchoring junctions. They provide strong adhesion between cells as intracellularly they link to the intermediate filament cytoskeleton or actin microfilaments, respectively (Simpson et al., 2011). Tetraspanins function as membrane organisers and are able to regulate the function of their partner proteins in this way. While the role of the tetraspanin CD82 in cadherin mediated adhesion has been described (Abe et al., 2008; Chigita et al., 2012; Marjon et al., 2016), a role for CD82 in desmosomal adhesion has not been studied.

The aim of this chapter was to investigate the role of CD82 in the maintenance of cell-cell adhesion, in control and CD82 overexpressing mammary epithelial (HB2) cells. To assess the adhesiveness of control and CD82 overexpressing cells dispase assays were carried out. The adhesiveness of HB2 cells expressing a CD82 N-terminal deletion mutant and a palmitoylation deficient mutant of CD82 were also tested. These mutants were tested because it is thought that the N- and C-terminal domains of tetraspanins are important for interactions with cytoplasmic signalling proteins such as PKCα, which has been shown to regulate desmosomal adhesion (Garrod et al., 2005; Thomason et al., 2012), and palmitoylation of tetraspanins is important for stabilising associations in tetraspanin-enriched microdomains (TERMs) (Yang et al., 2002; Berditchevski et al., 2002). To test whether CD82 plays a role in desmosomal adhesion, siRNA oligonucleotides were

used to knockdown desmosomal components, and adhesiveness of control and CD82 overexpressing HB2 cells assessed by dispase assays. This part of the study was expanded to include the adherens junction proteins E-cadherin and β-catenin to determine whether CD82 increases adherens junction mediated adhesion in HB2 cells. The expression and intracellular distribution of desmosomal and adherens junction proteins in response to knockdown of desmosomal and adherens junction components was also assessed.

3.2 Results

3.2.1 CD82 strengthens cell-cell adhesion

To analyse whether CD82 affects the maintenance of cell-cell adhesion, control HB2 cells (HB2PURO) and HB2 cells overexpressing CD82 (HB2CD82) were used. A CD82 mutant lacking the N terminus (HB2CD82ΔN) and a palmitoylation deficient mutant of CD82 (HB2CD82Cys5), in which all five membrane proximal cysteines were mutated to alanine, were used to test whether the N-terminus and membrane proximal cysteines of CD82 play a role in cell-cell adhesion (Figure 7A). The stable transfectants were generated by the Odintsova laboratory using a retroviral transduction method (Odintsova et al., 2013) which involved transfecting FLY A13 packaging cells with an empty retroviral construct with a selectable marker conferring resistance against puromycin (PURO) and retroviral constructs encoding CD82, CD82ΔN, and CD82Cys5 with the same selectable marker. These individual constructs were co-transfected with retroviral packaging and envelope plasmids. The medium on the packaging cells was used to infect HB2 cells. Cells that have incorporated the vectors in their genome were selected for

with puromycin. Figure 7B shows the expression level of CD82 in HB2PURO, HB2CD82, HB2CD82ΔN, and HB2CD82Cys5 cells. CD82 from HB2 cells runs as at 25-55 kDa on SDS-PAGE and appears as a smear as a result of glycosylation (White et al., 1998).

To investigate the adhesiveness of control HB2 cells and the various CD82 transfectants dispase assays were carried out. The cells were grown to confluence and treated with dispase, which cleaves extracellular matrix components, to release the confluent monolayer from the culture dish. This was then subjected to mechanical stress by placing it onto a rotating platform (Figure 8). The assay provides a measure of the strength of cell-cell adhesion. The greater the number of fragments that are generated the weaker the adhesion between cells, and the fewer the number of fragments the stronger the adhesion between cells. Quantification of the number of fragments generated after the monolayers were subjected to mechanical stress shows that CD82 increases cell-cell adhesion compared to HB2PURO cells (Figure 9).

Previous studies have proposed that the N-terminus of CD82 is involved with the interaction of cytoplasmic signalling proteins such as PKCα which could potentially modulate cell-cell adhesion (Termini and Gillette, 2017). A reduction in adhesion was observed when compared to the CD82 overexpressing cells. However, the results were not significant, due to lack of reproducibility of the dispase assays, a problem encountered throughout this study, indicating that the N-terminus of CD82 is probably not required for the CD82 mediated increase in cell-cell adhesion

(Figure 9). Palmitoylation of tetraspanins is important for interactions with other tetraspanins and partner proteins (Yang et al., 2002; Berditchevski et al., 2002). Therefore, loss of palmitoylation could affect the assembly of TERMs. However, the results indicate that palmitoylation of CD82 is not essential for the CD82 mediated increase in cell-cell adhesion, suggesting that interactions with other tetraspanins are not important for the CD82 mediated increase in cell-cell adhesion (Figure 9). However, this interpretation does not account for the high expression of CD82 in HB2CD82Cys5 cells (Figure 7). Therefore, the possibility that higher expression of CD82 increases cell-cell adhesion in HB2CD82Cys5 cells remains.

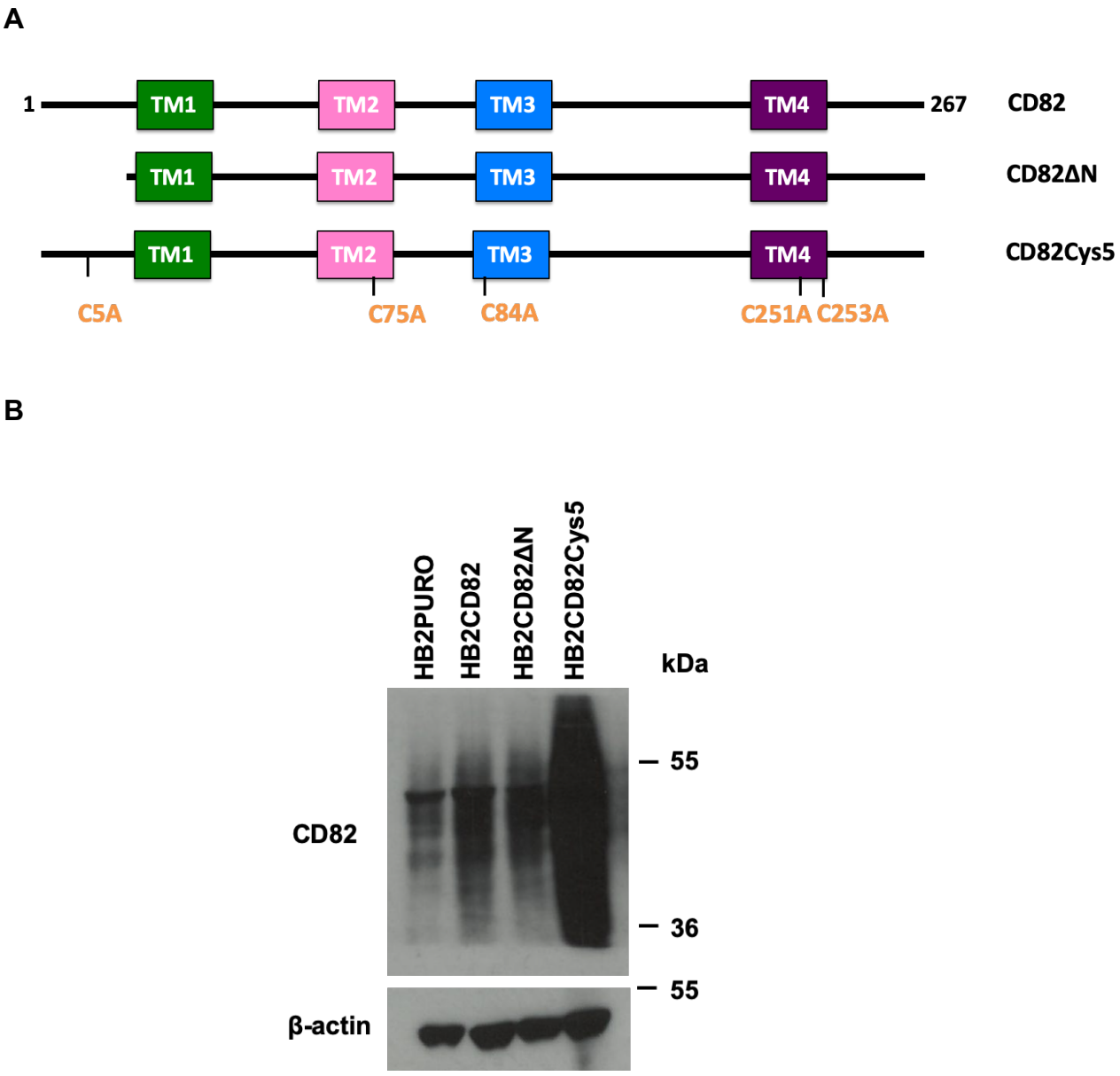

Figure 7 CD82 domain structure and expression.

(A) Domain architecture of CD82. Tetraspanins contain four transmembrane domains, and short N- and C- terminal tails. To generate the CD82ΔN mutant the N-terminal tail was deleted. CD82 also contains five membrane proximal cysteine residues which can be palmitoylated. These residues (highlighted in orange) were mutated to alanine to produce the palmitoylation deficient protein. (B) To generate control and CD82 overexpressing HB2 cells, cells were stably transfected with control (Puro), CD82, CD82ΔN and CD82Cys5 constructs. Lysates were prepared and analysed by western blotting using antibodies against CD82 and β-actin (loading control). Data are from one experiment.

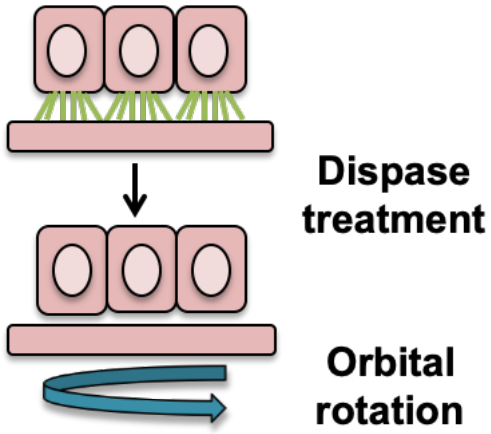

Figure 8 Summary of dispase assay.

Cells are plated onto 6 well plates and grown for 72 h. Confluent monolayers are then treated with dispase in PBS at 37°C to release the monolayer. Dispase cleaves extracellular matrix components such as collagen and fibronectin leaving cell-cell junctions intact. The released monolayer is then is subjected to mechanical stress by placing it onto rotating platform. The number of fragments generated is an indicator of the strength of adhesion between cells.

A

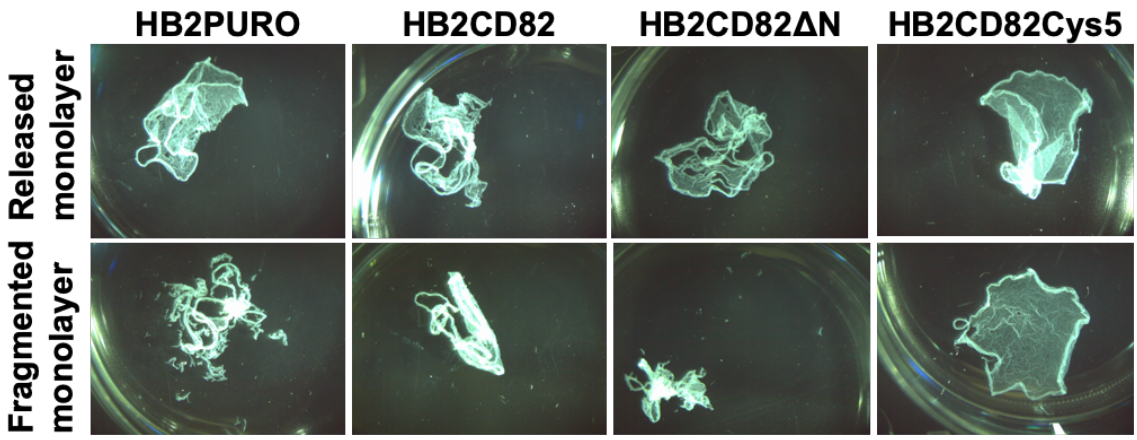

B

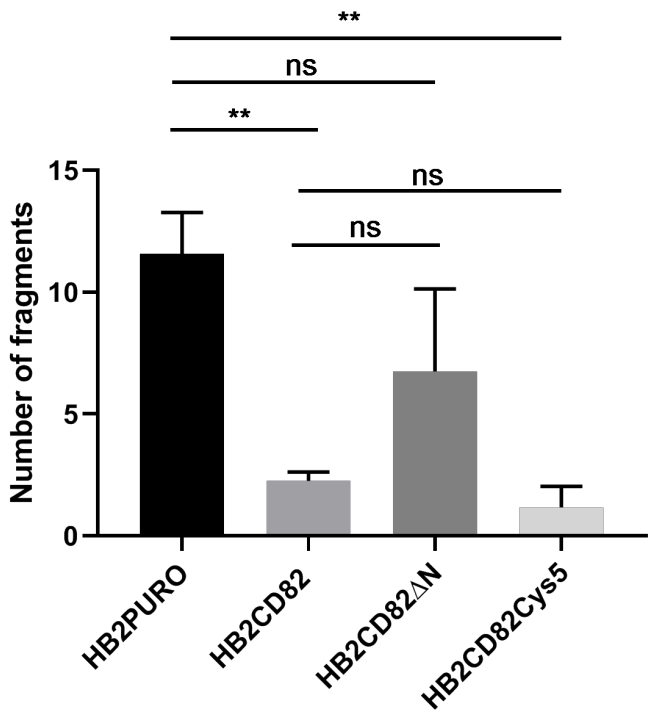

Figure 9 CD82 strengthens cell-cell adhesion in HB2 cells.

(A) Confluent HB2 cells were treated with dispase to release monolayers (top row) and subjected to mechanical stress (bottom row). (B) Quantification of fragments generated. Data are the mean, standard error, and t-test of four independent experiments (** P<0.01).

3.2.2 PG and DSG2 contribute to the CD82 mediated increase in cell-cell adhesion

To investigate whether desmosomal proteins contribute to the CD82 mediated increase in cell-cell adhesion (Figure 9), the desmosomal proteins, PG and DSG2 were transiently depleted in HB2PURO and HB2CD82 cells. PG is found primarily in desmosomes, although it can replace β-catenin in adherens junctions in certain circumstances, and is essential for desmosomal adhesion. DSGs are exclusively found in desmosomes and the presence of at least one DSG is essential for desmosomal adhesion (Garrod and Chidgey, 2008). HB2PURO and HB2CD82 cells were reverse transfected with siRNA oligonucleotides (oligos) against PG (siPG) and DSG2 (siDSG2), with non-silencing control (siCtrl) oligos acting as controls. Lysates were prepared 72 h after transfection to assess the level knockdown of PG and DSG2 by western blotting (Figure 10). Densitometric analysis of the western blots shows 76-81% knockdown of PG and 96-97% knockdown of DSG2 in HB2PURO and HB2CD82 cells 72 h after transfection.

Loss of expression of DSG isoforms can be compensated for by gain of expression of other isoforms (Hanakawa et al., 2002). Therefore, the expression levels of DSG 1 and 3 in DSG2 depleted HB2PURO and HB2CD82 cells were analysed by western blotting. Human keratinocyte (HaCaT) cells were used as a positive control as they express both DSG1 and 3. DSG1 and 3 were not detected in siCtrl and siDSG2 samples of both HB2PURO and HB2CD82 cells following western blotting with an antibody that recognises both DSG1 and 3 (Figure 11).

This confirms that DSG isoforms 1 and 3 do not compensate for the loss of DSG2 expression as they are not expressed in HB2 cells.

The adhesive strength of the cells was assessed by dispase assays. The cells were reverse transfected with siPG and siDSG2, and siCtrl. 72 h after transfection the cells were treated with dispase and subjected to mechanical stress. Transient depletion of PG resulted in a decrease in cell-cell adhesion in both HB2PURO cells and HB2CD82 cells (Figure 12 A-B). Expressing the data as fold change, relative to the siCtrl transfections shows that the decrease in adhesion is greater in HB2PURO cells compared to HB2CD82 cells. Knockdown of DSG2 in HB2PURO cells resulted in a decrease in adhesion, but this was not statistically significant. This may be due to the variability of the dispase assay as highlighted by the large standard error of the mean. However, depletion of DSG2 resulted in a significant decrease in adhesion in CD82 overexpressing HB2 cells (Figure 13 A-B). Expressing the data as fold change (Figure 13C) shows that there is a greater reduction in adhesion relative to siCtrl in HB2CD82 cells compared to HB2PURO cells. However, the standard error of the mean is high when normalised to siCtrl for HB2CD82 cells further highlighting the variable nature of the dispase assays. These data show that both PG and DSG2 contribute to the CD82 mediated increase in cell-cell adhesion.

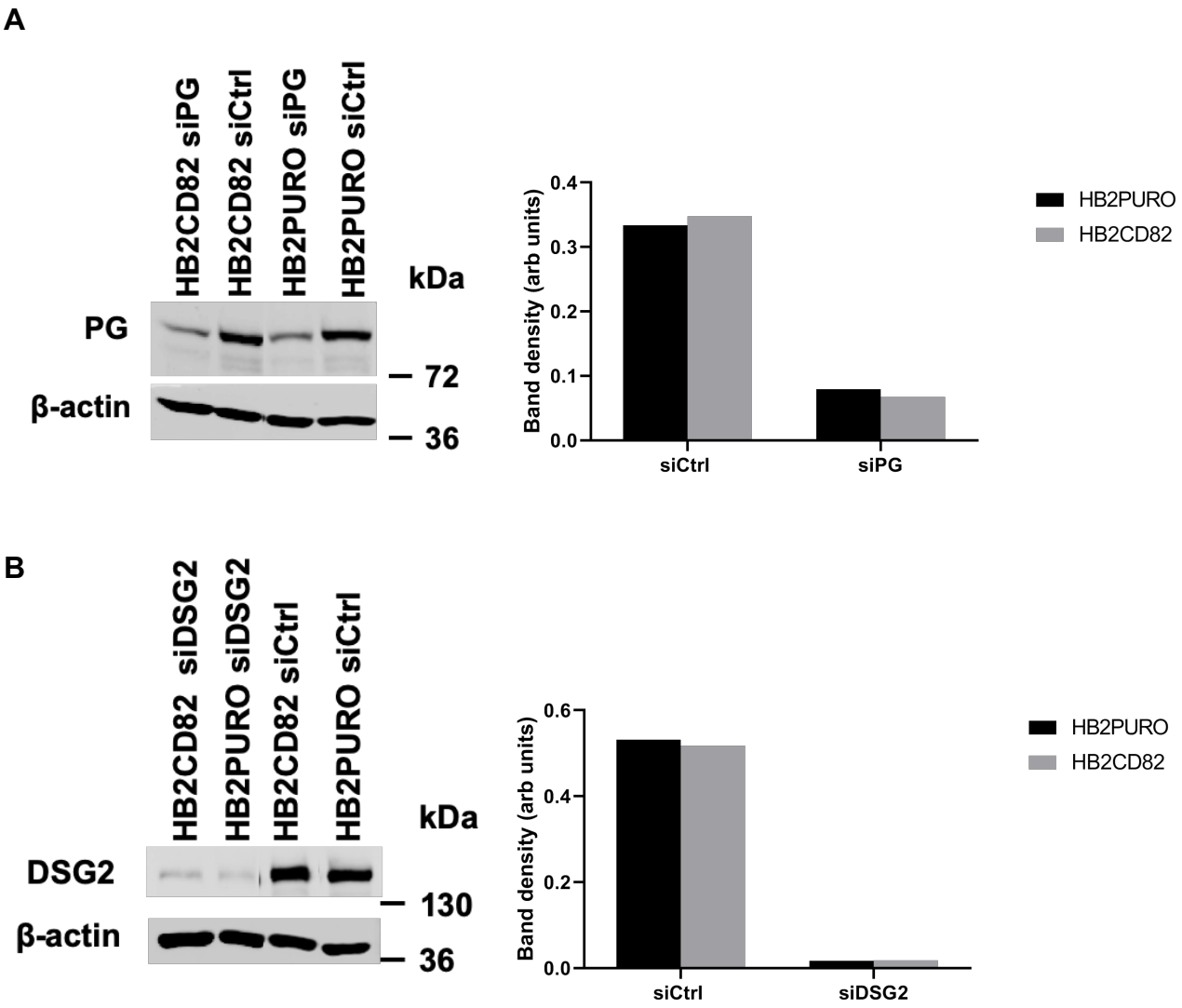

Figure 10 Transient knockdown of PG and DSG2 expression using siRNA.

HB2PURO and HB2CD82 cells were transfected with siRNA oligos against PG (siPG), DSG2 (siDSG2) and non-silencing control oligos (siCtrl). Lysates were prepared 72 h after transfection and the level of knockdown was assessed by western blotting using antibodies against PG (A), DSG2 (B) and β-actin (loading control). Western blots were quantified by densitometry and normalised with respect to β-actin. Data presented are from one experiment.

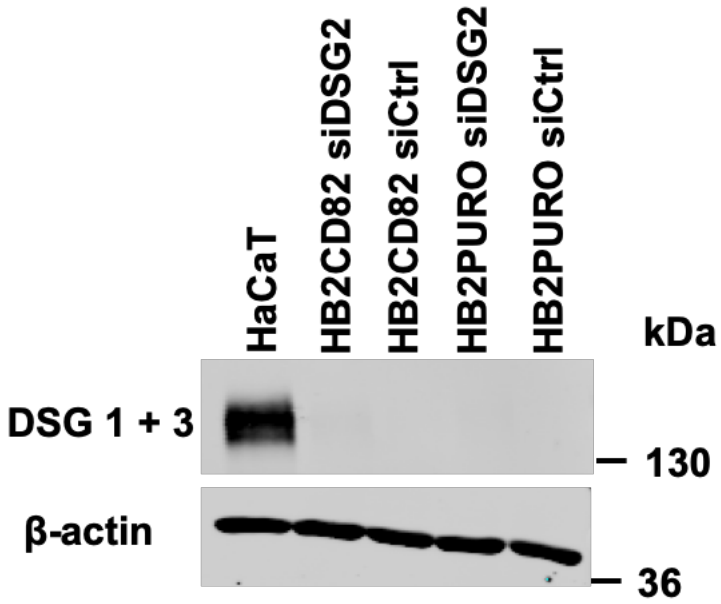

Figure 11 DSG1 and 3 are not expressed in HB2 cells and are not upregulated in response to loss of DSG2 expression

HB2PURO and HB2CD82 cells were transfected with siRNA oligonucleotides against DSG2. Lysates were prepared 72 h after transfection and analysed by western blotting using an antibody that recognises both DSG1 and 3, and β-actin (loading control). HaCaT cells were used as a positive control. Data are from one experiment.

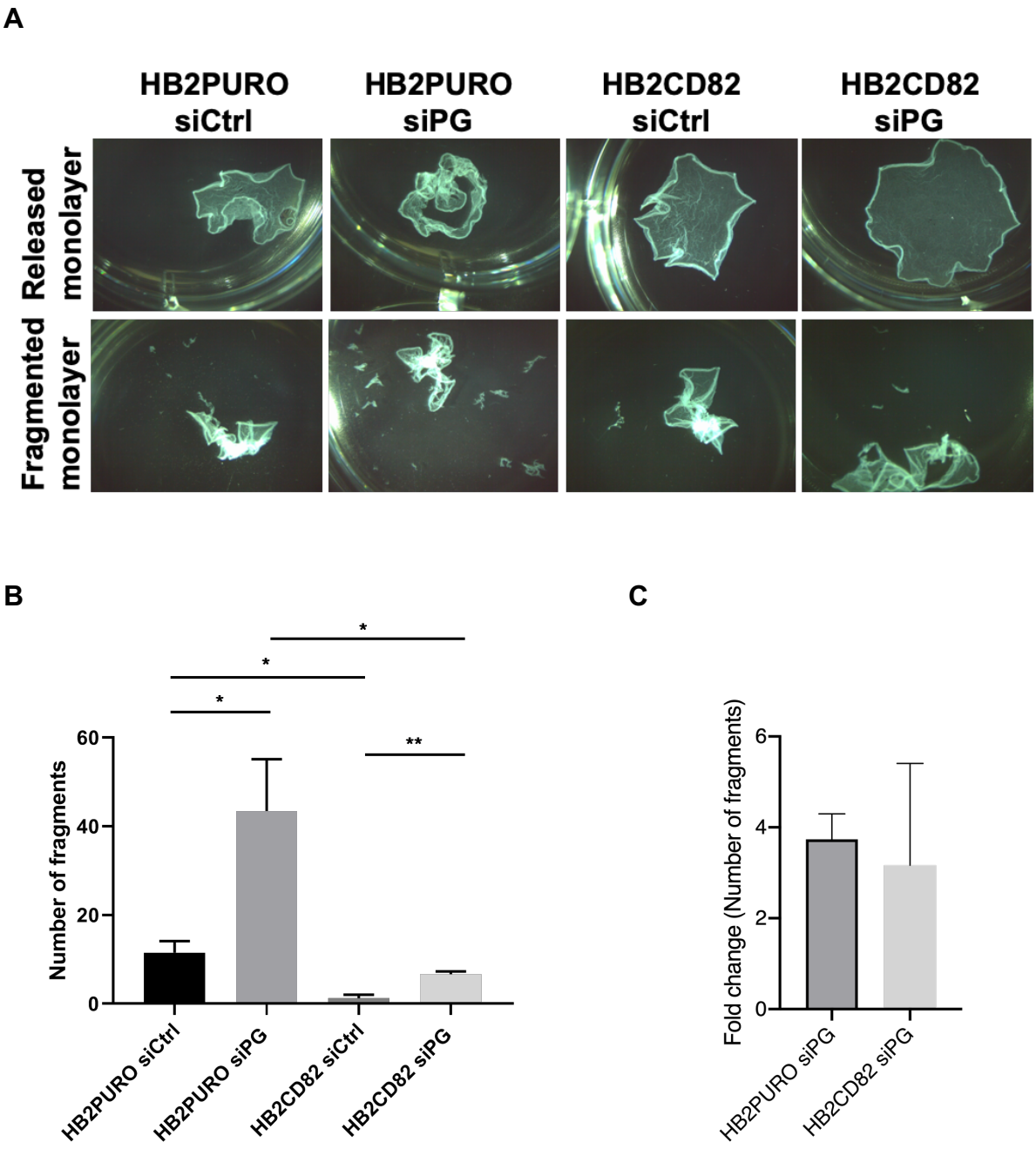

Figure 12 PG contributes to the CD82 mediated increase in cell-cell adhesion.

(A) HB2PURO and HB2CD82 cells were reverse transfected with control (siCtrl) and siRNA oligos against PG (siPG). 72 h after transfection the cells were treated with dispase and subjected to mechanical stress. Representative images are shown. (B) Quantification of the fragments generated. (C) Data from B expressed relative to siCtrl of each transfectant and expressed as fold change. Results are the mean, standard error, and t-test of four (HB2PURO) and three (HB2CD82) independent experiments (* $P<0.05$, ** $P<0.01$).

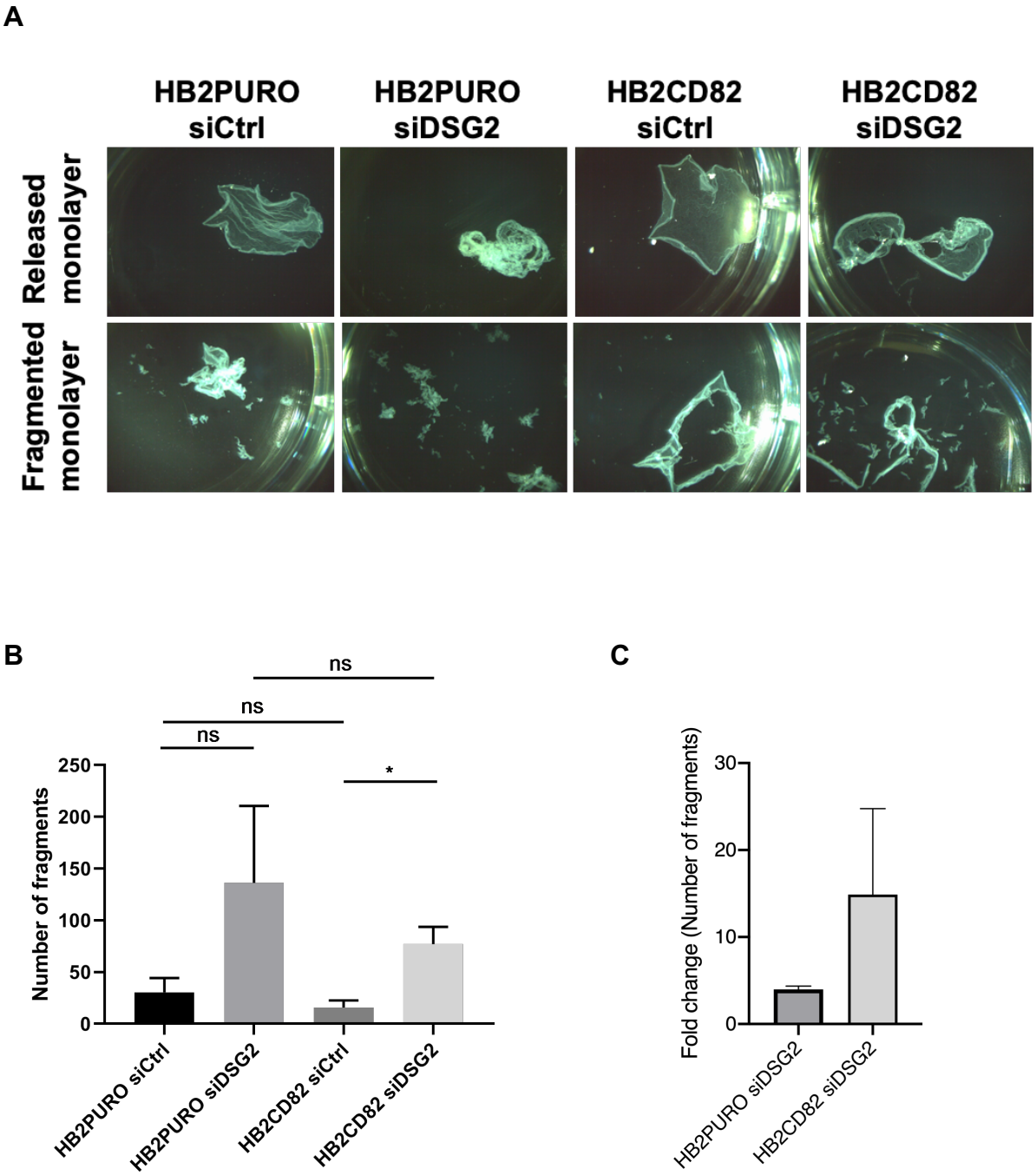

Figure 13 DSG2 contributes to CD82 mediated increase in cell-cell adhesion.

(A) HB2PURO and HB2CD82 cells were reverse transfected with control (siCtrl) and siRNA oligos against DSG2 (siDSG2). 72 h after transfections the cells were treated with dispase and subjected to mechanical stress. Representative images are shown. (B) Quantification of the fragments generated. (C) Data from B expressed relative to siCtrl of each transfectant and expressed as fold change. Results are the mean, standard error, and t-test of three independent experiments (* $P<0.05$).

3.2.3 No firm conclusion can be drawn regarding the role of DP in the CD82 mediated increase in cell-cell adhesion in HB2 cells

Desmosomes provide strong adhesion as they intracellularly link to the intermediate filament (IF) network (Garrod and Chidgey, 2008). DP is an essential component of desmosomes. Loss or mutation of DP can result in skin blistering diseases and cardiomyopathies. The C-terminus of DP interacts with IFs while the N-terminus interacts with PG and PKP. To investigate whether DP contributes to the CD82 mediated increase in cell-cell adhesion, HB2 cells were transfected with siRNA oligos targeted against DP (siDP) and non-silencing control oligos (siCtrl). The level of knockdown was assessed by western blotting and immunofluorescence microscopy. DP was difficult to detect by western blotting despite loading a high concentration of protein (Figure 14A). Therefore, knockdown efficiency was assessed by immunofluorescence microscopy. HB2PURO and HB2CD82 cells were reverse transfected on glass coverslips with siDP and siCtrl oligos and 72 h after transfection, the cells were fixed, stained with an anti-DP antibody and imaged with a confocal microscope (Figure 14B). The acquired images confirm knockdown of DP in both HB2PURO and HB2CD82 cells, with the knockdown efficiency being higher in HB2CD82 cells in this experiment.

The strength of adhesion of DP depleted HB2 cells was assessed by dispase assay 72 h after transfection. Treatment with siDP had no effect in HB2PURO cells. A decrease in adhesion was observed in HB2CD82 cells although this was not significant (Figure 15 A-B). Expressing the data as fold change (Figure 15C)

shows that the decrease in adhesion is greater in HB2CD82 cells compared to HB2PURO cells. Hence no firm conclusion could be reached. For this reason, the same experiment was carried out using a different set of siRNA oligos (siDPpool) targeting different sequences of DP. The level of knockdown was first assessed by western blotting, but this was again difficult to confirm due to low signal detection (Figure 16A). However, confocal imaging of the cells shows efficient knockdown of DP with siDPpool 72 h after transfection (Figure 16B). Following knockdown of DP in HB2 cells with siDPpool, the strength of cell-cell adhesion was assessed by dispase assay. The results show that siDP pool caused an apparent, albeit not significant, increase in adhesion in HB2PURO cells, and a decrease in adhesion in HB2CD82 cells (Figure 17). The latter data showed borderline significance (P= 0.0346). The treatment with both siDP and siDPpool resulted in an apparent decrease in adhesion in HB2CD82 cells as expected. However, this was not the case in control HB2PURO cells. Expressing the data as fold change relative to siCtrl transfection for each transfectant shows that there is a decrease in adhesion in HB2CD82 cells when compared to HB2PURO cells. Thus, the contradictory nature of the data, combined with lack of significance, means that no firm conclusion can be made about the role of DP in the CD82 mediated increase in cell-cell adhesion in HB2 cells.

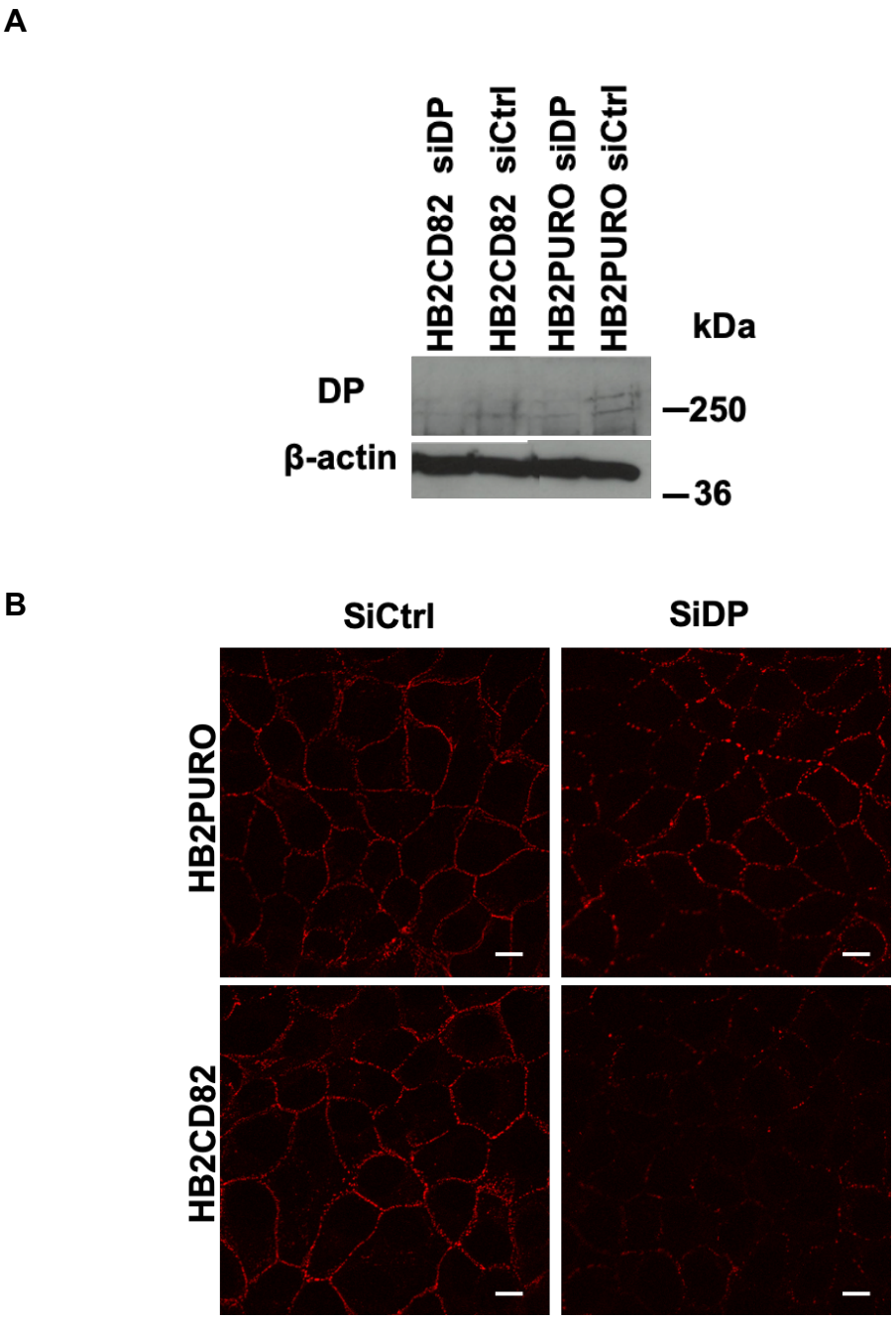

Figure 14 Knockdown of DP expression using siRNA.

(A) HB2PURO and HB2CD82 cells were reverse transfected with control siRNA oligos and oligos against DP. 72 h after transfection, the cells were lysed and expression of DP was assessed by western blot analysis using antibodies against DP and β-actin (loading control). (B) HB2PURO and HB2CD82 cells were reverse transfected on glass coverslips with control siRNA oligos and oligos against DP. 72 h after transfection the cells were fixed with methanol and stained with an anti-DP antibody. The cells were imaged using the same gain and offset settings. Scale bar, 10 μm. Data are from one experiment.

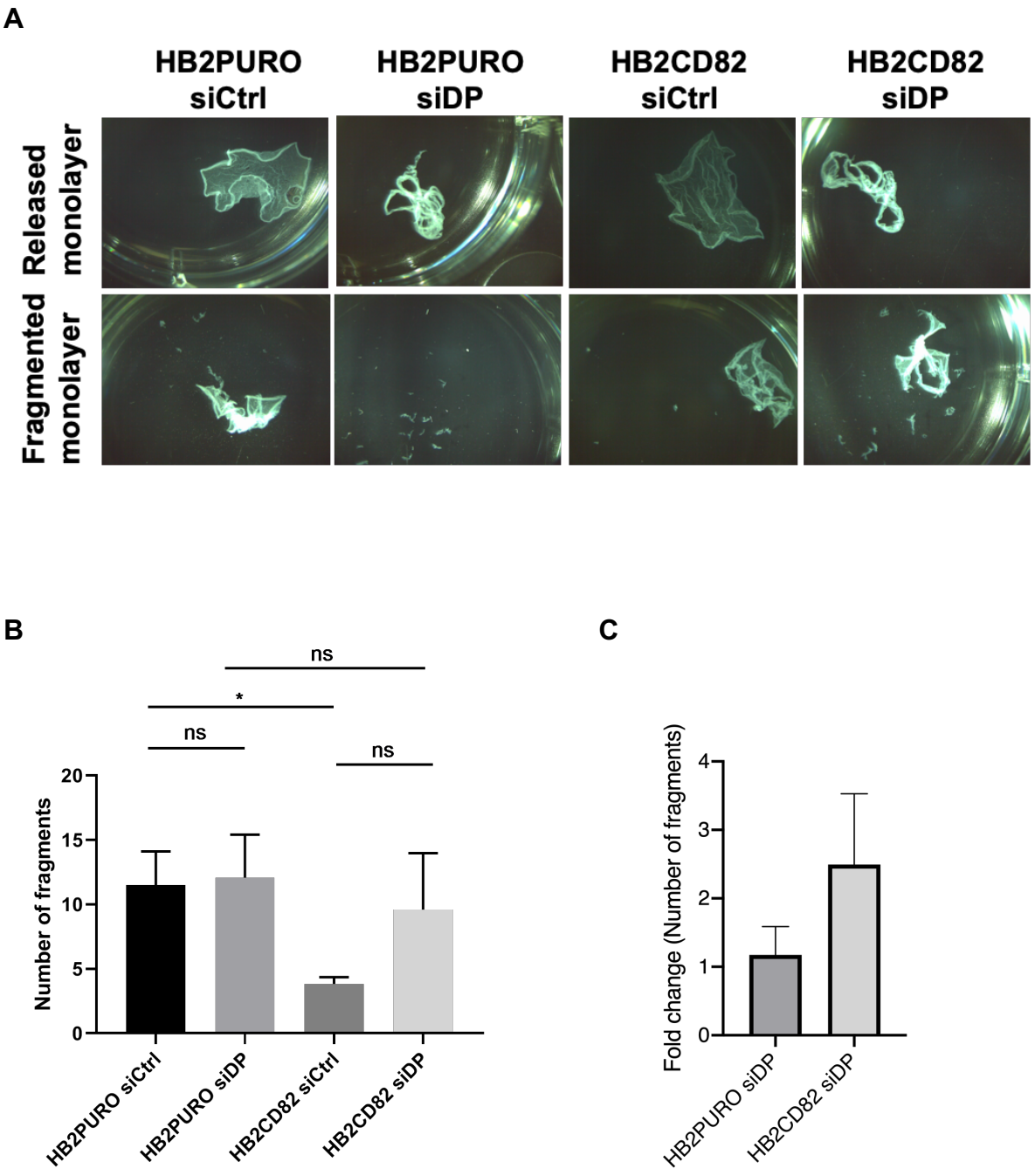

Figure 15 Knockdown of DP expression with siDP does not result in a decrease in adhesion.

(A) HB2PURO and HB2CD82 cells were reverse transfected with control (siCtrl) siRNA oligonucleotides (oligos) and with siRNA oligos against DP (siDP). 72 h after transfections the cells were treated with dispase and subjected to mechanical stress. Representative images are shown. (B) Quantification of the number of fragments. (C) Data from B expressed relative to siCtrl of each transfectant and expressed as fold change. Results are the mean, standard error, and t-test of three independent experiments (*P<0.05).

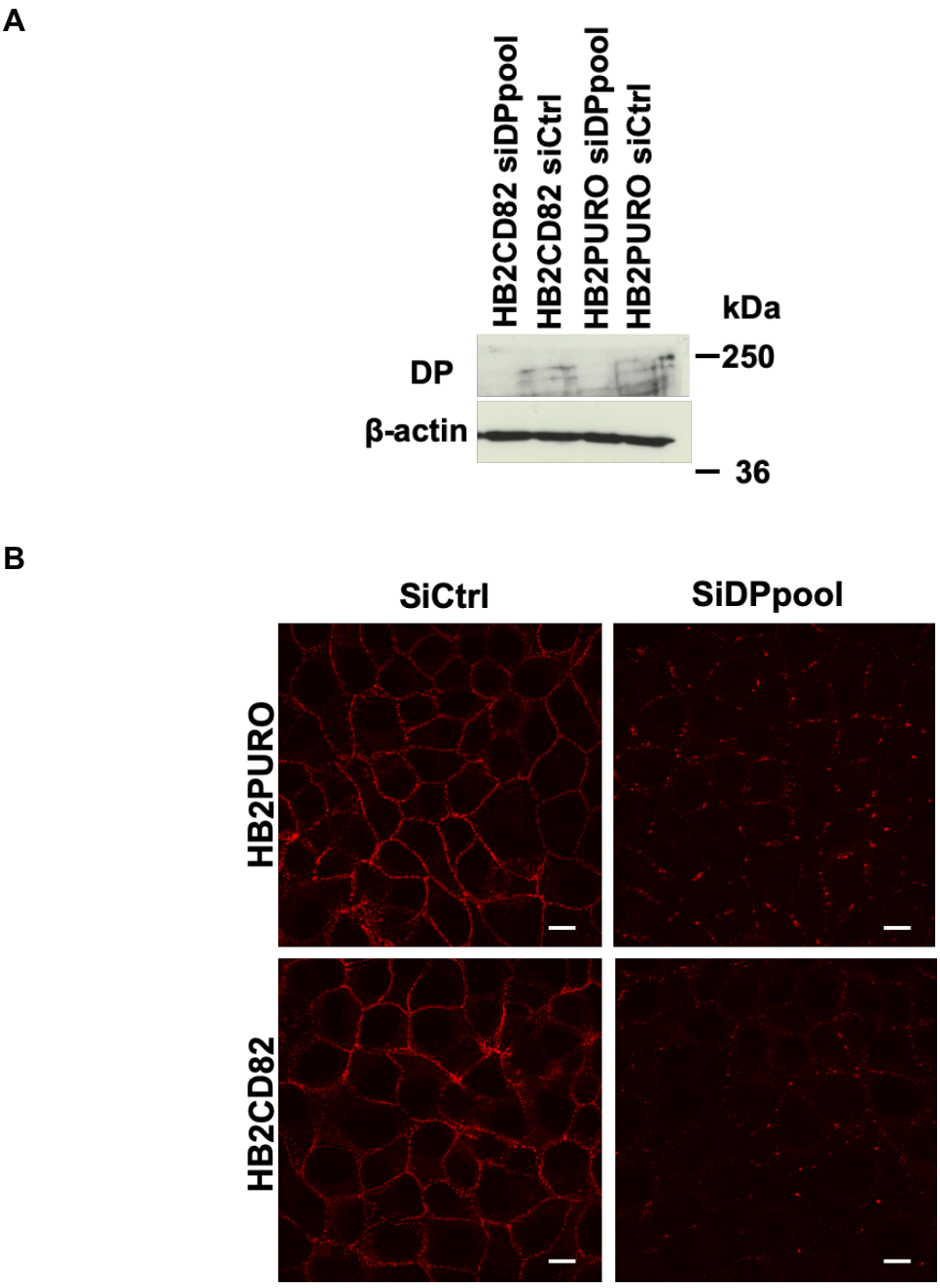

Figure 16 Knockdown of DP using a pool of siRNA oligonucleotides.

(A) HB2PURO and HB2CD82 cells were reverse transfected with control siRNA oligos and a pool of oligos against DP (siDPpool). 72 h after transfection, the cells were lysed and expression of DP was assessed by western blot analysis using antibodies against DP and β-actin (loading control). (B) HB2PURO and HB2CD82 cells were reverse transfected on coverslips with control siRNA oligos and a pool of oligos against DP. 72 h after transfection the cells were fixed with methanol and stained with an anti-DP antibody. The cells were imaged using the same gain and offset settings. Scale bar, 10 μm. Data are from one experiment.

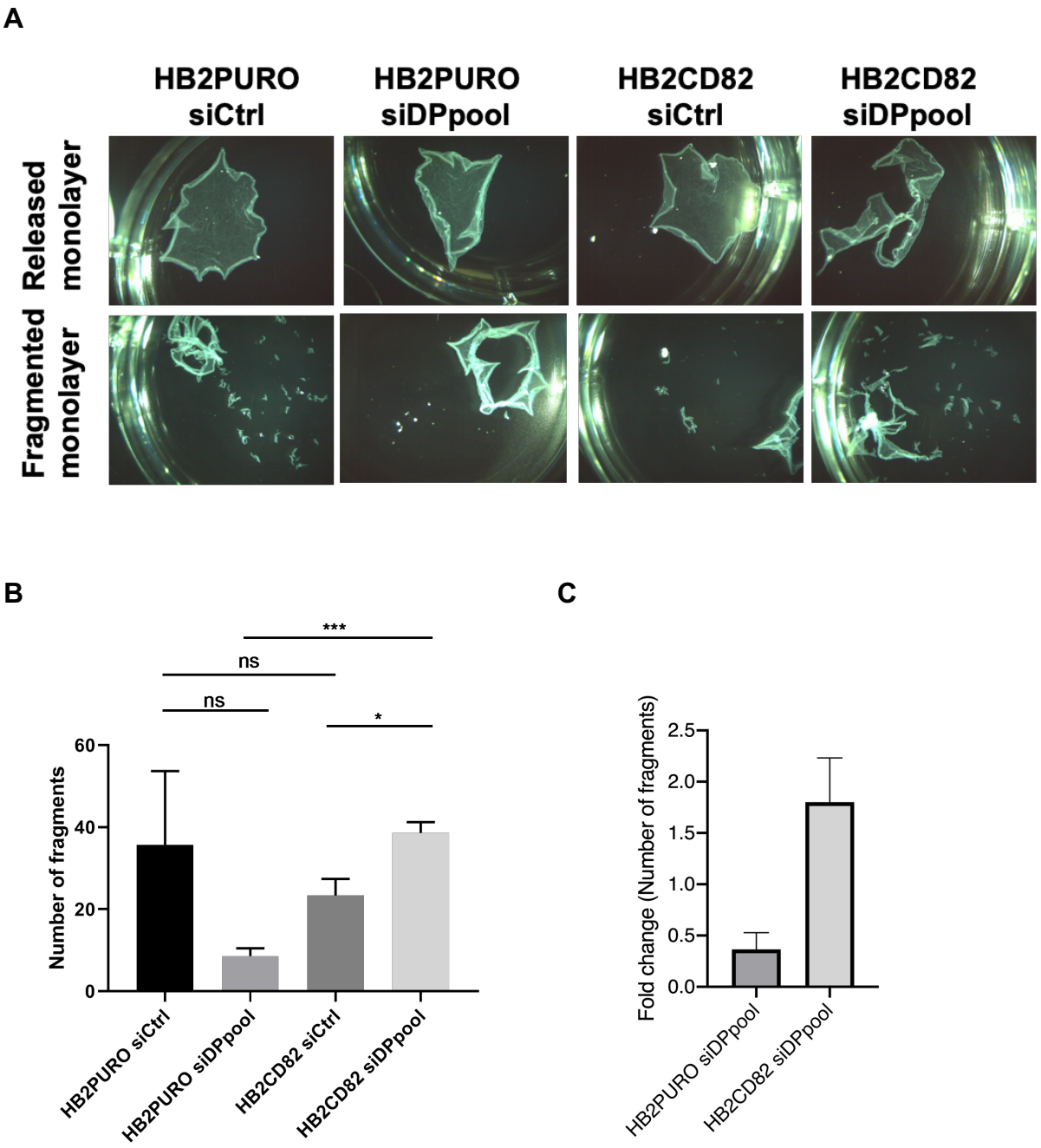

Figure 17 Knockdown of DP with siDP pool results in a decrease in adhesion in HB2CD82 cells.

(A) HB2PURO and HB2CD82 cells were reverse transfected with control (siCtrl) siRNA oligonucleotides (oligos) and with siRNA oligos against DP (siDPpool). 72 h after transfections the cells were treated with dispase and subjected to mechanical stress. Representative images are shown. (B) Quantification of the number of fragments. (C) Data from B expressed relative to siCtrl of each transfectant and expressed as fold change. Results are the mean, standard error, and t-test of three independent experiments (* $P<0.05$).

3.2.4 Depletion of PG does not result in an increase in cell migration in HB2 cells

During wound healing, desmosomal components are downregulated to facilitate cell migration (Garrod et al., 2005; McHarg et al., 2014). In addition, PG has been shown to suppress cell migration by strengthening cell-cell adhesion (Yin et al., 2005b). Having observed a decrease in the CD82 mediated increase in cell-cell adhesion in PG depleted HB2CD82 cells, gap closure assays were carried out to test whether depletion of PG results in increased cell migration. HB2PURO and HB2CD82 cells were initially reverse transfected with siPG and siCtrl oligos in 6 well plates. 48 h after transfection, the cells were counted and plated at a high density to ensure confluence the next day, in the chambers of a 35 mm Ibidi µ-Dish culture insert. 24 h after plating, the insert was removed, and the gap area, initially 500 µm, was imaged at specific time points over 24 h (Figure 18A). The gap area relative to the control gap area was then measured for each time point using ImageJ by thresholding the individual images to highlight the gap area.

The results show that there is no difference in cell migration between HB2PURO and HB2CD82 cells transfected with siCtrl at the time points studied, and it appears that HB2PURO and HB2CD82 cells migrate at a similar rate over the 24 h period. Overall knockdown of PG does not result in an increase in cell-migration in both HB2PURO and HB2CD82 cells (Figure 18B). Therefore, the CD82 mediated increase in cell-cell adhesion does not suppress cell migration. It may be that either knockdown of PG was not sufficient to show an effect on migration or that depletion of more than one desmosomal component is required for increased

migration.

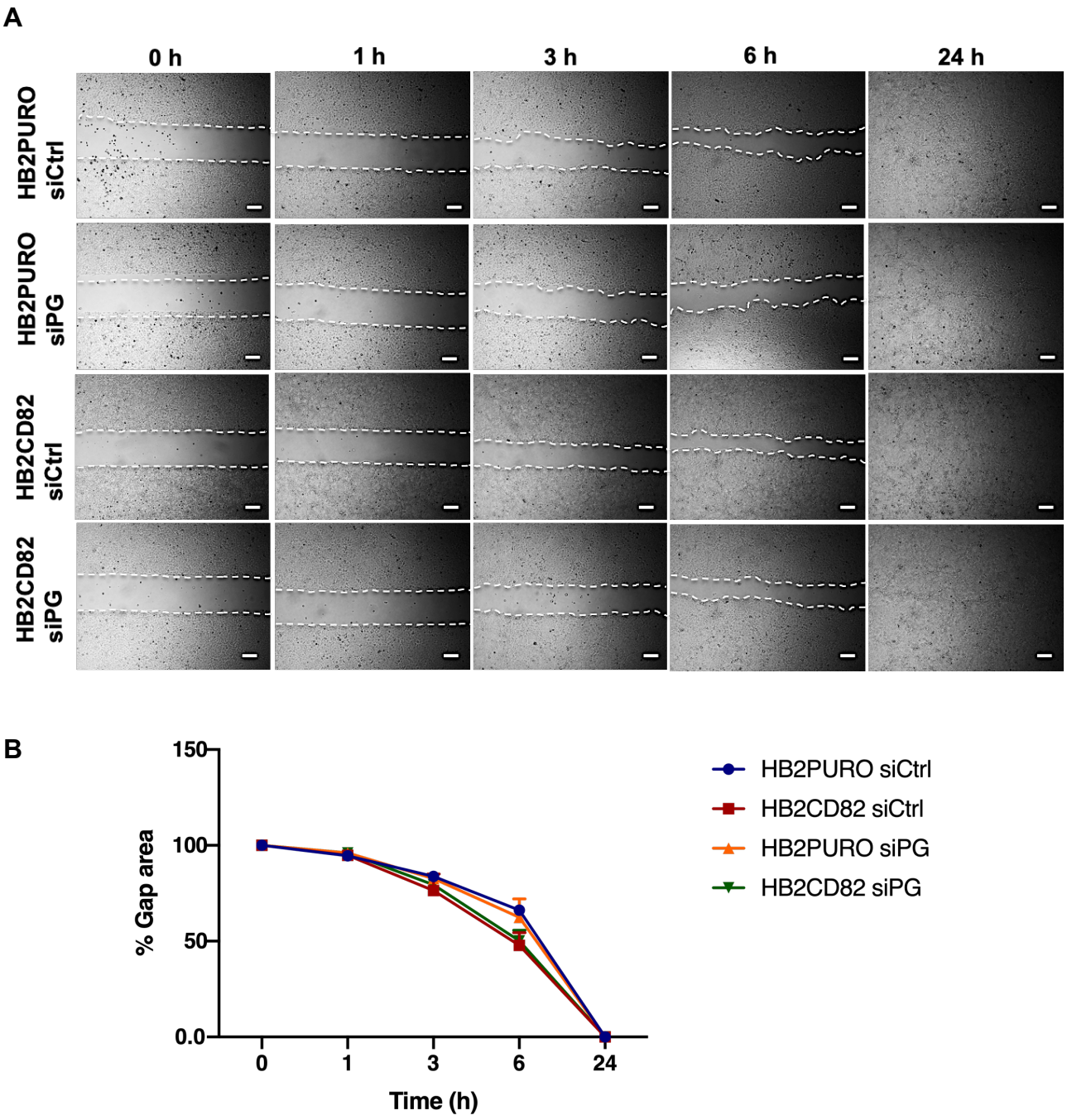

Figure 18 Gap-closure assay of PG depleted HB2 cells.

(A) HB2PURO and HB2CD82 were reverse transfected with control (siCtrl) oligos and oligos against PG (siPG). 48 h after transfection the cells were trypsinised and seeded in the chambers of the insert. The insert was removed 24 h after seeding to allow cells to close the gap. Representative images were taken at the indicated time points after removal of the insert. Scale bars, 200 µm. (B) Quantification of % gap area at the indicated time points. Data are the mean and standard deviation of two independent experiments.

3.2.5 E-cadherin and β-catenin are not upregulated in response to knockdown of desmosomal proteins

It is possible that upregulation of adherens junction proteins occurs in response to knockdown of desmosomal proteins, compensating, at least to some extent, for the lack of the latter in adhesion assays. Therefore, I investigated whether E-cadherin and β-catenin are upregulated in response to knockdown of PG, DSG2 and DP. HB2PURO and HB2CD82 cells were reverse transfected with siRNA oligos against PG (siPG), DSG2 (siDSG2) and DP (siDP). The cells were lysed 72 h after transfection and expression levels of E-cadherin and β-catenin were analysed by western blotting. Densitometric analysis of the western blots shows that expression of the adherens junction proteins, E-cadherin and β-catenin is unchanged following knockdown of PG, DSG2 and DP (Figure 19).

To analyse the localisation of E-cadherin and β-catenin following depletion of PG, DSG2 and DP, HB2PURO and HB2CD82 cells were reverse transfected with siPG, siDSG2 and siDP on glass coverslips. The cells were fixed 72 h after transfection and stained with anti-E-cadherin and anti-β-catenin antibodies. The cells were then imaged with a confocal microscope. The images obtained show that the localisation of E-cadherin and β-catenin is unchanged in PG, DSG2 and DP depleted control and CD82 overexpressing HB2 cells (Figure 20). These data indicate that knockdown of desmosomal components in HB2 cells does not result in a change of expression or localisation of E-cadherin and β-catenin.

A

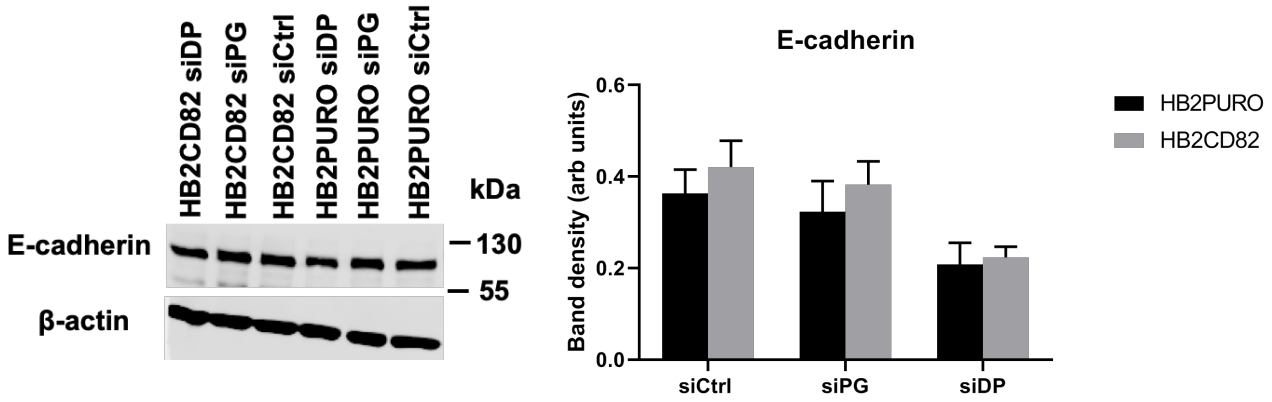
HB2CD82 siDP
HB2CD82 siPG
HB2CD82 siCtrl
HB2PURO siDP
HB2PURO siPG
HB2PURO siCtrl
kDa
E-cadherin
130
55
β-actin
E-cadherin
Band density (arb units)
0.6
0.4
0.2
0.0
siCtrl
siPG
siDP
HB2PURO
HB2CD82

B

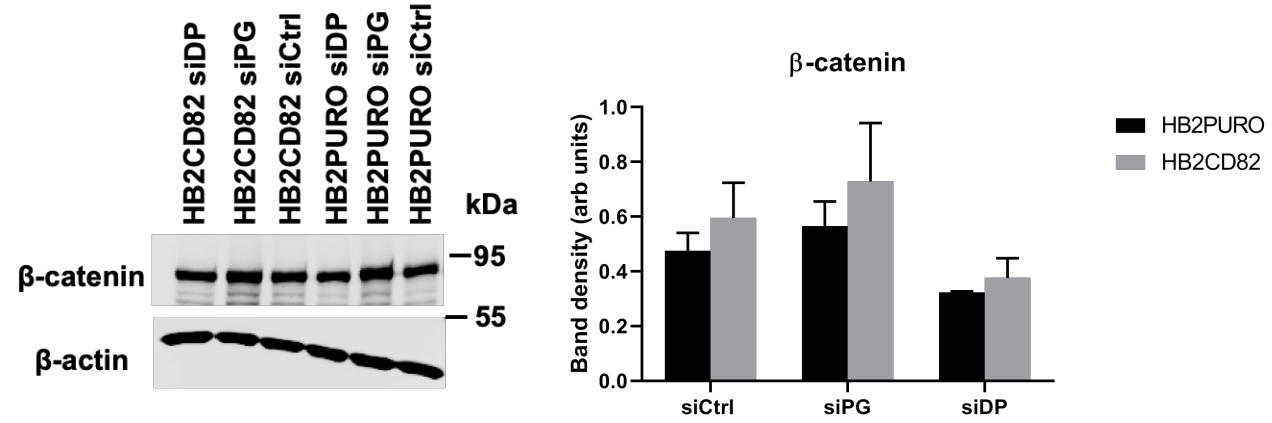
HB2CD82 siDP
HB2CD82 siPG
HB2CD82 siCtrl
HB2PURO siDP
HB2PURO siPG
HB2PURO siCtrl
kDa
β-catenin
95
55
β-actin
β-catenin
Band density (arb units)
1.0
0.8
0.6
0.4
0.2
0.0
siCtrl
siPG
siDP
HB2PURO
HB2CD82

C

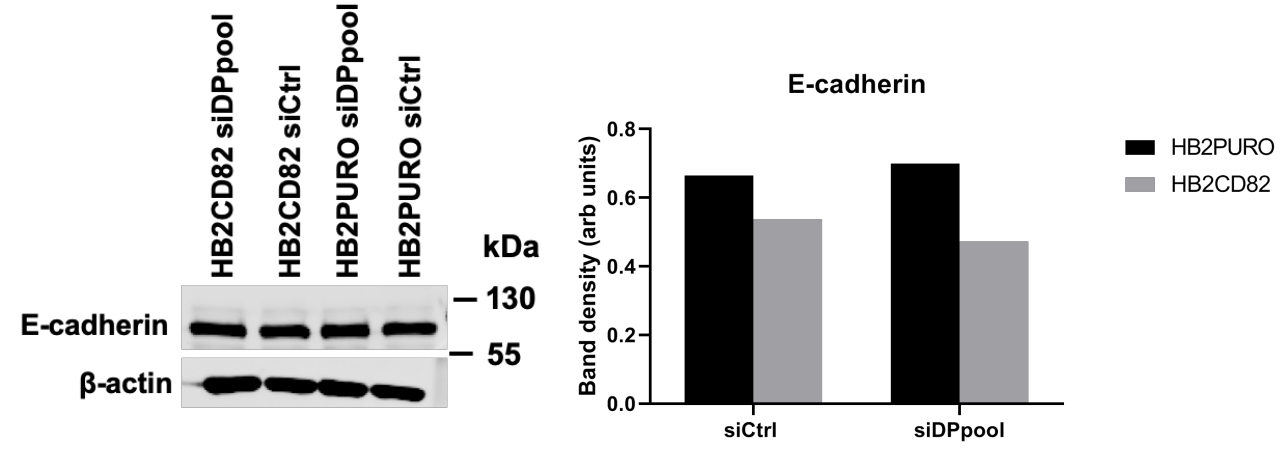
HB2CD82 siDPpool
HB2CD82 siCtrl
HB2PURO siDPpool
HB2PURO siCtrl
kDa
E-cadherin
130
55
β-actin
E-cadherin
Band density (arb units)
0.8
0.6
0.4
0.2
0.0
siCtrl
siDPpool
HB2PURO
HB2CD82

D

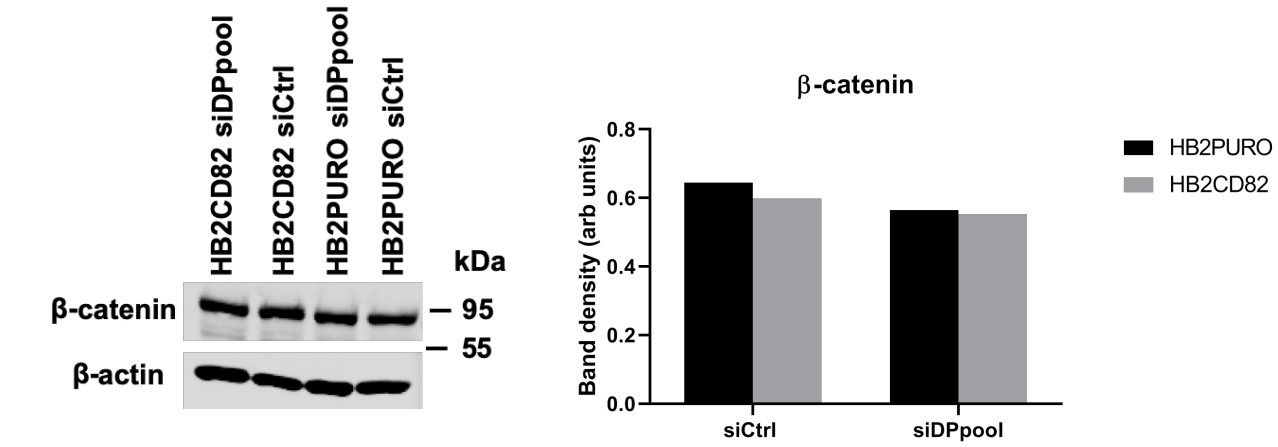
HB2CD82 siDPpool
HB2CD82 siCtrl
HB2PURO siDPpool
HB2PURO siCtrl
kDa
β-catenin
95
55
β-actin
β-catenin
Band density (arb units)
0.8
0.6
0.4
0.2
0.0
siCtrl
siDPpool
HB2PURO
HB2CD82

E

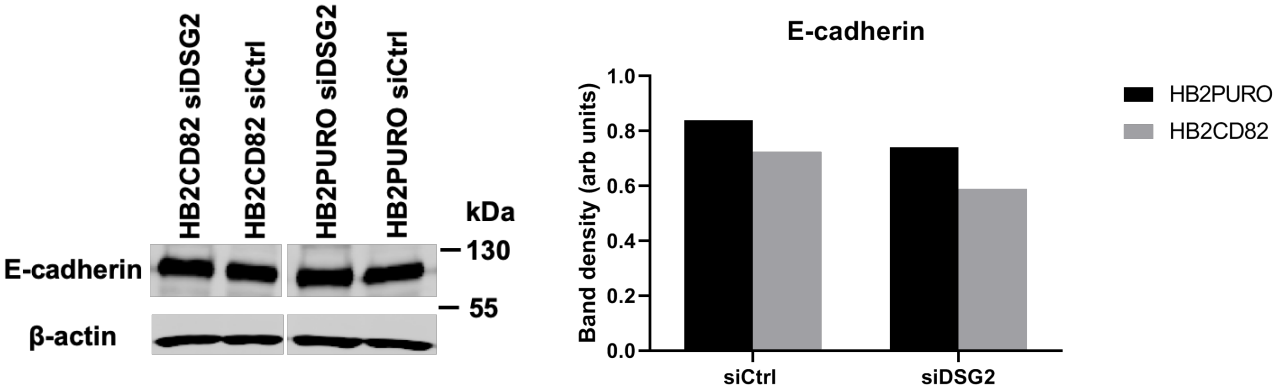
HB2CD82 siDSG2
HB2CD82 siCtrl
HB2PURO siDSG2
HB2PURO siCtrl
kDa
E-cadherin
130
55
β-actin
E-cadherin
Band density (arb units)
1.0
0.8
0.6
0.4
0.2
0.0
siCtrl
siDSG2
HB2PURO
HB2CD82

F

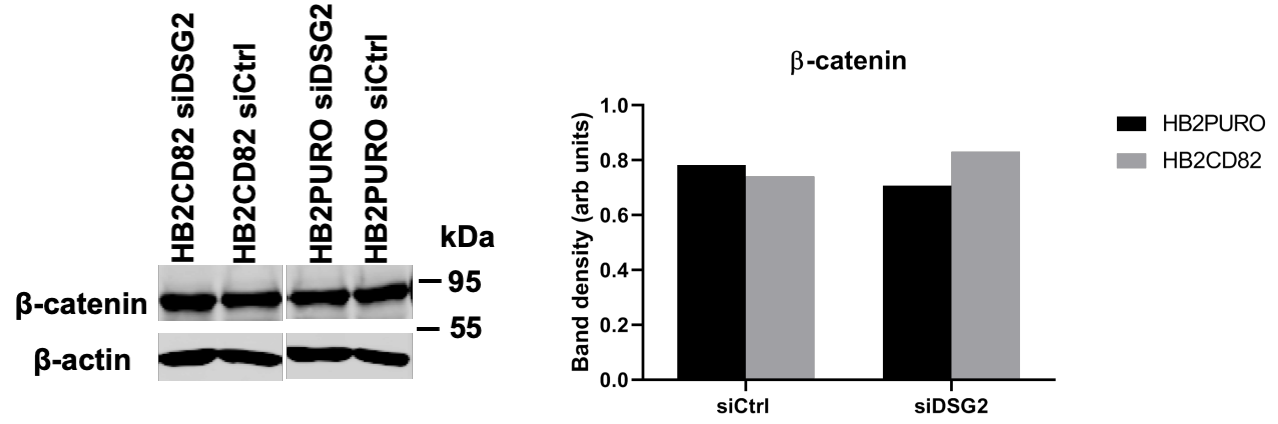
HB2CD82 siDSG2
HB2CD82 siCtrl
HB2PURO siDSG2
HB2PURO siCtrl
kDa
β-catenin
95
55
β-actin
β-catenin
Band density (arb units)
1.0
0.8
0.6
0.4
0.2
0.0
siCtrl
siDSG2
HB2PURO
HB2CD82

Figure 19 Expression of adherens junction proteins is unchanged in PG, DSG2, DP depleted HB2 cells.

HB2PURO and HB2CD82 cells were reverse transfected with control siRNA oligos (siCtrl) and with oligos against PG (siPG) and DP (siDP) (A-B), DP with a pool of oligos (C-D), and DSG2 (E-F). The cells were lysed 72 h after transfection and the expression of the adherens junction proteins E-cadherin and β-catenin were assessed by western blotting. Western blots were quantified by densitometry and normalised with respect to β-actin. Results are mean (and standard error) of three (A-B), two (C-D), and one (E-F) independent experiment(s).

A

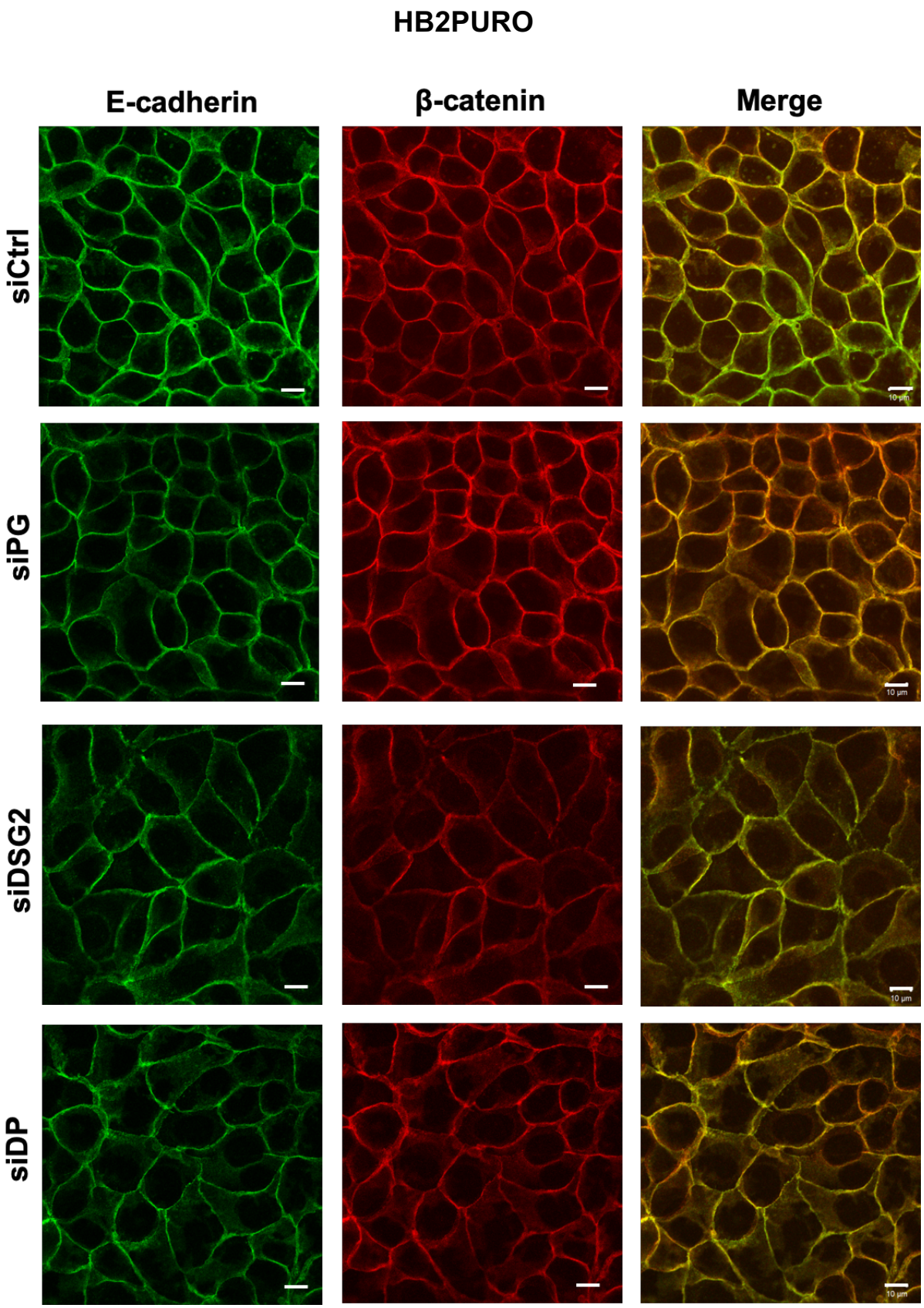
HB2PURO
E-cadherin
β-catenin
Merge
siCtrl
siPG
siDSG2
siDP
10 µm

B

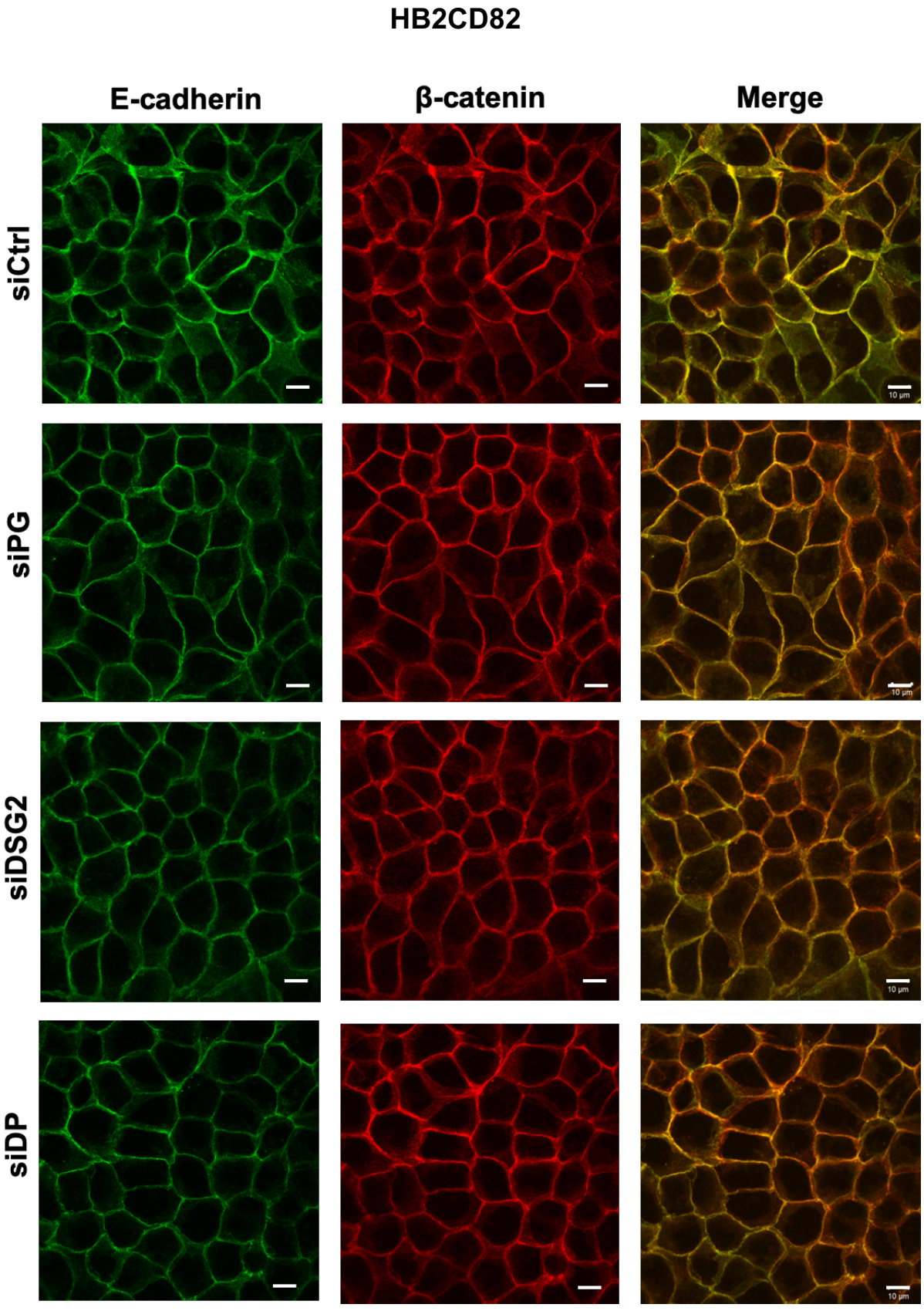
HB2CD82
E-cadherin
β-catenin
Merge
siCtrl
siPG
siDSG2
siDP
10 µm

Figure 20 Localisation of E-cadherin and β-catenin in PG, DSG2 and DP depleted HB2 cells.

(A) HB2PURO and (B) HB2CD82 cells were reverse transfected on glass coverslips with control (siCtrl) oligos, and oligos against PG (siPG), DP (siDP) and DSG2 (siDSG2). 72 h after transfection, cells were fixed with methanol and stained with anti-E-cadherin and anti- β-catenin antibodies. Scale bars, 10 μm. Images are from one experiment.

3.2.6 Knockdown of E-cadherin results in a decrease in cell-cell adhesion in both control and CD82 overexpressing HB2 cells

Next, the study was expanded to examine adherens junction mediated adhesion in HB2 cells, as CD82 has been shown to strengthen E-cadherin and β-catenin interactions (Abe et al., 2008; Chigita et al., 2012). To assess whether E-cadherin and β-catenin contribute to the CD82 mediated increase in cell-cell adhesion, HB2PURO and HB2CD82 cells were reverse transfected with siRNA oligos against E-cadherin (siEcad) and β-catenin (si-βcat). The cells were lysed 72 h after transfection and western blot analysis was first carried out to assess the level of knockdown. Densitometric analysis of the western blots shows 81-83% knockdown E-cadherin and 76-90% knockdown of β-catenin in HB2PURO and HB2CD82 cells (Figure 21).

Dispase assays were carried out 72 h after transfection as above, and the results from the dispase assays indicate that knockdown of E-cadherin attenuates the CD82 mediated increase in cell-cell adhesion, resulting in a decrease in adhesion (Figure 22). There was also decrease in adhesion in HB2PURO cells in response to E-cadherin depletion. Expressing the data as fold change shows that there is a greater reduction in cell-cell adhesion in HB2CD82 cells (Figure 22C). However, knockdown of β-catenin did not have an effect on the strength of cell-cell adhesion in both HB2PURO and HB2CD82 cells (Figure 23), but there was a large variation in the number of fragments generated between experiments. This is also evident when the data is expressed as fold change (Figure 23C). When the data is

expressed relative to siCtrl transfetions, there is a greater decrease in cell-cell adhesion in HB2CD82 cells.

Western blot analysis revealed that the expression of desmosomal proteins PG and DSG2 is not upregulated following depletion of E-cadherin and β-catenin in both HB2PURO and HB2CD82 cells (Figure 24). Further to this, immunofluorescence and confocal microscopy analysis of the cells showed that the localisation of PG and DP was also unaffected in these cells (Figure 25). This suggests that desmosomal proteins are not upregulated in response to knockdown of E-cadherin and β-catenin in HB2 cells, and probably do not compensate for loss of E-cadherin and β-catenin.

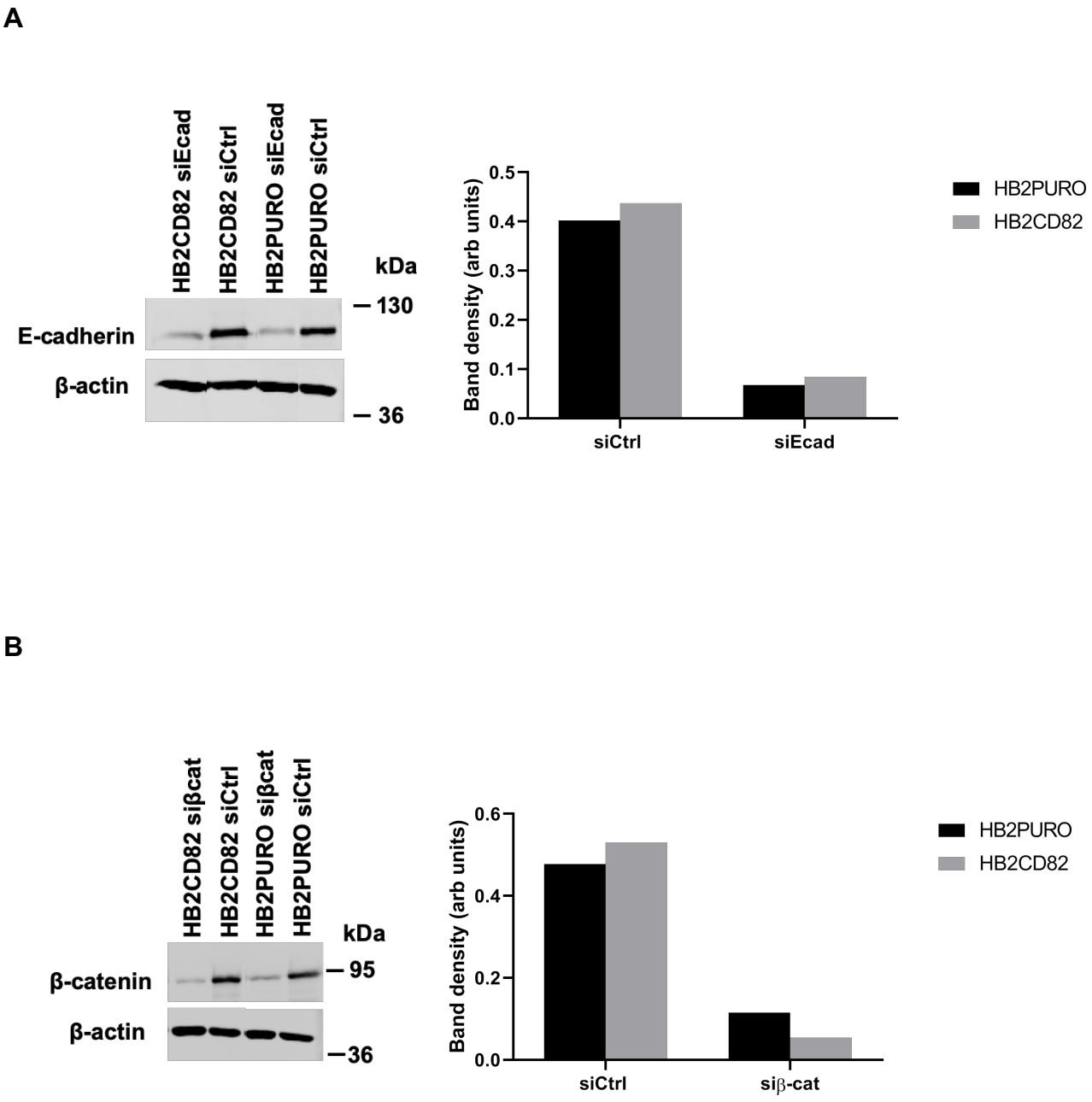

Figure 21 Transient knockdown of E-cadherin and β-catenin expression using siRNA.

HB2PURO and HB2CD82 cells were transfected with siRNA oligonucleotides against E-cadherin and β-catenin and non-silencing control oligonucleotides (siCtrl). Lysates were prepared 72 h after transfection and the level of knockdown was assessed by western blotting using antibodies against E-cadherin (A), β-catenin (B) and β-actin (loading control). Western blots were quantified by densitometry and normalised with respect to β-actin. Data presented are from one experiment.

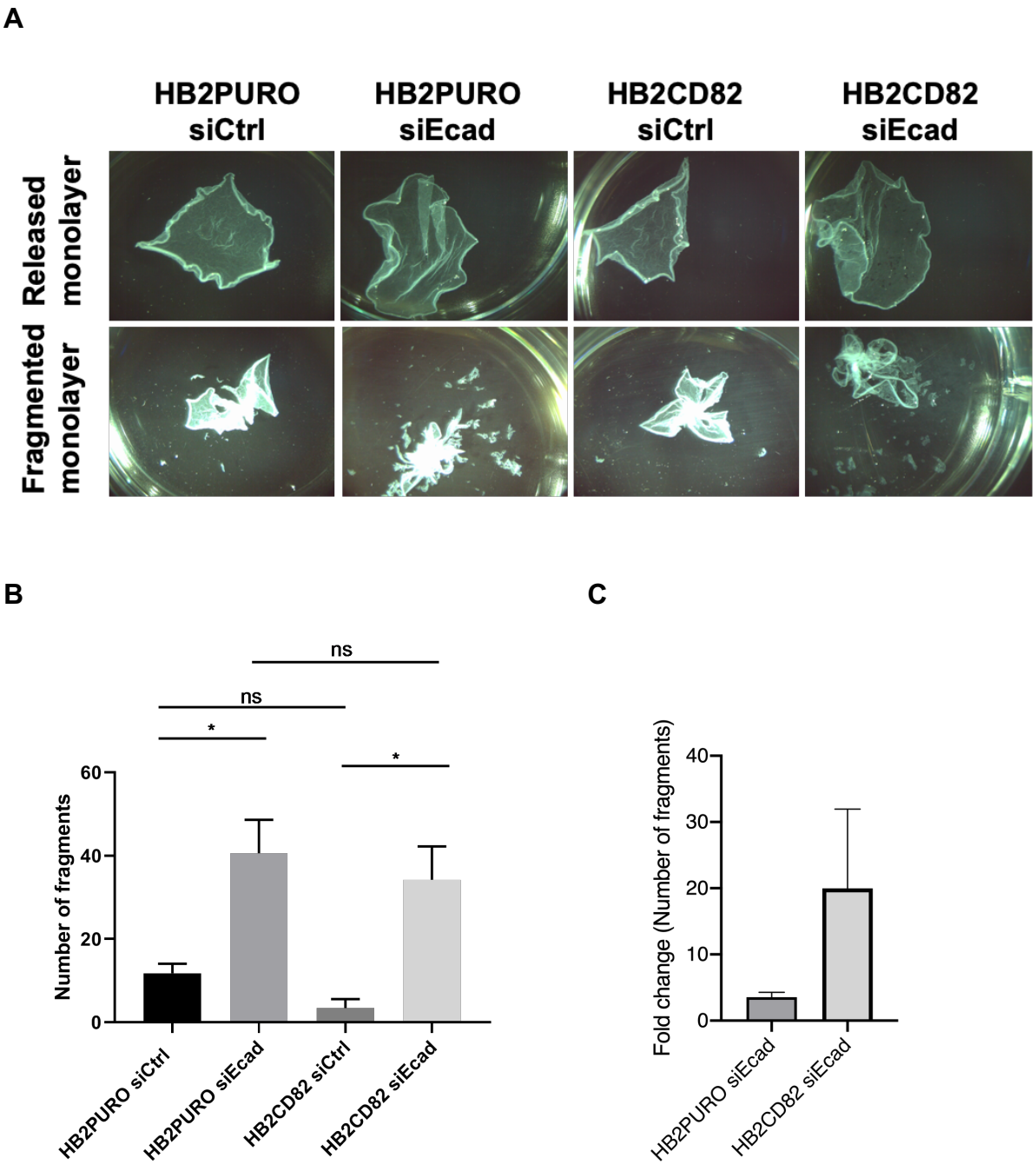

Figure 22 E-cadherin contributes to the CD82 mediated increase in cell-cell adhesion.

(A) HB2PURO and HB2CD82 cells were reverse transfected with control (siCtrl) siRNA oligonucleotides (oligos) and with siRNA oligos against E-cadherin (siEcad). 72 h after transfections the cells were treated with dispase and subjected to mechanical stress. Representative images are shown. (B) Quantification of the fragments generated. (C) Data from B expressed relative to siCtrl of each transfectant and expressed as fold change. Results are the mean, standard error, and t-test of three independent experiments (* $P<0.05$).

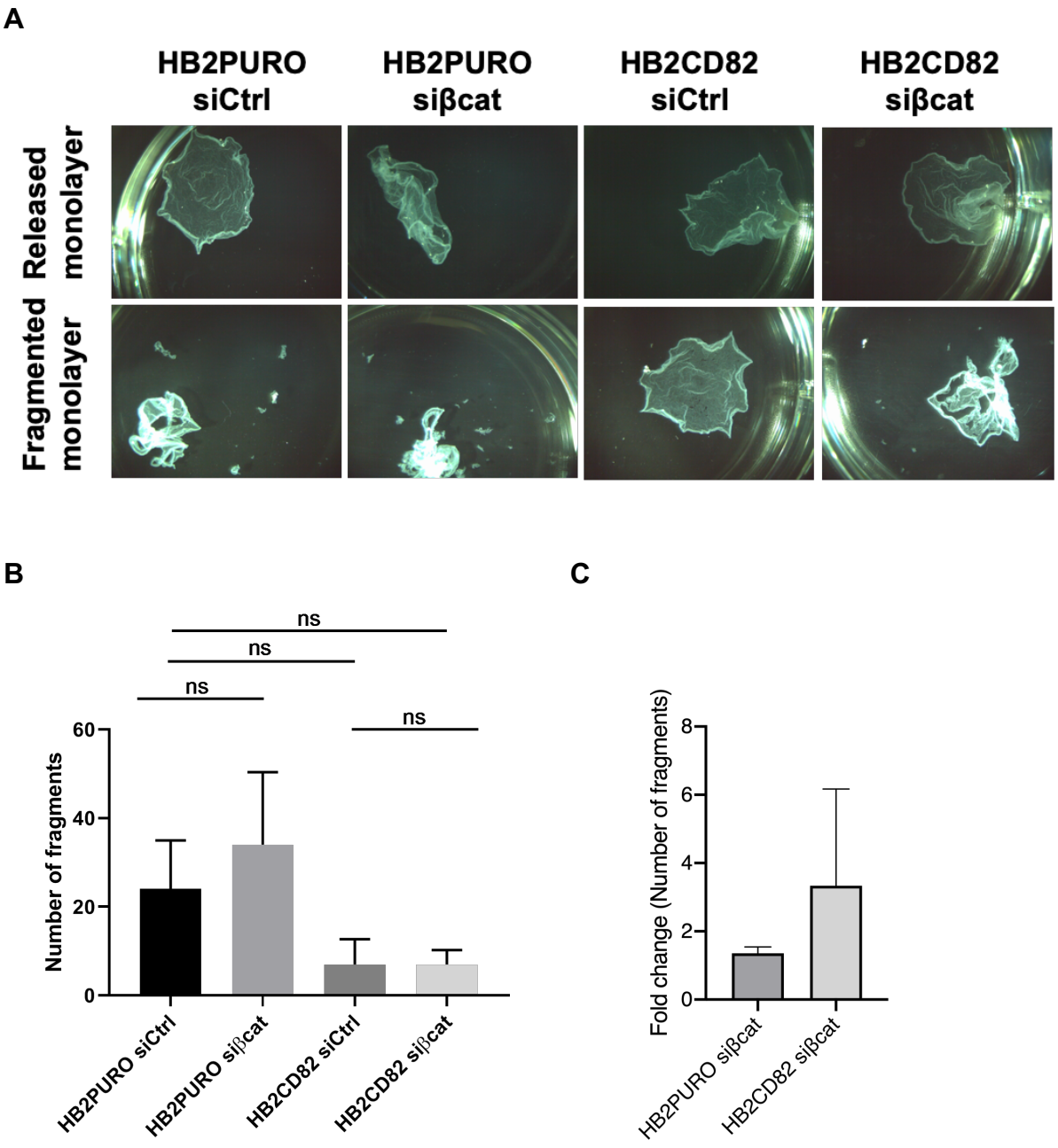

Figure 23 β-catenin does not contribute to the CD82 mediated increase in cell-cell adhesion.

(A) HB2PURO and HB2CD82 cells were reverse transfected with control (siCtrl) siRNA oligonucleotides (oligos) and with siRNA oligos against β-catenin (siβ-cat). 72 h after transfections the cells were treated with dispase and subjected to mechanical stress. Representative images are shown. (B) Quantification of the number of fragments. (C) Data from B expressed relative to siCtrl of each transfectant and expressed as fold change. Results are the mean, standard error, and t-test of three independent experiments.

A

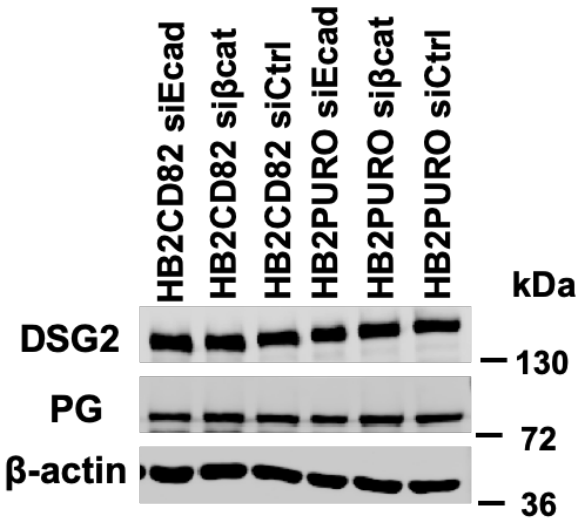

B

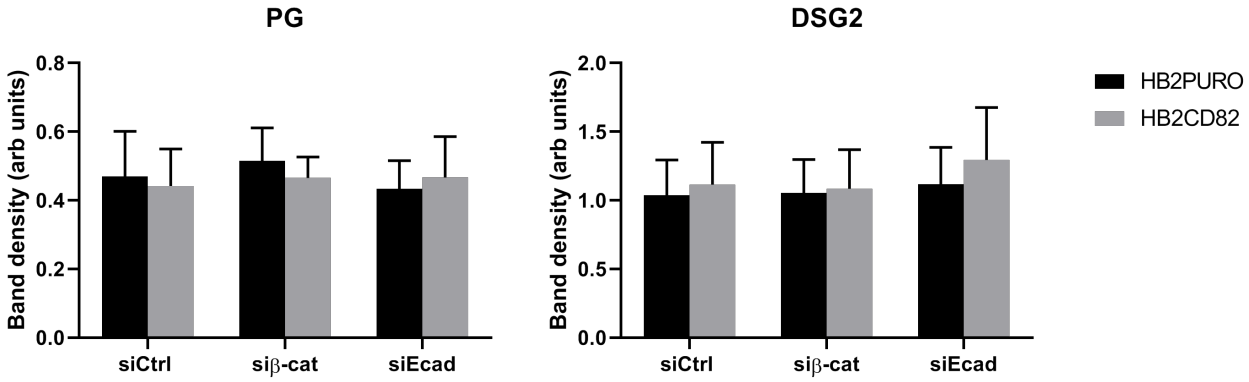

Figure 24 Expression levels of desmosomal proteins are unchanged in E-cadherin and β-catenin depleted cells.

(A) HB2PURO and HB2CD82 cells were reverse transfected with control siRNA oligos (siCtrl) and with oligos against E-cadherin (siEcad) and β-catenin (siβ-cat). The cells were lysed 72 h after transfection and the expression of the desmosomal proteins was assessed by western blotting with anti-DSG2, anti-PG, and anti-β-actin antibodies. Western blots were quantified by densitometry and normalised with respect to β-actin. Representative western blots are shown. Results are the mean and standard error or of three independent experiments.

A

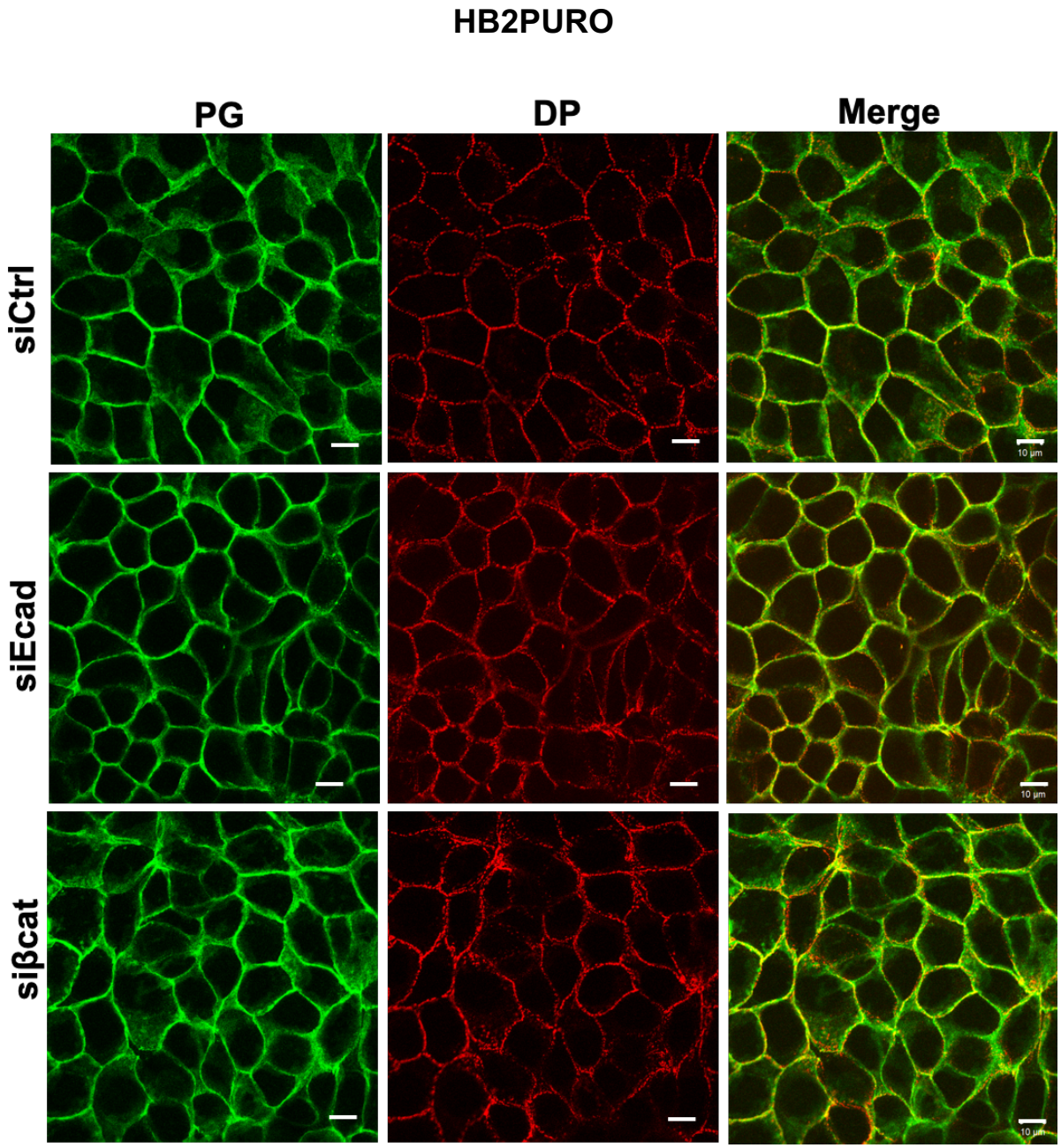

B

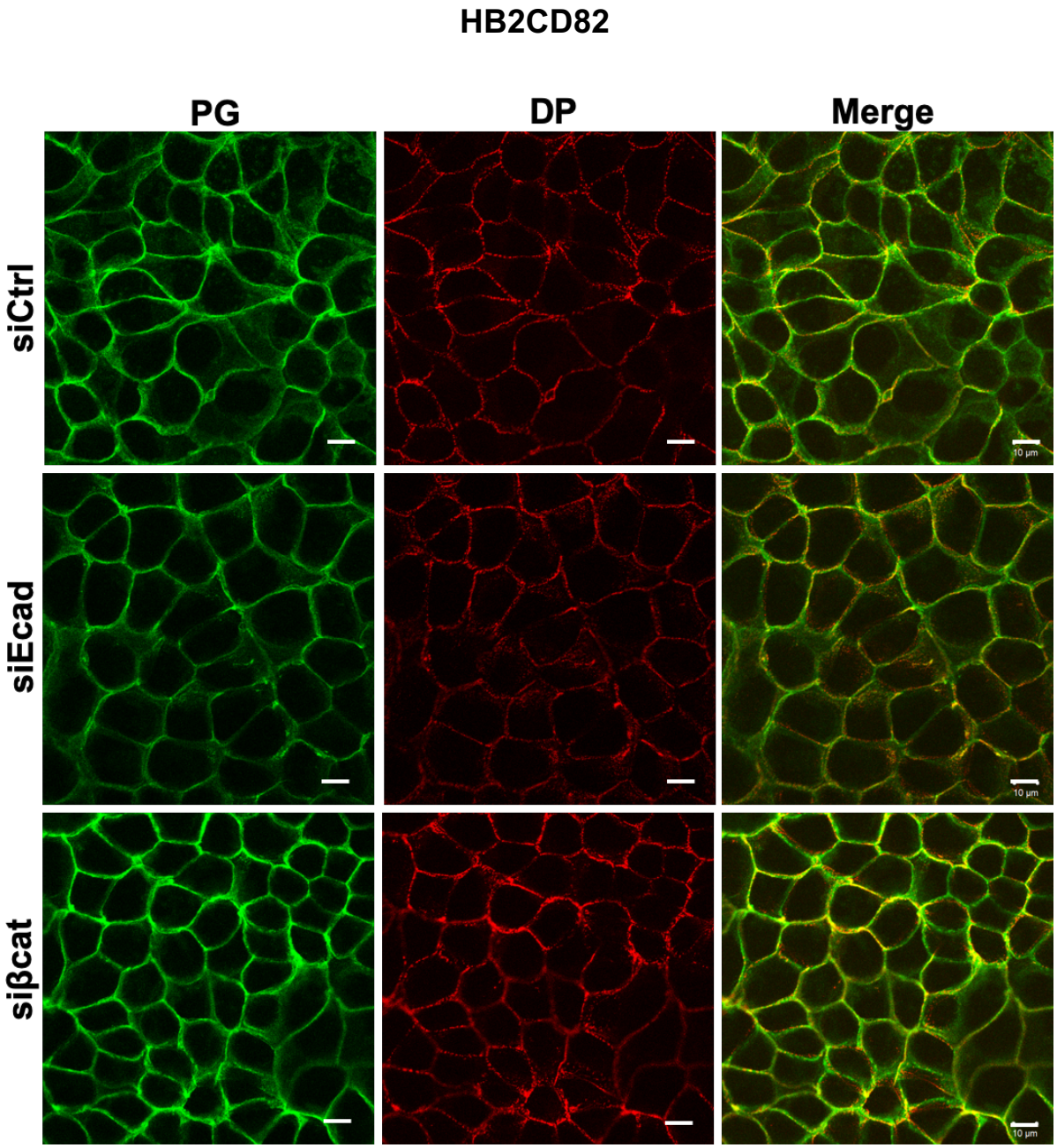

Figure 25 Localisation of PG and DP is unaffected in E-cadherin and β-catenin depleted HB2 cells.

(A) HB2PURO and (B) HB2CD82 cells were reverse transfected on glass coverslips with control (siCtrl) oligos, and oligos against β-catenin (siβ-cat) and E-cadherin (siEcad). 72 h after transfection, cells were fixed with methanol and stained with anti-PG and anti-DP antibodies. Scale bars, 10 µm. Images are from one experiment.

3.2.7 CD82 increases both DSG2 and E-cadherin mediated adhesion

Previous data (section 3.2.2 or 3.2.6) showed that depletion of DSG2 and E-cadherin attenuated the CD82 mediated increase in cell-cell adhesion. DSG2 and E-cadherin are members of the desmosomal and classical cadherin family, respectively. They are the transmembrane components of their respective junctions. To investigate whether CD82 increases both DSG2 and E-cadherin mediated adhesion, HB2PURO and HB2CD82 cells were simultaneously transfected with siDSG2 and siEcad oligos, and non-silencing control oligos. The cells were treated with dispase 72 h after transfection and subjected to mechanical stress to assess their adhesive strength. The results show that double knockdown of DSG2 and E-cadherin results in a decrease in cell-cell adhesion in both HB2PURO cells and HB2CD82 cells (Figure 26). HB2CD82 cells treated with siDSG2 and siEcad appear more adhesive than HB2PURO cells based on the number of fragments generated. Expressing the data as fold change relative to siCtrl transfections shows that the decrease in adhesion is slightly greater in HB2CD82 cells (Figure 26C). These data indicate that CD82 strengthens both DSG2 and E-cadherin mediated adhesion.

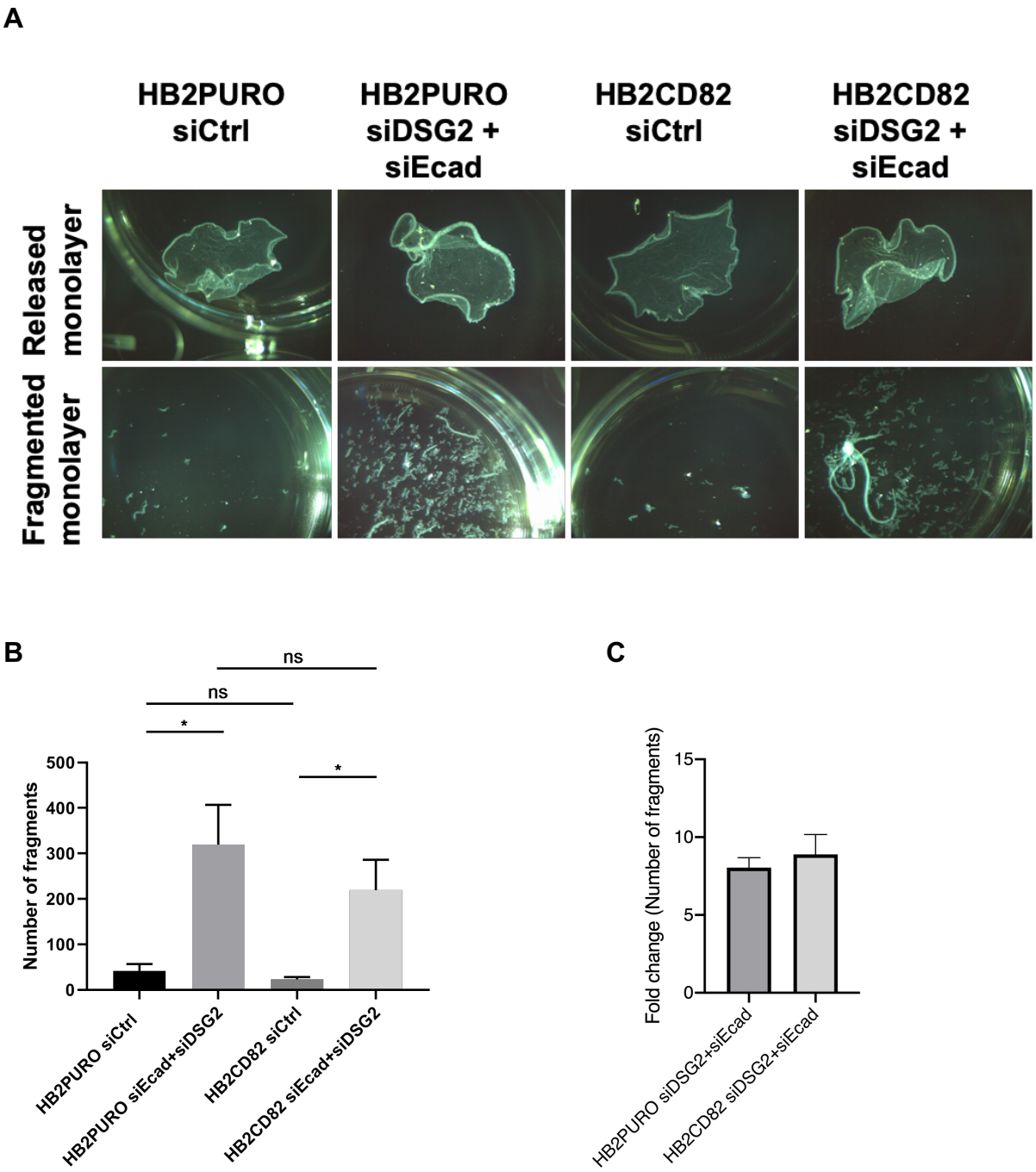

Figure 26 CD82 increases both DSG2 and E-cadherin mediated adhesion.

(A) HB2PURO and HB2CD82 cells were reverse transfected with control (siCtrl) siRNA oligonucleotides (oligos) and simultaneously with siRNA oligos against DSG2 (siDSG2) and E-cadherin (siEcad). 72 h after transfections the cells were treated with dispase and subjected to mechanical stress. Representative images are shown. (B) Quantification of the fragments generated. (C) Data from B expressed relative to siCtrl of each transfectant and expressed as fold change. Results are the mean, standard error, and t-test of three independent experiments (* $P<0.05$).

3.3 Discussion

A number of studies have demonstrated a role for CD82 in cell-cell adhesion (Jee et al., 2003; Abe et al., 2008; Lee et al., 2018). Transfection of CD82 into prostate cancer cells results in an increase in homotypic cell aggregation (Jee et al., 2003). CD82 has also been shown to specifically increase E-cadherin mediated adhesion by strengthening E-cadherin-β-catenin interactions at the membrane (Abe et al., 2008). A recent study demonstrated that CD82 upregulates the expression of E-cadherin by decreasing Snail expression in human prostate cancer cell lines (Lee et al., 2018), and this also resulted in increased β-catenin membrane localisation and stronger cell-cell adhesion. The data generated in my study is consistent with these findings in that CD82 increases cell-cell adhesion. Overexpression of CD82 in HB2 cells results in increased cell-cell adhesion (Figure 9), and knockdown of E-cadherin attenuated the CD82 mediated increase in cell-cell adhesion (Figure 22). This further supports a role for CD82 in cadherin mediated adhesion.

The results obtained with the palmitoylation deficient mutant of CD82 suggest that the formation of tetraspanin enriched microdomains is not required for the CD82 mediated increase in cell-cell adhesion (Figure 9). Overexpression of the N-terminal deletion mutant of CD82 appeared to impair cell-cell adhesion but was not statistically significant. It has been proposed that the N- and C- termini of tetraspanins might mediate tetraspanin interactions with cytoplasmic signalling proteins, such as PKCα and β-catenin (Zhang et al., 2001). This has been demonstrated for the tetraspanin CD53, as the interaction between this tetraspanin and PKCβ is mediated by the N-terminus of CD53 (Zuidscherwoude et al., 2017).

The results suggest that the N-terminus of CD82 does not directly contribute to the CD82 mediated increase in cell-cell adhesion but could perhaps be involved in initiating changes in signalling in response to mechanical stress.

Depletion of the desmosomal proteins PG and DSG2 in HB2CD82 cells attenuated the CD82 mediated increase in cell-cell adhesion (Figure 12,13). The expression and localisation patterns of E-cadherin and β-catenin were unaffected upon knockdown of PG and DSG2. These results indicate that CD82 promotes desmosomal adhesion, and that knockdown of desmosomal proteins does not result in compensatory increases in expression of adherens junction proteins. Stronger cell-cell adhesion in CD82 overexpressing HB2 cells did not correlate with a decrease in cell migration (Figure 18) which might have been expected given that desmosomal components are downregulated to facilitate cell migration during wound healing (Garrod et al., 2005; McHarg et al., 2014).

The results obtained following knockdown of DP are difficult to interpret (Figure 15, 17). Knockdown of DP with the siDP oligo had no effect on HB2PURO cells but resulted in a decrease in adhesion in HB2CD82 cells, though this was not statistically significant. However, knockdown with a set of oligos targeting different sequences in DP (siDPpool) resulted in an apparent increase in adhesion in HB2PURO cells and a decrease in adhesion of borderline significance in HB2CD82 cells. Based on these results no firm conclusion could be drawn on the role of DP in the CD82 mediated increase in cell-cell adhesion. DP is required for normal desmosomal adhesion. DP knockout mouse embryos die early during

development from adhesive defects (Gallicano et al., 1998). The keratin filament-desmosome links are compromised in these embryos. Consistent with this, failure in attachment to keratin intermediate filaments and weakening of the epidermis is observed in epidermis specific DP knockout mice (Vasioukhin et al., 2001). Other plaque proteins are unable to sufficiently anchor keratin intermediate filaments in the absence of DP. These studies highlight the importance of DP in cell-cell adhesion and the maintenance of tissue integrity. It should be noted that there is one report in the literature that suggests that DP is not essential for cell adhesion Sumigray and Lechler (2012). In this study the authors specifically knocked out DP in the intestinal epithelium of mice. The mice did not exhibit defects in the organisation of the intestinal epithelium and the authors concluded that cell-cell adhesion was unaffected by lack of DP. This may be the case, but it may simply be that intestinal epithelial cells are not subjected to the strong mechanical forces that are experienced in other tissues such as the epidermis and heart. Furthermore, the authors did not perform adhesion assays to determine whether the loss of DP actually affected the adhesiveness of cells. Nevertheless, it is possible that the role of DP may vary depending on the tissue in question. However, in my study it is more likely that the contradictory results obtained with the DP siRNA are due to the variability of the dispase assays, which was a problem with all of the dispase assays presented in this chapter and in chapter 4. This variability is also highlighted when the data are expressed as fold change relative to the control of each experiment. Further, the level of knockdown achieved with the siRNA oligonucleotides was not checked for each individual

experiment. This may also contribute to the variability observed as the level of knockdown could potentially vary between experiments.

Several studies have shown that E-cadherin is required for the assembly of desmosomes (Jones, 1988; Wheelock and Jensen, 1992; Lewis et al., 1994; Michels et al., 2009). Increasing calcium concentration induces the re-localisation of E-cadherin and desmosomal proteins to cell-cell borders (Wheelock and Jensen, 1992; Michels et al., 2009). Addition of an anti-E-cadherin antibody delays the calcium induced formation of both adherens junctions and desmosomes (Wheelock and Jensen, 1992). In a recent study E-cadherin was reported to interact with DSG2 in a calcium independent manner (Shafraz et al., 2018). Following E-cadherin homodimersation from opposing cells, E-cadherin interacts with DSG2 to form a heterodimer. E-cadherin continues to be associated with DSG2 in nascent desmosomes. DSG3 has also been shown to interact with E-cadherin (Tsang et al., 2010), and could perhaps interact with E-cadherin in a similar manner as DSG2. However, PG and E-cadherin complex formation can also initiate desmosome assembly (Lewis et al., 1997). These data highlight the interconnected nature of adherens junction mediated and desmosomal adhesion and the importance of classical cadherins in the assembly of desmosomes. In my study knockdown of E-cadherin did not appear to have an adverse effect on desmosomal adhesion (and vice versa) as adhesiveness was retained upon individual silencing of E-cadherin (and DSG2) as compared to that obtained upon simultaneous knockdown of both E-cadherin and DSG2 (Figure 26). The

adhesiveness of double knockdown of PG and E-cadherin in HB2 cells were not investigated in my study.

In summary, the data presented in this chapter show for the first time that CD82 promotes desmosomal adhesion. The mechanism by which this is achieved will be addressed in the following chapter by examining interactions between PKCα, CD82 and DP, to determine whether CD82 recruits PKCα to DP to facilitate phosphorylation of DP by PKCα. Phosphorylation of DP by PKCα is required for the assembly of desmosomes, and this could potentially contribute to the CD82 mediated increase in cell-cell adhesion.

Chapter 4 – PKCα interacts with CD82 and DP

4.1 Introduction

Strong adhesion is necessary for the maintenance of tissue integrity but is incompatible with processes that occur during development and wound healing. Desmosomes are able to switch between two different adhesive states (Wallis et al., 2000; Garrod et al., 2005; Kimura et al., 2007). Desmosomes in tissues and in confluent cultures are strongly adhesive and are calcium independent. This strongly adhesive state is referred to as 'hyperadhesion' (Garrod et al., 2005). Hyperadhesive desmosomes are unaffected upon chelation of extracellular calcium ions. However, treatment of cells with PKC activators results in the transition of desmosomes to calcium dependence (Kimura et al., 2007). Transition to calcium dependence also occurs during wound healing, where PKCα becomes associated with desmosomes at a wound edge and phosphorylates desmosomal components. This results in the conversion of desmosomes to a less adhesive calcium dependent state, facilitating cell migration (Wallis et al., 2000; Garrod et al., 2005; McHarg et al., 2014). Phosphorylation of DP in hyperadhesive desmosomes results in weaker adhesion, and a reduced association with the intermediate filament cytoskeleton (Hobbs and Green, 2012). However, phosphorylation of DP by PKCα, and reduced interaction with the intermediate filament cytoskeleton is also required for the incorporation of DP into desmosomes during desmosome assembly, where PKP2 recruits PKCα to DP (Godsel et al., 2005; Bass-Zubek et al., 2008). This highlights the important role of PKCα in the downregulation and assembly of desmosomes and that the role of PKCα may vary depending on the cellular context.

CD82 has been shown to recruit PKCα to membrane in the presence of the PKC activator, TPA (Zhang et al., 2001). In addition, CD82 membrane organisation regulates the size of PKCα clusters which can have an impact on downstream effector signalling (Termini et al., 2016). This chapter addresses the CD82 mediated increase in desmosomal adhesion reported in the chapter 3 by investigating whether CD82 is found in a complex with PKCα and DP, and to determine whether CD82 is involved in the recruitment of PKCα to DP. CD82 and PKCα were co-expressed in HEK293T cells to determine which portions of CD82 that are involved in mediating the interaction between CD82 and PKCα. HEK293T cells are derivatives of human embryonic kidney 293 cells containing the SV40 T-antigen and, unlike HB2 cells, can be transfected with high efficiency. They were used to maximise the likelihood of detecting interactions between transfected proteins. Immunoprecipitation and FLAG-agarose pull-down experiments were carried out to test whether CD82, PKCα and DP form a complex. The ability of the DP C-terminal domain in binding of PKCα was also assessed. In addition, the phosphorylation of desmosomal components by PKCα was investigated to determine the mechanism by which CD82 strengthens desmosomal adhesion.

4.2 Results

4.2.1 PKCα interacts with CD82

CD82 has been shown to interact with PKCα in Jurkat cells when stimulated with the PKC activator TPA and lysed in 1% Brij 98 (Zhang et al., 2001). To replicate this finding HEK293T cells were co-transfected with full-length GFP tagged human PKCα (GFP-PKCα) (residues 2-672) and CD82 constructs, or with empty vectors (pcDNA-GFP and pZeo) as a negative control. 48 h after transfection, the cells were treated with TPA for 1 h to stimulate PKC translocation. The cells were then lysed in 1% Brij 98 or 1% Triton X-100. GFP-PKCα was immunoprecipitated with an anti-GFP antibody. Western blot analysis of the immunoprecipitation samples with an anti-CD82 antibody shows detection of CD82 in the test sample (GFP-PKCα and CD82). The CD82 signal detected in the control (Ctrl) GFP immunoprecipitation sample are non-specific bands. Hence CD82 interacts with PKCα in 1% Brij 98 when treated with TPA, corroborating the findings of Zhang et al. (2001) (Figure 27). Western blot analysis of the immunoprecipitation samples with an anti-PKCα antibody confirms efficient transfection and immunoprecipitation of GFP- PKCα.

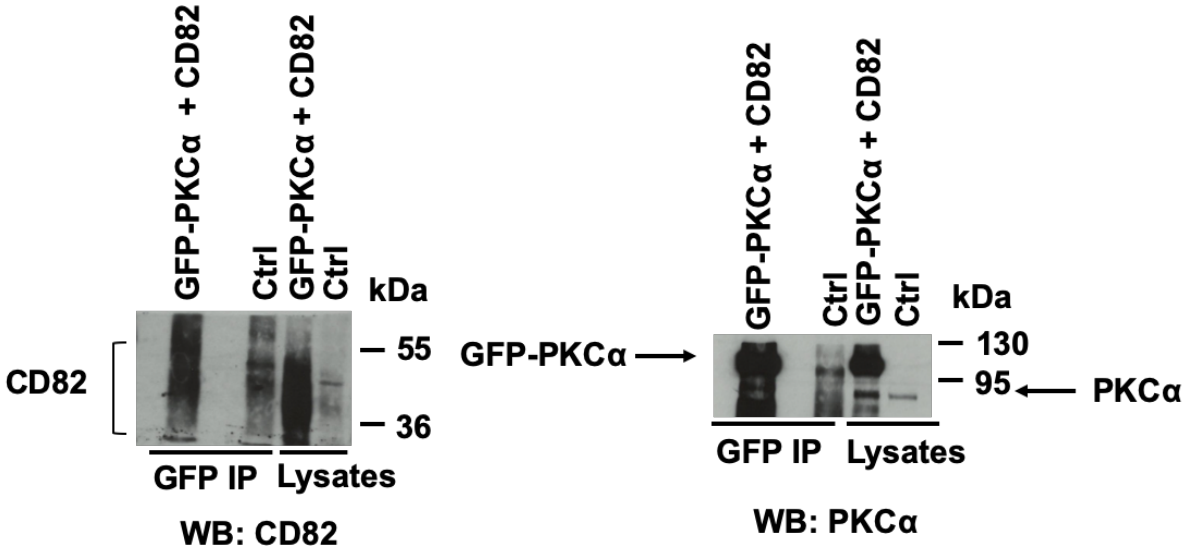

Figure 27 PKCα interacts with CD82 in 1% Brij 98

(A) HEK293T cells were co-transfected with GFP-PKCα and CD82 constructs, or with empty vectors (pcDNA-GFP and pZeo) as a negative control (Ctrl). 48 h after transfection the cells were treated with TPA for 1 h and then lysed with 1% Brij 98. GFP-PKCα was immunoprecipitated with an anti-GFP antibody. Results are from three independent experiments.

4.2.2 PKCα interacts with both N- and C-terminal deletion mutants of CD82

Transmembrane domain one and two and the N- and C- termini of tetraspanins are thought to mediate interactions with cytoplasmic signalling proteins such as PKCα (Zhang et al., 2001). It has recently been demonstrated that the N-terminus of the tetraspanin CD53 mediates the interaction between PKCβ and CD53 (Zuidscherwoude et al., 2017). However, while the interaction between CD82 and PKCα has been documented previously, it has not been shown which terminus of CD82 that is involved in this interaction (Zhang et al., 2001). To test whether the N-terminus of CD82 is responsible for the CD82 and PKCα interaction similar to the results reported for CD53, HEK293T cells were co-transfected with GFP-PKCα and a CD82 construct lacking the N-terminus, or with GFP-PKCα and CD82, which was used as a positive control, and with empty vectors (Ctrl) as a negative control. 48 after transfection the cells were treated with TPA for 1 h. The cells were then lysed in 1% Brij 98 and GFP-PKCα was immunoprecipitated with an anti-GFP antibody. The immunoprecipitation samples were analysed by western blotting with anti-CD82 and anti-PKCα antibodies. The results show that the N-terminal deletion mutant of CD82 is able to interact with PKCα as CD82 is detected in the GFP immunoprecipitation of the test sample (GFP-PKCα and CD82ΔN) (Figure 28A). GFP immunoprecipitation of the GFP-PKCα and CD82 samples shows that CD82 interacts with PKCα, as CD82 is also detected in this sample. The anti-PKCα western blot confirm that the transfection and immunoprecipitation were successful. This raised the possibility that the C-terminus of CD82 might mediate the interaction between CD82 and PKCα. To test this, the experiment above was carried out in the same manner but with a CD82 C-terminal deletion mutant

construct. The results show that this mutant is also capable of interacting with PKCα because CD82 is detected in the test sample and in the positive control (Figure 28B). However, a signal was detected in the negative control GFP immunoprecipitation sample which perhaps could be due to non-specific binding to the protein G agarose beads. In addition, this experiment was carried out once and to confirm this interaction it needs to be repeated, and potentially be carried out with a new batch of protein G agarose beads. Another caveat is that the CD82 N- and C-terminal truncation constructs are expressed at different levels and it is therefore difficult to make a direct comparison between the two. Overall, based on these results the PKCα and CD82 interaction could be mediated by either one of the N- or C- terminal tails or potentially by transmembrane domains one and two which were not tested in my study.

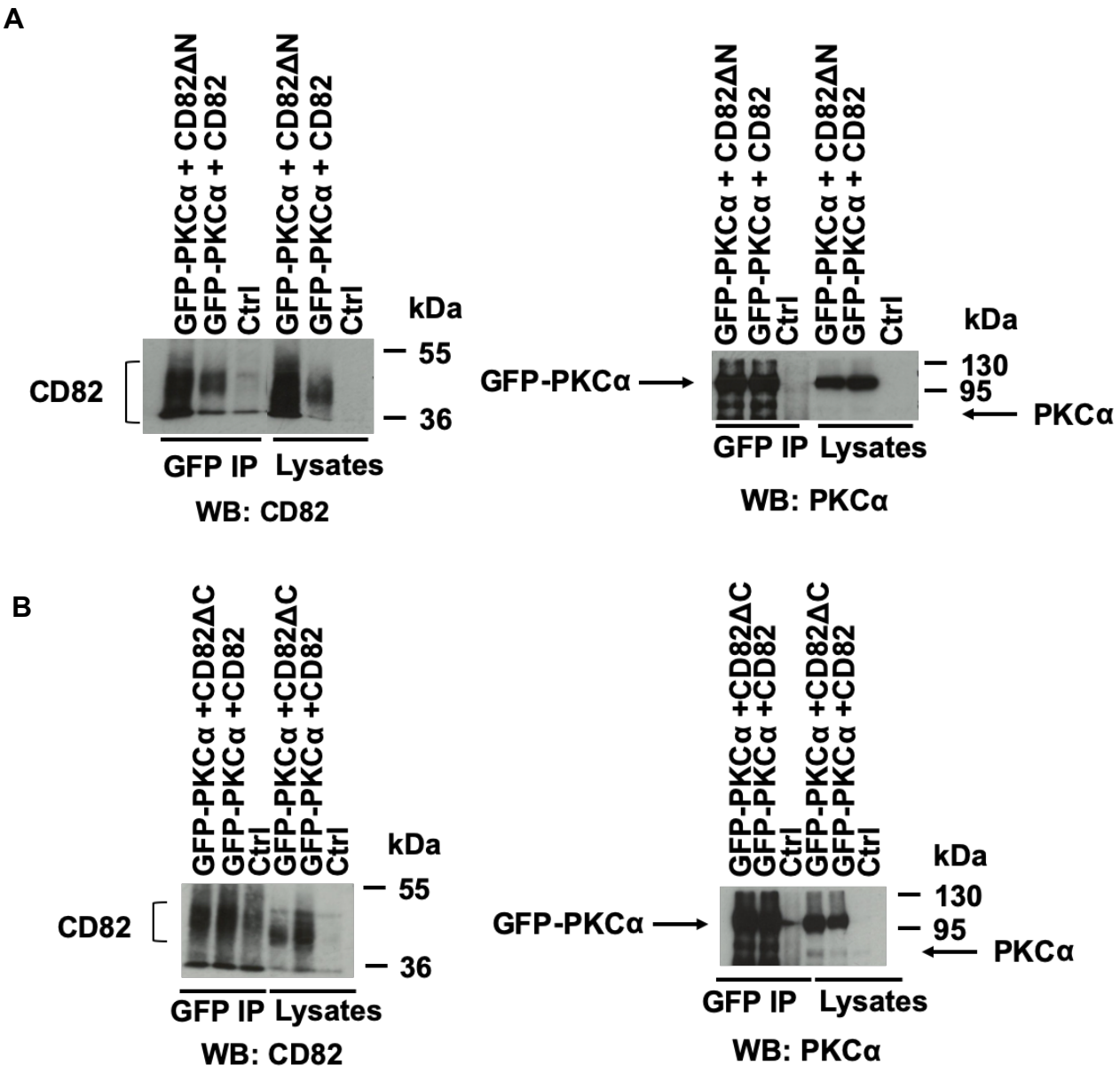

Figure 28 PKCα interacts with both N- and C- terminal deletion mutants of CD82

(A) HEK293T cells were co-transfected with GFP-PKCα and a CD82 N-terminal mutant (CD82ΔN), or with empty vectors (pcDNA-GFP and pZeo) as a negative control (Ctrl). 48 h after transfection the cells were treated with TPA for 1 h. The cells were then lysed with 1% Brij 98. GFP-PKCα was immunoprecipitated with an anti-GFP antibody. (B) The same experiment as in (A) was carried out but the cells were transfected with a C-terminal mutant of CD82 (CD82ΔC). Results are from one experiment.

4.2.3 Endogenous DP or transfected full-length FLAG-tagged DP is not detected in a complex with PKCα

During desmosome assembly, PKP2 recruits PKCα to DP, where PKCα phosphorylates DP (Bass-Zubek et al., 2008). Endogenous DP interacts with PKCα in the presence of PKP2 in HEK293 cells in the absence of TPA treatment (Bass-Zubek et al., 2008). To test whether DP is found in a complex with PKCα and CD82, HEK293T cells were co-transfected with GFP- PKCα and CD82 constructs. Cells transfected with empty vectors (pcDNA-GFP and pZeo) were used as a negative control. 48 hours after transfection the cells were treated with or without TPA for 1 h. The cells were then lysed in 1% Triton X-100 and GFP-PKCα was immunoprecipitated with an anti-GFP antibody. The immunoprecipitation samples were analysed by western blotting with the anti-DP antibody 11-5F. The antibody detects both isoforms of DP, DPI and the shorter isoform DPII. In contrast to Bass-Zubek et al., 2008, the results show that DP is not expressed at sufficient levels in HEK293T cells and is therefore not detected in a complex with PKCα in both the absence and presence of TPA (Figure 29).

To increase the probability of detecting DP in a complex with PKCα, or CD82, HEK293T cells were co-transfected with GFP-PKCα and FLAG-tagged human full-length DP (residues 1-2871) (DP-FLAG) or GFP-CD82 and DP-FLAG constructs. 48 h after transfection, the cells were lysed in 1% Triton X-100, and another set of GFP-CD82 and DP-FLAG transfected cells were lysed in 1% Brij 98. GFP-PKCα was immunoprecipitated with an anti-GFP antibody, and the immunoprecipitation samples analysed with anti-DP, anti-PKCα, and anti-CD82 antibodies. Western

blot analysis showed low transfection efficiency of DP-FLAG, as there is only a slight increase in DP above the endogenous expression level (Figure 30). No interaction was detected between DP and PKCα, and DP and CD82 in both buffers. The PKCα and CD82 western blots show that the immunoprecipitations reactions were successful. The low transfection efficiency is probably due to the large size of DP.

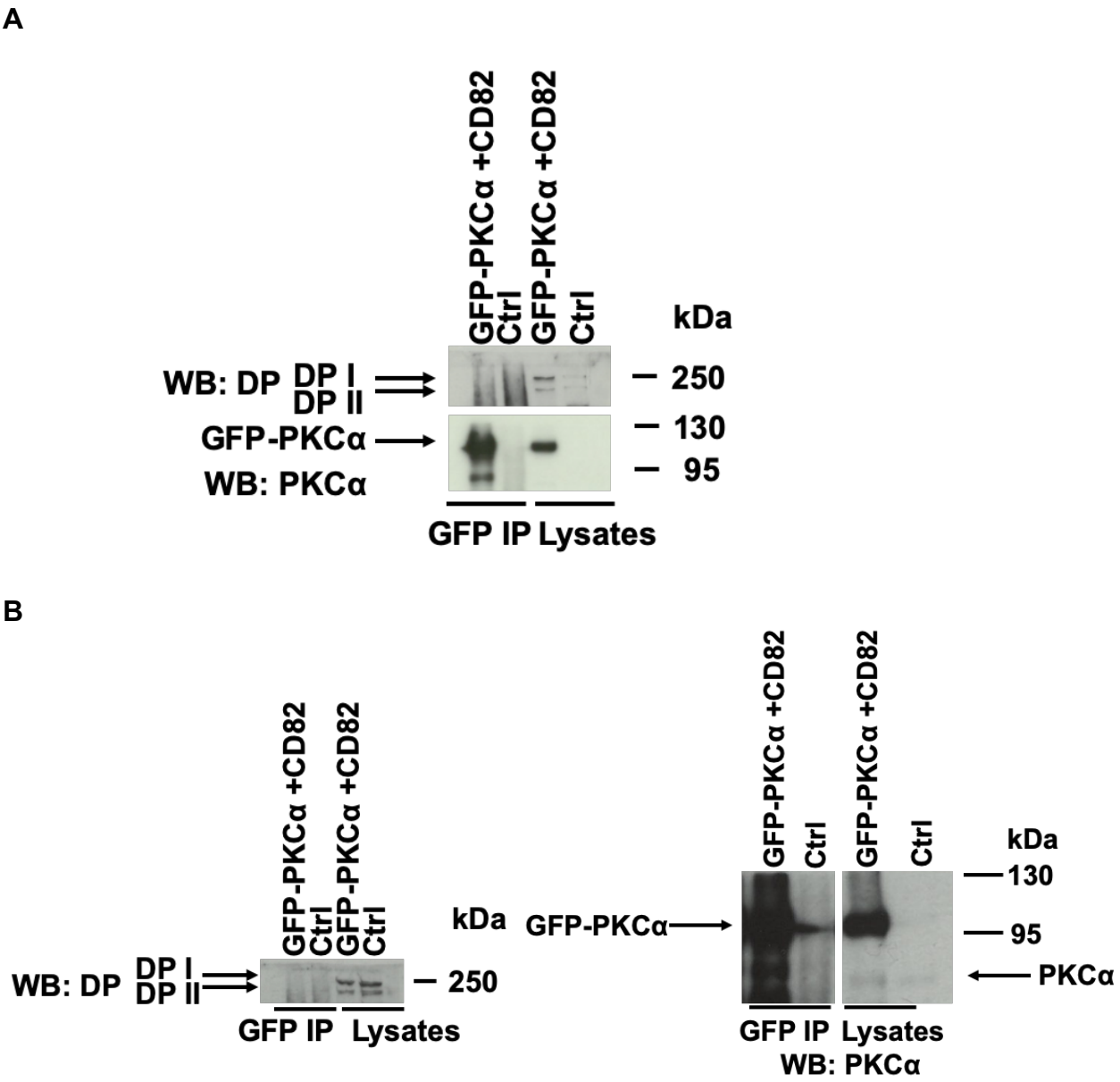

Figure 29 DP is not expressed at sufficient levels and not found in a complex with PKCα in HEK293T cells

HEK293T cells were co-transfected with GFP-PKCα and CD82), or with empty vectors (pcDNA-GFP and pZeo) as a negative control (Ctrl). 48 h after transfection the cells were treated without TPA (A) or with TPA (B) for 1 h. The cells were lysed in 1% Triton X-100. GFP- PKCα was immunoprecipitated with an anti-GFP antibody. The immunoprecipitation samples were analysed by western blotting with anti-DP and anti- PKCα antibodies. (PKCα blot for 29B immunoprecipitation samples are those shown in figure 28B). Results are from one experiment.

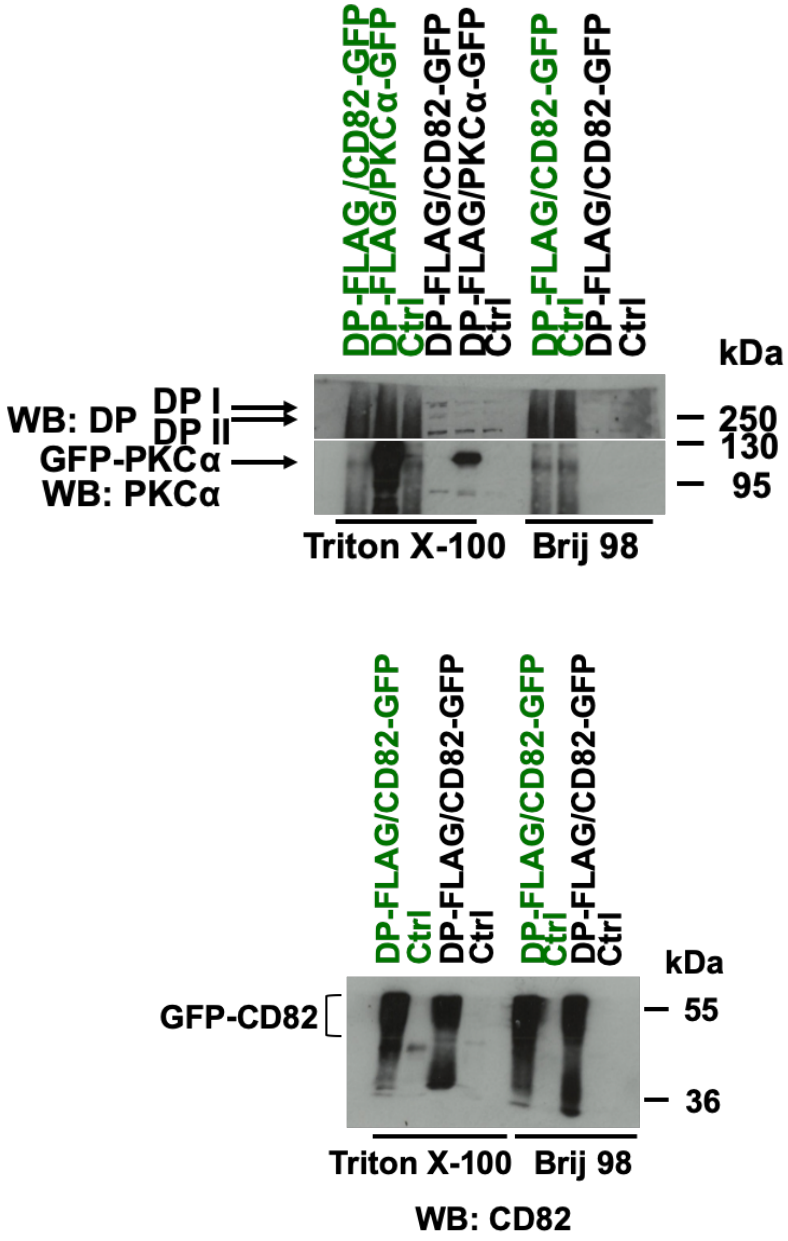

Figure 30 Full-length FLAG tagged DP is not detected in a complex with PKC α or CD82

HEK293T cells were co-transfected with GFP- PKCα and DP-FLAG or DP-FLAG and CD82 constructs), or with empty vectors (pcDNA-GFP and pZeo) as a negative control (Ctrl). 48 h after transfection the cells were lysed in 1% Triton X-100 or in 1% Brij 98. Proteins (black label) were immunoprecipitated with an anti-GFP antibody (green label). The immunoprecipitation samples were analysed by western blotting with anti-DP, anti- PKCα and anti-CD82 antibodies. Results are from one experiment.

4.2.4 Construction of a DP-ABC-GSR-FLAG plasmid

PKCα can regulate the strength of desmosomal adhesion by phosphorylating DP. Phosphorylation of serine 2849 of DP results in decreased adhesion in calcium independent desmosomes (Hobbs and Green, 2012). However, phosphorylation of DP is also required for the assembly of desmosomes. Previous data (Figure 30) showed a low transfection efficiency of full-length FLAG tagged DP. Given that PKCα phosphorylates S2849 which is within the glycine-serine-arginine (GSR) rich region of the C-terminus of DP, the interaction between DP and PKCα is likely mediated by the C-terminal domain of DP. To overcome the difficulty of transfecting full-length DP, a construct encoding the C-terminus of DP was produced. pcDNA-DP-ABC-FLAG was used as starting material. This construct encodes residues 1960-2822 which encompasses all of the C-terminal tail domains of DP except the GSR rich region. PCR was used to amplify DP residues 2822-2871, which includes the GSR rich region, using a full-length human DP cDNA clone (p931) as a template and PCR primers P1 which incorporates an *Eco*RV site, and P2 which incorporates DNA encoding a FLAG tag sequence and a stop codon, followed by a *Xho*I site for cloning (Figure 31A).

The resulting 250 bp PCR product and pcDNA-DP-ABC-FLAG were cut with the restriction enzymes *Eco*RV and *Xho*I (Figure 31B). The digested and purified PCR product was then ligated with the digested, electroeluted and purified pcDNA-DP-ABC-FLAG backbone. The ligation mix was transformed into XL-1 blue cells and plated onto LB agar plates containing ampicillin and incubated overnight at 37 ºC. To isolate DNA, single colonies were picked and inoculated in 5 ml of LB with

ampicillin overnight at 37 ºC. The cultures were harvested the next day and Qiaprep spin kits were used to isolate DNA. Seven clones were screened for the presence of the insert by digestion with the restriction enzyme *Eco*RV. pcDNA-DP-ABC-FLAG was cut with *Eco*RV and *Xho*I for size comparison. Fragments were resolved by agarose gel electrophoresis. Appreciable amounts of DNA was obtained from only two of the seven clones and it was difficult to determine whether these contained the insert due to the small size difference between the digested clones and parent vector backbone (Figure 32A). Therefore, both were selected for sequencing to confirm presence of the insert. The sequencing results showed that both clones contained the insert, and that the sequence was as expected. The chromatograms for one (clone 4) are shown in Figure 32B and C. Clone 4 was designated construct pc-DNA-ABC-GSR-FLAG.

To confirm that construct pcDNA-ABC-GSR-FLAG was expressed, HEK293T cells were transfected with pcDNA-DP-ABC-FLAG and pcDNA-ABC-GSR-FLAG. 48 h after transfection, transfected cells and untransfected control cells were lysed, and expression of DP analysed by western blotting using anti-DP and anti-FLAG antibodies. The results confirm expression of pcDNA-ABC-GSR-FLAG at the correct size of ~95 kDa (Figure 33).

A

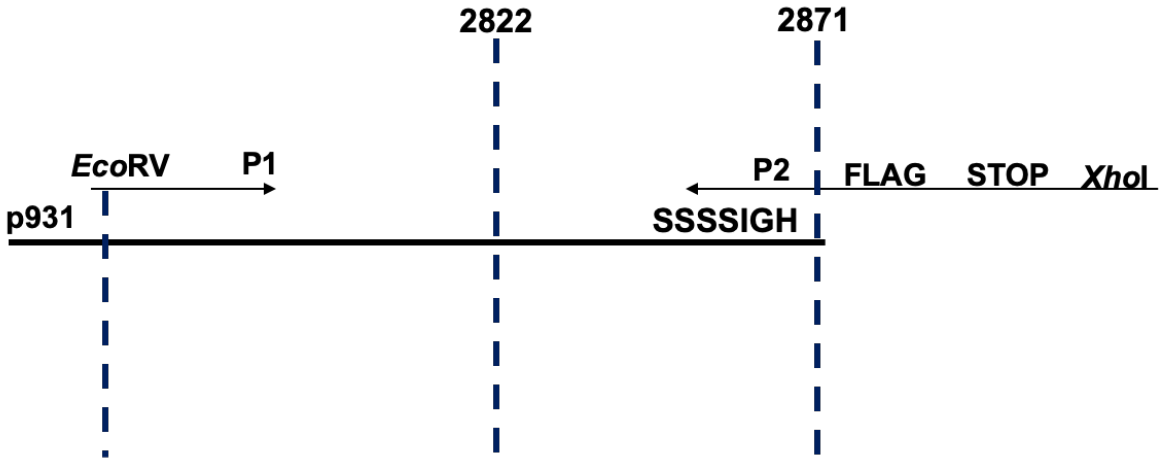

B

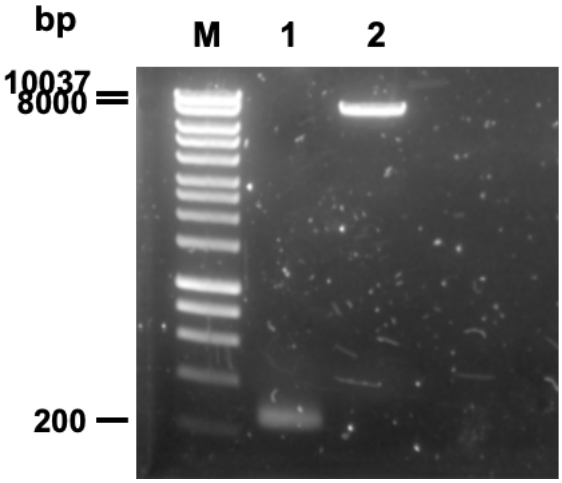

Figure 31 Generation of a PCR product encoding a FLAG tagged GSR rich domain

(A) Schematic representation of the strategy used. PCR primers P1 and P2 were used to amplify DP residues 2822-2871, using p931 encoding full length DP as a template. The PCR product was digested with *Eco*RV and *Xho*I, and ligated with *Eco*RV/*Xho*I digested pcDNA3-DP-ABC-FLAG vector. (B) M; Ladder. Lane 1, *Eco*RV and *Xho*I digested 250 bp PCR product obtained following amplification with primers P1 and P2. Lane 2, *Eco*RV and *Xho*I digested pcDNA3-DP-ABC-FLAG vector backbone.

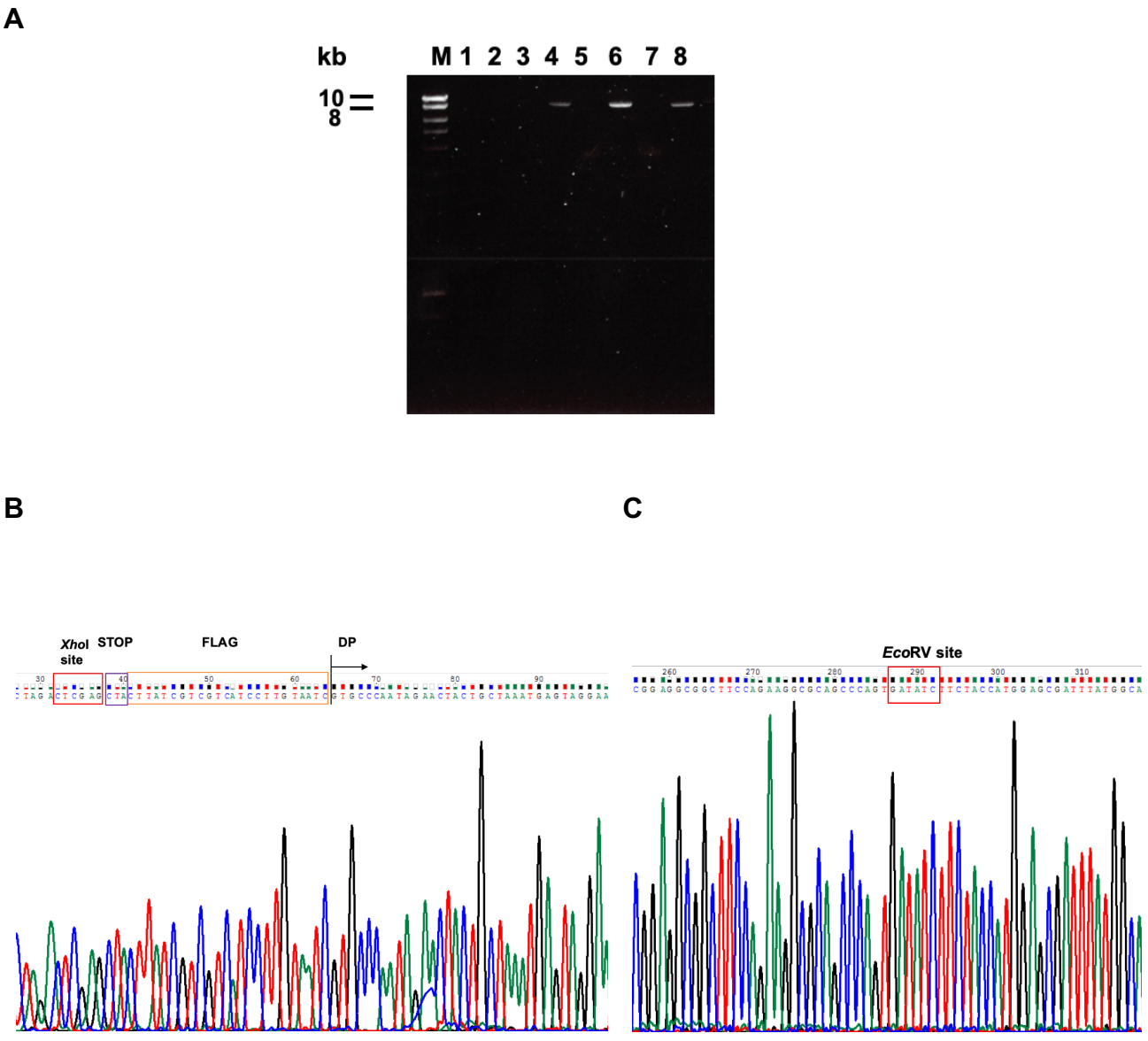

Figure 32 Verification of the presence of the insert

(A) Seven clones (lanes 1-7) were screened for the presence of the insert by digestion with the restriction enzyme *Eco*RV and size comparison with the parent vector pcDNA-DP-ABC-FLAG cut with with *Eco*RV and *Xho*I (lane 8). It was difficult to distinguish the clones which contained the insert as there is a small size difference between pcDNA-DP-ABC-FLAG and pcDNA-DP-ABC-GSR-FLAG. M; ladder. (B-C) Sequencing of clone 4 with primer P3 which hybridises to the pcDNA3 backbone, confirmed the presence of the insert and that the sequences around the restriction sites are as expected. (B) Chromatogram of the sequence surrounding the *Xho*I cloning site. (C) Chromatogram of the sequence surrounding the *Eco*RV cloning site. Red (Thymine), Green (Adenine), Black (Guanine), Blue (Cytosine).

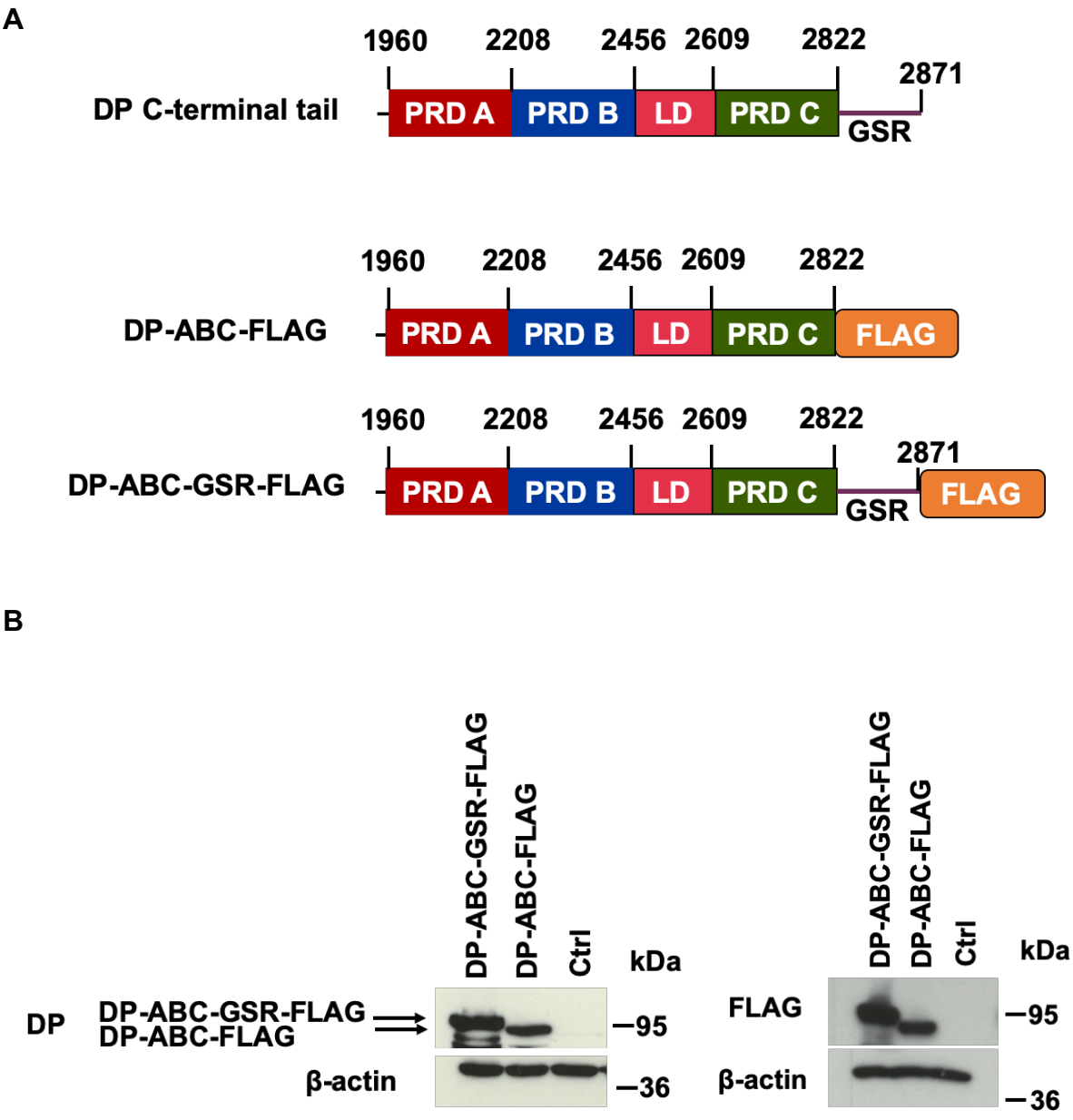

Figure 33 Expression of pcDNA-DP-ABC-GSR-FLAG construct in HEK293T cells

(A) Schematic representation of the DP C-terminal tail and DP-ABC-FLAG and DP-ABC-GSR-FLAG constructs. (B) HEK293T cells were transfected with pcDNA-DP-ABC-FLAG and pcDNA-ABC-GSR-FLAG. Untransfected cells were used as a negative control (Ctrl). 48 h after transfection, control and transfected cells were lysed and expression of the constructs analysed by western blotting with anti-DP, anti-FLAG, and β-actin (loading control) antibodies. Results are from one experiment.

4.2.5 PKCα interacts with the C-terminal domain of DP

The C-terminus of DP interacts with the intermediate filament cytoskeleton. This interaction can be modulated by phosphorylation of DP serine residue 2849 found within the GSR rich region of DP. Section 4.2.3 showed that transfection studies with DP were difficult due to its large size. Therefore, a DP C-terminal construct, containing the GSR region was generated for use in transfection studies. HEK293T cells were co-transfected with GFP-PKCα and DP-ABC-FLAG which lacks the GSR rich region, or DP-ABC-GSR-FLAG. Untransfected cells were used as a negative control. 48 h after transfection the cells were lysed in 1% Triton X-100. FLAG agarose beads were used to pull down DP-ABC-FLAG and DP-ABC-GSR-FLAG. The beads were washed, and bound proteins eluted from the beads with sample buffer and analysed by western blotting with anti-PKCα and anti-FLAG antibodies. The results show that both DP-ABC-FLAG and DP-ABC-GSR-FLAG bound PKCα (Figure 34). However, it appears that DP-ABC-FLAG interacts less robustly with PKCα than DP-ABC-GSR-FLAG, but this could also be due to lower transfection efficiency of DP-ABC-FLAG. These possibilities need to be investigated further. An additional band was also detected below the GFP-PKCα band in the DP-ABC-FLAG pull-down, the identity of this band is unclear.

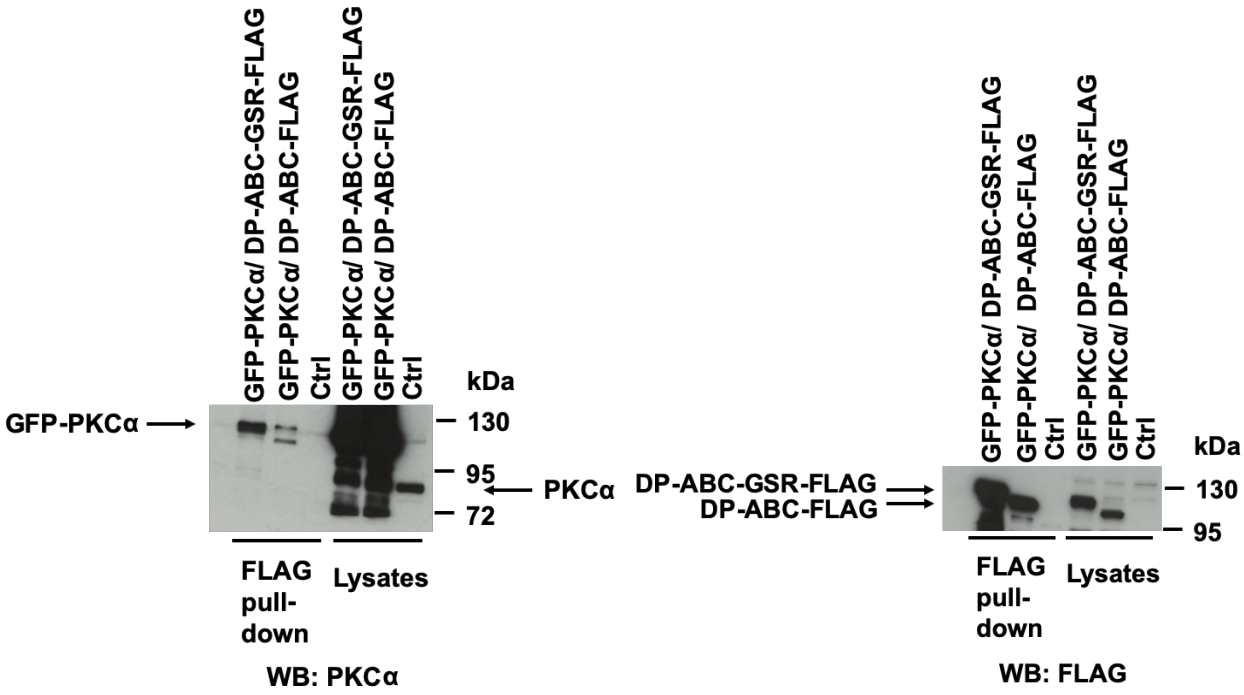

Figure 34 Both DP-ABC-FLAG and DP-ABC-GSR-FLAG bind PKCα

HEK293T cells were co-transfected with GFP-PKCα and DP-ABC-FLAG or DP-ABC-GSR-FLAG. Untransfected cells were used as a negative control (Ctrl). 48 h after transfection control and transfected cells were lysed in 1% Triton X-100. DP-ABC-FLAG and DP-ABC-GSR-FLAG were pulled down with FLAG agarose beads. Bound proteins were eluted from the beads with sample buffer. Pull-down samples were analysed by western blotting using anti-PKCα and anti-FLAG antibodies. Results are from two independent experiments for DP-ABC-GSR-FLAG and one experiment for DP-ABC-FLAG.

4.2.6 Phosphorylation of desmosomal components

Phosphorylation of desmosomal components regulates the strength of adhesion. To determine whether PKCα phosphorylates desmosomal proteins, HEK293T cells were co-transfected with GFP-PKCα, and either DP-ABC-FLAG or DP-ABC-GSR-FLAG constructs. Untransfected cells were used as a negative control. 48 h after transfection the cells were treated with TPA for 1 h and lysed in 1% Triton X-100, and proteins immunoprecipitated with an anti-phosphoserine antibody. The samples were analysed by western blotting with an anti-DP antibody. Phosphorylated DP was detected in both DP-ABC-FLAG and DP-ABC-GSR-FLAG transfections (Figure 35A). The DP-ABC-GSR-FLAG construct contains serine residue 2849 that is important for the interaction of desmosomes with IFs. Phosphorylation of DP-ABC-GSR-FLAG is not detected in the absence of TPA when DP-ABC-GSR-FLAG is pulled down with FLAG agarose and analysed by western blotting with an anti-phosphoserine antibody (Figure 36). The detection of phosphorylated DP with the DP-ABC-FLAG construct suggests that ABC domains of DP contain serine residues that could be phosphorylation targets of PKCα (Figure 35A). To confirm that the phosphorylation of DP on serine residues is PKC dependent, the cells were co-transfected with GFP-PKCα and DP-ABC-GSR-FLAG. Untransfected cells were used as a negative control. 48 h after transfection, the cells were treated with TPA or the PKC inhibitor Gö6976 for 1 h. The inhibitor is selective for PKCα and PKCβ. The cells were then lysed in 1% Triton X-100 and proteins immunoprecipitated with an anti-phosphoserine antibody. The samples were analysed by western blotting with an anti-DP antibody to detect phosphorylated DP. The results show that phosphorylation of DP persisted in the

presence of the PKC inhibitor (Figure 35B), suggesting involvement of other PKC isozymes or other serine/threonine kinases. However, no conclusion can be drawn as the experiment was carried out once and the optimal incubation time of the inhibitor or its activity was not determined.

Phosphorylation of PG by PKCα was also investigated in a similar manner as above. HEK293T cells were co-transfected with GFP-PKCα and a construct encoding full-length EGFP tagged human PG (EGFP-PG) (residues 1-745). Untransfected cells were used as a negative control. 48 h after transfection the cells were treated with TPA for 1 h and lysed in 1% Triton X-100 and proteins immunoprecipitated with an anti-phosphoserine antibody. Western blotting with an anti-PG antibody detected both endogenous and transfected PG in the lysates, and serine phosphorylated PG in the test sample (Figure 37). To determine whether serine phosphorylation of PG is PKC dependent HEK293T cells were co-transfected with GFP-PKCα and EGFP-PG. Untransfected cells were used as a negative control. 48 h after transfection the cells were treated with the PKC inhibitor Gö6976 for 1 h, lysed in 1% Triton X-100, and proteins immunoprecipitated with an anti-phosphoserine antibody. Western blotting with anti-PG antibody shows that phosphorylation of PG persisted under these conditions, again suggesting the involvement of other PKC isozymes or other serine/threonine kinases (Figure 37). Similar to the results obtained with DP, no conclusion can be drawn as the experiment was carried out once and the optimal incubation time of the inhibitor or its activity was not determined.

Phosphorylation of DSG2 by PKCα was investigated by co-transfecting HEK293T cells with GFP-PKCα and a construct encoding a mCherry-full length human DSG2 (residues 1-1118) fusion protein (mCherry-DSG2). Untransfected cells were used as a negative control. 48 h after transfection the cells were treated with TPA for 1 h and lysed with 1% Triton X-100 and proteins immunoprecipitated with an anti-phosphoserine antibody. Both endogenous and transfected DSG2 were detected in the lysates by western blotting with an anti-DSG2 antibody (Figure 38). However, phosphorylated DSG2 was not detected in the immunoprecipitation samples.

Finally, phosphorylation of DSC2 by PKCα was investigated by co-transfecting HEK293T cells with GFP-PKCα and a construct encoding full-length human DSC2a (residues 1-901). Untransfected cells were used as a negative control. 48 h after transfection the cells were treated with TPA for 1 h and lysed in 1% Triton X-100, and proteins immunoprecipitated with an anti-phosphoserine antibody. The samples were analysed by western blotting with anti-DSC2 antibody. This antibody detected both isoforms of DSC2, DSC2a and the shorter isoform DSC2b in the control and test lysates and, transfected DSC2a in the test lysate (Figure 39). The results show that phosphorylated DSC2a was not detected in the immunoprecipitation test sample.

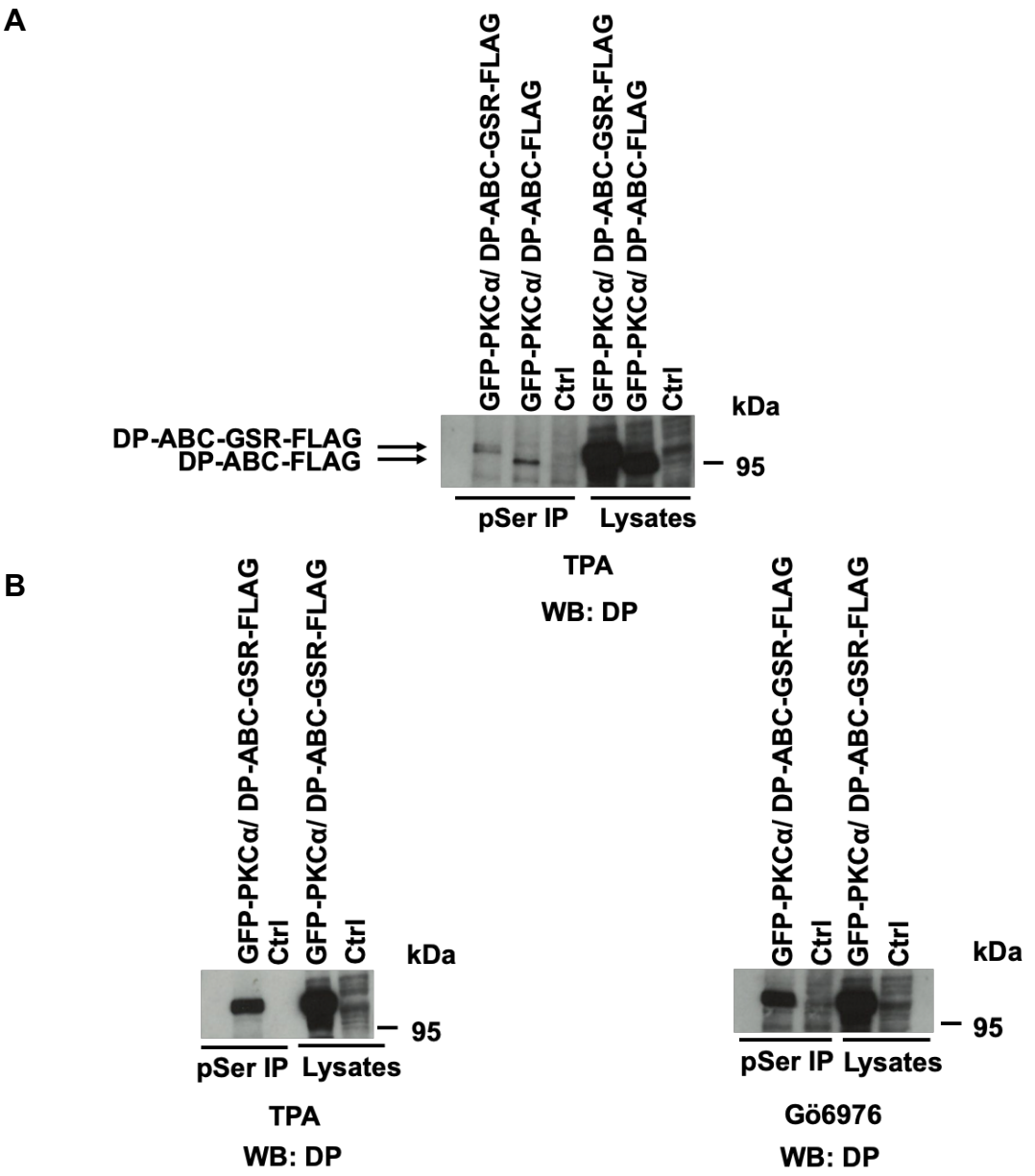

Figure 35 DP is phosphorylated on serine residues

(A) HEK293T cells were co-transfected with GFP-PKCα and DP-ABC-GSR-FLAG, and DP-ABC-GSR-FLAG. Untransfected cells were used as a negative control (Ctrl). 48 h after transfection control and transfected cells were treated with TPA with 1 h and lysed in 1% Triton X-100. GFP-PKCα was expressed at similar levels in the lysates of transfected cells (see Figure 35). Proteins were immunoprecipitated with an anti-phosphoserine antibody and analysed samples analysed by western blotting with an anti-DP antibody. Results are from one experiment. (B) HEK293T cells were co-transfected with GFP-PKCα and DP-ABC-GSR-FLAG and treated with TPA or Gö6976. TPA blot is representative of three independent experiments. Gö6976 blot is from one experiment.

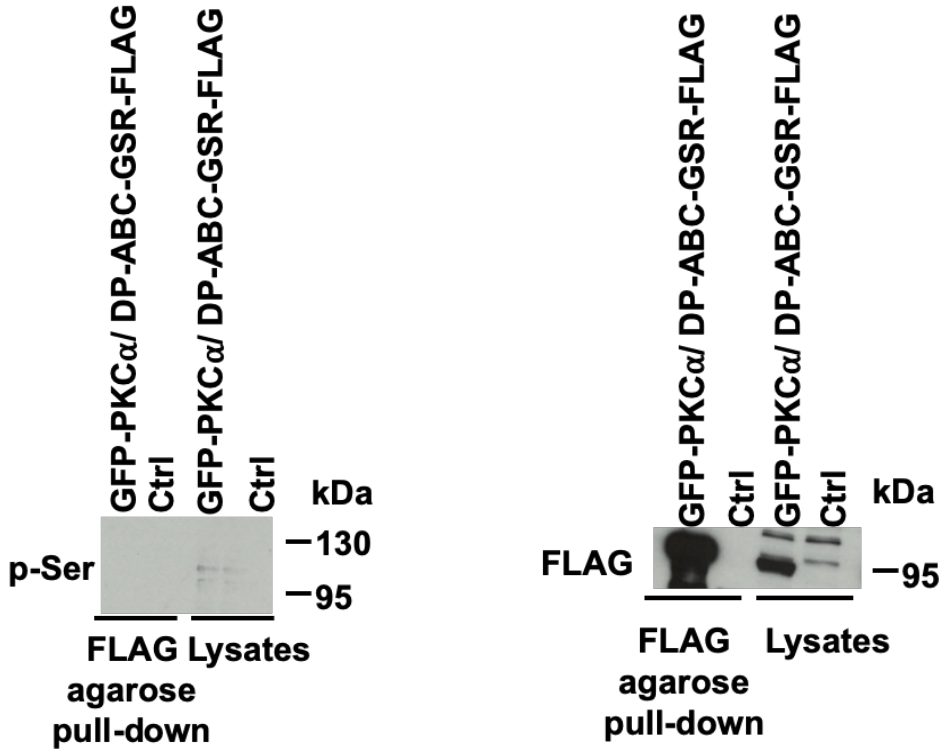

Figure 36 DP-ABC-GSR-FLAG is not phosphorylated on serine residues in the absence of TPA

HEK293T cells were co-transfected with GFP-PKCα and DP-ABC-GSR-FLAG. Untransfected cells were used as a negative control (Ctrl) 48 h after transfection control and transfected cells were lysed in 1% Triton X-100. GFP-PKCα was expressed at similar levels in the lysates of transfected cells (see Figure 35). DP-ABC-GSR-FLAG was pulled down with FLAG agarose beads. Bound proteins were eluted from the beads with sample buffer. Samples were analysed by western blotting with anti-phosphoserine and anti-FLAG antibodies. Results are from one experiment.

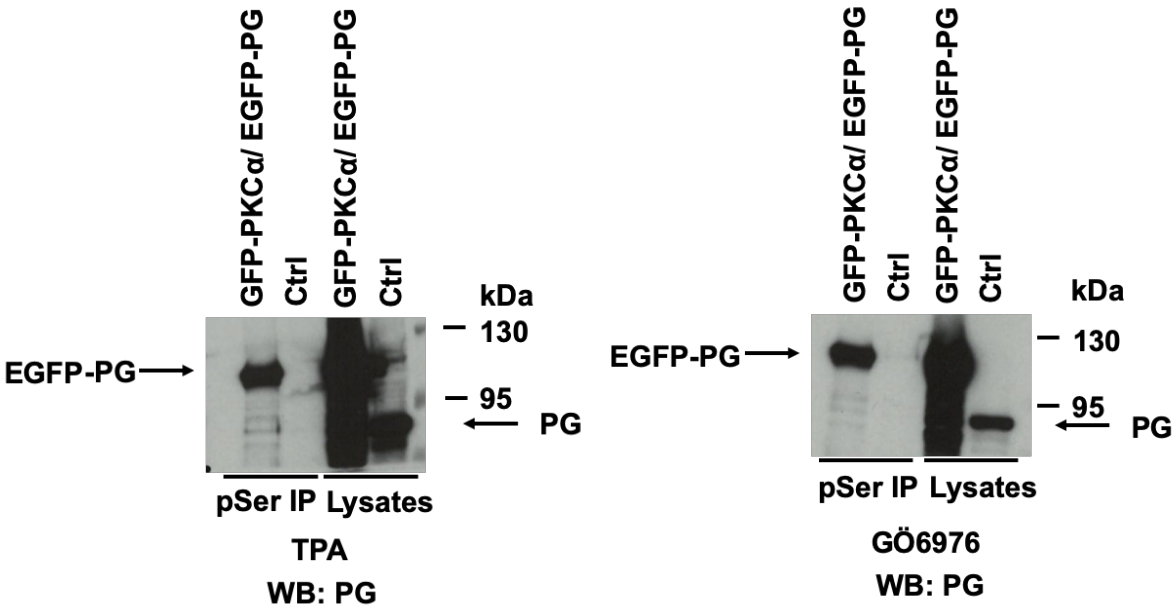

Figure 37 PG is phosphorylated on serine residues

(A) HEK293T cells were co-transfected with GFP-PKCα and EGFP-PG. Untransfected cells were used as a negative control (Ctrl). 48 h after transfection control and transfected cells were treated with TPA or Gö6976 for 1 h and lysed in 1% Triton X-100. GFP-PKCα was expressed at similar levels in the lysates of transfected cells (see Figure 35). Proteins were immunoprecipitated with an anti-phosphoserine antibody and samples analysed by western blotting with an anti-PG antibody. TPA blot is representative of three independent experiments, Gö6976 blot is from one experiment.

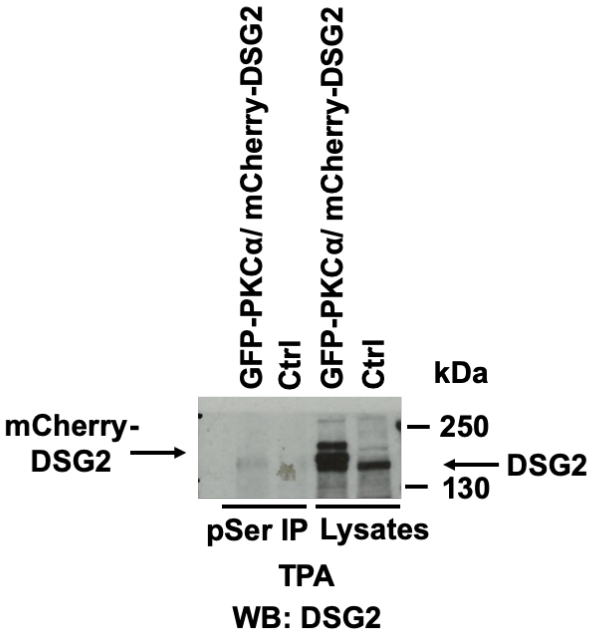

Figure 38 DSG2 is not phosphorylated on serine residues

HEK293T cells were co-transfected with GFP-PKCα and mCherry-DSG2. Untransfected cells were used as a negative control (Ctrl). 48 h after transfection control and transfected cells were treated with TPA for 1 h and lysed in 1% Triton X-100. GFP-PKCα was expressed at similar levels in the lysates of transfected cells (see Figure 35). Proteins were immunoprecipitated with an anti-phosphoserine antibody and samples analysed by western blotting with an anti-DSG2 antibody. Western blots are from one experiment.

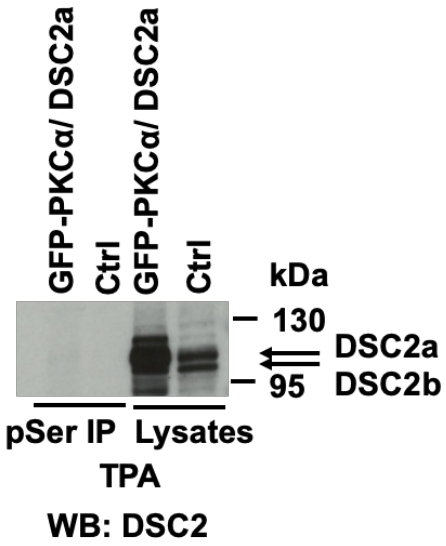

Figure 39 DSC2 is not phosphorylated on serine residues

(A) HEK293T cells were co-transfected with GFP-PKCα and DSC2. Untransfected cells were used as a negative control (Ctrl). 48 h after transfection control and transfected cells were treated with TPA for 1 h and lysed in 1% Triton X-100. GFP-PKCα was expressed at similar levels in the lysates of transfected cells (see Figure 35). Proteins were immunoprecipitated with an anti-phosphoserine antibody and samples analysed by western blotting with an anti-DSC2 antibody that recognises the alternatively spliced isoforms of DSC2. Western blots are from one experiment.

4.2.7 Knockdown of PKCα does not significantly reduce cell-cell adhesion in HB2 cells

PKCα plays an important role in regulating desmosomal adhesion and its activation has two somewhat contradictory effects. In the early stages of desmosome formation PKCα activation drives assembly (Bass-Zubek et al., 2008). Later, PKCα activation can promote the transition from mature, strongly adhesive, calcium independent desmosomes to weakly adhesive calcium dependent desmosomes (Kimura et al., 2007). Given that PKCα interacts with DP (Section 4.2.5) and is involved in regulating desmosome-intermediate filament interactions (Stappenbeck et al., 1994; Bass-Zubek et al., 2008; Hobbs and Green, 2012), the role of PKCα was investigated in the CD82 mediated increase in cell-cell adhesion. HB2PURO and HB2CD82 cells were treated with a PKC activator (TPA) and PKC inhibitor (Gö6976) for 1 h, 72 h after plating. At this stage the cultures had been confluent for 24 h. The monolayers were detached from the plates with dispase and subjected to mechanical stress (Figure 40A). The results indicate that stimulation with TPA results in an increase in adhesion and treatment with Gö6976 in a decrease in adhesion HB2CD82 cells (Figure 40B). Neither activation nor inhibition of PKC with the above compounds had a significant effect on HB2PURO cells.

To confirm whether PKCα specifically increased adhesion in HB2CD82 cells, HB2PURO and HB2CD82 cells were reverse transfected with non-silencing control (siCtrl) siRNA and siRNA oligos against PKCα. Figure 43 shows 86-90% knockdown of PKCα 72 h after transfection (Figure 41). 72 h after transfection, the

monolayers were detached with dispase and subjected to mechanical stress (Figure 42A). Quantification of the number of fragments shows that depletion of PKCα does not significantly decrease adhesion in both HB2PURO and HB2CD82 cells (Figure 42B). Expressing the data as fold change relative to siCtrl shows that there is a greater reduction in adhesion in HB2CD82 cells.

A

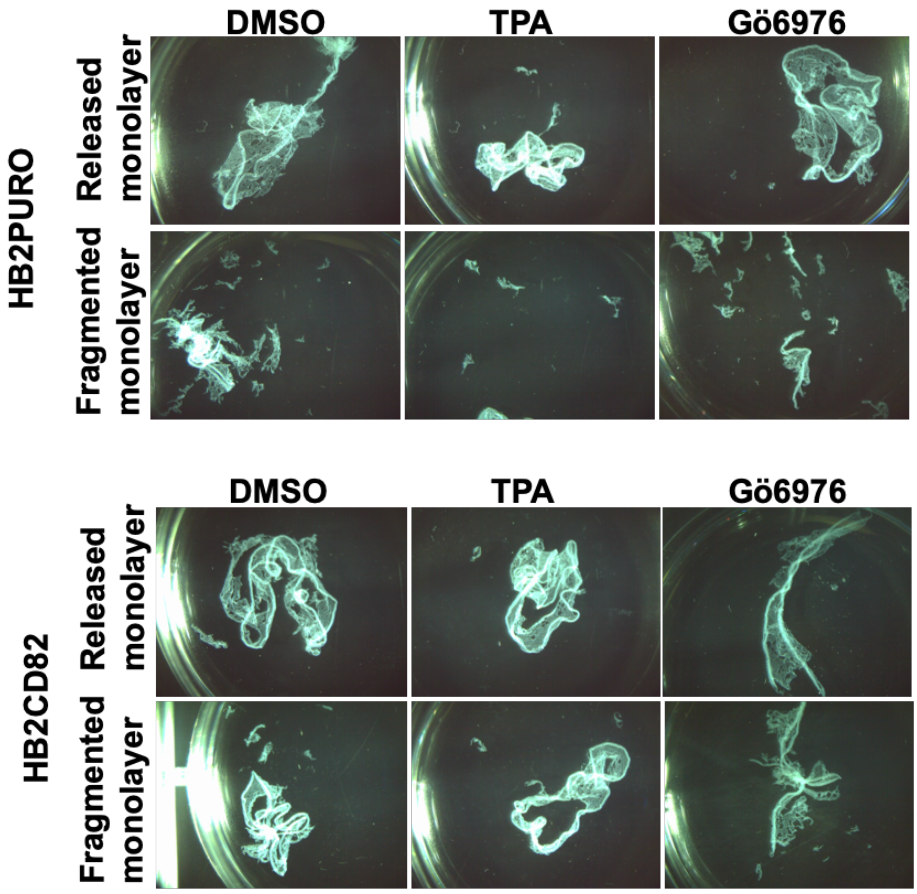
DMSO
TPA
Gö6976
HB2PURO
Released monolayer
Fragmented monolayer
DMSO
TPA
Gö6976
HB2CD82
Released monolayer
Fragmented monolayer

B

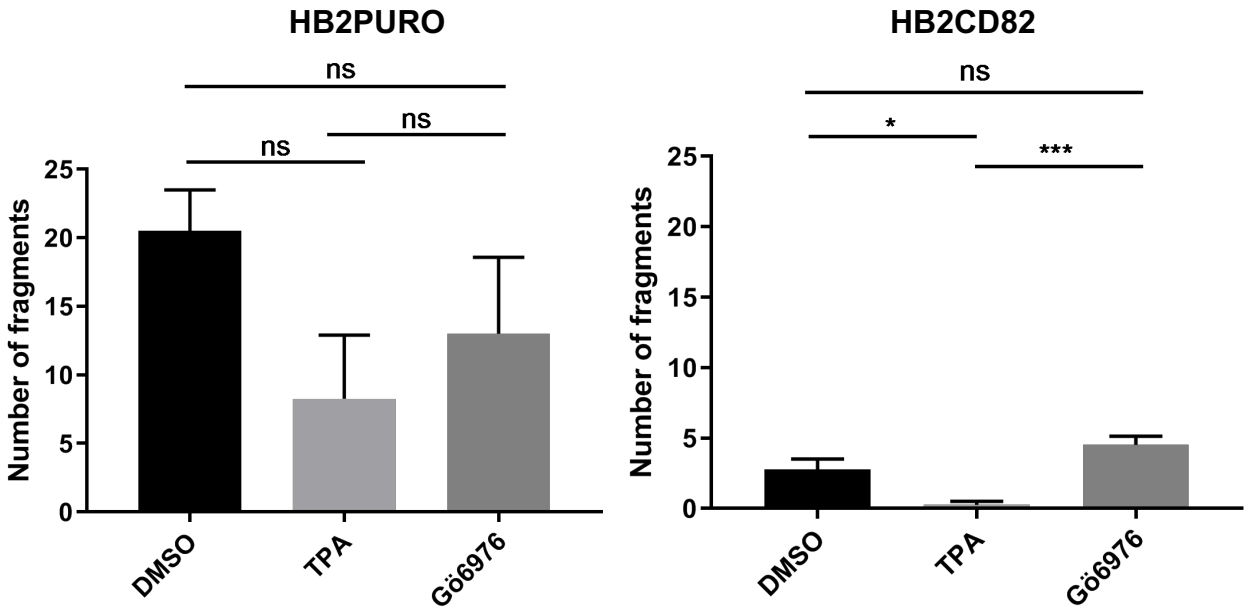
HB2PURO
ns
ns
ns
Number of fragments
25
20
15
10
5
0
DMSO
TPA
Gö6976
HB2CD82
ns
*
***
Number of fragments
25
20
15
10
5
0
DMSO
TPA
Gö6976

Figure 40 Pharmacological activation of PKC results in an increase in adhesion in HB2CD82 cells

(A) HB2PURO and HB2CD82 cells were treated with either TPA or Gö6976 and then detached with dispase 72 h after plating to release confluent monolayers, which were then subjected to mechanical stress. (B) Quantification of the number fragments. Data are the mean number of fragments, standard error and t-test of four independent experiments (*P<0.05, ***P<0.001).

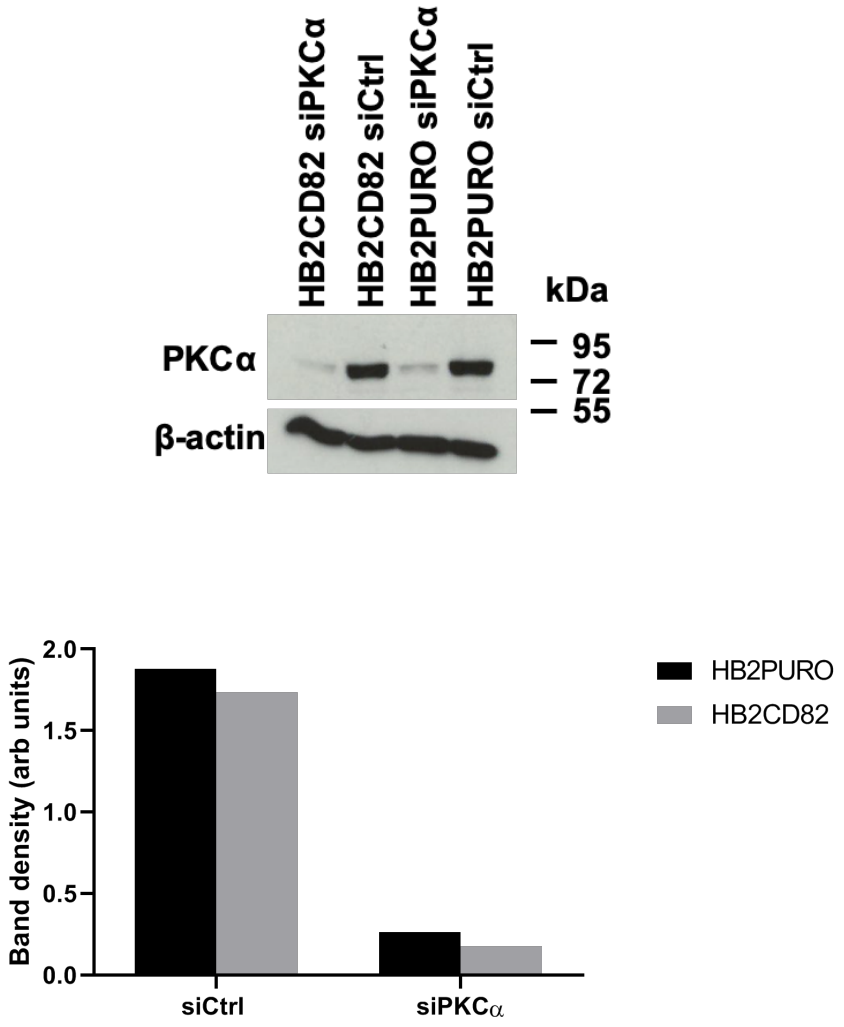

Figure 41 Knockdown of PKCα in HB2PURO and HB2CD82 cells

HB2PURO and HB2CD82 cells were reverse transfected with siRNA oligos against PKCα. 72 h after transfection, the cells were lysed, and knockdown efficiency analysed by western blotting with anti-PKCα and anti-β-actin antibodies (loading control). The western blot was quantified by densitometry and normalised with respect to β-actin. Results are from one experiment.

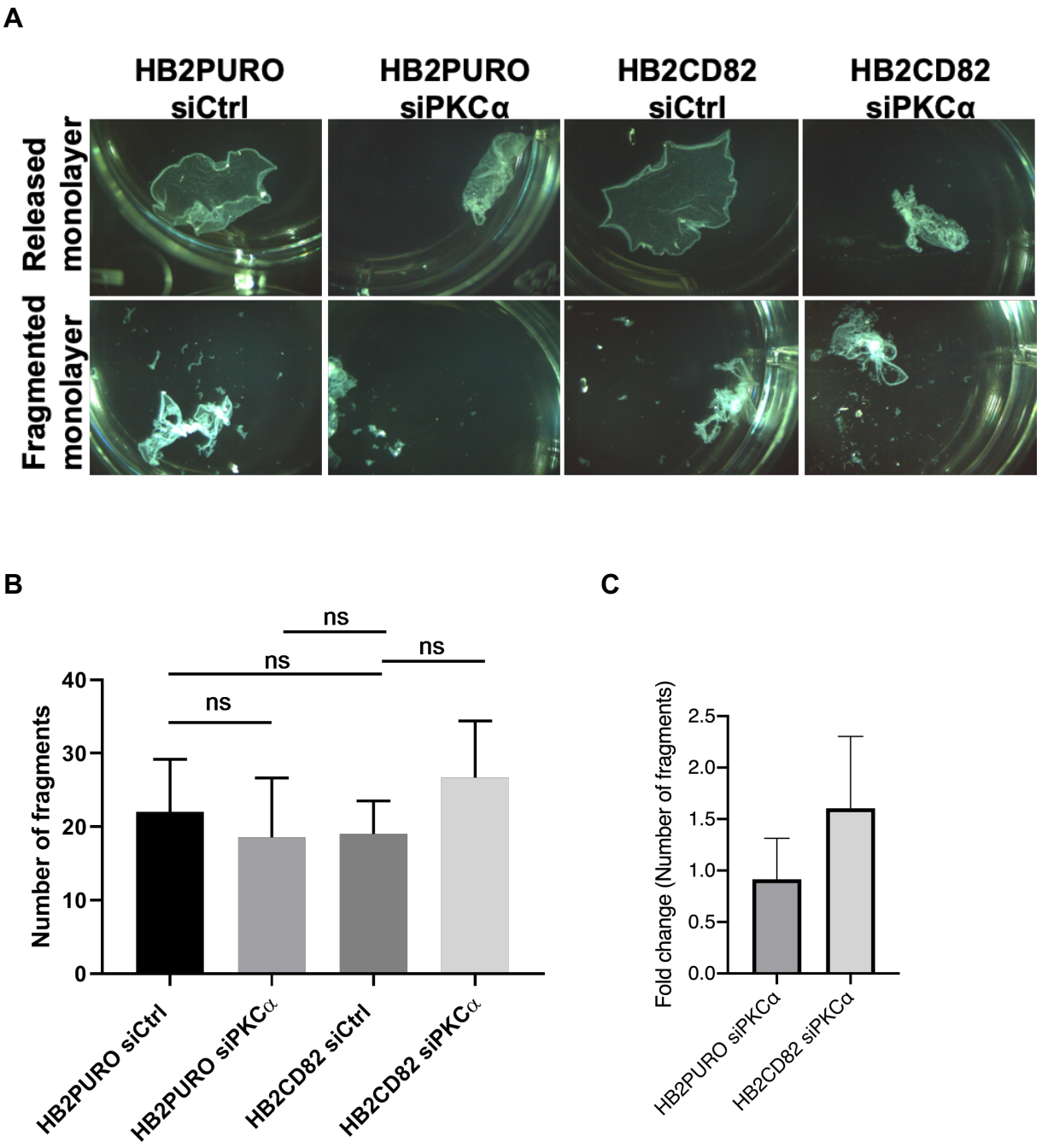

Figure 42 Depletion of PKCα does not result in a significant decrease in cell-cell adhesion in HB2 cells

(A) HB2PURO and HB2CD82 cells were reverse transfected with non-silencing (siCtrl) siRNA oligos and oligos against PKCα. 72 h after transfection, the monolayers were detached with dispase to release confluent monolayers, which were then subjected to mechanical stress. (B) Quantification of the number fragments. (C) Data from B expressed relative to siCtrl of each transfectant and expressed as fold change. Data are the mean number of fragments, standard error and t-test of three independent experiments.

4.3 Discussion

Previous work has established that CD82 interacts with PKCα in Jurkat cells when treated with TPA to stimulate PKCα translocation to the membrane (Zhang et al., 2001). TPA mimics diacylglycerol to activate PKCα. I have also shown the interaction between PKCα and CD82 when treated with TPA in HEK293T cells. In addition, I have demonstrated that this interaction is not preserved in more stringent conditions (1% Triton X-100). Using a chimeric mapping approach, where fragments of the tetraspanin CD9 which are capable of interacting with PKCα were replaced with fragments of the tetraspanin A15/Talla1 which does not interact with PKCα, Zhang et al. (2001) have shown that the PKCα tetraspanin interaction sites are likely to be transmembrane domains 1 and 2 or the N- and C-terminal tails. A recent study showed that the N-terminus of CD53 is involved in mediating the interaction between CD53 and PKCβ (Zuidscherwoude et al., 2017). This led me to investigate whether the N- and C-terminal domains of CD82 are involved in the interaction between CD82 and PKCα. In my study, HEK293T cells were co-transfected with GFP-PKCα and CD82 constructs lacking either the N- or C-terminus. Immunoprecipitation experiments showed that both N- and C-terminal deletion mutants of CD82 are capable of interacting with PKCα (Figure 28). This suggests that transmembrane loops 1 and 2 which were not investigated in my study could also be involved in the interaction.

CD82 membrane organisation regulates PKCα signalling (Termini et al., 2016). Prolonged treatment with TPA results in a reduced association between palmitoylation deficient CD82 and PKCα. In addition, CD82 regulates the size of

PKCα clusters and this is linked to alterations in downstream signalling pathways. Given that CD82 interacts with PKCα, I investigated whether CD82 is found in a complex with PKCα and DP. PKCα is involved in the regulation of desmosomal adhesion. During desmosome assembly, PKP2 plays a scaffolding role and recruits PKCα to DP in the cytoplasm. DP is then phosphorylated by PKCα and incorporated into desmosomes (Bass-Zubek et al., 2008). Phosphorylation of DP results in a reduced association with intermediate filaments (IFs) which may be necessary for the incorporation of DP into desmosomes. The importance of PKCα in desmosome assembly is further highlighted in PKP2 depleted cells where the disruption of the PKP2 scaffolding role results in a delay in desmosome assembly, and assembly is rescued by pharmacological activation of PKC (Bass-Zubek et al., 2008). Phosphorylation of a DP serine residue at position 2849 which falls within a PKC consensus sequence is thought to be responsible for mediating DP-IF interactions. A phosphorylation deficient point mutant of DP S2849 delays desmosome assembly and results in an increased association with IFs (Godsel et al., 2005). Bass-Zubek et al. (2008) showed that endogenous DP immunoprecipitated with PKCα in HEK293 cells. However, in my immunoprecipitation experiments I was unable to detect this interaction as DP is not expressed at sufficient levels in HEK293T cells (Figure 29). Transfection studies with full-length DP were largely unsuccessful, perhaps due to its large size (Figure 30). Therefore, I used DP C-terminal domain constructs for transfections. DP-ABC-FLAG contains three plakin repeat domains (PRDs) A, B and C, and a linker domain, and DP-ABC-GSR-FLAG contains the three PRDs, the linker domain and the C-terminal GSR rich region where S2849 is found. Both are

phosphorylated by PKCα, and FLAG-agarose pull-downs confirmed that both DP-ABC-FLAG and DP-ABC-GSR-FLAG interact with PKCα (Figure 34). This shows that PKCα phosphorylates and interacts with serine residues in other parts of DP, not just in the GSR rich region (such as S2849). While Bass-Zubek et al. (2008) have shown that PKP2 scaffolds a complex with DP and PKCα, and that DP is phosphorylated by PKCα, and therefore a substrate of PKCα, the possibility that this also involves direct binding of DP to PKCα remains to be established.

Mature desmosomes adopt a strongly adhesive state, referred to as 'hyperadhesion' in tissues and confluent monolayers in culture (Wallis et al., 2000; Garrod et al., 2005). Hyperadhesive desmosomes are calcium-independent, in other words chelation of extracellular calcium ions does not result in a decrease of adhesion or splitting of desmosomes and loss of adhesion. By contrast newly formed desmosomes, such as those found in recently formed confluent cultures, or desmosomes at a wound edge, are calcium dependent and chelation of calcium results in desmosome splitting and loss of adhesion (Kimura et al., 2007). Phosphorylation of DP by PKCα regulates the transition between these adhesive states. Thus weakly adhesive calcium dependent desmosomes transition to the hyperadhesive state when treated with PKC inhibitors (Wallis et al., 2000) and expression of a DP serine point mutant at position 2849 in A431 epidermoid carcinoma cells results in increased adhesion and resistance to mechanical stress in newly confluent cells (Hobbs and Green, 2012). PKCα-mediated phosphorylation of DP has been shown in keratinocytes lacking keratin expression by immunoprecipitation with an anti-phosphoserine antibody (Kröger et al., 2013).

Consistent with this finding, I have shown that both DP-ABC-FLAG and DP-ABC-GSR-FLAG are phosphorylated on serine residues when treated with TPA (Figure 35). This suggests that phosphorylation sites in PRDs A, B, and C, and the C-terminal linker domain, may be involved (in addition to S2849) in the regulation of desmosomal adhesion. The linker domain, located between PRDs B and C contains several consensus serine and threonine phosphorylation sites that have yet to be characterised (Kang et al., 2016). In my experiments treatment with Gö6976 did not result in a decrease in DP phosphorylation, so it is likely that other isoforms of PKC, or perhaps other serine/threonine kinases, are involved. However, I did not optimise the most effective concentration of the Gö6976 inhibitor in HEK293T cells. The concentration I used in my study has been shown to be effective in HaCaT cells (Kimura et al., 2007), and this concentration may not have been sufficient for inhibition of PKC in HEK293T cells. In addition, I did not evaluate the activity of the inhibitor or optimal time of incubation with the inhibitor as this was also based on the work of Kimura et al., (2007). The concentration of various PKC inhibitors was also previously determined for HB2 cells (Odintsova et al., 2013) and fell within this range but I was unable to use these cells for phosphorylation studies as they are somewhat refractory to transfection. Another caveat is that these experiments were performed once and further experiments need to be carried out to draw conclusions.

Other desmosomal proteins can also be phosphorylated. Epidermal growth factor (EGF) treatment results in tyrosine phosphorylation of PG and DSG2 (Gaudry et al., 2001). Tyrosine phosphorylated PG maintains its interaction with DSG2 but not

DP compromising the link to the IF cytoskeleton. PG can be phosphorylated on three tyrosine residues in its C-terminal domain at positions 693, 724 and 729. A phospho-deficient triple point mutant of tyrosine 693, 724, and 729, can maintain its interaction with DP when treated with EGF. Inhibition of epidermal growth factor receptor (EFGR) strengthens intercellular adhesion and promotes desmosome assembly (Lorch et al., 2004). Introduction of the phospho-deficient triple point mutant of PG into PG null cultured keratinocytes prevents the EGF dependent loss of interaction between PG and DP (Yin et al., 2005a). However, phosphorylation of PG does not always result in a loss of association with DP. Phosphorylation of PG by Src on tyrosine residue at position 643 results in an increased association with DP while phosphorylation of PG tyrosine 549 by Fyn or Fer tyrosine kinases has the opposite effect (Miravet et al., 2003). The effect of phosphorylation of Tyr643 and Tyr549 residues on the maintenance of cell-cell adhesion has not been investigated. I have shown that PG can also be phosphorylated on serine residues when treated with TPA (Figure 37). However, treatment with Gö6976 did not reduce phosphorylation of PG (Figure 37). This suggests that other isoforms of PKC or other serine/threonine kinases might be responsible for the phosphorylation of PG. However, the same limitations as with the Gö6976 experiments with DP apply and more replicates are needed in order to draw a conclusion.

I was unable to detect serine phosphorylated DSG2 in my experiments. Similarly, I was unable to detect serine phosphorylated DSC2 although serine phosphorylation of DSC2 has been reported following metabolic labelling and

immunoprecipitation (Parrish et al., 1990). However, there is a high abundance of proteins that are phosphorylated on serine residues, and the approach I used of immunoprecipitating with an anti-phosphoserine antibody is non-specific and is unable to detect all proteins that are phosphorylated on serine residues as some are more abundant than others and are therefore more readily immunoprecipitated.

One day confluent cultures of HB2CD82 cells treated with TPA are more adhesive than DMSO or Gö6976 treated HB2CD82 cells (Figure 40). Treatment of six days confluent cultures of HaCaT cells with TPA results in a decrease in adhesion (Kimura et al., 2007) so the effect of TPA on HB2PURO and HB2CD82 cells in my experiments may be desmosome assembly related. In support of this idea activation of PKC is required for the assembly of desmosomes and a decreased association of DP with IFs (Bass-Zubek et al., 2008). In my experiments, treatment of one day confluent HB2PURO and HB2CD82 cultures with Gö6976 did not significantly increase adhesion. By contrast treatment of one day confluent HaCaT cells with Gö6976 did result in an increase in adhesion (Kimura et al., 2007). The reason for this discrepancy is not clear but may simply be a difference in response between the two cell types. Knockdown of PKCα did not have a significant effect on cell-cell adhesion in my experiments (Figure 42) so other PKC isoforms may be involved in regulation of desmosomal adhesion in HB2 cells.

In summary, PKCα interacts with both CD82 and DP and increases the phosphorylation of the DP C-terminal tail (and PG). How then is the CD82

mediated increase in desmosomal adhesion brought about? One possibility is that CD82 which has been shown to regulate the clustering of PKCα at the membrane, localises PKCα to the membrane where it is able to phosphorylate DP, reducing its interaction with intermediate filaments and promoting desmosomes assembly (Bass-Zubek et al., 2008; Termini et al., 2016). Another is it is able to mediate clustering of desmosomal proteins during desmosome assembly. In addition to PKCα, a clustering role for CD82 has been demonstrated for other proteins such as integrin α4 which has not been shown to directly interact with CD82 but through its interactions with other tetraspanins affects its clustering, and N-cadherin (Termini et al., 2014; Marjon et al., 2016; Termini et al., 2016). Clustering of desmosomal proteins during desmosome assembly would in all probability increase interactions between desmosomal proteins and so increase the strength of desmosomal adhesion. This possibility will be explored in the next chapter.

Chapter 5 – CD82 reorganises the desmosomal plaque

5.1 Introduction

The organisation of desmosomal proteins is important for the maintenance of strong adhesion. Strong adhesion is associated with an ordered arrangement of the desmosomal cadherins giving rise to an electron dense midline (Odland, 1958; North et al., 1999; Garrod et al., 2005). Thus strongly adhesive calcium independent desmosomes have a dense midline whereas weakly adhesive calcium dependent desmosomes lack a midline and show a narrowing of the intercellular space (Garrod et al., 2005). Overexpression of PKP1 results in the reorganisation of several desmosomal components in the plaque, resulting in reduced plaque to plaque distances and hyperadhesion (Tucker et al., 2014; Stahley et al., 2016a). CD82 can regulate the clustering of membrane proteins and cytoplasmic signalling proteins (Termini et al., 2014; Marjon et al., 2016; Termini et al., 2016). Overexpression of CD82 increases the density of α4 integrin clusters resulting in increased cell-matrix adhesion (Termini et al., 2014). This raises the question whether CD82 increases cell-cell adhesion through clustering of desmosomal proteins.

The organisation of desmosomes has been studied using electron microscopy, immunogold labelling electron microscopy, cryoelectron tomography and more recently using the super-resolution microscopy technique, direct stocachastic optical reconstruction microscopy (dSTORM) (Odland, 1958; North et al., 1999; Al-Amoudi et al., 2011; Stahley et al., 2016a). These techniques are able to produce a detailed map of desmosomes. Desmosomes consist of two plaques that are

contributed by two interacting cells, and these techniques typically allow these plaques to be resolved. The experiments described in this chapter investigate the role of CD82 on the intracellular distribution of desmosomal and adherens junction proteins using confocal microscopy and a cell-cell boundary detection software to quantify fluorescence intensities at the membrane. Further, the role of CD82 on the clustering and organisation of desmosomal proteins is investigated using dSTORM which involves stochastically activating fluorophores to determine their localisation. Clustering of desmosomal proteins refers to how tightly packed desmosomal proteins (referred to as molecules throughout the text, as fluorophores are detected) are within a plaque and this was investigated using the density-based spatial clustering of applications with noise (DBSCAN) algorithm which is discussed further in 5.2.3, along with the optimisation of the algorithm. The organisation of desmosomes was studied by measuring the distances between DP plaques contributed by adjacent cells.

5.2 Results

5.2.1 Quantification of fluorescence intensities of cell-cell junction proteins

The distribution of the desmosomal proteins PG and DSG2 was analysed in HB2PURO and HB2CD82 cells using immunofluorescence and confocal microscopy. The cells were stained with anti-PG and anti-DSG2 antibodies and labelled with fluorescently conjugated secondary antibodies. Z-stacks were collected using a 0.35 μm step size and analysed using a cell-cell boundary quantification software (Stroe et al., 2016) (Figure 43). The software detects cell-cell boundaries in the green channel by applying second-order steerable Gaussian filters at different angles. To quantify the fluorescence intensity of the detected cell-cell borders, a threshold is applied to the image followed by morphological thinning to produce a skeleton image which is then expanded to create a mask that covers the cell-cell boundaries that allows the fluorescence intensities of the green and red channels to be computed. The software was used to determine the mean fluorescence intensity of each slice in a z-stack. Analysis of the z-stacks shows that PG fluorescence intensity at cell-cell borders was greater in HB2PURO cells (Figure 43B). However, the fluorescence intensity of DSG2 at cell-cell borders is greater in HB2CD82 cells compared to control cells (Figure 43B). This suggests that CD82 could affect the clustering of PG and DSG2 at the membrane. HB2PURO and HB2CD82 cells were also stained with anti-β-catenin and anti-E-cadherin antibodies to investigate whether CD82 affects their intracellular distribution (Figure 44B). Analysis of the z-stacks shows similar β-catenin fluorescence intensities at cell-cell borders for both HB2PURO and HB2CD82 cells

(Figure 44B). The fluorescence intensity of E-cadherin at cell-cell borders was slightly higher in HB2CD82 cells.

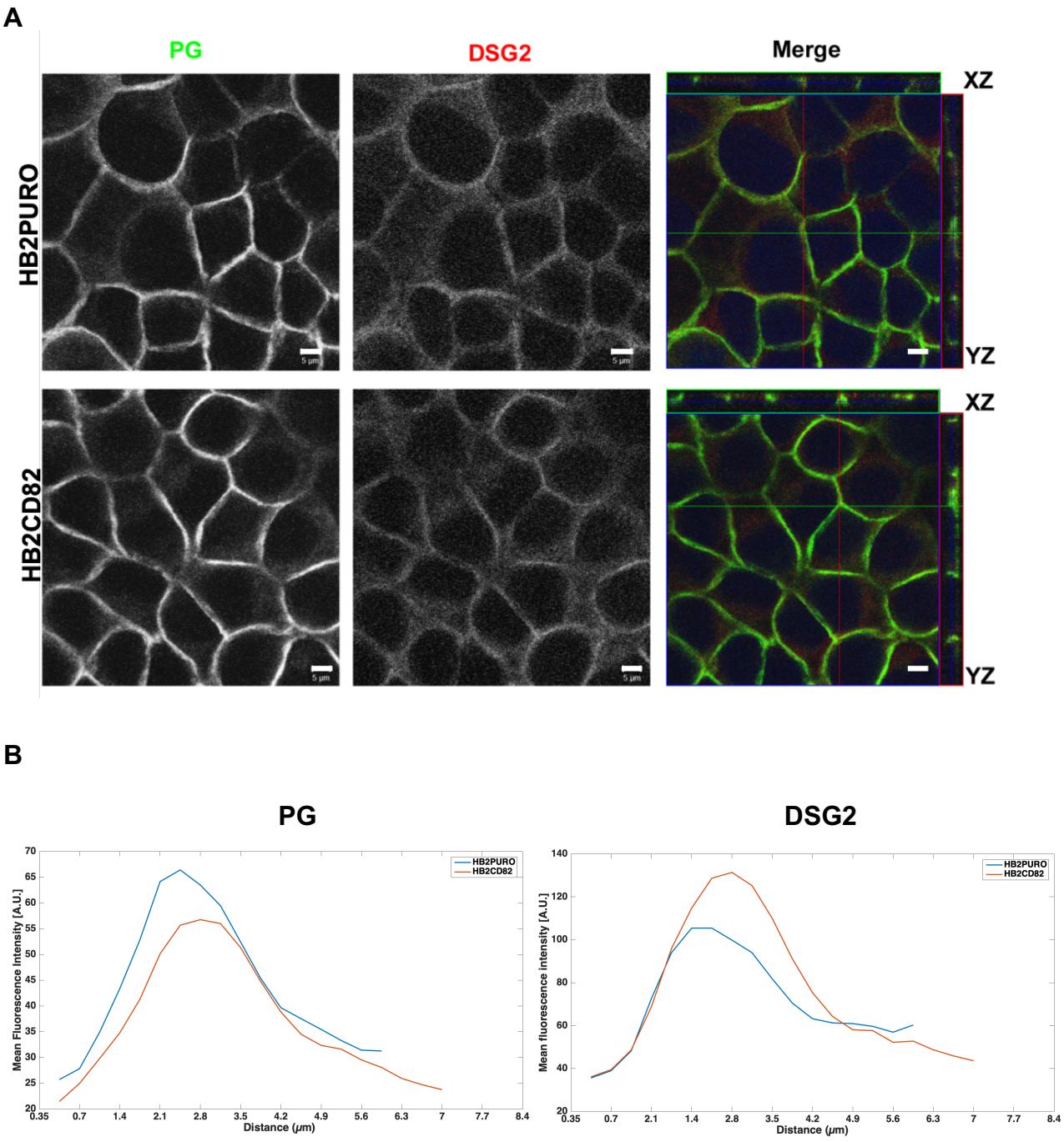

Figure 43 Quantification of PG and DSG fluorescence intensities at cell-cell borders

(A) HB2PURO and HB2CD82 were fixed with methanol and stained with anti-PG and anti-DSG2 antibodies followed by fluorescently conjugated secondary antibodies. Scale bar, 5μm. (B) Z-stacks were collected and analysed using a cell-cell boundary detection software that detects boundaries using second order steerable Gaussian filters. The detected boundaries are then thresholded to compute fluorescence intensities of each slice in a z-stack. Results are from one z-stack and one experiment.

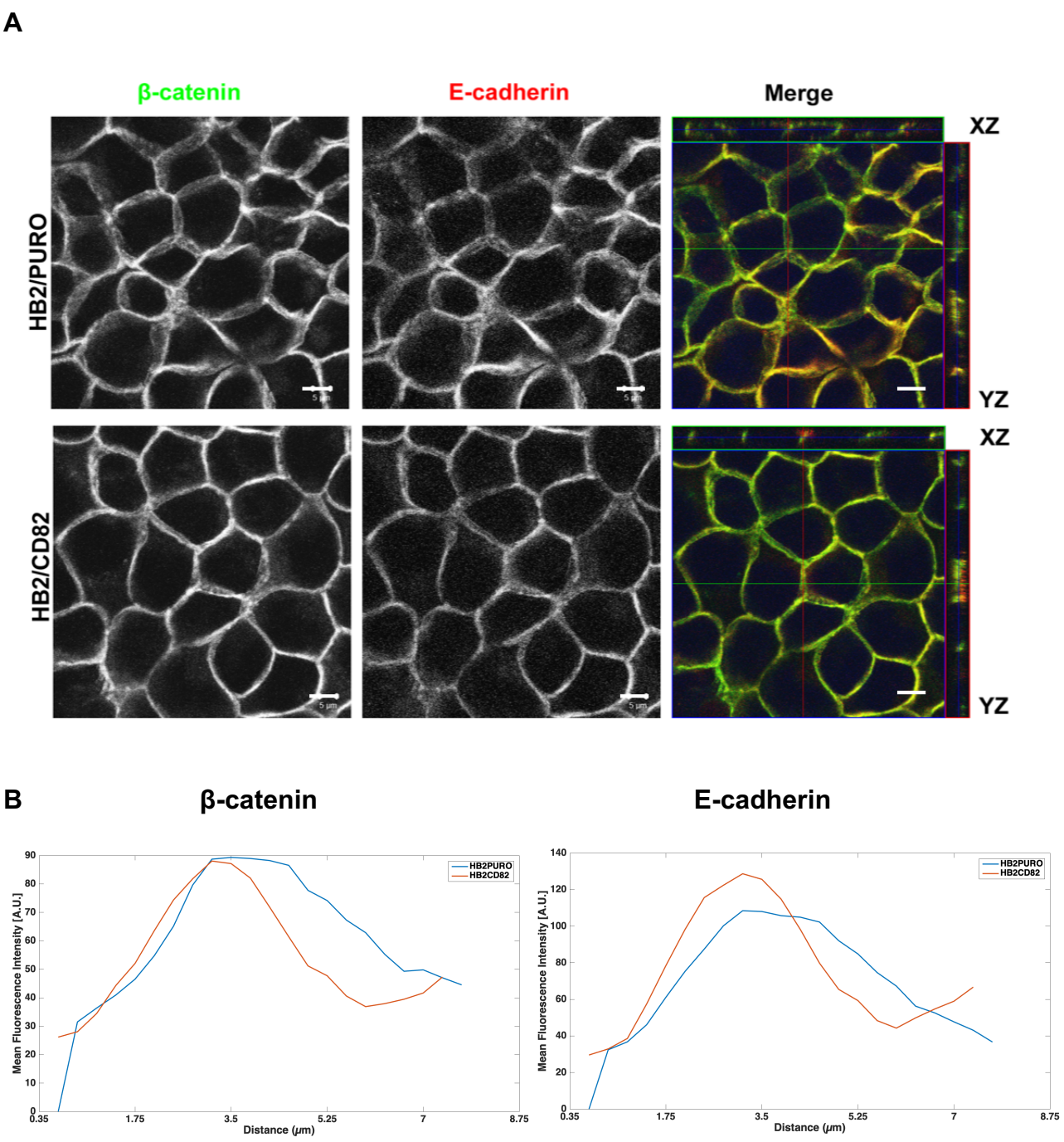

Figure 44 Quantification of β-catenin and E-cadherin fluorescence intensities at cell-cell borders

(A) HB2PURO and HB2CD82 were fixed with methanol and stained with anti- β-catenin and anti-E-cadherin antibodies followed by fluorescently conjugated secondary antibodies. Scale bar, 5μm. (B) Z-stacks were collected and analysed using a cell-cell boundary detection software that detects boundaries using second order steerable Gaussian filters. The detected boundaries are then thresholded to compute fluorescence intensities of each slice in a z-stack. Results are from one z-stack and one experiment.

5.2.2 Methanol fixation clearly delineates cell-cell contacts

HB2PURO cells were grown to confluence on glass bottom dishes. The medium was removed, and the cells were rinsed with PBS before fixation. To determine an optimal method for STORM sample preparation three different fixation methods were tested. In the first method the cells were pre-extracted with sucrose and Triton X-100 before being fixed with paraformaldehyde (PFA). This method has previously been used for resolving desmosomes by dSTORM (Stahley et al., 2016). For the second method the cells were fixed with PFA and permeabilised with Triton X-100. The final method tested was fixation with 100% methanol, a method which gave satisfactory results with confocal microscopy throughout my study. In addition, methanol fixation has also been reported to yield better staining patterns of DP compared with PFA fixation (Ma and Lorincz, 1988). The cells were then stained with an antibody against the C-terminus of PG and labelled with Alexa Fluor (AF) 647. STORM switching buffer was added to the cells and 20000 frames were collected in 3D-STORM mode. The images were reconstructed in Nikon NIS-Elements. A super-resolution image is reconstructed from the stack of images by determining the positions of the molecules. The methanol fixation method clearly delineated cell-cell contacts and gave the lowest level of non-specific staining, highlighting that this is a suitable method for sub-diffraction imaging of desmosomes, and was used for all dSTORM experiments (Figure 45). However, it was difficult to select distinct desmosomes with the anti-PG C-term antibody. Therefore, cells were stained for DSG2 and DP to resolve single desmosomes for clustering analysis.

A

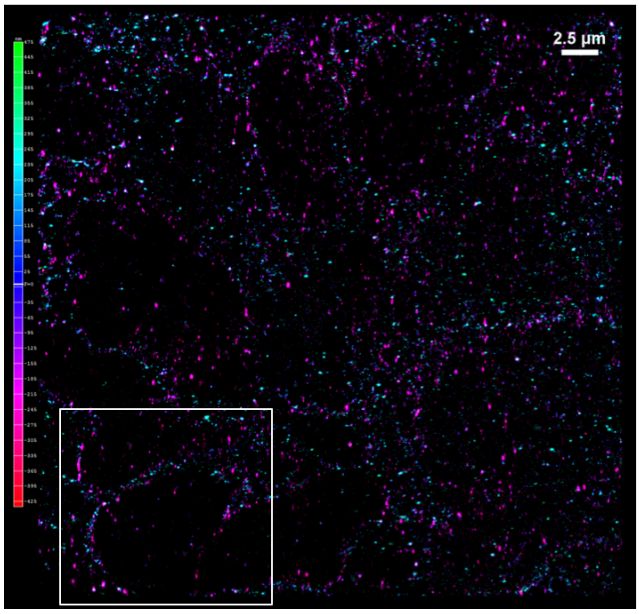

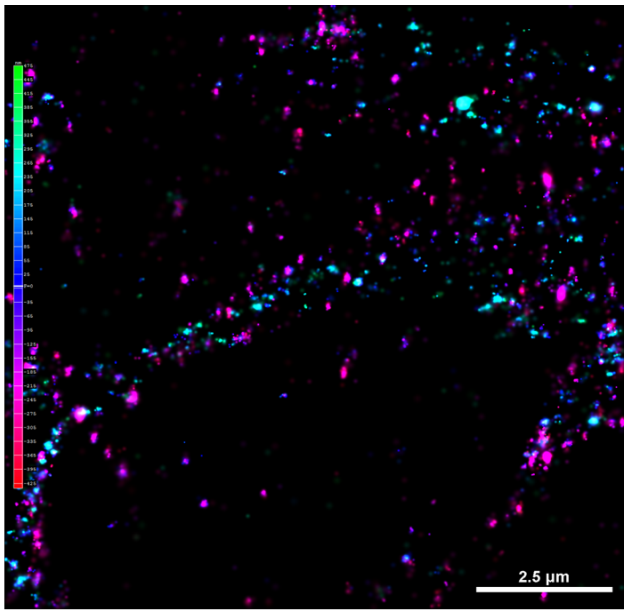

B

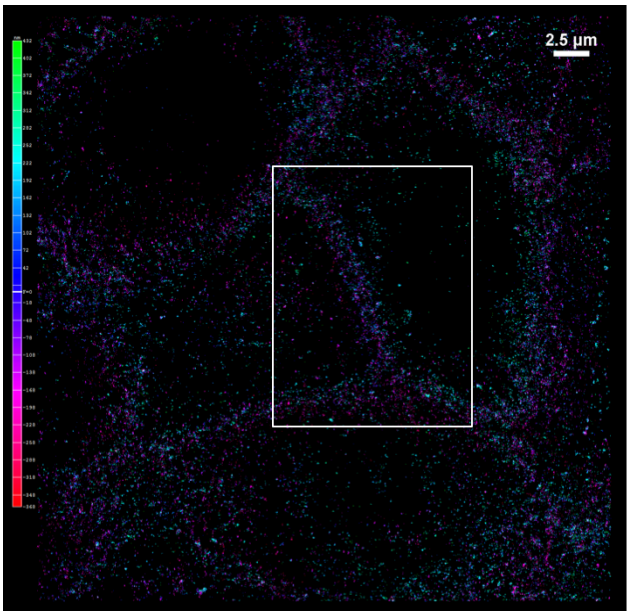

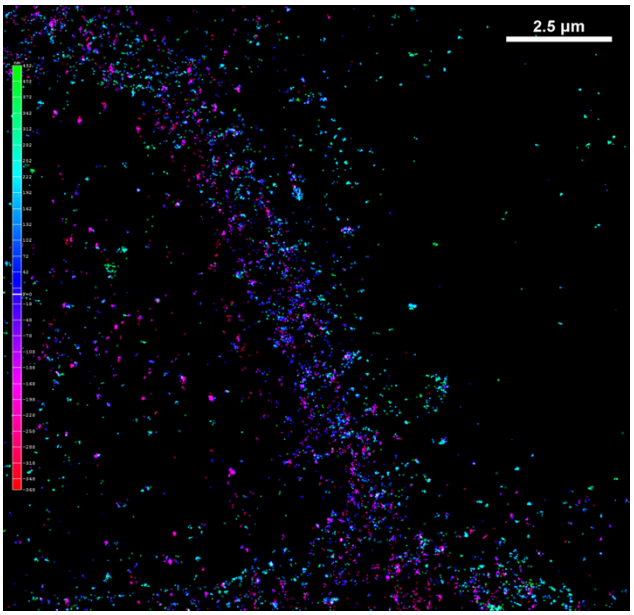

C

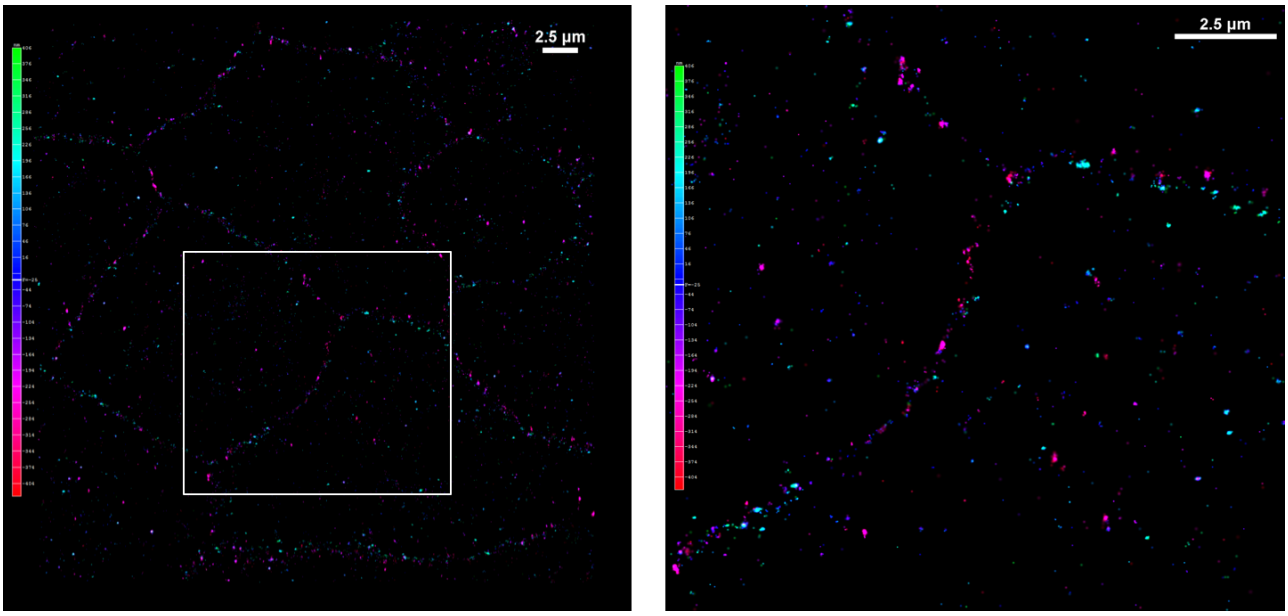

Figure 45 PG resolved by 3D-STORM using different fixation methods

HB2PURO cells were stained with an anti-PG antibody against the C-terminus of PG and labelled with AF647. Images of the whole field of view and regions of interest (white box) for each fixation method are shown. (A) HB2PURO cells were pre-extracted with 300mM sucrose, 0.2% Triton X-100 in PBS, and then fixed with 4% PFA. The cells were then blocked and permeabilised in 3% BSA, 0.2% Triton X-100. (B) Cells were fixed with 4% PFA and permeabilised with 0.1% Triton X-100/PBS, and blocked with 20% heat inactivated goat serum/PBS (C) The cells were fixed with 100% methanol at -20°C, and blocked with 20% heat inactivated goat serum/PBS. Frames were collected in 3D-STORM mode and reconstructed in Nikon NIS-Elements. Scale bar, 2.5 µm. Three images were collected per fixation condition. Representative images are shown. Images are from one experiment.

5.2.3 CD82 does not affect the clustering of DSG2 and DP molecules

To test whether CD82 affects the clustering or 'packing' of DSG2 molecules within desmosomes, HB2PURO and HB2CD82 cells were grown to confluence on glass bottom dishes, and fixed with methanol. The cells were stained with an antibody against the C-terminal domain of DSG2 (DSG2 C-term) and labelled with AF647. STORM switching buffer was added and the cells were imaged in 3D-STORM mode. 20000 frames were collected and reconstructed in the ThunderSTORM software (Ovesný et al., 2014). In contrast to the PG super-resolution images (Figure 45), the reconstructed images of DSG2 show that distinct desmosomes were resolved (Figure 46). Single desmosomes were then selected from the reconstructed images and analysed using a density-based spatial clustering of applications with noise (DBSCAN) algorithm based imaging workflow (Ester et al., 1996). The streamlined imaging workflow used to analyse the dSTORM images was developed by Dr Jeremy Pike at the Centre of Membrane Proteins and Receptors (COMPARE). The workflow was applied to all dSTORM data sets analysed in my study. The DBSCAN algorithm arbitrarily selects a core point and searches for points that have at least a minimum number of points (MinPts) within a given search radius (ε) (Figure 47) (Ester et al., 1996; Nicovich et al., 2017). These points become part of a cluster if they meet these criteria. The neighbouring points are then analysed to determine if they are part of the cluster. All points that do not have MinPts neighbours in the given search radius are not classified as part of a cluster and are considered background. The algorithm then visits the next point till all the points have been classified as part of a cluster or as background. The DBSCAN algorithm also gives information on the area, volume, and density of

clusters. A drawback of method is that the search radius (ε) and MinPts are user defined (Nicovich et al., 2017). Selection of these parameters can be based on values reported for the structures to be analysed or on the distribution of the data to be analysed. Statistical models can be applied to overcome the difficulties associated with selecting appropriate parameters that reflect clustering behaviour (Griffié et al., 2017; Nicovich et al., 2017). However, this requires prior knowledge of the distribution of the molecules and this was not available. A search radius (ε) of 30 nm with 10 MinPts was selected for clustering analysis in my study after optimisation of running the algorithm with different values for these parameters. These values were selected because the points detected were part of more than one cluster rather than being grouped as one large cluster within a plaque of a single desmosome.

Clustering analysis of desmosomes stained with DSG2 C-term using DBSCAN shows that that there is no significant difference in the number of detections between HB2PURO and HB2CD82 cells. The number of detections are the number of molecules that are detected within desmosomes. A similar number of clusters were detected in HB2PURO and HB2CD82 cells (Figure 48, Figure 49). Figure 48 shows 2D and 3D cluster maps of the desmosomes presented in Figure 46. These desmosomes were shown because they showed similar clustering. However, these desmosomes vary in length and this was not measured. Therefore, it is not clear whether CD82 also affects the length of desmosomes. The mean number of detections per cluster was higher in HB2PURO cells compared to HB2CD82 cells. However, this is not significant as only one data

point accounts for the high standard deviation. A similar pattern was also observed for the area and volume of clusters detected. There is also no significant difference in the density (molecules per μm^3) of molecules found within clusters in HB2PURO and HB2CD82 cells. The values for the properties of the clusters are summarised in Table 5. Overall these data indicate that CD82 does not affect the clustering of DSG2 molecules.

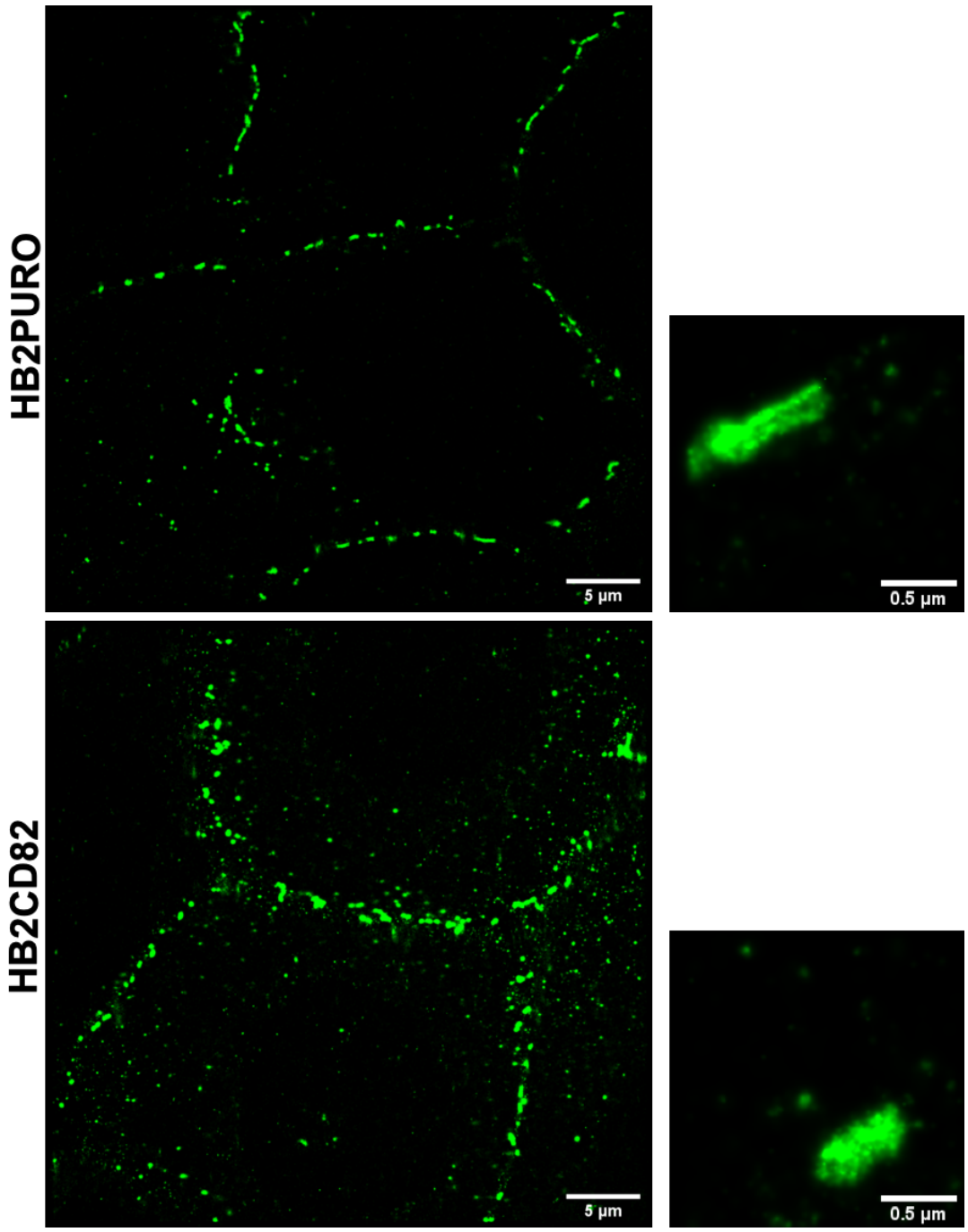

Figure 46 DSG2 C-term resolved by 3D-STORM

HB2PURO and HB2CD82 cells were grown on glass bottom dishes and fixed with 100% methanol. The cells were then stained with an antibody against the C-terminal domain of DSG2 and labelled with AF647. 20000 frames were collected in 3D-STORM mode. The reconstructed images with regions of interest containing single desmosomes are shown. Images are representative of 3 independent experiments. Three images were analysed per experiment. In total 75 desmosomes were analysed per condition. Scale bars, 5 µm full field of view images and 0.5 µm regions of interest.

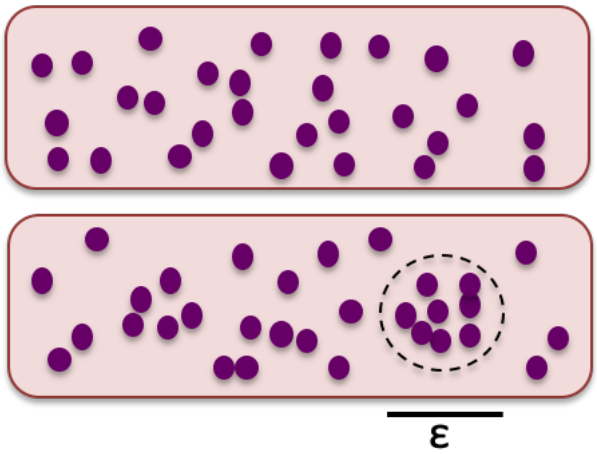

Figure 47 Schematic illustration of the DBSCAN algorithm

DBSCAN groups together points that are tightly packed together in a given radius ε into clusters depending on the number of neighbouring points. The example shown here has been applied to desmosomes. Adapted from Nicovich et al. (2017).

A

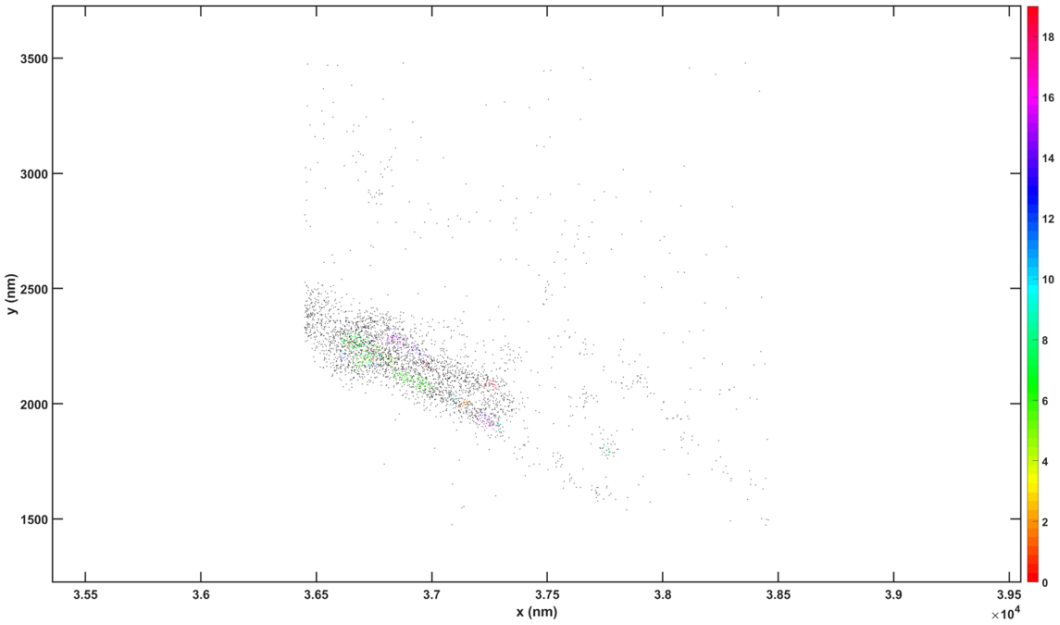

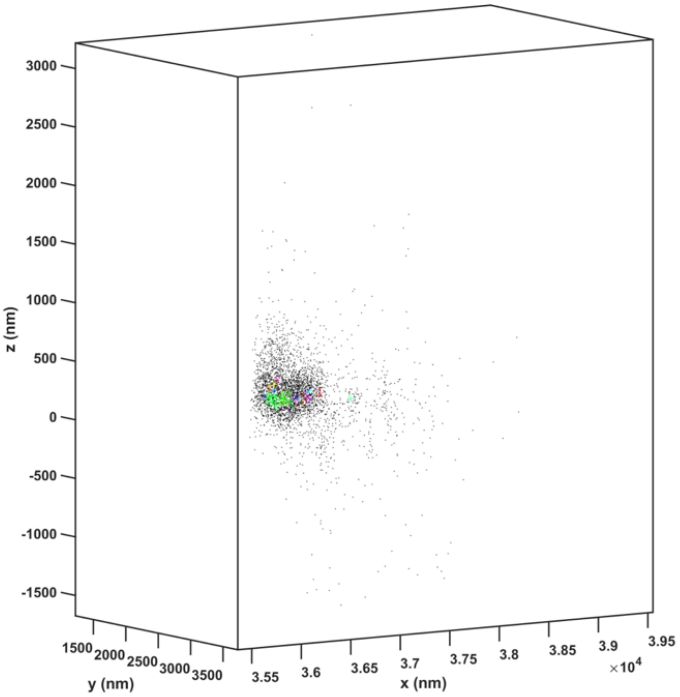

B

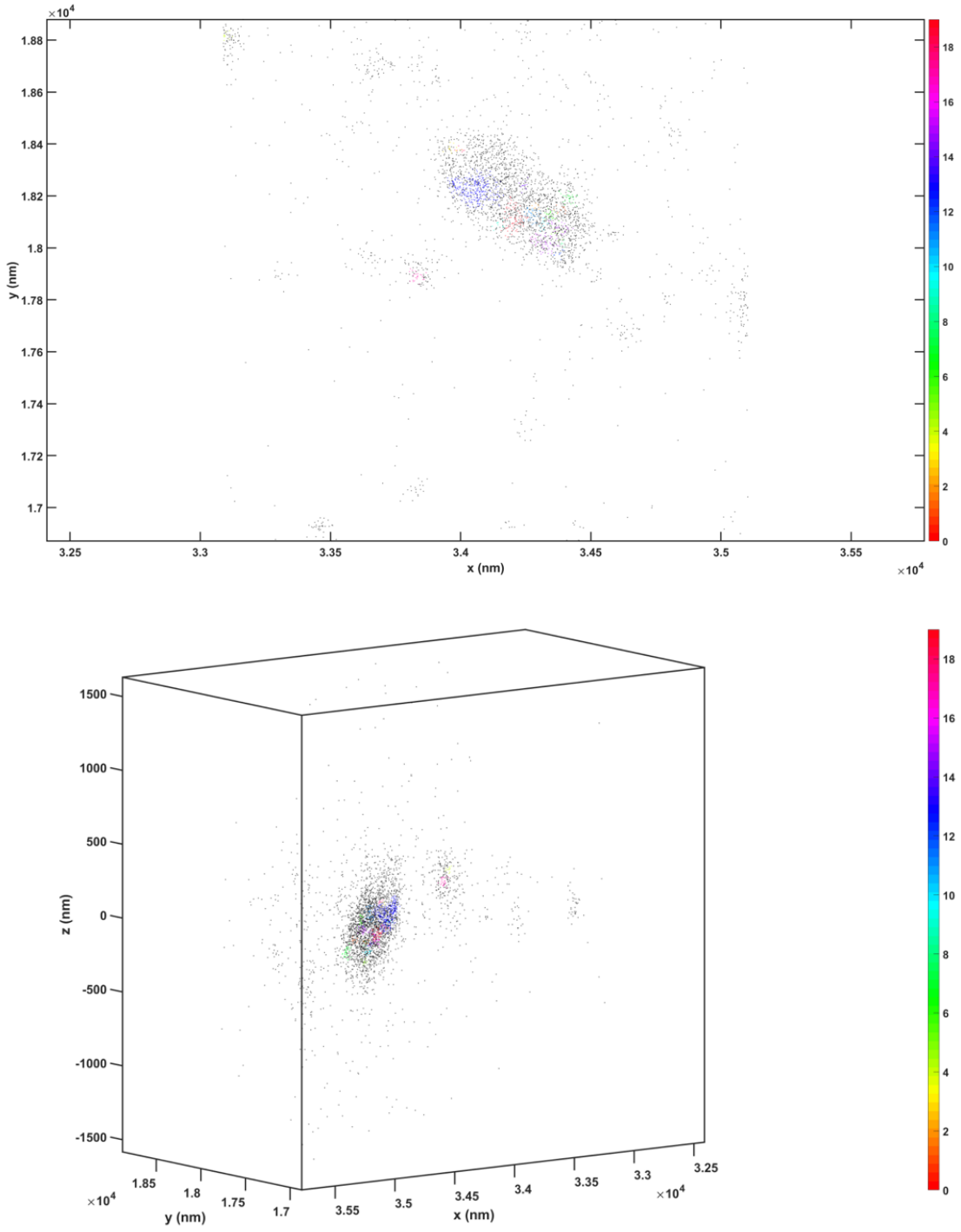

Figure 48 Cluster maps of DSG2 C-term

Cluster maps of DSG2 C-term generated by the DBSCAN image analysis workflow. The images are colour coded according to the number of clusters. (A) HB2PURO 2D and 3D cluster maps of DSG2 C-term. (B) HB2CD82 2D and 3D cluster maps of DSG2 C-term.

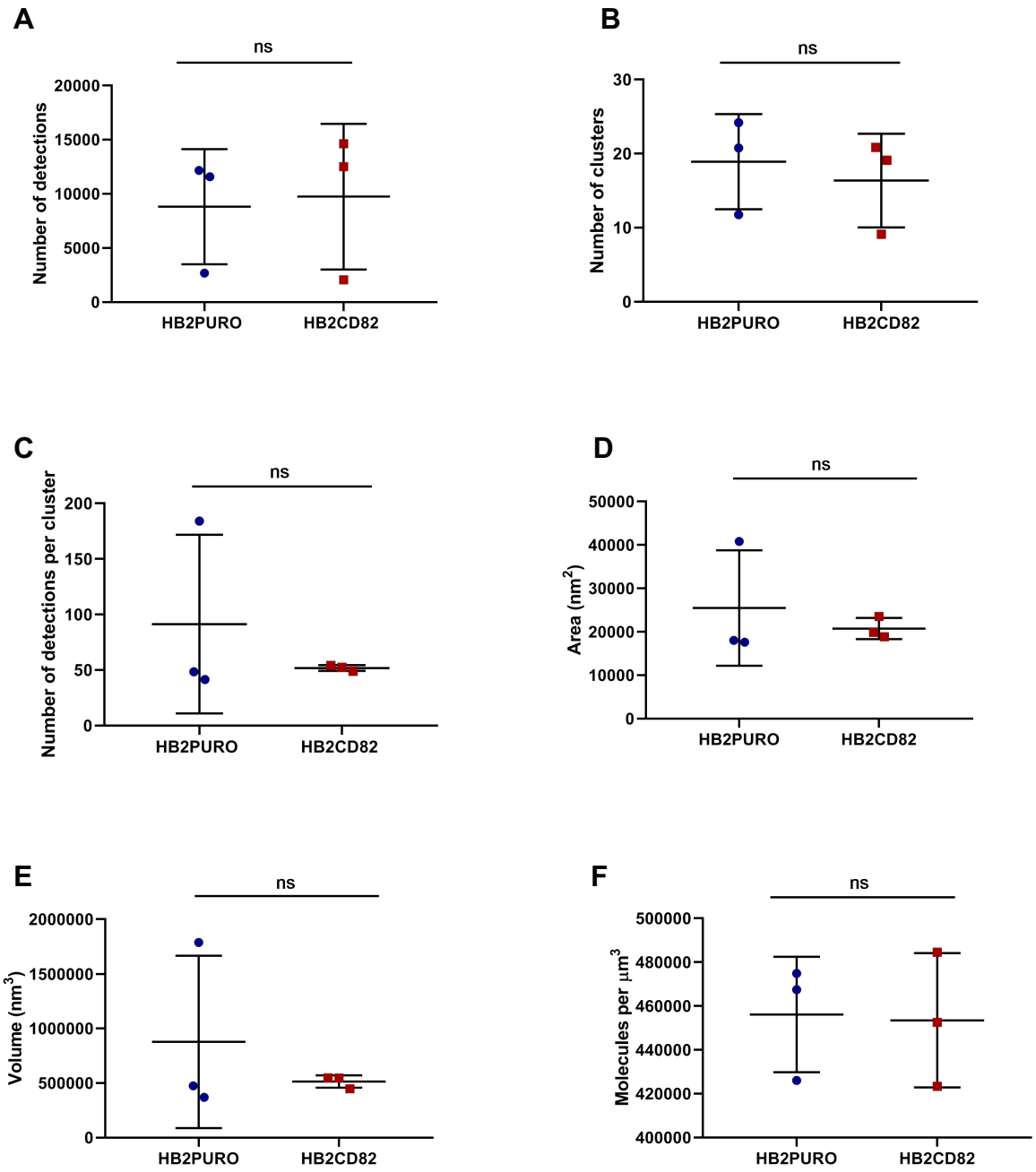

Figure 49 CD82 does not affect the clustering of DSG2 molecules

Cluster analysis of DSG2 C-term with the DBSCAN image analysis workflow. (A) The mean number of molecules detected. (B) The number of clusters detected. (C) The number of molecules detected per cluster. (D) Area of the clusters. (E) Volume of the clusters. (F) Mean density of clusters. 25 desmosomes were analysed from 3 reconstructed images per experiment. Data are the mean, SD and t-test of three independent experiments.

Table 5 DSG2 C-term cluster properties.

	HB2PURO	HB2CD82
Number of detections	8808±5313	9736±6729
Number of clusters	19±6	16±6
Number of detections per cluster	91±80	52±3
Area (nm^2)	25475±13291	20749±2452
Volume (nm^3)	876884±789772	513846±57046
Molecules per μm^3	456128±26343	453497±30611

Values are mean±SD

To analyse whether CD82 affects the clustering of DP molecules within desmosomes, HB2PURO and HB2CD82 were stained with an antibody against the C-terminus of DP (DP C-term) and labelled with AF647. Images were collected and analysed as described above. The reconstructed images show the desmosomal plaques contributed by adjacent cells (Figure 50). Figure 51 shows the 2D and 3D cluster maps obtained with clustering algorithm of the desmosomes shown in Figure 50. These desmosomes were selected because they showed similar clustering. The length of the desmosomes in this dataset was not measured. Clustering analysis of the dataset with the DBSCAN imaging workflow shows there is no significant difference in the number of DP molecules detected in HB2PURO and HB2CD82 cells (Figure 52). A similar number of DP clusters were detected in HB2PURO and HB2CD82 cells. The number of detections per cluster was higher in HB2CD82 cells but this was not significant. The area and volume of DP clusters detected was greater in HB2CD82 but this also not statistically

significant. The density of DP molecules inside clusters (molecules per μm^3) was higher HB2CD82 cells compared to HB2PURO cells but this not statistically significant. The values of the DP cluster properties are summarised in Table 6. These results suggest that CD82 does not regulate the clustering of DP molecules within desmosomes.

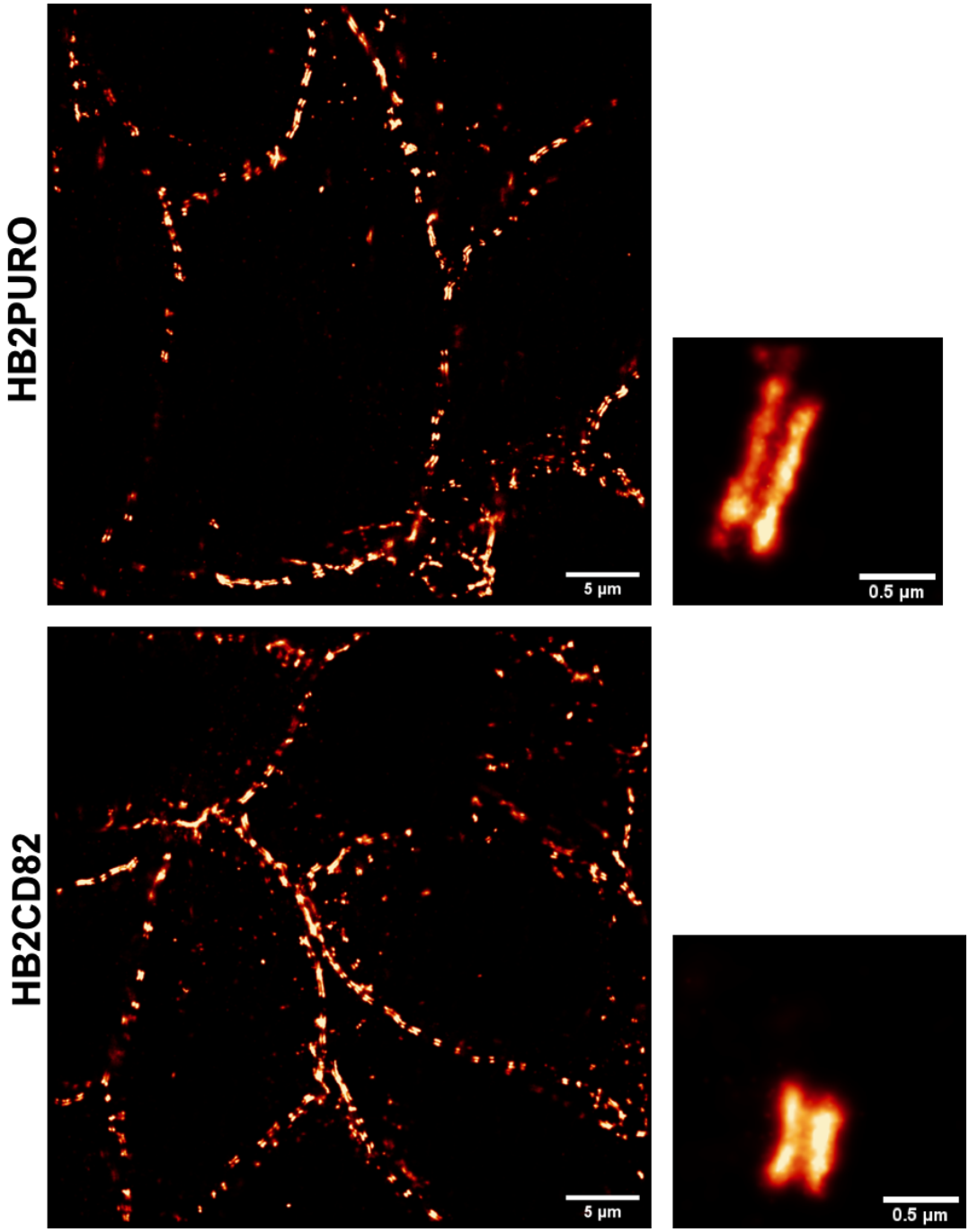

Figure 50 DP C-term resolved by 3D-STORM

HB2PURO and HB2CD82 cells were grown on glass bottom dishes and fixed with 100% methanol. The cells were then stained with an antibody against the C-terminal domain of DP and labelled with AF647. 20000 frames were collected in 3D-STORM mode. The reconstructed images with regions of interest containing single desmosomes are shown. Images are representative of 3 independent experiments. Three images were analysed per experiment. In total 75 desmosomes were analysed per condition. Scale bars, 5 µm full field of view images and 0.5 µm regions of interest.

A

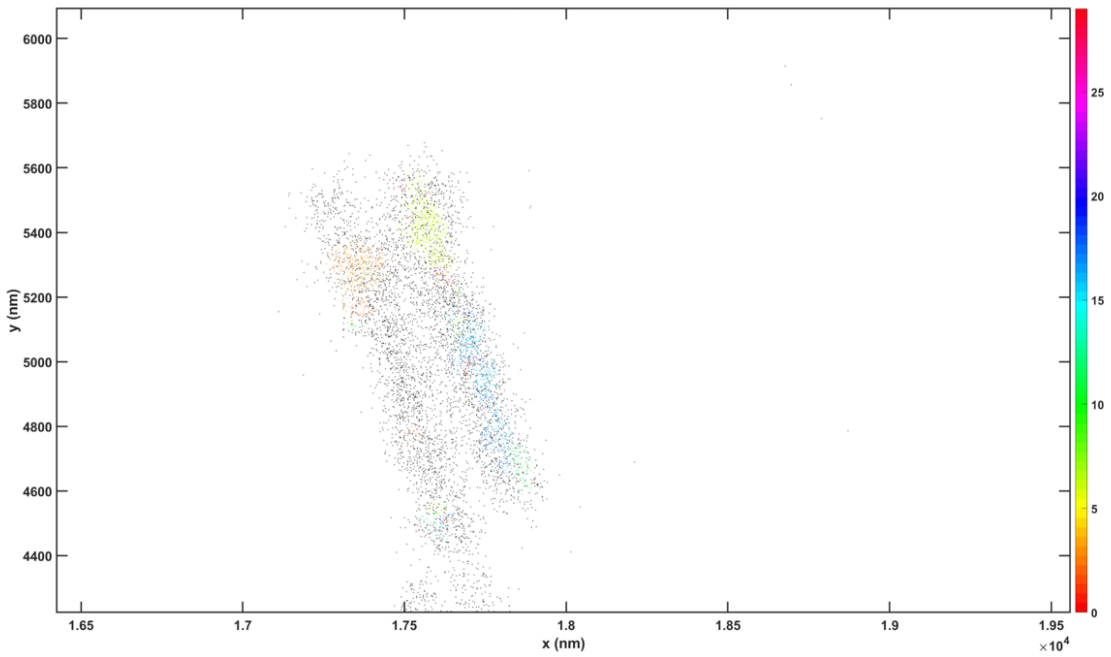
6000
5800
5600
5400
5200
5000
4800
4600
4400
y (nm)
1.65
1.7
1.75
1.8
1.85
1.9
1.95
x (nm)
×10^4
25
20
15
10
5
0

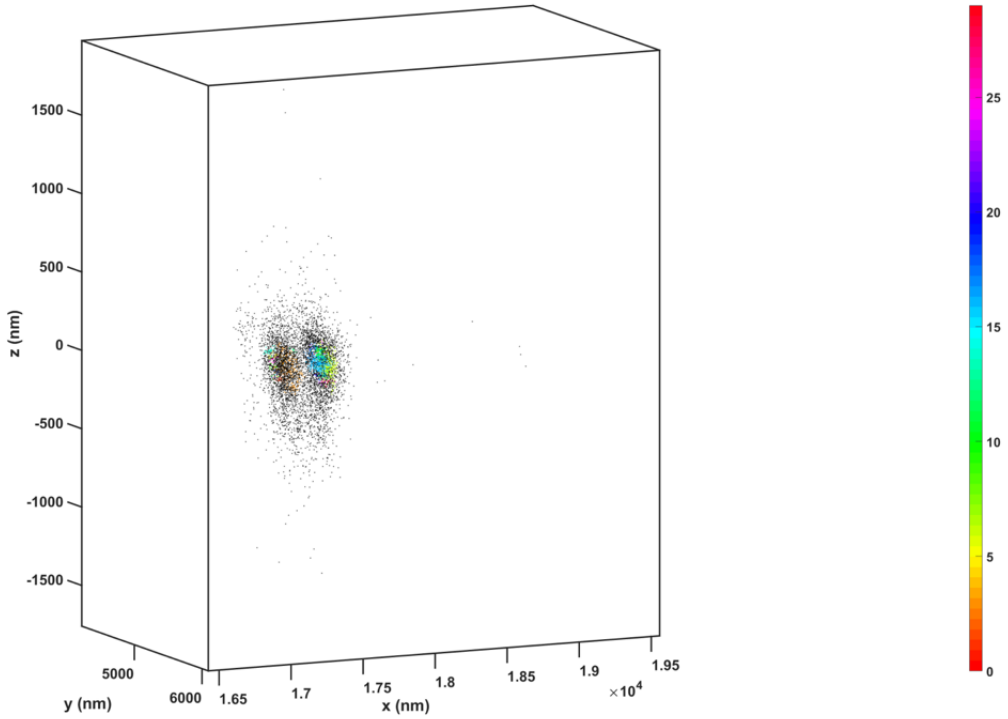
1500
1000
500
0
-500
-1000
-1500
z (nm)
5000
6000
y (nm)
1.65
1.7
1.75
1.8
1.85
1.9
1.95
x (nm)
×10^4
25
20
15
10
5
0

B

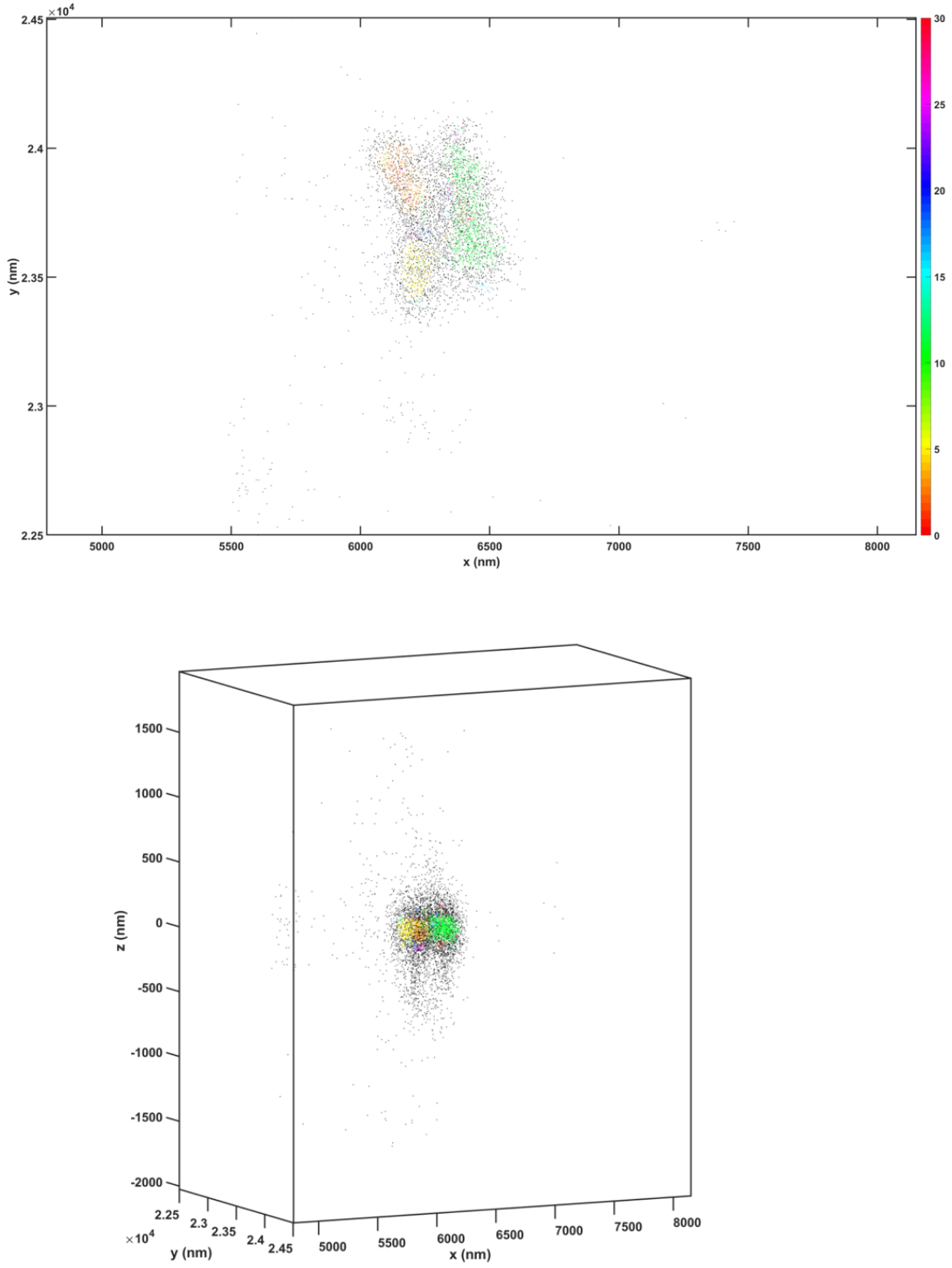

Figure 51 Cluster maps of DP C-term

Cluster maps of DP C-term generated by the DBSCAN image analysis workflow. The images are colour coded according to the number of clusters. (A) HB2PURO 2D and 3D cluster maps. (B) HB2CD82 2D and 3D cluster maps.

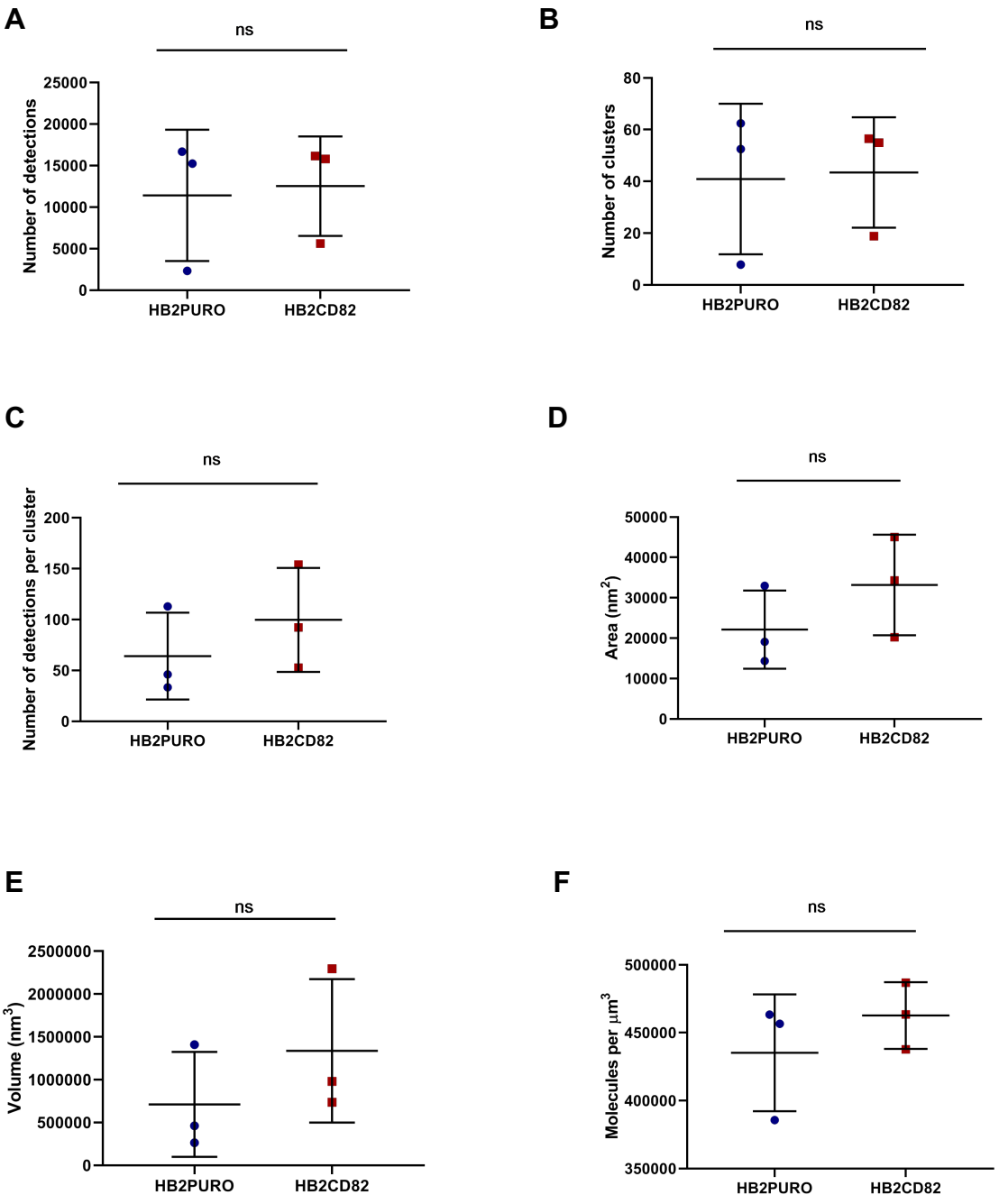

Figure 52 CD82 does not affect clustering of DP molecules

Cluster analysis of DP C-term with the DBSCAN image analysis workflow. (A) The mean number of molecules detected. (B) The number of clusters detected. (C) The number of molecules detected per cluster. (D) Area of the clusters. (E) Volume of the clusters. (F) Mean density of clusters. 25 desmosomes were analysed from 3 reconstructed images per experiment. Data are the mean, SD and t-test of three independent experiments.

Table 6 DP C-term cluster properties.

	HB2PURO	HB2CD82
Number of detections	11412±7904	12525±5989
Number of clusters	41±29	43±21
Number of detections per cluster	64±43	100±51
Area (nm^2)	22141±9688	33205±12455
Volume (nm^3)	712141±612478	1336698±838026
Molecules per μm^3	435209±42998	462635±24550

Values are mean±SD

5.2.4 CD82 alters the organisation of the desmosomal plaque

Section 5.2.3 showed that CD82 did not affect the clustering of DSG2 and DP. This led me to investigate the organisation of the desmosomal plaque as this may correlate with changes in adhesion (Stahley et al., 2016). The DP C-terminal domain super-resolution images clearly show the plaques contributed by adjacent cells (Figure 50). The same data set was used to study the organisation of desmosomes. To test whether CD82 affects the organisation of the desmosomal plaque, the distance between the two plaques was measured. The plaque to plaque distances were measured on 2D images. The plaque to plaque distance of the DP C-terminal domains was determined using the plot profile function in Fiji. This function determines the intensities of pixels within a selection along with the distance through the selection. This allowed the distance between the two intensity peaks corresponding to each plaque perpendicular to the plasma membrane to be calculated. The results show that overexpression of CD82 reduces the plaque to plaque distance for DP C-term (Figure 53). A plaque to plaque distance of 261 nm

was observed in CD82 overexpressing HB2 cells compared to 307 nm in HB2PURO cells. The separation between the plaques is also maintained in 3D as shown in the cluster maps (Figure 51). The plaque to plaque distance for DSG2 C-term was not determined because the plaques were closer together and it was difficult to distinguish between peaks. Moreover, the length of desmosomes or width of individual plaques were not measured due to time constraints. Therefore, it is not clear whether these features contribute to the CD82 mediated increase in cell-cell adhesion. Further analysis of the dataset is required to determine whether overexpression of CD82 affects these features.

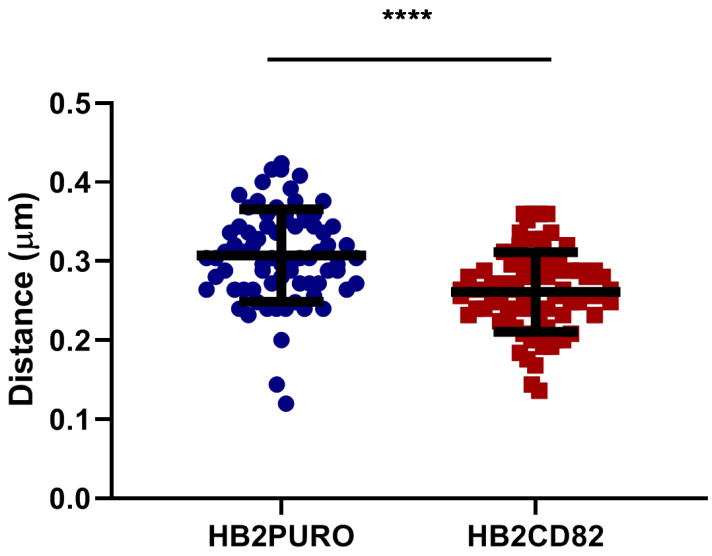

Figure 53 Expression of CD82 reduces the plaque to plaque distance of the DP C-terminal domains

Quantification of the plaque to plaque distance of the DP C-terminal domains. Results are the plaque to plaque distances of 75 desmosomes, SD and t-test from three independent experiments (**** P<0.0001).

5.3 Discussion

Studies have reported that CD82 can regulate the clustering of membrane proteins and cytoplasmic signalling proteins such as PKCα (Termini et al., 2014; Marjon et al., 2016; Termini et al., 2016). Using confocal immunofluorescence microscopy and cell boundary detection software (Stroe et al., 2016) increased levels of PG and reduced levels of DSG2 were detected at cell-cell borders in CD28 overexpressing cells. It is possible that changes in expression at the membrane correlate with clustering. Hence I decided to investigate whether CD82 affects the clustering of desmosomal proteins, as this may contribute to the CD82 mediated increase in cell-cell adhesion (Section 3.2.1). Single desmosomes were resolved using dSTORM and the clustering of proteins within desmosomes was analysed using the clustering algorithm DBSCAN (Figure 47). The clustering of PG was not investigated as it was difficult to select single desmosomes to permit clustering analysis. However, it was possible to investigate the clustering of DSG2 and DP. The results suggest that clustering of DSG2 and DP does not contribute to the CD82 mediated increase in cell-cell adhesion (Figure 49, Figure 52).

One drawback of DBSCAN is that the two key parameters, search radius and minimum number of points are user defined. The values selected are usually informed by previous values used for similar structures. There was no previous data available for desmosomal proteins and the values used were selected as they gave rise to clusters in the region of interests. The lack of prior knowledge could perhaps have contributed to the non-significant results obtained for DSG2 and DP with the DBSCAN algorithm and may not reflect their clustering behaviour. To

overcome this, alternative density-based clustering algorithms such as OPTICS (ordering points to identify clustering structure) that do not heavily rely on the key parameters mentioned above could be used (Nicovich et al, 2017). Another possibility that has not been explored is that clustering of PKCα by CD82 could perhaps indirectly contribute to the recruitment of PKCα by PKP2 to DP to allow DP assembly into desmosomes (Bass-Zubek et al., 2008; Termini et al., 2016).

Ultrastructural studies have shown that calcium independent hyperadhesive desmosomes possess an electron-dense midline in the intercellular space between two adjacent cells (Odland, 1958; North et al., 1999; Garrod et al., 2005). The midlines arise from the highly organised arrangement of the desmosomal cadherins (Garrod et al., 2005). Desmosomes found at a wound edge lack midlines and are calcium dependent (Garrod et al., 2005). The intercellular space of these desmosomes is also narrower suggesting a loss of the ordered arrangement of the desmosomal cadherins resulting in weakly adhesive desmosomes. Given that the organisation of desmosomal components affects adhesive strength I investigated whether CD82 affects the organisation of the desmosomal plaque. Using dSTORM, plaques contributed by adjacent cells were resolved with distinct separation with an anti-DP C-term antibody. This allowed the distance between the DP C-terminal domains to be measured. The results suggest that CD82 reduces the DP C-term plaque to plaque distance (Figure 53). The value obtained for the DP C-term plaque to plaque distance in CD82 overexpressing HB2 cells is close to the plaque to plaque distance of 235 nm reported for DP C-terminal domains in human keratinocytes obtained using

dSTORM (Stahley et al., 2016). Overexpression of PKP1 increases cell-cell adhesion and reduces the plaque to plaque distances of DSG2 C-term, DP rod and C-terminal domains in human keratinocytes (Tucker et al., 2014; Stahley et al., 2016). This suggests that CD82 strengthens desmosomal adhesion by altering the organisation of the desmosomal plaque.

My data show that the CD82 mediated increase in cell adhesion is accompanied by a decrease in DP plaque to plaque distance (Figure 53). How then is this achieved? North et al. (1999) using immunogold labelling and electron microscopy found that the DP C terminus was located 52 nm from the membrane in sections of bovine nasal epidermis that contained both the DPI and DPII isoforms. This distance is consistent with the shorter DPII isoform being orientated perpendicular to the membrane. If this is the case then the longer DPI isoform must adopt an alternative conformation, being either folded or coiled, or oriented at an angle to the membrane, as suggested by Stahley et al. (2016a). Stahley et al. (2016a) showed that the plaque to plaque distance for the DP N-terminal domain does not change upon PKP1 overexpression in cultured human keratinocytes whilst the DP C-terminal domain moves closer to the membrane. Hence to achieve a decrease in plaque to plaque distance for the DP C-terminal domain (Figure 53) both DP isoforms must either fold or coil to a greater extent or adopt a less perpendicular, more acute orientation to the membrane.

The N-terminus of DP contains a short N-terminal unstructured region and a plakin domain which consists of six spectrin repeats (SR3-8) and a Src homology domain

embedded in SR5. The plakin domain is comprised of two rigid arms, a long arm consisting of SR3-6 (and the SH3 domain), and a short arm consisting of SR7-8, with a flexible hinge between the two (Al-Jassar et al., 2013). Therefore, it may be that the flexible hinge in the DP plakin domain allows for movement of the DP C-terminal domain, allowing DP to adopt an extended or contracted conformation as required. Extension of the hinge may occur when desmosomes are subjected to mechanical stress, preventing damage to the long and short arms and perhaps other domains of the protein (Ortega et al., 2016). The DP C-terminal domain contains three plakin repeat domains (PRD A, B and C) and a linker domain that separates PRDs B and C (Choi et al., 2002; Kang et al., 2016). The linker region of DP contains residues that are important for intermediate filament binding and confers specificity for vimentin and simple epithelial keratins (Fontao et al., 2003). The linker domain is followed by a short unstructured flexible region which may offer some flexibility to the DP tail region. However, small angle X-ray scattering analysis of the DP tail region suggests that flexibility of the linker is limited (Kang et al., 2016). Therefore, it is likely that the flexible hinge within the plakin domain is more likely to facilitate movement of the DP C-terminal domain, and so account for the reduced plaque to plaque distance in CD82 overexpressing cells.

In summary, the results presented in this chapter indicate that CD82 does not strengthen desmosomal adhesion by regulating the clustering of DSG2 and DP. However, though not investigated in my study, it could be that CD82 alters the orientation of DP in the plaque causing DP C-termini to move closer to the membrane, resulting in a reduced plaque to plaque distance upon CD82

overexpression. The reorganisation in the desmosomal plaque could contribute to the CD82 mediated increase in desmosomal adhesion. The challenge that remains will be to prove that this is the case.

Chapter 6 – Discussion and future work

6.1 CD82 increases desmosomal adhesion

Desmosomal adhesion is vital for the maintenance of tissue integrity. Loss of desmosomal adhesion can have devastating consequences for human health and it is important to understand the mechanisms by which desmosomal adhesion is regulated. Herein for the first time I have shown that the tetraspanin CD82 is able to increase desmosomal adhesion. The mammary epithelial cell line HB2 was used for the majority of my experiments because they have been used as model system for studying CD82 interactions and they express desmosomal and adherens junction proteins (Odintsova et al., 2000; Odintsova et al., 2003; Odintsova et al., 2013). Overexpression of CD82 in HB2 cells resulted in both increased desmosomal and adherens junction mediated cell-cell adhesion. A number of studies have reported that CD82 increases cell-cell adhesion (Jee et al., 2003; Abe et al., 2008; Lee et al., 2018) but none have previously documented the contribution of desmosomes to this process.

It is clear that both desmosomes and adherens junctions contribute to cell-cell adhesion, both in control HB2 cells and in HB2 cells that overexpress CD82. In control HB2 cells siRNA against DSG2 (and PG) results in a decrease in adhesion. Similarly, siRNA against E-cadherin (and β-catenin) results in a decrease in adhesion. Addition of siRNAs against both DSG2 and E-cadherin results in a further decrease in adhesion. A similar picture emerges when HB2 cells overexpressing CD82 are examined, although in each case the cells are more adhesive than their control counterparts. Thus, in HB2CD82 cells siRNA

against DSG2 (and PG) and E-cadherin, results in a decrease in adhesion. As in control HB2 cells siRNA against both DSG2 and E-cadherin results in a further decrease in adhesion. Together these data clearly show that both desmosomes and adherens junctions play a part in the CD82 mediated increase in cell-cell adhesion in HB2 cells. HB2CD82 cells treated with siRNAs against DSG2 and E-cadherin appear to be slightly more adhesive than their control counterparts (Figure 26) so it may be that CD82 increases adhesion by another, as yet undefined mechanism.

My siRNA data clearly implicate DSG2 in the CD82 mediated increase in adhesion. DSG2 is the only desmoglein expressed in HB2 cells and both a DSG and DSC are required for desmosomal adhesion (Chidgey et al., 1996; Tselepis et al., 1998). DP is also required for desmosomal adhesion, but no firm conclusion could be drawn on the role of DP in the CD82 mediated increase in cell-cell adhesion. The data showing that DP is essential for normal desmosomal adhesion is extensive and clear-cut. To give just one example loss of DP in keratinocytes results in weaker adhesion as a result of failure of attachment to IFs (Vasioukhin et al., 2001). Hence the contradictory results obtained with the DP knockdown experiments in HB2 cells are difficult to explain. Knockdown of DP should have resulted in loss of adhesion, in both HB2 control and HB2 cells overexpressing CD82. It is almost inconceivable that knockdown of DP could have any other effect on adhesion. One possible explanation could be that the rotational forces experienced by HB2 mammary epithelial cells in dispase assays are different to those that are experienced by keratinocytes in the skin and by cells in other

tissues *in vivo* subjected to strong mechanical forces. However, lack of reproducibility was a problem with all of the dispase assays, particularly those involving DP siRNAs, and this is the most likely explanation for the contradictory nature of the data obtained. This variation is also evident when the data is expressed as fold change relative to the control transfection for each experiment.

Knockdown/ knockout experiments often result in upregulation and redistribution of related molecules. For example, β-catenin is localised to desmosomes in PG null mice (although it is unable to fully compensate for the lack of PG) (Bierkamp et al., 1999) and upregulation of PG compensates for the absence of β-catenin in adult cardiomyocytes (Zhou et al., 2007). Hence, I considered the possibility that adherens junction proteins could be upregulated in response to knockdown of desmosomal proteins, and so compensate at least in part for loss of desmosomal adhesiveness in siRNA experiments. This was not the case as neither E-cadherin nor β-catenin was upregulated in HB2 cells in response to knockdown of either DSG2, PG or DP (Figure 19). Furthermore, there was no discernible change in the intracellular localisation of either of any of these proteins (Figure 20).

Palmitoylation of CD82 is not required for the CD82 mediated increase in cell-cell adhesion (Figure 9). CD82 contains five membrane proximal cysteines that can be palmitoylated (Termini and Gillette, 2017). HB2 cells overexpressing palmitoylation deficient CD82 (HB2CD82Cys5) (i.e. CD82 with five cysteine residues mutated to alanine) showed similar adhesiveness to HB2CD82 cells (Figure 9). Palmitoylation is important for the formation of tetraspanin-enriched microdomains (TERMs) and

stabilises tetraspanin-tetraspanin interactions and tetraspanin interactions with other proteins (Yang et al., 2002; Berditchevski et al., 2002; Charrin et al., 2002), and mutation of tetraspanin palmitoylation sites has been shown to reduce tetraspanin interactions with integrins which in turn affects associated signalling pathways. Further to this overexpression of palmitoylation deficient CD82 in KG1a human acute myeloid leukaemia cells results in decreased adhesion to fibronectin which has been linked to a reduced density of α4β1 integrin clusters (Termini et al., 2014). CD82 does not directly interact with α4β1 integrin and, α4β1 integrin is linked to CD82 through associations with other tetraspanins (Termini et al., 2014). The result obtained with HB2 cells expressing palmitoylation deficient CD82 suggest that the CD82 mediated increase in cell-cell adhesion arises through a mechanism that does not entirely rely on interactions within TERMs.

6.2 CD82 interacts with PKCα which in turn interacts with, and phosphorylates, DP

For immunoprecipitation and pull-down experiments the HEK293T cell line was used. This is a human embryonic kidney cell line and was used because it is possible to transfect these cells with much greater efficiency than HB2 cells, which are somewhat refractory to transfection, so maximising the chances of observing interactions between transfected proteins. I co-transfected HEK293T cells with constructs encoding CD82 and a GFP-PKCα fusion protein and immunoprecipitated the fusion protein with an antibody against GFP. Using this methodology I showed that CD82 interacts with PKCα in the presence of the PKC

activator TPA (and using 1% Brij 98 to lyse the transfected cells) (Figure 27). This is consistent with the findings of Zhang et al. (2001) who showed by immunoprecipitation with an anti-CD82 antibody that CD82 interacts with PKCα in TPA treated Jurkat cells. In addition, I showed that both N- and C-terminal deletion constructs of CD82 are capable of interacting with PKCα (Figure 28). Thus, neither N- nor C-terminal domains are essential for binding PKCα. These results build on the findings of Zhang et al. (2001) as they further implicate transmembrane loops 1 and 2 in the interaction between tetraspanins and PKCα. In contrast to the results obtained in my study, using fluorescence lifetime imaging, it was shown that CD53 and PKCβ are within close proximity in TPA treated B cells (Zuidscherwoude et al., 2017), and that this interaction is mediated by the N-terminus of CD53 as removal of the N-terminal domain disrupted the interaction between CD53 and PKCβ. This suggests that that different PKC isoforms could preferentially bind to either the N- and C- terminal tail of tetraspanins or possibly both.

I then went on to investigate the interaction of PKCα with DP. While DP has been shown to be a substrate of PKCα, little is known about whether DP is also a binding partner of PKCα. Two DP C-terminal domain constructs were expressed in HEK293T cells, of which one encompassed PRDs A, B and C (DP-ABC-FLAG), and the other PRDs ABC and GSR rich region (DP-ABC-GSR-FLAG). The GSR rich region contains residue S2849 which can be phosphorylated by PKCα (Stappenbeck et al., 1994; Fontao et al., 2003). FLAG-agarose pull-downs show that both DP constructs can interact with PKCα (Figure 34). However, it appears

that the construct with the GSR rich region interacts more robustly with PKCα. This may be because the construct containing the GSR rich region is more efficiently expressed or that there is indeed a stronger interaction between this construct and PKCα. It will be important to repeat this experiment to distinguish between these two possibilities as little is known of PKCα interactions and phosphorylation of residues outside of the DP GSR rich region.

To confirm that PKCα is able to phosphorylate DP I co-transfected HEK293T cells with DP and PKCα constructs and stimulated the cells with TPA. Immunoprecipitation experiments with an anti-phosphoserine antibody showed that PKCα is able to phosphorylate DP on serine residues. Phosphorylation of both DP constructs (i.e. both with and without the GSR rich domain) was detected (Figure 35). Hence it is clear that PKC is able to interact with and phosphorylate serine residues outside of the GSR rich region. Phosphorylation of DP persisted in the presence of the PKC inhibitor Gö6976, suggesting the potential involvement of other PKC isoforms or other serine/threonine kinases such as PKA. The latter has been implicated in the phosphorylation of plakin proteins. Thus phosphorylation of plakin family member plectin on residue S4642, which is equivalent residue to DP S2849, by PKA results in reduced association with IFs, which facilitates wound healing (Bouameur et al., 2013). Similarly, treatment of HeLa cells with forskolin activates PKA and results in phosphorylation of DP and reduced attachment to IFs which in turn promotes desmosome assembly (Stappenbeck et al., 1994; Godsel et al., 2005). However, the experiments with the Gö6976 inhibitor were carried out once and more replicates are needed. In addition, to this the concentration and

incubation time with the inhibitor needs to be determined for HEK293T cells, as the conditions used in my study were determined to be appropriate for HaCaT cells by Kimura et al., (2007).

Tyrosine phosphorylation of PG is thought to modulate its interactions with other desmosomal proteins (Gaudry et al., 2001; Miravet et al., 2003) but little is known regarding the role of serine phosphorylation. I co-transfected HEK293T cells with PG and PKCα constructs and stimulated the cells with TPA. Immunoprecipitation experiments with an anti-phosphoserine antibody showed that PKCα is able to phosphorylate PG on serine residues (Figure 37). Phosphorylation of PG persisted in the presence of Gö6976 so other PKCs that are not inhibited by this compound may be involved. It is also difficult to draw a conclusion based on this result as the same limitations with DP and Gö6976 experiments apply. However, I did not test whether PG interacts with PKCα in the same way that DP does, and it will be important to carry out this experiment in the future. Endogenous DSG1 is phosphorylated on serine residues in MDCK cells (Pasdar et al., 1995) but I was unable to detect serine phosphorylation of exogenous DSG2 and DSC2a following transfection experiments in HEK293T cells.

One limitation of this part of my study is that although the phosphorylation studies clearly show that PKCα is able to phosphorylate DP and PG, they do not prove that phosphorylation of DP and/or PG by PKCα occurs in HB2 cells and is subsequently responsible for the CD82 mediated increase in cell-cell adhesion. Treatment of control and CD82 overexpressing HB2 cells with TPA indicated that

activation of PKC is involved in the observed increase in adhesion, but it does not show that either DP or PG is the target of the kinase, and if so whether phosphorylation of either of these proteins affects cell-cell adhesion. Further, TPA is not specific for the PKCα isoform, so other PKCs, or indeed other serine/threonine kinases, could be involved in regulating adhesion in HB2 cells. Knockdown of PKCα in control and CD82 overexpressing HB2 cells does not result in a significant decrease in adhesion (Figure 42), suggesting the potential involvement of either other PKC isoforms or other kinases. It will be important to determine whether any difference in DP and/or PG phosphorylation can be seen in control and CD82 overexpressing cells. Endogenous desmosomal proteins are difficult to immunoprecipitate because they are incorporated into insoluble desmosomes but it may be possible to distinguish differences in phosphorylation in DP and/or PG constructs transfected into HB2 control and HB2 cells overexpressing CD82.

CD82 has previously been shown to act as a scaffolding protein (Termini et al., 2014; Marjon et al., 2016; Termini et al., 2016). CD82 regulates the density of α4β1 clusters within TERMs leading to increased cell-matrix adhesion (Termini et al., 2014) but it is not clear whether this also has an effect on adhesion related signalling. CD82 also regulates the clustering of N-cadherin molecules at the membrane (Marjon et al., 2016), which contributes to increased adhesion of acute myeloid leukaemia cells to the bone marrow. This is brought about by an increased density but reduced size of N-cadherin clusters. The CD82 scaffold stabilises PKCα at the membrane and regulates the size the of PKCα clusters

(Termini et al., 2016). The stabilisation of the CD82 and PKCα interaction and clustering of PKCα leads to sustained ERK1/2 signalling in TPA treated KG1a cells (Termini et al., 2016). I showed an interaction between CD82 and PKCα but was unable to show an interaction between CD82 and DP. Hence, it is unlikely that CD82 acts as a scaffold for both proteins. However, CD82 could potentially localise PKCα to the membrane, enabling it to interact with and phosphorylate DP, and potentially other desmosomal proteins, during desmosome assembly. This is important because phosphorylation of DP reduces its affinity for IFs, promoting assembly and cell-cell adhesion (Bass-Zubek et al., 2008).

6.3 CD82 reduces DP C-terminal domain plaque to plaque distance

To further investigate the mechanism by which CD82 increases desmosomal adhesion, I investigated the possibility that CD82 could increase desmosomal adhesion by increasing the clustering of desmosomal proteins. Clustering analysis performed on dSTORM images of single desmosomes with DBSCAN showed that CD82 does not affect the clustering of DP and DSG2 (Figure 49,52). However, overexpression of CD82 reduced the distance between the DP C-terminal domains (Figure 53). This could be as a result of a narrower intercellular space, which is unlikely as this feature is associated with weakly adhesive desmosomes (Garrod et al., 2005; Garrod, 2010). Another possibility is that DP adopts a less extended conformation. The DP N-terminal plakin domain contains a flexible hinge (Al-Jassar et al., 2013) that could enable DP to adopt a less extended, more compact, conformation if required. A further possibility is that the reduced DP C-terminal domain plaque to plaque distance could be caused by a change in the

orientation of DP so that it is less perpendicular to membrane (North et al., 1999; Stahley et al., 2016) (Figure 54).

Clearly the reduction in DP plaque-plaque distance correlates with an increase in desmosomal adhesion. The question remains as to whether the reduction in DP plaque to plaque distance observed upon overexpression of CD82 has functional consequences for cell-cell adhesion or whether it is simply a consequence of demosomes becoming more adhesive, and eventually hyperadhesive. It may be that cytoplasmic proteins are drawn in closer to the membrane as desmosomes assemble, mature, form a midline and become hyperadhesive. Such 'compression' would likely induce a change in conformation of DP and would not necessarily have a direct effect on intercellular adhesion. It is worth noting that such 'compression' would not necessarily be accompanied by increased clustering within the plaque if it was confined to one direction (i.e. towards the membrane). If 'compression' were to occur, one would expect other desmosomal proteins to behave in the same way as DP. Unfortunately, plaque to plaque distance of the DSG2 C-terminal domains were difficult to determine in HB2 cells as the intensity profiles overlapped so the question that remains as to whether overexpression of CD82 affects the plaque to plaque distance of other desmosomal proteins. Interestingly overexpression of PKP1 has been shown to induce hyperadhesion in keratinocytes (Bornslaeger et al., 2001; Hatzfeld et al., 2000; Tucker et al., 2014) and reduce plaque-plaque distance for the DP C-terminal and rod domains (Stahley et al., 2016) so it is unlikely that this phenomenon is unique to HB2 cells.

In summary, CD82 forms a complex with PKCα which phosphorylates DP. Phosphorylation of DP reduces interactions with IFs and promotes desmosome assembly (Bass-Zubek et al., 2008). Assembly of desmosomes could then trigger a change in conformation in DP, resulting in a decrease in DP C-terminal domain plaque to plaque distance and a subsequent increase in cell-cell adhesion. Alternatively the decrease in the DP plaque to plaque distance could occur as a consequence of increased adhesion and ‘compression’. A potential mechanism for the CD82 mediated increase in desmosomal adhesion is shown in Figure 55.

Weakly adhesive desmosome

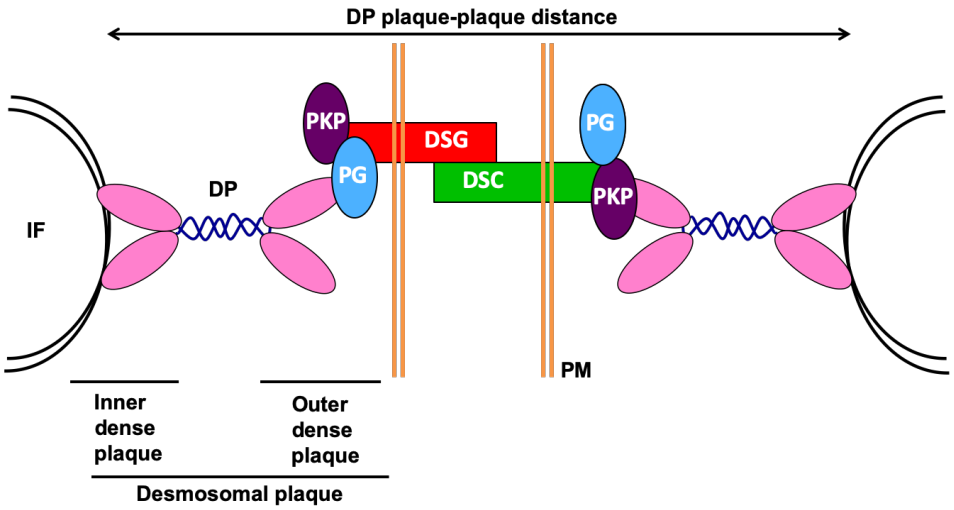

Hyperadhesive desmosome

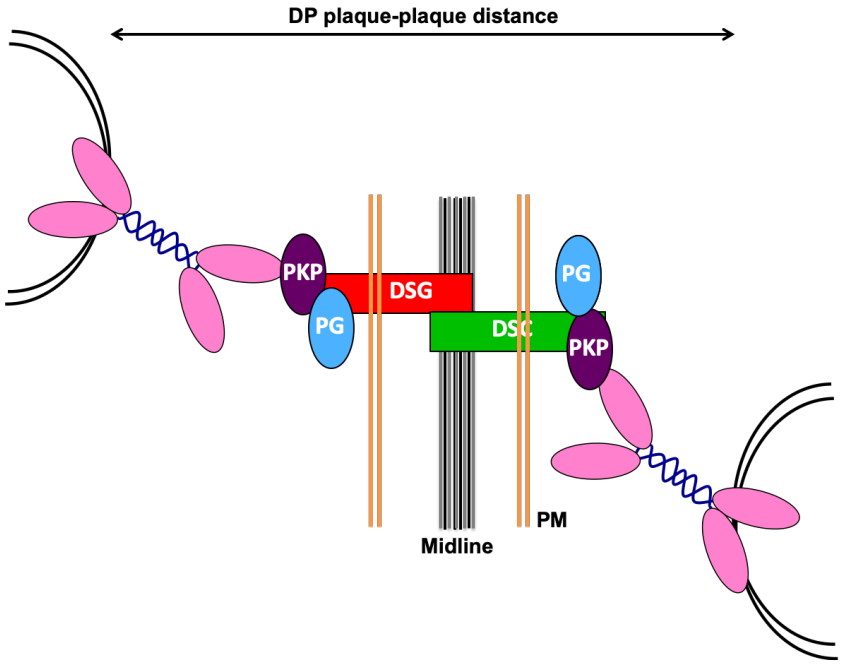

Figure 54 CD82 reduces the plaque to plaque distance of the DP C-terminal domains

The plaque to plaque distances were calculated between the DP C-terminal domains of DP molecules contributed by adjacent cells (arrow). Overexpression of CD82 reduces this distance. In the hyperadhesive desmosome shown in this figure, the orientation of DP to the membrane is altered to account for the decreased DP plaque-plaque distance. However, other explanations are possible (see text). PM; plasma membrane

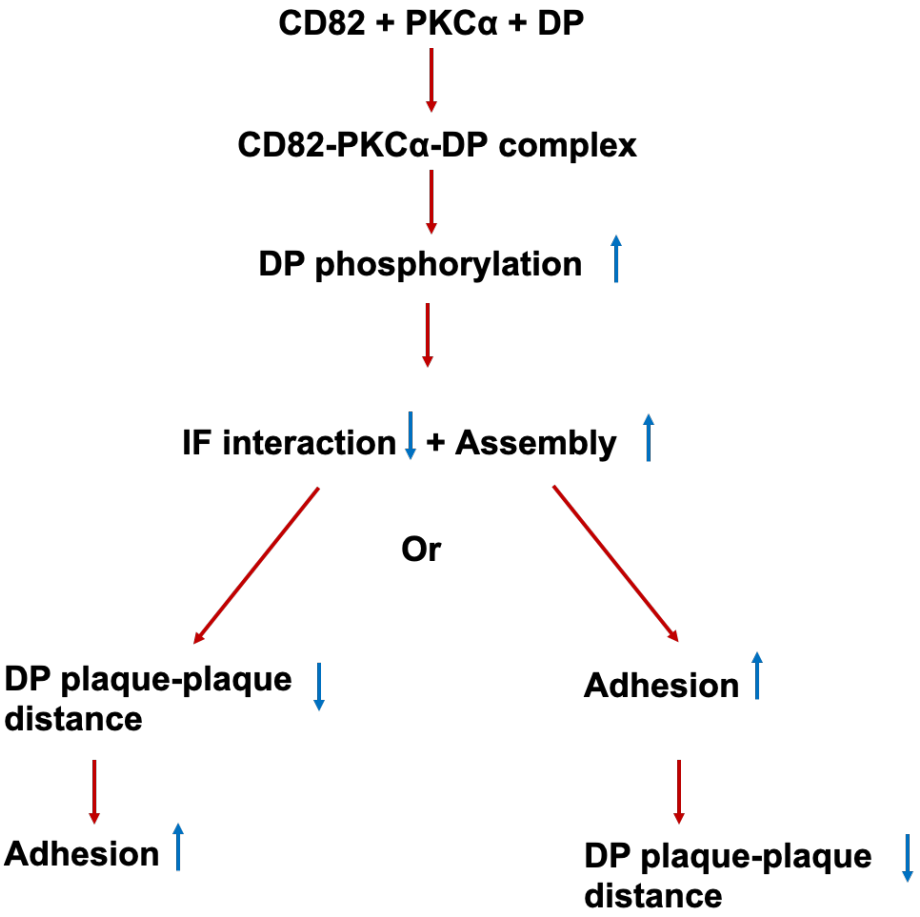

Figure 55 Potential mechanism for the CD82-mediated increase in desmosomal adhesion

CD82 forms a complex with PKCα, which phosphorylates DP, resulting in reduced interactions with intermediate filaments and increased assembly (Bass-Zubek et al., 2008). This in turn causes an increase in cell-cell adhesion. The decrease in DP plaque-plaque distance could be either a cause or a consequence of the latter (see text).

6.4 Future work

6.4.1 What is the relationship between CD82, PKCα, DP phosphorylation and increased cell adhesion?

I have shown that PKCα is able to phosphorylate DP in HEK293T cells (Figure 35). However, I have not yet shown that DP phosphorylation is increased in CD82 overexpressing cells and if it is whether PKCα is responsible. To investigate the relationship between CD82 and DP phosphorylation, DP could be immunoprecipitated in TPA treated control and CD82 overexpressing cells, and anti-phosphoserine or phospho-specific antibodies could be used to directly compare the level of phosphorylation of DP. The same experiment could be carried out on cells treated with forskolin to determine whether PKA is also involved in the relationship between CD82 and DP phosphorylation. As stated these experiments might be difficult due to the insoluble nature of DP in desmosomes but it may be possible to compare phosphorylation of transfected DP proteins in HB2PURO and HB2CD82 cells. Similar experiments could be carried out to examine the effect of PG phosphorylation. Pharmacological activation of PKC increases adhesion in HB2 cells (Figure 40). However, knockdown of PKCα did not decrease adhesion in HB2 cells as expected (Figure 42) so it is possible that other PKC isoforms compensate for loss of PKCα or are themselves involved in DP phosphorylation. Other PKC isoforms could be knocked down with siRNA to determine whether they contribute to the CD82 mediated increase in cell-cell adhesion. Overexpressing PCKα, and perhaps other PKC isoforms, in HB2 cells to see whether they increase adhesion would be another option.

6.4.2 Does CD82 affect desmosome assembly?

Another consequence of the CD82 mediated increase in cell-cell adhesion could be an increase in the assembly of desmosomes. The increase in the assembly of desmosomes could come about by increased phosphorylation of DP by PKCα, so reducing its association with IFs (Bass-Zubek et al., 2008), or by increased recruitment of desmosomal cadherins to the membrane, a process which also involves PG and PKP and has been shown to strengthen intercellular adhesion (Lorch et al., 2004; Nekrasova et al., 2011). To investigate this possibility, the trafficking of desmosomal proteins to the membrane could be studied in control and CD82 overexpressing cells by chelating extracellular calcium ions with EGTA to induce the internalisation of desmosomes, and then increasing the calcium concentration back to physiological levels. The trafficking of desmosomal proteins to the membrane could be tracked by fixing the cells at specific time points and carrying out immunofluorescence staining for desmosomal proteins. The cell-cell boundary software discussed in chapter 5 could then be used to quantify fluorescence intensities at the membrane.

6.4.3 What is the relationship between the decrease in the DP C-terminal domain plaque to plaque distance and increased adhesion?

The question arises as to whether the reduction in DP plaque to plaque distance is responsible for increased adhesion in CD82 overexpressing cells, or whether it is a consequence of increased adhesion, reorganisation of the desmosomal cadherins and the acquisition of a midline, or some combination of the two. Using CRISPR-Cas9 genome editing it would be possible to modify either DSG2 or

DSC2, or both, in HB2 cells so that they are unable to interact in the intercellular space and form a midline. Presumably overexpression of CD82 in the modified cells would not increase cell adhesion but would DP plaque to plaque distance be reduced? Interestingly, DPII, the shorter of the two major DP isoforms, is more adhesive than DPI (Cabral et al., 2012). Genome editing of HB2 cells so that they exclusively express a DPI isoform might be informative. Would cell adhesion increase more than expected with a pre-existing reduction in DP plaque to plaque distance? Producing a DP hinge domain mutant protein by genome editing could be an alternative way of addressing the same question.

6.5 Concluding remarks

In this study, I have demonstrated that overexpression of CD82 increases cell-cell adhesion in HB2 cells, and that desmosomal and adherens junction proteins contribute to the CD82 mediated increase in cell-cell adhesion. The increase in desmosomal adhesion is most likely brought about by the interaction between CD82, PKCα and DP. CD82 may form a scaffold for PKCα allowing PKCα to phosphorylate DP. The latter has been shown to reduce IF interactions and in turn promote desmosome assembly (Bass-Zubek et al., 2008). Assembly of desmosomes could then trigger a change in conformation of DP, accounting for the reduced plaque to plaque distance of the DP C-terminal domains and the increase in adhesion. Alternatively, the reduced plaque to plaque distance could be a consequence of increased adhesion. Overall my results prove that CD82 is able to induce an increase in desmosomal adhesion and suggest that it does so in

a process that involves PKCα, DP phosphorylation and a reorganisation of the desmosomal plaque.

References

Abe, M., Sugiura, T., Takahashi, M., Ishii, K., Shimoda, M., Shirasuna, K. (2008) A novel function of CD82/KAI-1 on E-cadherin-mediated homophilic cellular adhesion of cancer cells. *Cancer Letters*. 266(2), 163–170.

Al-Amoudi, A., Castano-Diez, D., Devos, D.P., Russell, R.B., Johnson, G.T., Frangakis, A.S. (2011) The three-dimensional molecular structure of the desmosomal plaque. *Proceedings of the National Academy of Sciences*. 108(16), 6480–6485.

Al-Jassar, C., Bernadó, P., Chidgey, M., Overduin, M. (2013) Hinged Plakin Domains Provide Specialized Degrees of Articulation in Envoplakin, Periplakin and Desmoplakin. *PLoS ONE*. 8(7), e69767.

Alexander, M.S., Rozkalne, A., Colletta, A., Spinazzola, J.M., Johnson, S., Rahimov, F., Meng, H., Lawlor, M.W., Estrella, E., Kunkel, L.M., Gussoni, E. (2016) CD82 Is a Marker for Prospective Isolation of Human Muscle Satellite Cells and Is Linked to Muscular Dystrophies. *Cell Stem Cell*. 19(6), 800–807.

Bass-Zubek, A.E., Hobbs, R.P., Amargo, E. V., Garcia, N.J., Hsieh, S.N., Chen, X., Wahl, J.K., Denning, M.F., Green, K.J. (2008) Plakophilin 2: a critical scaffold for PKCα that regulates intercellular junction assembly. *The Journal of Cell Biology*. 181(4), 605–613.

Baum, B., Georgiou, M. (2011) Dynamics of adherens junctions in epithelial establishment, maintenance, and remodeling. *The Journal of Cell Biology*. 192(6): 907-917.

Berditchevski, F., Gilbert, E., Griffiths, M.R., Fitter, S., Ashman, L., Jenner, S.J. (2001) Analysis of the CD151·α3β1 Integrin and CD151·Tetraspanin Interactions by Mutagenesis. *Journal of Biological Chemistry*. 276(44), 41165–41174.

Berditchevski, F., Odintsova, E., Sawada, S., Gilbert, E. (2002) Expression of the Palmitoylation-deficient CD151 Weakens the Association of alpha 3beta 1 Integrin with the Tetraspanin-enriched Microdomains and Affects Integrin-dependent Signaling. *Journal of Biological Chemistry*. 277(40), 36991–37000.

Berditchevski, F., Tolias, K.F., Wong, K., Carpenter, C.L., Hemler, M.E. (1997) A novel link between integrins, transmembrane-4 superfamily proteins (CD63 and CD81), and phosphatidylinositol 4-kinase. *Journal of Biological Chemistry*. 272(5), 2595–8.

Berdichevsky, F., D Alford, B. D., D'Souza, Taylor-Papadimitriou, J. (1994). Branching morphogenesis of human mammary epithelial cells in collagen gels. *Journal of Cell Science.* 107: 3557-3568.

Bierkamp, C., Mclaughlin, K.J., Schwarz, H., Huber, O., Kemler, R. (1996) Embryonic Heart and Skin Defects in Mice Lacking Plakoglobin. *Developmental Biology*. 180(2), 780–785.

Bierkamp, C., Schwarz, H., Huber, O., Kemler, R. (1999) Desmosomal localization of beta-catenin in the skin of plakoglobin null-mutant mice. *Development*. 126(2), 371–81.

Bornslaeger, E.A., Godsel, L.M., Corcoran, C.M., Park, J.K., Hatzfeld, M., Kowalczyk, A.P., Green, K.J. (2001) Plakophilin 1 interferes with plakoglobin binding to desmoplakin, yet together with plakoglobin promotes clustering of desmosomal plaque complexes at cell-cell borders. *Journal of Cell Science*. 114(4), 727–38.

Bouameur, J.-E., Schneider, Y., Begre, N., Hobbs, R.P., Lingasamy, P., Fontao, L., Green, K.J., Favre, B., Borradori, L. (2013) Phosphorylation of serine 4642 in the C-terminus of plectin by MNK2 and PKA modulates its interaction with intermediate filaments. *Journal of Cell Science*. 126(18), 4195–4207.

Boucheix, C., Rubinstein, E. (2001) Tetraspanins. *Cellular and Molecular Life Sciences*. 58(9), 1189–1205.

Brouhard, G.J., Rice, L.M. (2018) Microtubule dynamics: an interplay of biochemistry and mechanics. *Nature Reviews Molecular Cell Biology*. 19(7), 451–463.

Cabral, R.M., Tattersall, D., Patel, V., McPhail, G.D., Hatzimasoura, E., Abrams, D.J., South, A.P., Kelsell, D.P., Magee, A.I., Garrod, D.R. (2012) The DSPII splice variant is crucial for desmosome-mediated adhesion in HaCaT keratinocytes. *Journal of Cell Science*. 125(12), 2853–61.

Cabral, R.M., Wan, H., Cole, C.L., Abrams, D.J., Kelsell, D.P., South, A.P. (2010) Identification and characterization of DSPIa, a novel isoform of human desmoplakin. *Cell and Tissue Research*. 341(1), 121–129.

Caradonna, F., Luparello, C. (2014). Cytogenetic characterization of HB2 epithelial cells from the human breast. *In Vitro Cell Dev Biol Anim*. 50(1):48-55.

Charrin, S., Jouannet, S., Boucheix, C., Rubinstein, E. (2014) Tetraspanins at a glance. *Journal of Cell Science*. 127(17), 3641–3648.

Charrin, S., Manié, S., Oualid, M., Billard, M., Boucheix, C., Rubinstein, E. (2002) Differential stability of tetraspanin/tetraspanin interactions: role of palmitoylation. *FEBS Letters*. 516(1–3), 139–44.

Chen, J., Nekrasova, O.E., Patel, D.M., Klessner, J.L., Godsel, L.M., Koetsier, J.L., Amargo, E. V, Desai, B. V, Green, K.J. (2012) The C-terminal unique region of desmoglein 2 inhibits its internalization via tail-tail interactions. *The Journal of Cell Biology*. 199(4), 699–711.

Cheng, F., Eriksson, J.E. (2014) Intermediate Filaments. In *eLS*. Chichester, UK: John Wiley & Sons, Ltd.

Chidgey, M.A.J., Clarke, J.P., Garrod, D.R. (1996) Expression of Full-Length Desmosomal Glycoproteins (Desmocollins) Is Not Sufficient to Confer Strong Adhesion on Transfected L929 Cells. *Journal of Investigative Dermatology*. 106(4), 689–695.

Chigita, S., Sugiura, T., Abe, M., Kobayashi, Y., Shimoda, M., Onoda, M., Shirasuna, K. (2012) CD82 inhibits canonical Wnt signalling by controlling the cellular distribution of β-catenin in carcinoma cells. *International Journal of Oncology*. 41(6), 2021–8.

Chitaev, N.A., Leube, R.E., Troyanovsky, R.B., Eshkind, L.G., Franke, W.W., Troyanovsky, S.M. (1996) The binding of plakoglobin to desmosomal cadherins: patterns of binding sites and topogenic potential. *The Journal of Cell Biology*. 133(2), 359–69.

Choi, H.-J., Park-Snyder, S., Pascoe, L.T., Green, K.J., Weis, W.I. (2002) Structures of two intermediate filament-binding fragments of desmoplakin reveal a unique repeat motif structure. *Nature Structural Biology*. 9(8), 612–620.

Delva, E., Tucker, D.K., Kowalczyk, A.P. (2009) The desmosome. *Cold Spring Harbor Perspectives in Biology*. 1(2), a002543.

Dempsey, G.T., Vaughan, J.C., Chen, K.H., Bates, M., Zhuang, X. (2011) Evaluation of fluorophores for optimal performance in localization-based super-resolution imaging. *Nature Methods*. 8(12), 1027–36.

Desai, B. V, Harmon, R.M., Green, K.J. (2009) Desmosomes at a glance. *The Journal of Cell Science*. 122(24), 4401–7.

van Deventer, S.J., Dunlock, V.-M.E., van Spriel, A.B. (2017) Molecular interactions shaping the tetraspanin web. *Biochemical Society Transactions*. 45(3), 741–750.

Dogterom, M., Koenderink, G.H. (2019) Actin–microtubule crosstalk in cell biology. *Nature Reviews Molecular Cell Biology*. 20(1), 38–54.

Dong, J.T., Lamb, P.W., Rinker-Schaeffer, C.W., Vukanovic, J., Ichikawa, T., Isaacs, J.T., Barrett, J.C. (1995) Kal1, a metastasis suppressor gene for prostate cancer on human chromosome 11p11.2. *Science*. 268(5212), 884–886.

Dubash, A.D., Green, K.J. (2011) Desmosomes. *Current Biology.* 21(14), R529-31.

Ester, M., Kriegel, H.-P., Sander, J., Xu, X. (1996) A Density-Based Algorithm for Discovering Clusters in Large Spatial Databases with Noise. In *Proceedings of the 2nd International Conference on Knowledge Discovery and Data Mining*. 226–231.

Fanaei, M., Monk, P.N., Partridge, L.J. (2011) The role of tetraspanins in fusion. *Biochemical Society Transactions*. 39(2), 524–8.

Favre, B., Begré, N., Bouameur, J.-E., Lingasamy, P., Conover, G.M., Fontao, L., Borradori, L. (2018) Desmoplakin interacts with the coil 1 of different types of intermediate filament proteins and displays high affinity for assembled intermediate filaments. *PLoS ONE*. 13(10), e0205038.

Fletcher, D.A., Mullins, R.D. (2010) Cell mechanics and the cytoskeleton. *Nature*. 463(7280), 485–92.

Fontao, L., Favre, B., Riou, S., Geerts, D., Jaunin, F., Saurat, J.H., Green, K.J., Sonnenberg, A., Borradori, L. (2003) Interaction of the bullous pemphigoid antigen 1 (BP230) and desmoplakin with intermediate filaments is mediated by distinct

sequences within their COOH terminus. *Molecular Biology of the Cell*. 14(5), 1978–1992.

Gallicano, G.I., Kouklis, P., Bauer, C., Yin, M., Vasioukhin, V., Degenstein, L., Fuchs, E. (1998) Desmoplakin Is Required Early in Development for Assembly of Desmosomes and Cytoskeletal Linkage. *The Journal of Cell Biology*. 143(7), 2009–2022.

Garcia, M.A., Nelson, W.J., Chavez, N. (2018) Cell–cell junctions organize structural and signaling networks. *Cold Spring Harbor Perspectives in Biology*. 10(4), pii: a029181.

Garrod, D. (2010) Desmosomes in vivo. *Dermatology Research and Practice*. 2010(1), 212439.

Garrod, D., Chidgey, M. (2008) Desmosome structure, composition and function. *Biochimica et Biophysica Acta - Biomembranes*. 1778(3), 572–587.

Garrod, D., Tabernero, L. (2014) Hyper-adhesion: A unique property of desmosomes. *Cell Communication and Adhesion*. 21(5), 249–256.

Garrod, D.R., Berika, M.Y., Bardsley, W.F., Holmes, D., Tabernero, L. (2005) Hyper-adhesion in desmosomes: its regulation in wound healing and possible relationship to cadherin crystal structure. *Journal of Cell Science*. 118(24), 5743–5754.

Garrod, D.R., Fisher, C., Smith, A., Nie, Z. (2008) Pervanadate stabilizes desmosomes. *Cell Adhesion & Migration*. 2(3), 161–6.

Gaudry, C.A., Palka, H.L., Dusek, R.L., Huen, A.C., Khandekar, M.J., Hudson, L.G., Green, K.J. (2001) Tyrosine-phosphorylated Plakoglobin Is Associated with Desmogleins but Not Desmoplakin after Epidermal Growth Factor Receptor Activation. *Journal of Biological Chemistry*. 276(27), 24871–24880.

Getsios, S., Simpson, C.L., Kojima, S., Harmon, R., Sheu, L.J., Dusek, R.L., Cornwell, M., Green, K.J. (2009) Desmoglein 1-dependent suppression of EGFR signaling promotes epidermal differentiation and morphogenesis. *The Journal of Cell Biology*. 185(7), 1243–58.

Godsel, L.M., Hsieh, S.N., Amargo, E. V, Bass, A.E., Pascoe-McGillicuddy, L.T., Huen, A.C., Thorne, M.E., Gaudry, C.A., Park, J.K., Myung, K., Goldman, R.D., Chew, T.-L., Green, K.J. (2005) Desmoplakin assembly dynamics in four dimensions: multiple phases differentially regulated by intermediate filaments and actin. *The Journal of Cell Biology*. 171(6), 1045–59.

Green, K.J., Gaudry, C.A. (2000) Are desmosomes more than tethers for intermediate filaments? *Nature Reviews Molecular Cell Biology*. 1(3), 208-216.

Green, K.J., Getsios, S., Troyanovsky, S., Godsel, L.M. (2010) Intercellular Junction Assembly, Dynamics, and Homeostasis. *Cold Spring Harbor Perspectives in Biology*. 2(2), a000125.

Green, K.J., Parry, D.A., Steinert, P.M., Virata, M.L., Wagner, R.M., Angst, B.D., Nilles, L.A. (1990) Structure of the human desmoplakins. Implications for function in the desmosomal plaque. *Journal of Biological Chemistry*. 265(5), 2603–12.

Green, K.J., Simpson, C.L. (2007) Desmosomes: New Perspectives on a Classic. *Journal of Investigative Dermatology*. 127(11), 2499–2515.

Griffié, J., Shlomovich, L., Williamson, D.J., Shannon, M., Aaron, J., Khuon, S., L. Burn, G., Boelen, L., Peters, R., Cope, A.P., Cohen, E.A.K., Rubin-Delanchy, P., Owen, D.M. (2017) 3D Bayesian cluster analysis of super-resolution data reveals LAT recruitment to the T cell synapse. *Scientific Reports*. 7(1), 4077.

Griner, E.M., Kazanietz, M.G. (2007) Protein kinase C and other diacylglycerol

effectors in cancer. *Nature Reviews Cancer*. 7(4), 281–294.

Grossmann, K.S., Grund, C., Huelsken, J., Behrend, M., Erdmann, B., Franke, W.W., Birchmeier, W. (2004) Requirement of plakophilin 2 for heart morphogenesis and cardiac junction formation. *The Journal of Cell Biology*. 167(1), 149–160.

Gumbiner, B.M. (2005) Regulation of cadherin-mediated adhesion in morphogenesis. *Nature Reviews Molecular Cell Biology*. 6(8), 622–634.

Haining, E.J., Yang, J., Bailey, R.L., Khan, K., Collier, R., Tsai, S., Watson, S.P., Frampton, J., Garcia, P., Tomlinson, M.G. (2012) The TspanC8 Subgroup of Tetraspanins Interacts with A Disintegrin and Metalloprotease 10 (ADAM10) and Regulates Its Maturation and Cell Surface Expression. *Journal of Biological Chemistry*. 287(47), 39753–39765.

Hanakawa, Y., Matsuyoshi, N., Stanley, J.R. (2002) Expression of desmoglein 1 compensates for genetic loss of desmoglein 3 in keratinocyte adhesion. *The Journal of Investigative Dermatology*. 119(1), 27–31.

Harrison, O.J., Brasch, J., Lasso, G., Katsamba, P.S., Ahlsen, G., Honig, B., Shapiro, L. (2016) Structural basis of adhesive binding by desmocollins and desmogleins. *Proceedings of the National Academy of Sciences*. 113(26), 7160–7165.

Hatzfeld, M., Haffner, C., Schulze, K., Vinzens, U. (2000) The Function of Plakophilin 1 in Desmosome Assembly and Actin Filament Organization. *The Journal of Cell Biology*. 149(1), 209–222.

He, B., Liu, L., Cook, G.A., Grgurevich, S., Jennings, L.K., Zhang, X.A. (2005) Tetraspanin CD82 attenuates cellular morphogenesis through down-regulating integrin alpha6-mediated cell adhesion. *Journal of Biological Chemistry*. 280(5),

3346–54.

Hemler, M.E. (2005) Tetraspanin functions and associated microdomains. *Nature Reviews Molecular Cell Biology*. 6(10), 801–811.

Hobbs, R.P., Green, K.J. (2012) Desmoplakin regulates desmosome hyperadhesion. *The Journal of Investigative Dermatology*. 132(2), 482–5.

Hofmann, I., Casella, M., Schnölzer, M., Schlechter, T., Spring, H., Franke, W.W. (2006) Identification of the junctional plaque protein plakophilin 3 in cytoplasmic particles containing RNA-binding proteins and the recruitment of plakophilins 1 and 3 to stress granules. *Molecular Biology of the Cell*. 17(3), 1388–1398.

Huang, B., Wang, W., Bates, M., Zhuang, X. (2008) Three-dimensional super-resolution imaging by stochastic optical reconstruction microscopy. *Science*. 319(5864), 810–813.

Huang, Y., Zucker, B., Zhang, S., Elias, S., Zhu, Y., Chen, H., Ding, T., Li, Y., Sun, Y., Lou, J., Kozlov, M.M., Yu, L. (2019) Migrasome formation is mediated by assembly of micron-scale tetraspanin macrodomains. *Nature Cell Biology*. 21(8), 991–1002.

Jee, B., Jin, K., Hahn, J.H., Song, H.G., Lee, H. (2003) Metastasis-suppressor KAI1/CD82 induces homotypic aggregation of human prostate cancer cells through Src-dependent pathway. *Experimental and Molecular Medicine*. 35(1), 30–37.

Jiang, D., Jiang, Z., Lu, D., Wang, X., Liang, H., Zhang, J., Meng, Y., Li, Y., Wu, D., Huang, Y., Chen, Y., Deng, H., Wu, Q., Xiong, J., Meng, A., Yu, L. (2019) Migrasomes provide regional cues for organ morphogenesis during zebrafish gastrulation. *Nature Cell Biology*. 21(8), 966–977.

Johnson, J.L., Najor, N.A., Green, K.J. (2014) Desmosomes: regulators of cellular signaling and adhesion in epidermal health and disease. *Cold Spring Harbor Perspectives in Medicine*. 4(11), a015297.

Jones, J.C. (1988) Characterization of a 125K glycoprotein associated with bovine epithelial desmosomes. *The Journal of Cell Science*. 89(2), 207-16.

Jonkman, M.F., Pasmooij, A.M.G., Pasmans, S.G.M.A., van den Berg, M.P., Ter Horst, H.J., Timmer, A., Pas, H.H. (2005) Loss of desmoplakin tail causes lethal acantholytic epidermolysis bullosa. *American Journal of Human Genetics*. 77(4), 653–60.

Kami, K., Chidgey, M., Dafforn, T., Overduin, M. (2009) The Desmoglein-Specific Cytoplasmic Region Is Intrinsically Disordered in Solution and Interacts with Multiple Desmosomal Protein Partners. *Journal of Molecular Biology*. 386(2), 531–543.

Kang, H., Weiss, T.M., Bang, I., Weis, W.I., Choi, H.-J. (2016) Structure of the Intermediate Filament-Binding Region of Desmoplakin. *PLoS ONE*. 11(1), e0147641.

Kimura, T.E., Merritt, A.J., Garrod, D.R. (2007) Calcium-independent desmosomes of keratinocytes are hyper-adhesive. *Journal of Investigative Dermatology*. 127(4), 775–781.

Kitadokoro, K., Bordo, D., Galli, G., Petracca, R., Falugi, F., Abrignani, S., Grandi, G., Bolognesi, M. (2001) CD81 extracellular domain 3D structure: insight into the tetraspanin superfamily structural motifs. *The EMBO journal*. 20(1–2), 12–8.

Knudsen, K.A., Wheelock, M.J. (1992) Plakoglobin, or an 83-kD homologue distinct from beta-catenin, interacts with E-cadherin and N-cadherin. *The Journal of Cell Biology*. 118(3), 671–9.

Koch, P.J., Franke, W.W. (1994) Desmosomal cadherins: another growing multigene family of adhesion molecules. *Current Opinion in Cell Biology*. 6(5), 682–687.

Kowalczyk, A.P., Bornslaeger, E.A., Borgwardt, J.E., Palka, H.L., Dhaliwal, A.S., Corcoran, C.M., Denning, M.F., Green, K.J. (1997) The amino-terminal domain of desmoplakin binds to plakoglobin and clusters desmosomal cadherin-plakoglobin complexes. *The Journal of Cell Biology*. 139(3), 773–84.

Kowalczyk, A.P., Green, K.J. (2013) Structure, function, and regulation of desmosomes. *Progress in Molecular Biology and Translational Science*. 116, 95–118.

Kröger, C., Loschke, F., Schwarz, N., Windoffer, R., Leube, R.E., Magin, T.M. (2013) Keratins control intercellular adhesion involving PKC-α-mediated desmoplakin phosphorylation. *The Journal of Cell Biology*. 201(5), 681–92.

Lammerding, J., Kazarov, A.R., Huang, H., Lee, R.T., Hemler, M.E. (2003) Tetraspanin CD151 regulates 6 1 integrin adhesion strengthening. *Proceedings of the National Academy of Sciences*. 100(13), 7616–7621.

Lee, M.-S., Byun, H.-J., Lee, J., Jeoung, D.-I., Kim, Y.-M., Lee, H. (2018) Tetraspanin CD82 represses Sp1-mediated Snail expression and the resultant E-cadherin expression interrupts nuclear signaling of β-catenin by increasing its membrane localization. *Cellular Signalling*. 52, 83–94.

Lewis, J.E., Jensen, P.J., Wheelock, M.J. (1994) Cadherin Function Is Required for Human Keratinocytes to Assemble Desmosomes and Stratify in Response to Calcium. *Journal of Investigative Dermatology*. 102(6), 870–877.

Lewis, J.E., Wahl, J.K., Sass, K.M., Jensen, P.J., Johnson, K.R., Wheelock, M.J.

(1997) Cross-talk between adherens junctions and desmosomes depends on plakoglobin. *The Journal of Cell Biology*. 136(4), 919–34.

Lineberry, N., Su, L., Soares, L., Fathman, C.G. (2008) The single subunit transmembrane E3 ligase gene related to anergy in lymphocytes (GRAIL) captures and then ubiquitinates transmembrane proteins across the cell membrane. *Journal of Biological Chemistry*. 283(42), 28497–505.

Lorch, J.H., Klessner, J., Park, J.K., Getsios, S., Wu, Y.L., Stack, M.S., Green, K.J. (2004) Epidermal growth factor receptor inhibition promotes desmosome assembly and strengthens intercellular adhesion in squamous cell carcinoma cells. *Journal of Biological Chemistry*. 279(35), 37191–200.

Ma, A.S.P., Lorincz, A.L. (1988) Immunofluorescence localization of peripheral proteins in cultured human keratinocytes. *Journal of Investigative Dermatology*. 90(3), 331–335.

Mackay, H.J., Twelves, C.J. (2007) Targeting the protein kinase C family: are we there yet? *Nature Reviews Cancer*. 7(7), 554–562.

Marjon, K.D., Termini, C.M., Karlen, K.L., Saito-Reis, C., Soria, C.E., Lidke, K.A., Gillette, J.M. (2016) Tetraspanin CD82 regulates bone marrow homing of acute myeloid leukemia by modulating the molecular organization of N-cadherin. *Oncogene*. 35(31), 4132–40.

Matter, K., Balda, M.S. (2007) Epithelial tight junctions, gene expression and nucleo-junctional interplay. *Journal of Cell Science*. 120(9), 1505–11.

Matthews, A.L., Szyroka, J., Collier, R., Noy, P.J., Tomlinson, M.G. (2017) Scissor sisters: regulation of ADAM10 by the TspanC8 tetraspanins. *Biochemical Society Transactions*. 45(3), 719–730.

McHarg, S., Hopkins, G., Lim, L., Garrod, D. (2014) Down-Regulation of Desmosomes in Cultured Cells: The Roles of PKC, Microtubules and Lysosomal/Proteasomal Degradation. *PLoS ONE*. 9(10), e108570.

Meng, J.-J., Bornslaeger, E.A., Green, K.J., Steinert, P.M., Ip, W. (1997) Two-hybrid Analysis Reveals Fundamental Differences in Direct Interactions between Desmoplakin and Cell Type-specific Intermediate Filaments. *Journal of Biological Chemistry*. 272(34), 21495–21503.

Meşe, G., Richard, G., White, T.W. (2007) Gap Junctions: Basic Structure and Function. *Journal of Investigative Dermatology*. 127(11), 2516–2524.

Michels, C., Buchta, T., Bloch, W., Krieg, T., Niessen, C.M. (2009) Classical cadherins regulate desmosome formation. *Journal of Investigative Dermatology*. 129(8), 2072–2075.

Miravet, S., Piedra, J., Castaño, J., Raurell, I., Francí, C., Duñach, M., García de Herreros, A. (2003) Tyrosine phosphorylation of plakoglobin causes contrary effects on its association with desmosomes and adherens junction components and modulates beta-catenin-mediated transcription. *Molecular and Cellular Biology*. 23(20), 7391–402.

Mochly-Rosen, D., Das, K., Grimes, K. V. (2012) Protein kinase C, an elusive therapeutic target? *Nature Reviews Drug Discovery*. 11(12), 937–957.

Molder, L. Te, Juksar, J., Harkes, R., Wang, W., Kreft, M., Sonnenberg, A. (2019) Tetraspanin CD151 and integrin α3β1 contribute to the stabilization of integrin α6β4-containing cell-matrix adhesions. *Journal of Cell Science*, jcs.235366.

Nagar, B., Overduin, M., Ikura, M., Rini, J.M. (1996) Structural basis of calcium-induced E-cadherin rigidification and dimerization. *Nature*. 380(6572), 360–364.

Nekrasova, O.E., Amargo, E. V., Smith, W.O., Chen, J., Kreitzer, G.E., Green, K.J. (2011) Desmosomal cadherins utilize distinct kinesins for assembly into desmosomes. *The Journal of Cell Biology*. 195(7), 1185–1203.

Newton, A.C. (2010) Protein kinase C: poised to signal. *American journal of physiology. Endocrinology and metabolism*. 298(3), 395-402.

Newton, A.C. (2003) Regulation of the ABC kinases by phosphorylation: protein kinase C as a paradigm. *The Biochemical Journal*. 370(2), 361–71.

Nicovich, P.R., Owen, D.M., Gaus, K. (2017) Turning single-molecule localization microscopy into a quantitative bioanalytical tool. *Nature Protocols*. 12(3), 453–461.

Niessen, C.M. (2007) Tight junctions/adherens junctions: Basic structure and function. *Journal of Investigative Dermatology*. 127(11), 2525–2532.

Niessen, C.M., Gottardi, C.J. (2008) Molecular components of the adherens junction. *Biochimica et Biophysica Acta*. 1778(3), 562–71.

Norgett, E.E., Hatsell, S.J., Carvajal-Huerta, L., Ruiz Cabezas, J.-C., Common, J., Purkis, P.E., Whittock, N., Leigh, I.M., Stevens, H.P., Kelsell, D.P. (2000) Recessive mutation in desmoplakin disrupts desmoplakin-intermediate filament interactions and causes dilated cardiomyopathy, woolly hair and keratoderma. *Human Molecular Genetics*. 9(18), 2761–2766.

North, A.J., Bardsley, W.G., Hyam, J., Bornslaeger, E.A., Cordingley, H.C., Trinnaman, B., Hatzfeld, M., Green, K.J., Magee, A.I., Garrod, D.R. (1999) Molecular map of the desmosomal plaque. *Journal of Cell Science*, 112(23), 4325–36.

Odintsova, E., van Niel, G., Conjeaud, H., Raposo, G., Iwamoto, R., Mekada, E., Berditchevski, F. (2013) Metastasis Suppressor Tetraspanin CD82/KAI1

Regulates Ubiquitylation of Epidermal Growth Factor Receptor. *Journal of Biological Chemistry*. 288(36), 26323–26334.

Odintsova, E., Sugiura, T., Berditchevski, F. (2000) Attenuation of EGF receptor signaling by a metastasis suppressor, the tetraspanin CD82/KAI-1. *Current Biology.* 10(16), 1009–12.

Odintsova, E., Voortman, J., Gilbert, E., Berditchevski, F. (2003) Tetraspanin CD82 regulates compartmentalisation and ligand-induced dimerization of EGFR. *Journal of Cell Science*. 116(22), 4557–4566.

Odland, G.F. (1958) The fine structure of the interrelationship of cells in the human epidermis. *The Journal of Biophysical and Biochemical Cytology*. 4(5), 529–38.

Ortega, E., Manso, X.A., Buey, R.M., Carballido, A.M., Carabias, A., Sonnenberg, A., De Pereda, J.M. (2016) The structure of the plakin domain of plectin reveals an extended rod-like shape. *Journal of Biological Chemistry*. 291(36), 18643–18662.

Ovesný, M., Křížek, P., Borkovec, J., Švindrych, Z., Hagen, G.M. (2014) ThunderSTORM: a comprehensive ImageJ plug-in for PALM and STORM data analysis and super-resolution imaging. *Bioinformatics*. 30(16), 2389–2390.

Palka, H.L., Green, K.J. (1997) Roles of plakoglobin end domains in desmosome assembly. *Journal of Cell Science*. 110 (19), 2359–71.

Parrish, E.P., Marston, J.E., Mattey, D.L., Measures, H.R., Venning, R., Garrod, D.R. (1990) Size heterogeneity, phosphorylation and transmembrane organisation of desmosomal glycoproteins 2 and 3 (desmocollins) in MDCK cells. *Journal of Cell Science*. 96(2), 239–248.

Parrish, E.P., Steart, P. V., Garrod, D.R., Weller, R.O. (1987) Antidesmosomal monoclonal antibody in the diagnosis of intracranial tumours. *The Journal of*

Pathology. 153(3), 265–273.

Pasdar, M., Li, Z., Chan, H. (1995) Desmosome assembly and disassembly are regulated by reversible protein phosphorylation in cultured epithelial cells. *Cell Motility and the Cytoskeleton*. 30(2), 108–121.

Penn, E.J., Burdett, I.D., Hobson, C., Magee, A.I., Rees, D.A. (1987) Structure and assembly of desmosome junctions: biosynthesis and turnover of the major desmosome components of Madin-Darby canine kidney cells in low calcium medium. *The Journal of Cell Biology*. 105(5), 2327–2334.

Perrais, M., Chen, X., Perez-Moreno, M., Gumbiner, B.M. (2007) E-cadherin homophilic ligation inhibits cell growth and epidermal growth factor receptor signaling independently of other cell interactions. *Molecular Biology of the Cell*. 18(6), 2013–25.

Rübsam, M., Broussard, J.A., Wickström, S.A., Nekrasova, O., Green, K.J., Niessen, C.M. (2018) Adherens Junctions and Desmosomes Coordinate Mechanics and Signaling to Orchestrate Tissue Morphogenesis and Function: An Evolutionary Perspective. *Cold Spring Harbor Perspectives in Biology*. 10(11), a029207.

Ruiz, P., Brinkmann, V., Ledermann, B., Behrend, M., Grund, C., Thalhammer, C., Vogel, F., Birchmeier, C., Günthert, U., Franke, W.W., Birchmeier, W. (1996) Targeted mutation of plakoglobin in mice reveals essential functions of desmosomes in the embryonic heart. *The Journal of Cell Biology*. 135(1), 215–25.

Rust, M.J., Bates, M., Zhuang, X. (2006) Sub-diffraction-limit imaging by stochastic optical reconstruction microscopy (STORM). *Nature Methods*. 3(10), 793–796.

Seigneuret, M., Delaguillaumie, A., Lagaudrière-Gesbert, C., Conjeaud, H. (2001) Structure of the tetraspanin main extracellular domain. A partially conserved fold

with a structurally variable domain insertion. *Journal of Biological Chemistry*. 276(43), 40055–64.

Shafraz, O., Rübsam, M., Stahley, S.N., Caldara, A.L., Kowalczyk, A.P., Niessen, C.M., Sivasankar, S. (2018) E-cadherin binds to desmoglein to facilitate desmosome assembly. *eLife*. 7:e37629

Shapiro, L., Fannon, A.M., Kwong, P.D., Thompson, A.; (1995) *Structural basis of cell-cell adhesion by cadherins*. *Nature.* 374(6520), 327-37.

Simpson, C.L., Patel, D.M., Green, K.J. (2011) Deconstructing the skin: cytoarchitectural determinants of epidermal morphogenesis. *Nature Reviews Molecular Cell Biology*. 12(9), 565–80.

Stahley, S.N., Saito, M., Faundez, V., Koval, M., Mattheyses, A.L., Kowalczyk, A.P. (2014) Desmosome assembly and disassembly are membrane raft-dependent. *PLoS ONE*. 9(1), e87809.

Stahley, S.N., Bartle, E.I., Atkinson, C.E., Kowalczyk, A.P., Mattheyses, A.L. (2016a) Molecular organization of the desmosome as revealed by direct stochastic optical reconstruction microscopy. *The Journal of Cell Science*. 129(15), 2897–2904.

Stahley, S.N., Warren, F.W., Feldman, R.J., Swerlick, R.A., Mattheyses, A.L., Kowalczyk, A.P. (2016b) Super-resolution microscopy reveals altered desmosomal protein organization in pemphigus vulgaris patient tissue. *Journal of Investigative Dermatology*. 136(1):59-66.

Stappenbeck, T.S., Bornslaeger, E.A., Corcoran, C.M., Luu, H.H., Virata, M.L., Green, K.J. (1993) Functional analysis of desmoplakin domains: specification of the interaction with keratin versus vimentin intermediate filament networks. *The Journal of Cell Biology*. 123(3), 691–705.

Stappenbeck, T.S., Lamb, J.A., Corcoran, C.M., Green, K.J. (1994) Phosphorylation of the desmoplakin COOH terminus negatively regulates its interaction with keratin intermediate filament networks. *Journal of Biological Chemistry*. 269(47), 29351–4.

Stipp, C.S., Hemler, M.E. (2000) Transmembrane-4-superfamily proteins CD151 and CD81 associate with alpha 3 beta 1 integrin, and selectively contribute to alpha 3 beta 1-dependent neurite outgrowth. *Journal of Cell Science*. 113 (11), 1871–82.

Stroe, P., Claridge, E., Odintsova, E. (2016) Cell Boundary Detection for Quantitative Studies of the Role of Tetraspanin CD82 in Cell-cell Adhesion. *Procedia Computer Science*. 90, 107–112.

Stuck, M.W., Conley, S.M., Naash, M.I. (2015) Retinal Degeneration Slow (RDS) Glycosylation Plays a Role in Cone Function and in the Regulation of RDS·ROM-1 Protein Complex Formation. *Journal of Biological Chemistry*. 290(46), 27901–13.

Sumigray, K.D., Lechler, T. (2012) Desmoplakin controls microvilli length but not cell adhesion or keratin organization in the intestinal epithelium. *Molecular Biology of the Cell*. 23(5), 792–9.

Takahashi, M., Sugiura, T., Abe, M., Ishii, K., Shirasuna, K. (2007) Regulation of c-Met signaling by the tetraspanin KAI-1/CD82 affects cancer cell migration. *International Journal of Cancer*. 121(9), 1919–1929.

Takeda, M., Kanki, Y., Masumoto, H., Funakoshi, S., Hatani, T., Fukushima, H., Izumi-Taguchi, A., Matsui, Y., Shimamura, T., Yoshida, Y., Yamashita, J.K. (2018) Identification of Cardiomyocyte-Fated Progenitors from Human-Induced Pluripotent Stem Cells Marked with CD82. *Cell Reports*. 22(2), 546–556.

Termini, C.M., Cotter, M.L., Marjon, K.D., Buranda, T., Lidke, K.A., Gillette, J.M. (2014) The membrane scaffold CD82 regulates cell adhesion by altering α4 integrin stability and molecular density. *Molecular Biology of the Cell*. 25(10), 1560–73.

Termini, C.M., Gillette, J.M. (2017) Tetraspanins Function as Regulators of Cellular Signaling. *Frontiers in Cell and Developmental Biology*. 5, 34.

Termini, C.M., Lidke, K.A., Gillette, J.M. (2016) Tetraspanin CD82 Regulates the Spatiotemporal Dynamics of PKCα in Acute Myeloid Leukemia. *Scientific Reports*. 6, 29859.

Thomason, H.A., Cooper, N.H., Ansell, D.M., Chiu, M., Merrit, A.J., Hardman, M.J., Garrod, D.R. (2012) Direct evidence that PKCα positively regulates wound re-epithelialization: correlation with changes in desmosomal adhesiveness. *The Journal of Pathology*. 227(3), 346–356.

Thomason, H.A., Scothern, A., Mcharg, S., Garrod, D.R. (2010) Desmosomes: adhesive strength and signalling in health and disease. *The Biochemical Journal*. 429, 419–433.

Tonoli, H., Barrett, J.C. (2005) CD82 metastasis suppressor gene: A potential target for new therapeutics? *Trends in Molecular Medicine*. 11(12), 563–570.

Tsai, Y.C., Mendoza, A., Mariano, J.M., Zhou, M., Kostova, Z., Chen, B., Veenstra, T., Hewitt, S.M., Helman, L.J., Khanna, C., Weissman, A.M. (2007) The ubiquitin ligase gp78 promotes sarcoma metastasis by targeting KAI1 for degradation. *Nature Medicine*. 13(12), 1504–1509.

Tsang, S.M., Liu, L., Teh, M.-T., Wheeler, A., Grose, R., Hart, I.R., Garrod, D.R., Fortune, F., Wan, H. (2010) Desmoglein 3, via an Interaction with E-cadherin, Is Associated with Activation of Src. *PLoS ONE*. 5(12), e14211.

Tselepis, C., Chidgey, M., North, A., Garrod, D. (1998) Desmosomal adhesion inhibits invasive behavior. *Proceedings of the National Academy of Sciences*. 95(14), 8064–9.

Tucker, D.K., Stahley, S.N., Kowalczyk, A.P. (2014) Plakophilin-1 Protects Keratinocytes from Pemphigus Vulgaris IgG by Forming Calcium-Independent Desmosomes. *Journal of Investigative Dermatology*. 134(4), 1033–1043.

Vasioukhin, V., Bowers, E., Bauer, C., Degenstein, L., Fuchs, E. (2001) Desmoplakin is essential in epidermal sheet formation. *Nature Cell Biology*. 3(12), 1076–1085.

Vaughan, J.C., Dempsey, G.T., Sun, E., Zhuang, X. (2013) Phosphine quenching of cyanine dyes as a versatile tool for fluorescence microscopy. *Journal of the American Chemical Society*. 135(4), 1197–200.

Vilela, M.J., Hashimoto, T., Nishikawa, T., North, A.J., Garrod, D. (1995) A simple epithelial cell line (MDCK) shows heterogeneity of desmoglein isoforms, one resembling pemphigus vulgaris antigen. *Journal of Cell Science*. 108 (4), 1743–50.

Vilela, M.J., Parrish, E.P., Wright, D.H., Garrod, D.R. (1987) Monoclonal antibody to desmosomal glycoprotein 1—A new epithelial marker for diagnostic pathology. *The Journal of Pathology*. 153(4), 365–375.

Wallis, S., Lloyd, S., Wise, I., Ireland, G., Fleming, T.P., Garrod, D. (2000) The α Isoform of Protein Kinase C Is Involved in Signaling the Response of Desmosomes to Wounding in Cultured Epithelial Cells. *Molecular Biology of the Cell*. 11(3), 1077–1092.

Wheelock, M.J., Jensen, P.J. (1992) Regulation of keratinocyte intercellular

junction organization and epidermal morphogenesis by E-cadherin. *The Journal of Cell Biology*. 117(2), 415–25.

White, A., Lamb, P.W., Barrett, J.C. (1998) Frequent downregulation of the KAI1(CD82) metastasis suppressor protein in human cancer cell lines. *Oncogene.* 6(24), 3143-9.

Yáñez-Mó, M., Barreiro, O., Gordon-Alonso, M., Sala-Valdés, M., Sánchez-Madrid, F. (2009) Tetraspanin-enriched microdomains: a functional unit in cell plasma membranes. *Trends in Cell Biology*. 19(9), 434–446.

Yang, X., Claas, C., Kraeft, S.K., Chen, L.B., Wang, Z., Kreidberg, J.A., Hemler, M.E. (2002) Palmitoylation of tetraspanin proteins: Modulation of CD151 lateral interactions, subcellular distribution, and integrin-dependent cell morphology. *Molecular Biology of the Cell*. 13(3), 767–781.

Yang, Z., Bowles, N.E., Scherer, S.E., Taylor, M.D., Kearney, D.L., Ge, S., Nadvoretskiy, V. V., DeFreitas, G., Carabello, B., Brandon, L.I., Godsel, L.M., Green, K.J., Saffitz, J.E., Li, H., Danieli, G.A., Calkins, H., Marcus, F., Towbin, J.A. (2006) Desmosomal Dysfunction due to Mutations in Desmoplakin Causes Arrhythmogenic Right Ventricular Dysplasia/Cardiomyopathy. *Circulation Research*. 99(6), 646–655.

Yap, A.S., Duszyc, K., Viasnoff, V. (2018) Mechanosensing and Mechanotransduction at Cell-Cell Junctions. *Cold Spring Harbor Perspectives in Biology*. 10(8), a028761.

Yin, T., Getsios, S., Caldelari, R., Godsel, L.M., Kowalczyk, A.P., Müller, E.J., Green, K.J. (2005a) Mechanisms of plakoglobin-dependent adhesion: Desmosome-specific functions in assembly and regulation by epidermal growth factor receptor. *Journal of Biological Chemistry*. 280(48), 40355–40363.

Yin, T., Getsios, S., Caldelari, R., Kowalczyk, A.P., Muller, E.J., Jones, J.C.R., Green, K.J. (2005b) Plakoglobin suppresses keratinocyte motility through both cell-cell adhesion-dependent and -independent mechanisms. *Proceedings of the National Academy of Sciences*. 102(15), 5420–5425.

Zhang, X.A., Bontrager, A.L., Hemler, M.E. (2001) Transmembrane-4 Superfamily Proteins Associate with Activated Protein Kinase C (PKC) and Link PKC to Specific β_1 Integrins. *Journal of Biological Chemistry*. 276(27), 25005–25013.

Zhang, X.A., Lane, W.S., Charrin, S., Rubinstein, E., Liu, L. (2003) EWI2/PGRL associates with the metastasis suppressor KAI1/CD82 and inhibits the migration of prostate cancer cells. *Cancer Research*. 63(10), 2665–74.

Zhou, J., Qu, J., Yi, X.P., Graber, K., Huber, L., Wang, X., Gerdes, A.M., Li, F. (2007) Upregulation of γ-catenin compensates for the loss of β-catenin in adult cardiomyocytes. *American Journal of Physiology-Heart and Circulatory Physiology*. 292(1), 270–276.

Zimmerman, B., Kelly, B., McMillan, B.J., Seegar, T.C.M., Dror, R.O., Kruse, A.C., Blacklow, S.C. (2016) Crystal Structure of a Full-Length Human Tetraspanin Reveals a Cholesterol-Binding Pocket. *Cell*. 167(4), 1041-1051.

Zöller, M. (2009) Tetraspanins: push and pull in suppressing and promoting metastasis. *Nature Reviews Cancer*. 9(1), 40–55.

Zuidscherwoude, M., Dunlock, V.M.E., Van Den Bogaart, G., Van Deventer, S.J., Van Der Schaaf, A., Van Oostrum, J., Goedhart, J., In't Hout, J., Hämmerling, G.J., Tanaka, S., Nadler, A., Schultz, C., Wright, M.D., Adjobo-Hermans, M.J.W., Van Spriel, A.B. (2017) Tetraspanin microdomains control localized protein kinase C signaling in B cells. *Science Signaling*. 10(478), eaag2755.

Zuidscherwoude, M., Göttfert, F., Dunlock, V.M.E., Figdor, C.G., Van Den Bogaart,

G., Van Spriel, A.B. (2015) The tetraspanin web revisited by super-resolution microscopy. *Scientific Reports*. 5(1), 12201.